

University of Nottingham
UK | CHINA | MALAYSIA

# The Role of Mesenchymal Cells in Cholangiocarcinoma

Mireia Sueca-Comes

A thesis submitted to the University of Nottingham for the degree of Doctor of Philosophy (PhD)

Under supervision of Professor Anna M. Grabowska and Professor David O. Bates

December 2022

# Abstract

The process of tumour formation and progression is highly influenced by the components of the tumour microenvironment (TME) through a mutual and dynamic crosstalk. Cholangiocarcinoma (CCA) is a highly desmoplastic tumour; however, the role of its reactive TME is not fully elucidated. Treatments are limited and often ineffective due to the lack of biomarkers for its early diagnosis and the lack of understanding of its molecular pathogenesis. Therefore, we believe that investigating the TME and its role in CCA progression could lead to more effective therapeutic treatments for managing this devastating cancer.

Spheroid models were established from CCA patient-derived xenografts and a range of cell-lines. The models were characterised by live/dead staining; and stained for H&E, Vimentin (mesenchymal marker) and CK7 and CK19 (CCA markers). The effect of the mesenchymal stem cells (MSCs) in driving proliferation was evaluated by luminescence and Ki-67 staining. The transcriptome was also sequenced and analysed to identify potential signalling pathways that may be driving the proliferation.

CCA-derived spheroids remained viable, retained histological features frequently found in CCA tumours and stained positive for the hepatobiliary markers, confirming that it is a relevant system to investigate CCA. Interestingly, cell proliferation was found to be significantly promoted by the presence of mesenchymal cells. In the PDX-based models, it was also noted that the presence of stromal support enhanced the formation of spheroids, highlighting the importance of the crosstalk with the TME. In addition, RNA-sequencing expression data showed that the ECM-receptor and PI3K-AKT signalling pathways were upregulated in the presence of MSCs.

These results indicate that CCA proliferation could be driven by the crosstalk between the tumour and the stroma through these signalling pathways, and ultimately these pathways could be promising targets for the treatment of this disease.

# Acknowledgements

Firstly, I would like to express my most sincere gratitude to my primary supervisor, Professor Anna M. Grabowska, for her wisdom, invaluable guidance, and support over the last four years. From the very first day to the last, her passion for science has been inspirational and kept me motivated through times of difficulty. I would also like to thank my co-supervisor, Professor David O. Bates, for his support and valuable advice in various aspects of my work. I must also thank our collaborators Professor Nigel Mongan, Professor Jesper B. Andersen, Dr Dan Booth and Dr Sakaew Waraporn for their mentorship and their many contributions to this project. I thank Dr Isioma Egbuniwe and Elena Cristina Rusu too for their valuable input in this project.

I am also grateful to the friendship and support of the wonderful people in the Grabowska Lab who helped me along the way, especially Pam Collier, Catherine Probert, Phil Clarke and the *in* vivo team; and the beautiful people I met along the way in QMC and Biodiscovery Institute from other groups. There are too many of you to name individually, but I hope you know that your kindness got me through this PhD. Thank you for creating a fun, friendly and collaborative working environment.

I must mention my compatriot, Magda, who has been the best PhD friend I could ask for. I have so much respect for you, both as a scientist and a friend, and I am grateful I met you. I would also like to give special thanks to my best friend, Joan and my cousin Joana for their time and continuous advice. Thanks to the rest of my group of friends from both my town, (L'Ametlla de Mar) and my former University (Rovira i Virgili and University of Barcelona).

Finally, I would be greatly amiss if I did not thank my family, and family-in-law. To my family-in-law (especially my brother-in-law, Akbar) thank you for listening to me ramble on about my thesis and patiently suffering alongside me. I cannot even attempt to tell you how much you all mean to me. The biggest honour, however, must go to my parents, José Luis, and Candelaria; brother, Josep Lluis; grandparents, Paquito, Clarin, José Luis and Manolita; and my soulmate, Akmal. I simply would not be here without your unconditional love and never-ending support. You had to endure four years' worth of doubts and woes, and not once did you stop believing in me. For that, and for so much more, thank you. I am forever grateful to you all.

## Author's declaration

I, Mireia Sueca-Comes, confirm that the work presented in this thesis was carried out in accordance with the requirements of the University's Regulations and Code of Practice for Research Degree Programs and that it has not been submitted for any other academic award. I confirm that the work and views demonstrated in this thesis are my own. Where information has been derived from other sources, I confirm this has been indicated in the thesis.

SIGNED: 

DATE: 29/09/2022

# Table of Contents

**ABSTRACT** ..... **2**

**ACKNOWLEDGEMENTS** ..... **3**

**AUTHOR'S DECLARATION** ..... **4**

**LIST OF ABBREVIATIONS** ..... **10**

**LIST OF FIGURES** ..... **16**

**LIST OF TABLES** ..... **20**

**CHAPTER 1. INTRODUCTION** ..... **21**

1.1. CANCER AND HALLMARKS OF CANCER ..... 22

*1.1.1. Sustaining Proliferative Signalling* ..... *23*

*1.1.2. Evading Growth Suppressors* ..... *23*

*1.1.3. Resisting cell death* ..... *24*

*1.1.4. Enabling Replicative Immortality* ..... *24*

*1.1.5. Inducing Angiogenesis* ..... *24*

*1.1.6. Activating Invasion and Metastasis* ..... *24*

*1.1.7. Enabling Characteristic: Genome Instability and Mutations* ..... *25*

*1.1.8. Enabling Characteristic: Tumour-Promoting Inflammation* ..... *25*

*1.1.9. Emerging Hallmark: Reprogramming Energy Metabolism* ..... *26*

*1.1.10. Emerging Hallmark: Evading Immune Destruction* ..... *26*

*1.1.11. Unlocking Phenotypic Plasticity* ..... *26*

*1.1.12. Non-mutational Epigenetic Reprogramming* ..... *26*

*1.1.13. Polymorphic Microbiomes* ..... *27*

*1.1.14. Senescent Cells* ..... *27*

1.2. TUMOUR MICROENVIRONMENT ..... 28

*1.2.1. Cells of Mesenchymal Origin* ..... *29*

1.2.1.1. Fibroblasts ..... 29

1.2.1.2. Mesenchymal stem cells ..... 30

1.2.1.3. Cancer-Associated Fibroblasts ..... 31

1.3. CHOLANGIOCARCINOMA ..... 32

*1.3.1. Epidemiology and risk factors* ..... *32*

*1.3.2. Morphological Classification* ..... *35*

1.3.2.1. Intrahepatic Cholangiocarcinoma ..... 35

1.3.2.2. Perihilar and distal Cholangiocarcinoma ..... 35

*1.3.3. Clinical presentations and diagnostic* ..... *35*

*1.3.4. Treatments and clinical trials* ..... *36*

1.4. SIGNALLING AND MOLECULAR NETWORKS IN CHOLANGIOCARCINOMA ..... 38

*1.4.1. Cell survival and cell death-related pathways* ... *39*
1.4.1.1. Pathways associated to *FGFR2* ... 39
1.4.1.2. Pathways associated to *BRAF*, *KRAS* and *TP53* mutations ... 39
1.4.1.3. EGFR signalling pathway ... 39
1.4.1.4. Secretin and histamine signalling pathways ... 40
1.4.1.5. PI3K/AKT signalling pathway ... 41
1.4.1.6. Apoptosis and necroptosis signalling pathways ... 41
*1.4.2. Development-related pathways* ... *41*
1.4.2.1. Notch signalling pathway ... 41
1.4.2.2. Hedgehog signalling pathway ... 42
1.4.2.3. Wnt/β-catenin signalling pathway ... 43
*1.4.3. Metabolic and epigenetic pathways associated to IDH1/2 mutations* ... *43*
*1.4.4. Epigenetic and DNA damage response pathways associated to BAP1, PBRM1 and ARID1A mutations* ... *44*
1.5. TUMOUR MICROENVIRONMENT IN CCA ... 44
*1.5.1. Inflammatory cells* ... *45*
*1.5.2. Extracellular matrix* ... *46*
*1.5.3. Tumour Stromal Cells and Cancer-associated Fibroblasts* ... *46*
1.6. CHOLANGIOCARCINOMA EXPERIMENTAL MODELS ... 48
*1.6.1. 2D models* ... *49*
*1.6.2. 3D models* ... *49*
1.6.2.1. Spheroids and spheres ... 50
1.6.2.2. Hydrogel-based models ... 52
1.6.2.2.1. Organoids ... 52
*1.6.3. In vivo models* ... *53*
1.6.3.1. Patient-derived xenografts ... 54
*1.6.4. Ex vivo models* ... *55*
1.7. HYPOTHESIS AND AIMS ... 56
**CHAPTER 2. MATERIAL AND METHODS ... 57**
2.1. CELL-LINES ... 58
2.2. ROUTINE CULTURE OF CELL MONOLAYER ... 60
*2.2.1. Cell sub-culture* ... *60*
*2.2.2. Cell cryopreservation* ... *60*
*2.2.3. Cell revival* ... *60*
2.3. 3D *IN VITRO* MODELS ... 61
*2.3.1. Generation of a luminescent cell population and puromycin selection* ... *61*
*2.3.2. Establishment of cell-line-derived spheroids for the direct co-culture system* ... *61*
*2.3.3. Establishment of cell-line-derived spheroids for the indirect co-culture system* ... *62*
2.4. 3D *EX VIVO* MODELS ... 62

*2.4.1. Specimens and establishment of PDXs* ..... *62*
*2.4.2. Dissociation of the PDX tumours* ..... *63*
*2.4.3. Establishment of PDX-derived spheroids* ..... *64*
2.5. SPHEROID VIABILITY AND PROLIFERATION ..... 64
*2.5.1. AlamarBlue Assay* ..... *64*
*2.5.2. PrestoBlue Assay* ..... *64*
*2.5.3. Live/dead staining* ..... *65*
*2.5.4. Luciferase assay* ..... *65*
*2.5.5. Image analysis* ..... *66*
2.6. SPHEROID AND PDX MORPHOLOGY ..... 66
*2.6.1. Embedding spheroids in a microarray* ..... *66*
*2.6.2. Sectioning of the PDXs and spheroids* ..... *67*
*2.6.3. H&E Staining* ..... *67*
*2.6.4. Immunohistochemistry (IHC)* ..... *67*
2.6.4.1. IHC quantification ..... 68
2.6.4.1.1. Ki-67 ..... 68
2.6.4.1.2. Vimentin ..... 69
*2.6.5. Immunofluorescence (IF)* ..... *69*
*2.6.6. Scanning Electron Microscopy (SEM)* ..... *69*
2.7. BIOINFORMATIC ANALYSIS ..... 70
*2.7.1. RNA extraction* ..... *70*
*2.7.2. Analysis* ..... *70*
2.8. STATISTICAL ANALYSIS ..... 71

**CHAPTER 3. DEVELOPMENT AND CHARACTERISATION OF CELL-LINE-DERIVED CCA SPHEROIDS .... 72**

3.1. INTRODUCTION ..... 73
3.2. RESULTS ..... 75
*3.2.1. Optimisation of seeding density for CCA spheroid formation* ..... *75*
*3.2.2. Viability of the CCA cells in the spheroids* ..... *79*
3.2.2.1. Optimisation of the live/dead staining in the spheroid model ..... 80
*3.2.3. Morphology of the CCA spheroids* ..... *83*
*3.2.4. Characterisation of the cellular proliferation of the CCA spheroids* ..... *87*
*3.2.5. Expression of CK7 and CK19 in the CCA spheroids* ..... *89*
*3.2.6. Ultrastructural Characterisation of the CCA spheroids by SEM* ..... *91*
3.3. SUMMARY AND TECHNICAL DISCUSSION ..... 92

**CHAPTER 4. THE INFLUENCE OF MESENCHYMAL STEM CELLS ON CCA PROLIFERATION IN A SPHEROID MODEL ..... 96**

4.1. INTRODUCTION ..... 97

4.2. RESULTS ..... 99
*4.2.1. Generation of stable CCA luciferase-transduced cell-lines ..... 99*
*4.2.2. Effect of different co-culture ratios of CCA cells to hMSCs on CCA proliferation ..... 105*
*4.2.3. Effect of hMSCs and iMSCs on CCA proliferation in a direct co-culture system ..... 107*
*4.2.4. Effect of iMSCs on CCA proliferation in an indirect co-culture system ..... 111*
*4.2.5. Morphology of the mono- and co-culture spheroids ..... 116*
*4.2.6. Characterisation of the cellular proliferation mono- and co-culture spheroids ..... 118*
*4.2.7. Expression of Vimentin, CK7 and CK19 on the CCA spheroids ..... 120*
4.3. SUMMARY AND TECHNICAL DISCUSSION ..... 123

**CHAPTER 5. THE INFLUENCE OF MESENCHYMAL STEM CELLS ON PDX AND PDX-DERIVED SPHEROIDS ..... 126**

5.1. INTRODUCTION ..... 127
5.2. RESULTS ..... 129
*5.2.1. PDX characterisation ..... 129*
5.2.1.1. H&E Staining ..... 129
5.2.1.2. Vimentin expression ..... 131
5.2.1.3. CK7 and CK19 expression ..... 134
*5.2.2. PDX proliferation: Tumour volume and Ki-67 expression ..... 137*
*5.2.3. Generation of PDX-derived Spheroids ..... 141*
5.2.3.1. Group 1: CCA1, CCA7 and CCA11 ..... 143
5.2.3.2. Group 2: CCA2, CCA4, CCA5 and CCA6 ..... 145
*5.2.4. PDX-derived Spheroid characterisation ..... 147*
5.2.4.1. H&E staining ..... 147
5.2.4.2. Vimentin expression ..... 149
5.2.4.3. CK7 and CK19 expression ..... 149
*5.2.5. PDX-derived spheroid proliferation: Ki-67 expression ..... 151*
5.3. SUMMARY AND TECHNICAL DISCUSSION ..... 154

**CHAPTER 6. IDENTIFICATION OF ACTIVE SIGNALLING PATHWAYS IN CO-CULTURES OF CANCER CELLS AND MSCS ..... 158**

6.1. INTRODUCTION ..... 159
6.2. RESULTS ..... 161
*6.2.1. Experimental design and data pre-processing ..... 161*
*6.2.2. Activated pathways in the CCA co-culture spheroids ..... 162*
6.2.2.1. Pre-processing and Exploratory analysis ..... 163
6.2.2.2. Differentially expressed genes and enriched pathways ..... 166
6.2.2.3. Pathway analysis (GSEA) ..... 170
*6.2.3. Bioinformatic analysis of the PDXs ..... 173*
6.2.3.1. Pre-processing and Exploratory analysis ..... 173

6.2.3.2. Differentially expressed genes and GSEA ..... 176
*6.2.4. 3D CCA models* ..... *177*
6.3. SUMMARY AND TECHNICAL DISCUSSION ..... 178

**CHAPTER 7. DISCUSSION, CONCLUSIONS AND FUTURE DIRECTIONS ..... 182**

7.1. DISCUSSION ..... 183
7.2. FUTURE WORK ..... 199
7.3. CONCLUSIONS ..... 201

**APPENDIX A. ..... 202**

**ACHIEVEMENTS ..... 207**

- PUBLICATIONS ..... 207
- ORAL PRESENTATIONS ..... 207
- POSTER PRESENTATIONS ..... 207
- FUNDED TRAINING COURSES ..... 207
- GRANTS ..... 208

**COVID STATEMENT ..... 209**

**REFERENCES ..... 210**

# List of abbreviations

| | |
|---|---|
| 3D-TGA | 3D Tumour Growth Assay |
| ABC | Advanced Biliary Cancer |
| ADMSCs | Adipose-derived mesenchymal stem cells |
| AJCC | American Joint Committee on Cancer |
| AKT | Protein kinase B |
| ANOVA | Analysis of variance |
| B cells | Bone marrow-derived cells |
| BAF | Barrier-to-autointegration factor |
| Bak | Bcl-2 homologous antagonist/killer |
| Bax | Bcl-2-associated X protein |
| Bcl-2 | B-cell lymphoma-2 |
| Bcl-XL | B-cell lymphoma-extra-large |
| BL | Bioluminescence |
| BME | Basement membrane extract |
| BSA | Bovine serum albumin |
| C | Complement component |
| Ca-AM | Calcein Acetoxymethyl Ester |
| CAFs | Cancer-associated fibroblasts |
| CCA | Cholangiocarcinoma |
| CCL | Chemokine C-C motif ligand |
| CD | Cluster of differentiation |
| *CDH* | *Cadherin* |
| CEUS | Contrast-enhanced ultrasonography |
| CK | Cytokeratin |
| COL | Collagens |
| CPM | Counts per million |
| CSCs | Cancer stem cells |
| CT | Computed tomography |
| CTGF | Connective tissue growth factor |
| CTLs | Cytotoxic T lymphocytes |

| | |
|---|---|
| CXCL | Chemokine C-X-C motif ligand |
| CXCR | Chemokine C-X-C motif receptor |
| D-2HG | D-2-hydroxyglutarate |
| DAB | Diaminobenzidine |
| DCCA | Distal Cholangiocarcinoma |
| DEGs | Differential expressed genes |
| DHH | Desert hedgehog |
| DLL | Delta-like |
| DMEM | Dulbecco's Modified Essential Medium |
| DMSO | Dimethyl sulfoxide |
| DNA | Deoxyribonucleic acid |
| DPX | Dibutyl phthalate |
| E-cadherin | Epithelial cadherin |
| EC | Endothelial cells |
| ECCA | Extrahepatic Cholangiocarcinoma |
| ECM | Extracellular matrix |
| EDTA | Erthylenediamine tetraacetic acid |
| EGFR | Epidermal growth factor receptor |
| EMT | Epithelial to mesenchymal transition |
| ERBB | Erythroblastic oncogene B |
| ERK | Extracellular signal-regulated kinase |
| EthD-1 | Ethidium homodimer |
| FAP | Fibroblast activation protein |
| FBS | Fetal bovine serum |
| FDA | Food and Drug Administration |
| FDG PET | Fluorodeoxyglucose positron emission tomography |
| FDR | False discovery rate |
| FFs | FGFR2 fusions |
| FGF | Fibroblast growth factor |
| FGFR | Fibroblast growth factor receptor |
| GEMM | Genetically-engineered models |
| GEO | Expression Omnibus |

| | |
|---|---|
| GFP | Green fluorescent protein |
| GSEA | Gene Set Enrichment Analysis |
| H&E | Hematoxylin and eosin |
| $H_2O_2$ | Hydrogen peroxide |
| HB-EGF | Heparin binging-epidermal growth factor |
| HBSS | Hanks' Balanced Salt Solution |
| HCC | Hepatocellular carcinoma |
| HER | Human epidermal growth factor |
| HGF | Hepatocyte growth factor |
| HH | Hedgehog |
| HIF-1α | Hypoxia-inducible factor 1α |
| HisR | Histamine receptors |
| hMSCs | Primary bone marrow-derived mesenchymal stem cells |
| HNSCC | Head and neck squamous carcinoma |
| HSCs | Hematopoietic stem cells |
| ICCA | Intrahepatic Cholangiocarcinoma |
| iDEP | Integrated Differential Expression and Pathway analysis |
| IDH | Isocitrate dehydrogenase |
| IF | Immunofluorescence |
| IGF | Insulin-like growth factor |
| IHC | Immunohistochemistry |
| IHH | Indian hedgehog |
| IL | Interleukin |
| iMSCs | Immortalised bone marrow-derived mesenchymal stem cells |
| ITG | Integrin |
| IVIS | *In Vivo* Bioluminescent Imaging |
| JAG | Jagged |
| JAK | Janus tyrosine kinase |
| JNK | c-Jun N-terminal kinases |
| KRAS | Kirsten rat sarcoma |
| LEF | Lymphoid enhancer factor |
| MAPK | Mitogen-activated protein kinase |

| | |
|---|---|
| MC | Mast cells |
| Mcl | Myeloid leukemia cell differentiation protein |
| MEK | Mitogen-activated protein kinase kinase |
| MET | Mesenchymal to epithelial transition |
| MMP | Metalloproteinases |
| MRI | Magnetic resonance imaging |
| mRNA | Messenger RNA |
| MRTF | Myocardin-related transcription factor |
| MSCM | Mesenchymal stem cell medium |
| MSCs | Mesenchymal stem cells |
| mTOR | Mammalian target of rapamycin |
| NBF | Neutral Buffer Formalin |
| NCID | Notch intracellular domain |
| NCIN | National Cancer Intelligence Network |
| NF-κB | Nuclear factor-κB |
| NGS | Next Generation Sequencing |
| NK | Natural killer |
| Non-O-CCA | Non-Opisthorchis viverrini-related CCA |
| Notch | Neurogenic locus notch homolog protein |
| O-CCA | Opisthorchis viverrini-related CCA |
| PBS | Phosphate-buffered saline |
| PCA | Principal component analysis |
| PCCA | Perihilar |
| PCP | Planar cell polarity |
| PD-1 | Programmed cell death 1 |
| PD-L1 | Programmed cell death ligand 1 |
| PFA | Paraformaldehyde |
| PDAC | Pancreatic ductal adenocarcinoma |
| PDGF | Platelet-derived growth factor |
| PDXs | Patient-derived xenografts |
| PI | Propidium Iodide |
| PI3K | Phosphoinositide 3-kinases |

| | |
|---|---|
| POSTN | Periostin |
| PSC | Primary sclerosing cholangitis |
| PTEN | Phosphatase and tensin homolog |
| Puma | p53 upregulated modulator of apoptosis |
| QC | Quality checks |
| Rac | Ras-related C3 botulinum toxin substrate |
| RAS | Rat sarcoma |
| RB | Retinoblastoma-associated |
| RFU | Relative fluorescence |
| RIN | RNA integrity number |
| RLU | Relative luminescence |
| RNA | Ribonucleic acid |
| RNASeq | RNA Sequencing |
| rRNA | Ribosomal RNA |
| RTK | Receptor tyrosine kinases |
| SASP | Senescence-associated secretory phenotype |
| ScRNASeq | Single cell RNASeq |
| SCTR | Secretin receptors |
| SEM | Scanning Electron Microscopy |
| SEM | Standard error of the mean |
| SFD | Stromal cell-derived factor |
| SHH | Sonic hedgehog |
| SOX | SRY-box |
| STAT | Signal transducer and activator of transcription |
| T cells | Thymus cells |
| TAMs | Tumour-associated macrophages |
| TAZ | Transcriptional co-activator with PDZ-binding motif |
| TCF | T-cell factor |
| TCGA | The Cancer Genome Atlas |
| TEM | Transmission electron microscope |
| TGF-β | Transforming growth factor-β |
| TIMP | Tissue inhibitor of metalloproteinase |

| | |
|---|---|
| TME | Tumour microenvironment |
| TNF- α | Tumour necrosis factor-α |
| TNM | Tumour, nodes, and metastases |
| TP53 | Tumour protein p53 |
| TRK | Tropomyosin receptor kinase |
| tRNA | Transfer RNA |
| ULA | Ultra-low attachment |
| VEGF | Vascular endothelial growth factor |
| WB | Washing buffer |
| Wnt | Wingless-related integration site |
| YAP | Yes-associated protein |
| α-KG | α-ketoglutarate |
| α-SMA | α-smooth muscle actin |

# List of Figures

**Figure 1.1.** Hallmarks of cancer ..... 23

**Figure 1.2.** Tumour cells and cells of the tumour microenvironment ..... 29

**Figure 1.3.** Global age-standardised annual mortality rates for Cholangiocarcinoma (deaths per 100,000 inhabitants, including the 3 types of CCA) (Banales et al., 2020) ..... 34

**Figure 1.4.** Signalling pathways in Cholangiocarcinoma (Banales et al., 2020) ..... 38

**Figure 1.5.** Experimental models ..... 48

**Figure 3.1.** KKU-M055 spheroid formation ..... 76

**Figure 3.2.** KKU-M055 spheroid formation in the presence or absence of BME ..... 77

**Figure 3.3.** TFK-1 spheroid formation in the presence or absence of BME ..... 78

**Figure 3.4.** KKU-M055 and TFK-1 spheroid viability ..... 80

**Figure 3.5.** Live/dead staining optimisation ..... 82

**Figure 3.6.** Morphology of CCA cells cultured in 2D. ..... 83

**Figure 3.7.** Morphology of the CCA cell-line derived spheroids ..... 84

**Figure 3.8.** H&E staining of human CCA tumour and CCA cell-line-derived spheroids ..... 86

**Figure 3.9.** Ki-67 staining of CCA cell-line-derived spheroids ..... 87

**Figure 3.10.** Immunofluorescence staining of the KKU-M213-derived spheroids ... 89

**Figure 3.11.** CK7 and CK19 staining of CCA cell-line-derived spheroids ..... 90

**Figure 3.12.** SEM imaging of CCA-derived spheroids ..... 91

**Figure 4.1.** Diagram of the direct and indirect co-culture of CCA and MSCs ..... 99

**Figure 4.2.** Puromycin kill curves of CCA wild-type cells ..... 100

**Figure 4.3.** First attempt to generate bioluminescent transduced CCA cells ..... 102

**Figure 4.4.** Second attempt to generate bioluminescent transduced CCA cells ..... 103

**Figure 4.5.** Bioluminescent signal from transduced cells compared to their corresponding wild-type ..... 104

**Figure 4.6.** Different ratios of KKU-M213 and hMSCs co-culture spheroids ..... 106

**Figure 4.7.** Spheroid internal structure and morphology ..... 107

**Figure 4.8.** Growth of KKU-M213 cells in co-culture with hMSCs or iMSCs ..... 108

**Figure 4.9.** Effect of iMSCs on CCA-derived spheroid proliferation in a direct co-culture system ..... 110

**Figure 4.10.** Effect of iMSCs on CCA-derived spheroids in a co-culture transwell system ..... 113

**Figure 4.11.** Comparison between the direct and transwell system at day 5 ..... 115

**Figure 4.12.** Internal morphology of mono- and co-culture CCA spheroids ..... 117

**Figure 4.13.** Characterisation of the cellular proliferation of the CCA spheroids ... 119

**Figure 4.14.** Expression of Vimentin, CK7 and CK19 on CCA mono- and co-culture spheroids ..... 121

**Figure 5.1.** H&E staining of CCA patient tumours and matched patient-derived xenograft in presence or absence of hMSCs ..... 130

**Figure 5.2.** Vimentin staining of CCA patient-derived xenograft in presence or absence of hMSCs ..... 133

**Figure 5.3.** CK7 staining of CCA patient-derived xenograft in presence or absence of hMSCs ..... 135

**Figure 5.4.** CK19 staining of CCA patient-derived xenograft in presence or absence of hMSCs ..... 136

**Figure 5.5.** Tumour growth rates of patient-derived xenograft in presence or absence of hMSCs ..... 138

**Figure 5.6.** Ki-67 staining of CCA patient-derived xenograft in presence or absence of hMSCs ..... 140

**Figure 5.7.** CCA7 PDX-derived spheroids grown in a range of BME concentrations ..... 142

**Figure 5.8.** CCA 1, 7 and 11 PDX-derived spheroids in presence or absence of hMSCs or iMSCs ..... 144

**Figure 5.9.** CCA 2, 4, 5 and 6 PDX-derived spheroids in presence or absence of hMSCs or iMSCs ..... 146

**Figure 5.10.** H&E staining of CCA PDX-derived spheroids in presence or absence of hMSCs or iMSCs ..... 148

**Figure 5.11.** Vimentin staining of CCA PDX-derived spheroids in presence or absence of hMSCs or iMSCs ..... 149

**Figure 5.12.** CK17 staining of CCA PDX-derived spheroids in presence or absence of hMSCs or iMSCs ..... 150

**Figure 5.13.** CK19 staining of CCA PDX-derived spheroids in presence or absence of hMSCs or iMSCs ..... 150

**Figure 5.14.** Ki-67 staining of CCA PDX-derived spheroids in presence or absence of hMSCs or iMSCs ..... 152

**Figure 6.1.** Experimental design for RNASeq analysis .....162

**Figure 6.2.** Diagnostic plots of the KKU-M213-derived spheroids ..... 164

**Figure 6.3.** Exploratory analysis for the KKU-M213-derived spheroids ..... 165

**Figure 6.4.** DEGs genes identified by DESeq2 for the KKU-M213-derived spheroids ..... 167

**Figure 6.5.** Summary plots for differential expression analysis using DESeq2 for the KKU-M213-derived spheroids ..... 168

**Figure 6.6.** Overrepresentation analysis of KEGG pathways for the KKU-M213-derived spheroids ..... 169

**Figure 6.7.** Gene set enrichment analysis for the KKU-M213-derived spheroids ... 171

**Figure 6.8.** Heatmap of the EMT pathway ..... 172

**Figure 6.9.** Diagnostic plots of PDXs ..... 174

**Figure 6.10.** Exploratory analysis for the PDXs ..... 175

**Figure 6.11.** PCA plot of the PDXs after removing batch effect ..... 176

**Figure 6.12.** PCA plots of 3D CCA models ..... 177

**Figure 7.1.** Schematic pathway hypothesis of the biological effects of the mesenchymal cells in CCA proliferation ..... 197

**Figure A1.** Technical replicates of the cell-line derived spheroids in the spheroid-array ..... 202

**Figure A2.** Technical replicates of KKU-M213-derived spheroids in the spheroid-array ..... 203

**Figure A3.** Technical replicates of Group 1 PDX-derived spheroids in the spheroid-array ..... 204

**Figure A4.** Technical replicates of Group 2 PDX-derived spheroids in the spheroid-array ..... 205

# List of Tables

**Table 2.1.** Cholangiocarcinoma cell-lines information ..... 59

**Table 2.2.** List of antibodies (Ab) used in the IHC experiments ..... 68

**Table 3.1.** Conditions tested for live/dead staining optimisation in the spheroid model ..... 81

**Table A.1.** Summary of the concentration, purity (A260/A280 and A260/A230 ratios) and RIN of the RNA samples isolated for RNASeq ..... 206

# Chapter 1. Introduction

## 1.1. Cancer and Hallmarks of Cancer

Cancer is a worldwide health problem and according to Cancer Research UK 17 million incidents were reported in 2018 leading to 9.6 million deaths. In addition, population-based cancer data estimated that rates will keep increasing until 2040 reaching 27.5 million new cases of cancer per year (UK, 2018).

Rapid advances have also occurred in cancer research, where over the last quarter of century the knowledge has significantly increased, revealing the fundamental principles of cancer. These advances are reflected in the Hanahan *et al*. papers published every decade. In 2000 they defined cancer as a "disease involving dynamic changes in the genome" (Hanahan & Weinberg, 2000). The underlying principle was that mutations occurred in oncogenes with gain of function effects, and tumour suppressor genes with loss of function effects. They proposed six capabilities shared across all types of human tumours either as a novel capability or acquired during tumour development. These capabilities were defined as Hallmarks of Cancer (Hanahan & Weinberg, 2000). In 2011, the understanding of the mechanism underlying those capabilities was described. Two enabling characteristics key to the acquisition of the six hallmark capabilities and two new emerging hallmark capabilities were added to the Hallmarks (Hanahan & Weinberg, 2011). Most recently, in 2022, they have proposed new refinements either as discrete hallmarks or constituting distinctive enabling characteristics that facilitate the acquisition of hallmark capabilities. They have also recognised senescent cells as components of the tumour microenvironment (Hanahan, 2022). The Hallmarks of Cancer are briefly described in the following sections (Figure 1.1).

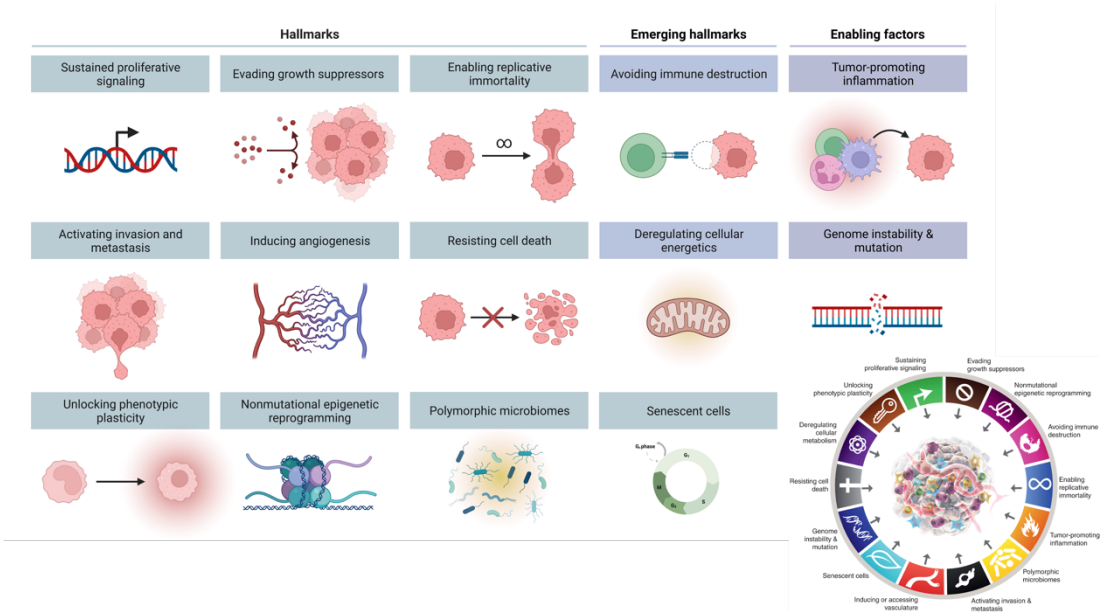



**Figure 1.1. Hallmarks of cancer.** Hallmarks that constitute the principle for the multistep development and complexities of cancer. Adapted from (Hanahan, 2022). Created with *BioRender.com*.

### 1.1.1. Sustaining Proliferative Signalling

Normal tissues ensure cell homeostasis by a controlled release of signals involved in cell division and growth. However, cancer cells can acquire the ability to deregulate all these cell mechanisms in different ways. They may have the ability to produce ligands themselves which subsequently bind to growth factor receptors generating an autocrine proliferative stimulation. Instead, cancer cells may stimulate cells within the supporting tumour stroma which consequently releases additional growth factors. Cell signalling may also be altered by increased numbers of receptors present on the surface of cancer cells encompassing a hyper-response. Additionally, tumours may have structural alterations in the receptors resulting in permanent activation. Finally, tumours can obviate the need for ligand-mediated receptor binding resulting in constitutive activation of downstream signalling pathways (Hanahan & Weinberg, 2011).

### 1.1.2. Evading Growth Suppressors

Tumour suppressor genes are genes that protect a cell from one important step on the path to cancer development by limiting cell growth. Cancer cells have developed the capability to inactivate the action of tumour suppressor genes. The two best-known

tumour suppressors inactivated in cancer are retinoblastoma-associated (RB) and tumour protein p53 (TP53) (Hanahan & Weinberg, 2011).

### 1.1.3. Resisting cell death

Apoptosis acts as a barrier to prevent neoplasia from occurring. Tumour cells evolve mechanisms to avoid cell death. The most common strategy is eliminating the damage sensor from the apoptosis-inducing circuitry by mutating the protein TP53. As an alternative, cancer cells can compromise the activity of TP53 by upregulating anti-apoptotic proteins such as B-cell lymphoma-2 (Bcl-2) and B-cell lymphoma-extra-large (Bcl-XL) or survival signals (insulin-like growth factor (IGF) 1/2); by downregulating pro-apoptotic proteins such as Bcl-2-associated X protein (Bax), Bcl-2 homologous antagonist/killer (Bak) and p53 upregulated modulator of apoptosis (Puma); or by short-circuiting the extrinsic ligand-induced death pathway (Hanahan & Weinberg, 2011).

### 1.1.4. Enabling Replicative Immortality

Normal cells bypass two barriers that control proliferation: senescence, where cells do not proliferate although they are still viable; and crisis, where cells are dead. Therefore, limiting the successive cell growth and division. These barriers are anticancer defences to stop the outgrowth of clones of pre-neoplastic and neoplastic cells. When cells become resistant to both barriers, it represents an essential step in tumour initiation and progression (Hanahan & Weinberg, 2011).

### 1.1.5. Inducing Angiogenesis

Angiogenesis is a process that generates tumour-associated neovasculature, which provides nutrients and oxygen to cells in addition to evacuating the carbon dioxide and metabolic wastes. During cancer development angiogenesis is always activated, thereby helping to sustain expanding neoplastic growths (Hanahan & Weinberg, 2011).

### 1.1.6. Activating Invasion and Metastasis

Carcinomas originate from epithelial cells and can develop a malignant phenotype resulting in local invasion and/or distant metastasis. Cancer cells normally develop changes in cell morphology, as well as their attachment to other kind of cells and to the extracellular matrix (ECM). The characteristic phenotypic change in metastatic

cancer cells is associated with the loss of Epithelial cadherin (E-cadherin). E-cadherin is a transmembrane protein responsible for key cell-to-cell adhesion and its decreased expression potentially activates invasion and metastasis (Berx & van Roy, 2009). In addition, the molecular mechanism underlying invasion and metastasis is known as epithelial to mesenchymal transition (EMT). During EMT epithelial cells lose their cell-cell junctions, re-organise their cytoskeleton and undergo changes in their cell shape and programme, consequently enabling an invasive phenotype. These cells are then recruited to specific locations where they can revert through mesenchymal to epithelial transition (MET). Cancer cells are able to initiate this mechanism to enable metastasis, resulting in the formation of a new tumour (Hanahan & Weinberg, 2011).

### 1.1.7. Enabling Characteristic: Genome Instability and Mutations

The acquisition of the functions previously described are possible by genome instability and mutations. Genomic alterations arise from many different pathways, such as damage in the telomeres, centrosome amplification, and from either endo- or exogenous sources. These mutations often lead to genomic instability, which predisposes the cell to become malignant. However, this has been expanded to incorporate epigenetic mechanisms, which include histone modifications, deoxyribonucleic acid (DNA) methylation, nucleosome positioning and non-coding ribonucleic acids (RNA) (Berdasco & Esteller, 2010). These epigenetic and genetic mechanisms interact at all stages of cancer development, working together to promote tumorigenesis through the acquisition of multiple hallmarks (Hanahan & Weinberg, 2011).

### 1.1.8. Enabling Characteristic: Tumour-Promoting Inflammation

Inflammation is considered as another enabling factor to acquire the Hallmarks of Cancer. Some neoplastic lesions are densely infiltrated by inflammatory cells. Historically, it was thought that the immune system attempted to eradicate tumours despite the ability of cancer cells to evade the immune destruction. By 2000, enough evidences demonstrated that the immune cells enhanced tumorigenesis by supplying growth factors that sustain survival and proliferation; as well as factors that increase angiogenesis, the expression of ECM-modifying enzymes and the activation of EMT resulting to higher invasion and metastasis (Hanahan & Weinberg, 2011).

### 1.1.9. Emerging Hallmark: Reprogramming Energy Metabolism

Reprogramming Energy Metabolism is an emerging hallmark that is known to facilitate tumour development and progression. Extensive research has been carried out in trying to understand the metabolic adjustments involved in uncontrolled cell proliferation (Hanahan & Weinberg, 2011).

### 1.1.10. Emerging Hallmark: Evading Immune Destruction

A second emerging hallmark is the capacity to avoid detection by the immune system and therefore, avoid being targeted by the immune response. Some components of the immune system are dispatched to eradicate cancer cells; however, cancer cells develop efficient mechanisms such as releasing transforming growth factor-β (TGF-β) to stop the infiltration of cytotoxic T lymphocytes (CTLs) and natural killer (NK) and subsequently, evade immune destruction. Currently, the immune checkpoint formed by programmed cell death 1 (PD-1) and programmed cell death ligand 1 (PD-L1) stands out as a key target due to its important role in helping cancer cells evade the immune system. Inhibitors are being investigated in numerous clinical trials and are licensed to treat some cancers (Hanahan & Weinberg, 2011).

### 1.1.11. Unlocking Phenotypic Plasticity

During tissue formation, cells undergo a series of developments until they reach a state of terminal differentiation where they stop proliferating. This constitutes a barrier to the continuing proliferation that occurs in neoplasia. Recent studies indicated that cancer cells can unlock the phenotypic plasticity and bypass the state of terminal differentiation. Cells can manifest this hallmark in various disruptions. Neoplastic cells may reverse the fully differentiated state by dedifferentiating back to a progenitor cell. In contrast, cancer cells may short-circuit the process, maintaining the neoplastic cells in a progenitor-like state; or cancer cells may go through transdifferentiation, where cells can change the destined differentiation (Hanahan, 2022).

### 1.1.12. Non-mutational Epigenetic Reprogramming

The hallmark of genome instability and mutation previously described (Chapter 1, Section 1.1.7) is widely accepted in the cancer research community. Currently, mutations are being catalogued in the different stages of the disease (development, metastasis or during treatment). There is also an appreciation of mutations in genes

that organise, modulate, and maintain the structure of the chromatin, and therewith regulate gene expression. Additionally, at present, there is the non-mutational epigenetic reprogramming, that involves only epigenetically regulated changes in gene expression. The proposition of epigenetic programming is raising interest in cancer research (Hanahan, 2022).

### 1.1.13. Polymorphic Microbiomes

The microbiota present in the internal mucosa and epidermis of the gastrointestinal tract, lungs, breast, and urogenital system lives in symbiosis with the barrier tissues of the body exposed to the environment. Recent studies suggest the microbiome to have either a positive or negative effect on cancer progression, development, and response to treatment (Hanahan, 2022).

### 1.1.14. Senescent Cells

The maintenance of homeostasis is protected by cellular senescence which is defined as an irreversible form of proliferation. The division cycle of unnecessary or dysfunctional cells is inactive and cell death occurs. Additionally, this programming evokes metabolism and morphology changes in addition to the activation of senescence-associated secretory phenotype (SASP) that involved a cascade of bioactive proteins (cytokines, chemokines, and proteases). A variety of conditions can induce senescence; some examples are DNA damage and nutrient deprivation, damage to cellular infrastructures and organelles, and imbalances in signalling pathways. Also, the mechanisms and functional determinants through which a particular senescent cell, in a specific TME, evokes a tumour-promoting or a tumour-antagonising SASP, are yet unresolved (Hanahan, 2022).

While these Hallmarks of Cancer and their enabling and emerging characteristics have proved a significant value in understanding the foundations of cancer; tumour formation and progression are also influenced by rearrangement of the components of the TME through mutual and dynamic crosstalk (Baghban et al., 2020).

## 1.2. Tumour microenvironment

In 1976 Peter Nowell described cancer as an evolutionary process, driven by step-wise somatic cell mutations with a sequential sub-clonal selection (Nowell, 1976). The concept of TME, however, was first proposed in 1863 when Virchow described the relationship between inflammation and cancer; and in 1889 upon the emergence of Pagets's theory of "seed and soil" (Jin & Jin, 2020; Langley & Fidler, 2011; Paget, 1989). In 2011, Hanahan and Weinberg recognised the emerging participation of TME in cancer development (Hanahan & Weinberg, 2011).

TME consists of immune and stromal cells, blood vessels and the non-cellular components of ECM (collagen, fibronectin, hyaluronan, laminin, etc.) (Baghban et al., 2020) (Figure 1.2). Tumour cells instruct, for their own benefit, the function of non-cellular and cellular components through complex signalling networks. The consequence of such interaction is reflected in tumour formation and maintenance as well as deficient response and resistance to treatment. The cells in the TME are also known to promote carcinogenesis in all phases of cancer development and metastasis (Hanahan & Coussens, 2012).

From a histological point of view, the TME consists of (Walter et al., 2021):

- Inflammatory cells: tumour-associated macrophages (TAMs), NK cells, neutrophils, mast cells (MC), dendritic cells, cluster of differentiation (CD) 4 and 8 positive, thymus cells (T cells), and bone marrow-derived cells (B cells).
- Vascular cells: microvascular cells, endothelial cells (EC), and pericytes.
- Extracellular matrix.
- Cells of mesenchymal origin: fibroblasts, mesenchymal stem cells, and cancer-associated fibroblasts (CAFs).

The cells of mesenchymal origin were the focus of this study and therefore, in the next section these cells are described in detail.

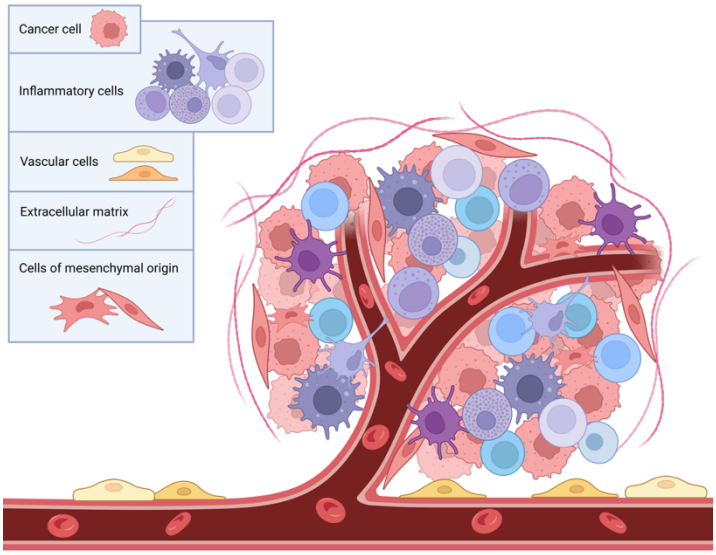



**Figure 1.2. Tumour cells and cells of the tumour microenvironment.** The TME consists of multiple cell types of diverse origins (inflammatory, vascular, and mesenchymal) and non-cellular components that forms the extracellular matrix. Created with *BioRender.com.*

### 1.2.1. Cells of Mesenchymal Origin

#### 1.2.1.1. Fibroblasts

Fibroblasts are a type of cells present in the TME and responsible for the generation of the ECM, including its synthesis, deposition, and structure. Normally, they are characterised by the presence of fibroblast activation protein (FAP). The presence of ECM proteins such as collagen type I, type IV, proteoglycan, and fibronectin generate a process called mechanoreciprocity, resulting in a mechanical stress of the ECM. ECM deposition is also characterised by the differentiation of fibroblasts into CAFs with d*e novo* expression of α-smooth muscle actin (α-SMA) (Bonnans, Chou, & Werb, 2014).

Fibroblasts express fibronectin upon the binding of TGF-β1, resulting in increased mechanical tension and leading to permanent ECM stiffness. The stiffness of the ECM enforces TGF-β1 release and results in a feedforward circuit, which is stopped in normal tissue by the activation of Yes-associated protein (YAP), transcriptional co-activator with PDZ-binding motif (TAZ) and myocardin-related transcription factor (MRTF). In normal tissue, this signalling pathway leads the de-differentiation of the fibroblasts back to quiescent fibroblasts or induces apoptosis. However, in tumour tissue, these functions are inactivated, and the fibroblasts are converted to CAFs through tumour cell-secreted platelet-derived growth factor (PDGF), fibroblast growth factor (FGF), sonic hedgehog (SHH), and interleukin (IL)-1β (Walter et al., 2021). Fibroblasts can also be converted into CAFs by tissue inhibitor of metalloproteinase

(TIMP)-1 and the subsequent activation of the IL-6/signal transducer and activator of transcription (STAT) 3 pathway (X. Zheng et al., 2016).

#### 1.2.1.2. Mesenchymal stem cells

Mesenchymal stem cells constitute a heterogeneous population which can be derived from perivascular regions of various adult organs and tissues such as bone marrow, adipose tissue, peripheral blood, among others (Hass, 2020). These multipotent cells are recruited and mobilised from the blood to the site of tissue injury by chemotaxis through growth factors like TGF-β, PDGF, IGF and FGF; and chemokines such as stromal cell-derived factor (SDF) 1; chemokine C-C motif ligand (CCL) 25 signalling; IL-6; and complement component (C) 1q, C3a, and C5a (Walter et al., 2021). There is evidence that in *in vivo* models, MSCs are attracted to tumour sites by similar signalling patterns (Du et al., 2008; M. G. Garcia et al., 2011).

In tissue injuries, MSCs are differentiated into activated fibroblasts, resident-like tissue stromal cells, or they directly mediate the activity of immune cells to promote tissue repair. The regenerative function of MSCs can be hijacked by malignant cells, and the majority of MSCs will subsequently differentiate into CAFs (Guo, Oshima, Kitmura, Taketo, & Oshima, 2008).

MSCs can also promote cancer metastasis and tumour angiogenesis in tumour tissue through the secretion of vascular endothelial growth factor (VEGF) and β-FGF (Schmidt et al., 2006). For instance, breast cancer cells have the capability to stimulate the MSCs, ultimately activating a cascade of paracrine signalling that results in higher motility, invasion, and metastasis (Aboulkheyr Es, Zhand, Thiery, & Warkiani, 2020; Karnoub et al., 2007). In addition, the secretion of IL-6 and chemokine C-X-C motif ligand (CXCL) 7 by MSCs can accelerate tumour growth through CSCs (C. Liu et al., 2011). MSCs are also involved in development of chemoresistance of tumours. In an infiltrating pancreatic ductal adenocarcinoma (PDAC) mouse model, a significant increase of MSCs was found when cells were exposed to gemcitabine, which was correlated to activation of the STAT3-CXCL10-CXC receptor (CXCR) 3 paracrine signalling axis and as a result CSCs survival was promoted (Timaner et al., 2018). The development of chemoresistance was also seen in an *in vitro* study using head and neck squamous carcinoma (HNSCC) cells exposed to paclitaxel, and co-cultured with bone marrow-derived MSCs (Scherzed et al., 2011). The effectiveness of hyperthermic

intraperitoneal chemotherapy therapy was also compromised by the activation of CXCL12 pathway through MSCs (Lis et al., 2011).

Nonetheless, evidence suggests that MSCs can also act as tumour suppressors (Walter et al., 2021). MSCs can act as tumour suppressors via the neurogenic locus notch homolog protein (Notch) 1(Walter et al., 2021) and wingless-related integration site (Wnt) signalling pathway (Walter et al., 2021) or secreting microvesicles or exosomes (Bruno et al., 2009). In this context, the proliferative activity was significantly reduced, and apoptosis was induced by the incorporation of MSC-released microvesicles by hepatic cells. Additionally, in a hepatocellular carcinoma (HCC) rat model, adipose-derived mesenchymal stem cells (ADMSCs)-derived exosomes reduced tumour volume (Ko et al., 2015). Similar, pulmonary metastasis was reduced by co-culturing a type of HCC cells with MSCs (G. C. Li et al., 2013). In Kaposi's sarcoma and HCC, MSCs hinder tumour progression by downregulating protein kinase B (AKT) activation (Khakoo et al., 2006; Zhao et al., 2012). In addition, cell proliferation was supressed when cells were treated with conditioned media of MSCs through the downregulation of the expression of nuclear factor-κB (NF-κB) (Qiao et al., 2008). Finally, a recent study showed that MSCs could inhibit proliferation, migration, and invasion in glioma cells using a 2D *in vitro* co-culture system through the downregulation of phosphoinositide 3-kinases (PI3K)/AKT signalling pathway (L. Lu et al., 2019).

These pro- and anti-tumour features of the MSCs and their potential for tumour-targeted therapies remain areas for further research and may be cancer type related.

#### 1.2.1.3. Cancer-Associated Fibroblasts

CAFs are differentiated fibroblasts localised in the TME. CAFs are an heterogenous population, α-SMA positive and they show high proliferative and metabolic activity. High density of CAFs correlated with tumour aggression, and metastasis potential in different tumour types (Walter et al., 2021).

CAFs are recruited to the tumour by a cascade of cytokine-signalling pathways, similar to those activated when fibroblasts are recruited to wounds, and first, CAFs may physically hinder tumour cells from invading surrounding tissue as they may account for a high percentage of the total tumour volume (Walter et al., 2021). However, as the tumour progresses, CAFs carry on depositing ECM proteins, secreting growth factors,

and remodelling and contracting the ECM. This process induces the stiffness of collagen fibres ultimately offering an advantage to the migrating cells (Gilkes, Bajpai, Chaturvedi, Wirtz, & Semenza, 2013; Piersma, Hayward, & Weaver, 2020). CAFs also facilitate metastasis by directing tumour cells away from the primary tumour (Erdogan et al., 2017). Once tumour cells have metastasised, tumour cells are capable of creating their own niche by transforming resident fibroblasts into CAFs (T. Fang et al., 2018).

## 1.3. Cholangiocarcinoma

Cholangiocarcinoma is the most common biliary tract malignancy and the second most common primary hepatic malignancy (Blechacz, 2017); comprising approximately 3% of all gastrointestinal cancers and 15% of all primary liver tumours (Banales et al., 2020). During liver development, hepatoblasts (bi-potent epithelial progenitor cells), can differentiate to hepatocytes, which establish the metabolic parenchyma of the liver; or cholangiocytes, which constitute the epithelium of the bile ducts and assist in the transport of toxic bile away from the liver (Martinez Lyons & Boulter, 2021). Cholangiocytes are actively involved in repairing the liver as well as modifying bile volume and composition. Moreover, cholangiocytes have a significant role in communication with other cells through paracrine secretion of various growth factors and peptides (Blechacz, 2017). Through the acquisition of the hallmarks (Raggi, Invernizzi, & Andersen, 2015), cholangiocytes can undergo a malignant transformation, ultimately forming CCA.

CCA is divided into three subtypes depending on their anatomical site of origin, intrahepatic (iCCA), perihilar (pCCA) and distal (dCCA) (Banales et al., 2016). These two last ones can also be collectively referred to as extrahepatic (eCCA). ICCAs arise above the second-order bile ducts, whilst the point of anatomical distinction between pCCA and dCCA is the insertion of the cystic duct (A. S. Khan & Dageforde, 2019).

### 1.3.1. Epidemiology and risk factors

CCA is an extremely heterogeneous cancer with significant regional variations in incidence. Data relating to the period 1971-2009 reported that CCA incidence is 0.3–6 per 100,000 inhabitants per year (Banales et al., 2016). However, this does not included places such as South Korea, China and Thailand, where incidence is >6 per 100,000 habitants (S. A. Khan, Genus, et al., 2019). The highest incidence varies from

85 per 100,000 in north-eastern Thailand to 0.4 per 100,000 in Canada (Strijker et al., 2019).

Patients with CCA have a devastatingly poor prognosis (UK, 2021). In 2008, the Public Health England's National Cancer Intelligence Network (NCIN) reported that only 5% of the diagnosed patients survive after 5 years (UK, 2021). Moreover, CCA mortality was different between genders and populations; it was found to be higher in men than in women, and in Asia than the West. Accordingly, Asian individuals had the highest mortality (2.81 per 100,000 men in Japan). In the USA, the more noticeable increases in mortality between 2004-2014 was for African American (45%), followed by Asian individuals (22%) and white individuals (20%) (Banales et al., 2020) (Figure 1.3). Nonetheless, the codes for the three CCA subtypes have not been accurate which has raised questions over the accuracy of the epidemiological data (Banales et al., 2020).

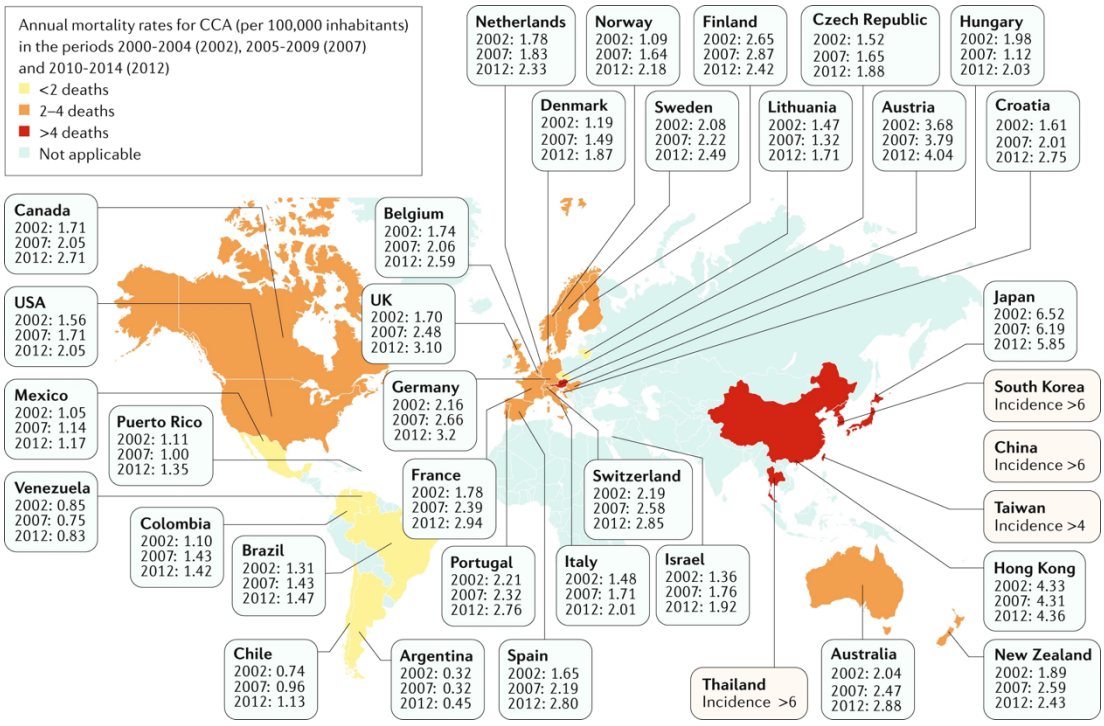



**Figure 1.3. Global age-standardised annual mortality rates for Cholangiocarcinoma (deaths per 100,000 inhabitants) (Banales et al., 2020).** Data refer to the periods 2000–2004 (2002), 2005–2009 (2007) and 2010–2014 (2012). Yellow illustrates regions with low mortality (<2 deaths), orange illustrates regions with mortality between 2 and 4 deaths, and red illustrates regions with high mortality (>4 deaths). Mortality in Thailand, China, Taiwan and South Korea was not reported and, therefore, CCA incidence is only shown.

Numerous risk factors are associated with CCA; some are common amongst the different types, and some are type-specific or seem to be significant in different areas. The most well-known and common shared risk factor is the chronic inflammation of the biliary epithelium and bile stasis (S. A. Khan, Tavolari, & Brandi, 2019). For instance, inflammatory agents such as high alcohol consumption, tobacco smoking and viral infections (hepatitis B and C virus), have been reported to increase the risk of developing CCA (Clements, Eliahoo, Kim, Taylor-Robinson, & Khan, 2020). In Thailand and the rest of Southeast Asia, the inflammation is, however, more associated to liver fluke parasitic infection (Opisthorchis viverrine or Clonorchis sinensis) (Pungpak et al., 1997; Smout et al., 2011). Obesity, primary sclerosing cholangitis, metabolic syndrome and/or presence of non-alcoholic fatty liver disease have been associated as a CCA risk factors too (Clements et al., 2020). Polymorphisms of host genes encoding enzymes involved in a variety of biological responses have also been linked to CCA development (S. A. Khan, Tavolari, et al., 2019). Nonetheless, some CCA cases are sporadic (Banales et al., 2020).

### 1.3.2. Morphological Classification

CCA was anatomically classified into extrahepatic and intrahepatic forms of the disease (Blechacz & Gores, 2008). However, the current term eCCA is now discouraged as it combines subtypes with different characteristics. iCCA can arise at any point of the intrahepatic biliary tree, ranging from the segmental bile ducts (Banales et al., 2020). pCCA emerge in the right and/or left hepatic duct and/or at their junction, and dCCA involves the common bile duct (Deoliveira et al., 2011; Nakanuma et al., 2010).

#### 1.3.2.1. Intrahepatic Cholangiocarcinoma

ICCA grows in three defined patterns: mass-forming, periductal-infiltrating, and intraductal-growing. ICCA can be histologically classified into small and large bile duct. Small bile duct is characterised by having small-sized tubular or acinar adenocarcinoma with nodular growth invading the liver parenchyma, and lack of mucin production. Those cells show isocitrate dehydrogenase (IDH) 1 and 2 mutations or FGF receptor (FGFR) 2 fusions. Large bile duct is known for the mucin-producing columnar tumour cells organised in a large duct or papillary architecture. Large bile duct iCCA cells can be characterised by kirsten rat sarcoma virus (*KRAS*) and/or *TP53* gene mutations (Banales et al., 2020).

#### 1.3.2.2. Perihilar and distal Cholangiocarcinoma

PCCA and dCCA are characterised by having poorly defined nodular sclerosing tumours or, less frequently, as intraductal papillary tumours. Histologically, both are defined as mucin-producing adenocarcinomas or papillary tumours. PCCA and dCCA, present high frequency mutations in *KRAS* oncogene and *TP53* suppressor gene (Banales et al., 2020).

### 1.3.3. Clinical presentations and diagnostic

In most cases, CCA is clinically silent at early stages and the specific symptoms only arise in the advanced stages (Banales et al., 2016). At initial stages, patients present with unspecific symptoms such as weight loss and fatigue, whereas patients with advanced stage of CCA present with symptoms such as abdominal pain, malaise, night sweats, painless jaundice, and cachexia (Endo et al., 2008).

CCA can be suspected based on several signs, such as abnormal liver function tests, biliary obstruction, elevated tumour markers, such as carbohydrate antigen 19-9 and carcinoembryonic antigen; or by ultrasonography which can highlight a bile structure or mass. Diagnosis and staging of CCA are carried out by magnetic resonance imaging (MRI), computed tomography (CT) scanning or contrast-enhanced ultrasonography (CEUS). However, differentiating between a benign and malignant bile duct structure, remains a challenge. When the diagnosis of CCA is unclear in MRI, CT or CEUS, an endoscopic tissue sampling is carried out, which is critical for CCA staging. Fluorodeoxyglucose positron emission tomography (FDG PET) is another approved diagnostic procedure (Endo et al., 2008).

Despite the multiple diagnostic methods available, the overall diagnosis of CCA remains limited; therefore, histopathological, or cytological analysis is necessary to confirm the diagnosis. This diagnosis is based on the world health organisation classification of biliary tract cancer. CCA is then staged according to the American Joint Committee on Cancer (AJCC) tumour, nodes, and metastases (TNM) system (Banales et al., 2020).

### 1.3.4. Treatments and clinical trials

Surgery is a potential curative option for CCA. Nonetheless, the relapse rate is 60%; therefore, and based on the partial benefits reported in the BILCAP study (Primrose et al., 2019), international guidelines published in 2019 recommended 6 months adjuvant capecitabine following curative resection of CCA as the current standard of care (Shroff, Kennedy, et al., 2019). The efficacy of liver transplantation in CCA, and especially pCCA, is still preliminary (Banales et al., 2020).

As CCA is initially asymptomatic, the malignancy is frequently found at advanced stages when the patient is unfit for resection. For patients who do not fit the criteria for surgical resection, palliative treatment remains the only possible option. For palliative treatment, the following points need to be considered: patient fitness, disease distribution and accessibility of tumour profiling (Banales et al., 2020).

The first-line treatment for advanced disease is cisplatin and gemcitabine combined chemotherapy. The Advanced Biliary Cancer (ABC)-02 trial showed that treating CCA with a combination of cisplatin and gemcitabine conferred a significant survival advantage, when compared to gemcitabine treatment alone (Okusaka et al., 2010; J.

Valle et al., 2010). Triple chemotherapy combinations are also currently being explored. For instance, combining cisplatin-gemcitabine and nab-paclitaxel (Shroff, Javle, et al., 2019) or -S1 (tegafur, gimeracil and oteracil) and FOLFIRINOX (Ioka et al., 2022) (NCT02591030). In addition, a first-in-class nucleotide analogue called Acelarin (NUC-1031) is combined with cisplatin (McNamara et al., 2021), and compared to the effect of cisplatin-gemcitabine effect in a phase III study (NCT04163900).

The second-line treatment for those patients who have already progressed on first-line is FOLFOX (folinic acid, 5-FU and oxaliplatin). This was tested in a phase III ABC-06 clinical trial (NCT01926236) that showed clinically significant benefits (Lamarca et al., 2021).

The standard for liver-directed therapies was also set by a subgroup analysis of the ABC trials for those patients who received cisplatin in combination of gemcitabine for unresectable iCCA and absence of extrahepatic metastasis; the 3-year OS was 0% and the median OS was 16.7 months (Banales et al., 2020). Intra-arterial therapy include transarterial radioembolization is another approach; however, the randomized SIRCCA clinical trial that evaluated its effect was interrupted due to lack of recruitment (NCT02807181). Other trials are studying the effect of combining systematic chemotherapy with local therapy (NCT02994251).

The use of targeted therapies is another attractive area; in iCCA patients, inhibitors against IDH1 (AG120, IDH305), IDH2 (AG221) and pan-IDH1–IDH2 (AG881) are currently being tested. AG120, commercially called ivosidenib, in a preliminary phase III trial showed significant evidence of efficacy (NCT03173248) (Zhu et al., 2021). In line with this, some FGFR inhibitors are currently being evaluated (NCT03656536 and NCT03773302). Moreover, for a very small group of CCA patients with neurotrophic receptor tyrosine kinases (RTK) fusions tropomyosin receptor kinase (TRK) inhibitors are found to be beneficial (Drilon et al., 2018; Drilon et al., 2017). Similarly, those with Wnt pathway alterations such as RNF43 mutations, the use of porcupine inhibitors is also beneficial (Banales et al., 2020) (NCT03447470). The Food and Drug Administration (FDA) granted accelerated approval to pemigatinib, the first treatment for adults with certain types of previously treated and advanced CCA (Rizzo, Ricci, & Brandi, 2021).

Finally, the role of immunotherapy in CCA is still limited and with minimal benefit (Yamamoto et al., 2005). Some CCA patients showed effective response using checkpoint inhibitors as shown in the KEYNOTE-028 trial using pembrolizumab in advanced biliary tract cancer (Ott et al., 2019) (NCT02054806). However, the KEYNOTE-158 trial did not confirm such activity in biliary tract tumours (Piha-Paul et al., 2020) (NCT02628067). Currently, there is an ongoing clinical trial (NCT03260712) targeting both the innate and adaptive immune system, which is proposed as the way forward for the development of immunotherapy in CCA (Banales et al., 2020). In fact, the TOPAZ-1 trial evaluated the effect of the immunotherapy durvalumab plus chemotherapy and showed a significantly improved overall survival in CCA (D. Y. Oh et al., 2022) (NCT03875235).

## 1.4. Signalling and molecular networks in Cholangiocarcinoma

In order to develop new treatments for the treatment of CCA, it is key to understand the molecular biology driving cholangiocarcinogenesis. The following sections describe pathways associated with CCA cell survival and death; with CCA development and pathways related to epigenetic alterations (Banales et al., 2020; Fouassier et al., 2019) (Figure 1.4).

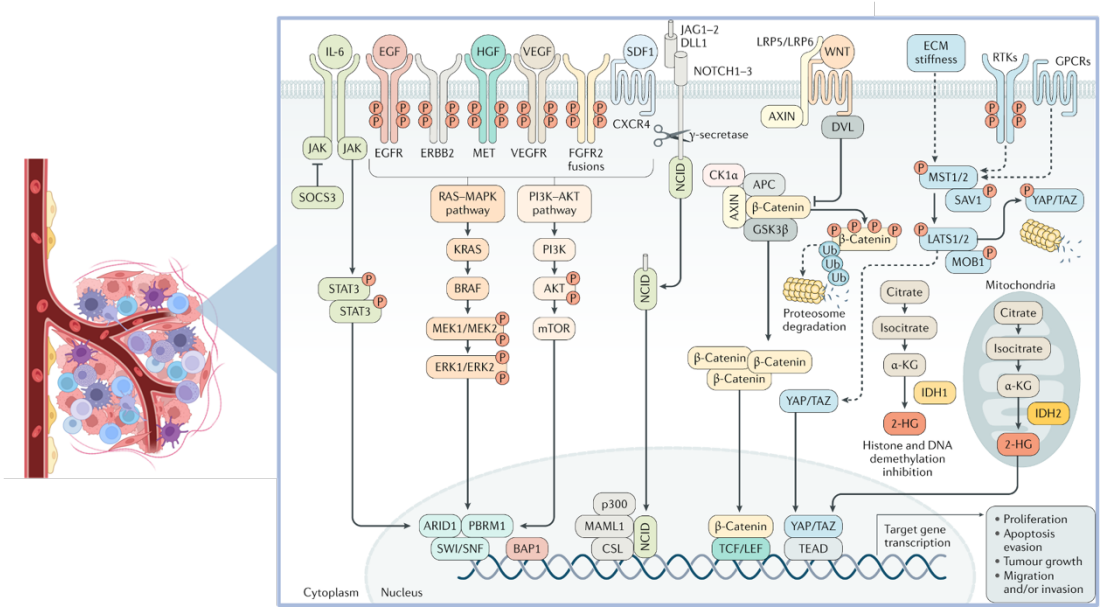



**Figure 1.4. Signalling pathways in Cholangiocarcinoma (Banales et al., 2020).** Pathways involved in the development, evolution, and growth of CCA. The activation of these signalling pathways occurs due to mutated or amplified genes and the interaction between the tumour cells and the TME.

### 1.4.1. Cell survival and cell death-related pathways

#### 1.4.1.1. Pathways associated to *FGFR2*

FGFR2 was found to be present in 10-15% of iCCA cases (Rizvi & Borad, 2016). FGFR2 fusions (FFs) are associated with constitutive tyrosine kinase activity (Fouassier et al., 2019). Extracellular signal-regulated kinase (ERK) 1/2 appeared to be the major tyrosine kinase oncogenic pathway activated by FFs (Arai et al., 2014; Lamberti et al., 2019). Nonetheless, the lack of i*n vitro* and *in vivo* models with FF-driven iCCA difficult the understanding of this oncogenic pathway (Fouassier et al., 2019).

#### 1.4.1.2. Pathways associated to *BRAF*, *KRAS* and *TP53* mutations

The prevalence of *BRAF* mutations in iCCA is 1-3% (Goeppert et al., 2014). The most frequent mutation is found in the V600 position (class 1 mutant), yet class 2 and class 3 mutants have also been described in iCCA (Dankner, Rose, Rajkumar, Siegel, & Watson, 2018). However, only class 1 tumours are sensitive to current licensed inhibitors (vemurafenib and dabrafenib). Although the differences in their underlying mutations, the 3 classes of inhibitors activate the mitogen-activated protein kinase kinase (MEK)/ERK module ultimately driving cell transformation (Dankner et al., 2018) .

*KRAS* and *TP53* are associated with both iCCA and eCCA. In iCCA, *KRAS* mutation occurs in cooperation with mutations in *TP53* and phosphatase and tensin homolog (*PTEN*) (Saborowski et al., 2013); in eCCA, in deletion of *TGFB-receptor 2* and *cadherin (CDH) 1* (Nakagawa et al., 2017). Regardless of the efforts in generating these genetic experimental models (Nakagawa et al., 2017; Saborowski et al., 2013), the oncogenic rat sarcoma (RAS) signalling and the downstream pathways have not yet been studied in detail (Fouassier et al., 2019).

#### 1.4.1.3. EGFR signalling pathway

The erythroblastic oncogene B (ERBB)/human epidermal growth factor (HER) family consists of four receptor tyrosine kinases: Her1 (epidermal growth factor receptor (EGFR), ErbB1), Her2 (Neu, ErbB2), Her3 (ErbB3), and Her4 (ErbB4) (Fouassier et al., 2019).

ERBB1-4 overexpression has been associated with poor prognostic in iCCA and eCCA (Pellat, Vaquero, & Fouassier, 2018). EGFR can integrate multiple internal and external signals to promote initiation and progression of CCA. For instance, CCA proliferation, migration and invasion are known to be promoted by the activation of janus tyrosine kinase (JAK)/STAT, RAS/MEK/ERK and PI3K/AKT downstream of EGFR and ERBB2 (Claperon et al., 2012; Claperon et al., 2014). Additionally, EGFR activation can be indirectly promoted by various compounds known to participate in CCA pathogenesis (Reich et al., 2016; J. H. Yoon et al., 2004). Oxidative stress is also known to induce heparin binging-epidermal growth factor (HB-EGF) expression in CCA through the MK2-dependendent transduction pathway (Nguyen Ho-Bouldoires et al., 2015). Interestingly, a recent study has reported continuous activation crosstalk between CAFs expressing EGFR ligands and CCA cells producing TGF-β (Claperon et al., 2013).

#### 1.4.1.4. Secretin and histamine signalling pathways

Secretin receptors (SCTR) are expressed in the biliary tree and play a key role in the physiology of cholangiocytes. SCTR are upregulated during cholestatic diseases; however, in CCA they are downregulated. *In vitro* and *in vivo* studies shown that secretin induces cell death ultimately reducing cell proliferation (Korner et al., 2006).

Histamine receptors (HisR) are expressed in CCA cells (Francis, Meng, Gaudio, & Alpini, 2012). ICCA, particularly, is known to chemoattract MC by secreting stem cell factor (C. Johnson et al., 2016). Once MC populate the stroma, they produce histamine (Francis, DeMorrow, et al., 2012). These facts have raised interest in the possibility that an autocrine and paracrine histamine circuit supports the progression of iCCA cells. Although this hypothesis has been supported by both *in vitro* and *in vivo* experiments, it remains unclear whether targeting this signalling will provide any clinical opportunity for CCA patients (Francis, DeMorrow, et al., 2012; C. Johnson et al., 2016). One approach already tested in Mdr2(-/-) primary sclerosing cholangitis (PSC) mouse model is the use of HisR antagonists, which reduced cholangiocyte proliferation, fibrosis and inflammation (Jones et al., 2016; Kennedy et al., 2018).

#### 1.4.1.5. PI3K/AKT signalling pathway

Important cellular processes such as proliferation, cytoskeletal rearrangements and apoptosis are regulated by the PI3K/AKT pathway. PI3K activates AKT, which integrates several downstream cascades (Fouassier et al., 2019).

In CCA, *PI3K* mutations provided a gain of function (Fouassier et al., 2019), and its downstream signalling influence CCA behaviour as evidenced in the following examples. In mice, tumour formation was found to be promoted by ectopic expression of AKT with YAP or NOTCH1 (Fan et al., 2012; S. Zhang et al., 2017). In eCCA, AKT activation correlated with shorter patient survival through mammalian target of rapamycin (mTOR) and loss of PTEN (J. Y. Chung et al., 2009). In pCCA, the signalling was driven by AKT2 (Guedj et al., 2009). Additionally, AKT can be activated by a family of phospho-serine binding proteins, which are known to be upregulated in CCA and associated with poor survival and metastasis (Kittirat et al., 2018). PIP60, is often downregulated in CCA, which acts as a tumour suppressor via controlling the PI3K/AKT pathway (Y. Zhang et al., 2018).

#### 1.4.1.6. Apoptosis and necroptosis signalling pathways

Resisting cell death is a hallmark of cancer (Chapter 1, Section 1.1.3). Apoptosis is the most well-known form of regulated cell death. However, necroptosis was recently discovered, and found to be triggered in liver parenchymal cells under acute and chronic injury in humans and experimental models (Gautheron et al., 2014)

Using experimental models, iCCA was found to be associated with necroptosis-driven epigenetic changes; and the pharmacological or genetic inhibition of necroptosis-associated hepatic cytokine microenvironment switched iCCA growth towards initiation of HCC. These facts were also observed in human tumours (Seehawer et al., 2018).

### 1.4.2. Development-related pathways

#### 1.4.2.1. Notch signalling pathway

Human genetic studies have highlighted Notch signalling as an important regulator of lineage specification during the growth of the liver (Martinez Lyons & Boulter, 2021). In mammals, the Notch system consists of four receptors (Notch 1-4), five canonical ligands (JAG1/2, and Delta-like (DLL)1/3/4), and various auxiliary factors that

regulate and transduce the signal. In canonical Notch signalling, the Notch intracellular domain (NICD) is released and translocated to the nucleus due to a conformational change and a proteolytic cleavage of the receptor. Inside the nucleus, a transcriptional repressor complex is displaced. Non-canonical Notch can be dependent or independent of ligand-receptor binding and the nuclear translocation of the NICD is not required. Notch signalling is becoming increasingly recognised as a key regulator of ductular morphogenesis and patterning (Martinez Lyons & Boulter, 2021).

The Notch pathway has been identified to potentially induce CCA. In eCCA, aberrant expression of Notch 1 and 3 correlated with cancer progression (H. A. Yoon et al., 2011). Conversely, in iCCA, the aberrant expression of Notch 1 and Notch 4 was reported to be associated with cancer progression (W. R. Wu et al., 2014). Additionally, Notch1 induced a cell migratory effect in iCCA by causing EMT and activating ras-related C3 botulinum toxin substrate (Rac) 1 (Q. Zhou, Wang, Peng, Liang, & Li, 2013), and its activation enhanced CCA cell proliferation and survival via upregulation of pro-survival protein myeloid leukemia cell differentiation protein (Mcl)-1 and Bcl-xL (Singrang, Kittisenachai, Roytrakul, Svasti, & Kangsamaksin, 2019). Notch 2 was found to be a major determinant of hepatocyte-derived iCCA formation in mice (J. Wang et al., 2018), and Notch 3 to sustain tumour cell survival through PI3K/AKT activation (Guest et al., 2016). Notch 4 was related to poor prognosis in iCCA (W. R. Wu et al., 2014). Additionally, AKT/mTOR and Notch cascades were activated in AKT/JAG1 iCCA tissues; and Notch signalling was important for iCCA development in AKT/JAG1 mice (Che et al., 2016).

#### 1.4.2.2. Hedgehog signalling pathway

The Hedgehog (HH) family comprises three ligands, SHH, Indian hedgehog (IHH), and desert hedgehog (DHH), which are involved in a variety of biological events including cell survival, differentiation, and proliferation (Fouassier et al., 2019). This pathway plays key roles in embryogenesis and adult stages; hence, alterations such as abnormal expression or gene mutations, and their downstream signalling cause a variety of malignancies (Sasai, Toriyama, & Kondo, 2019). For instance, hepatic inflammation, fibrosis and cholangiopathies have been associated with constitutive activation of the HH pathway (Y. Jung, McCall, Li, & Diehl, 2007; Machado & Diehl, 2018). In iCCA, SHH was significantly expressed (Al-Bahrani, Nagamori, Leng,

Petryk, & Sergi, 2015). The non-canonical HH signalling was activated in CCA cells and contributed to CCA progression (Razumilava et al., 2014).

#### 1.4.2.3. Wnt/β-catenin signalling pathway

Wnt/β-catenin signalling is a complex pathway that plays various roles in different cellular processes. Canonical Wnt signalling is β-catenin-dependent, whereas non-canonical Wnt signalling is β-catenin-independent (K. Shah & Kazi, 2022). In the canonical Wnt signalling, β-catenin enters the nucleus, and it associates with the T-cell factor (TCF)/lymphoid enhancer factor (LEF) family to trigger the expression of target genes involved in cell differentiation, migration, and apoptosis such as *CCND2*, *CDKN2A*, *BIRC5* (Boulter et al., 2015). The non-canonical Wnt signalling can be divided into Wnt/Ca2+ and Wnt/planar cell polarity (PCP) pathways (Lang, Chan, Veltri, & Lien, 2019).

It was demonstrated that CCA is a Wnt-high tumour, and the inflammatory macrophages maintained this state. The depletion of macrophages or inhibition of the canonical Wnt pathway results in reduced tumour burden in 3 pre-clinical models (xenografts of human CCA cells, a transgenic murine line that initiates CCA and a chemically induced rat model of CCA) (Boulter et al., 2015). It was also demonstrated that Wnt ligands associated with non-canonical Wnt signalling are upregulated in biliary injury (Wilson et al., 2020). Wnt/β-catenin signalling regulates SRY-box (SOX) 17 expression, and its overexpression in CCA cells (Merino-Azpitarte et al., 2017).

### 1.4.3. Metabolic and epigenetic pathways associated to *IDH1/2* mutations

IDH isoforms (*IDH1* and *IDH2*) mutations have been a breakthrough in CCA research. It has been reported to occur in 15−20% of iCCA (Salati et al., 2020). *IDH* mutations are considered gain of function and related to the disruption of the normal catalytic activity of IDH1/2, increasing the conversion of α-ketoglutarate (α-KG) to D-2-hydroxyglutarate (D-2HG), ultimately acting as a terminal metabolite, with a major impact on promoting tumour proliferation and metastasis through several pathways, such as activation of VEGFR and DNA methylation (Salati et al., 2020). Additional potential roles of 2-HG in mutant IDH cells include the disruption of hypoxia-inducible factor 1α (HIF-1α) regulation, altered collagen biogenesis and increased DNA damage (Dang & Su, 2017). In line with this, the mutant IDH subgroup showed

the highest level of DNA methylome alterations among iCCA samples based on the 3 most frequently mutated genes (*TP53*, *KRAS* and *IDH1/2*) (Nepal et al., 2018).

### 1.4.4. Epigenetic and DNA damage response pathways associated to *BAP1*, *PBRM1* and *ARID1A* mutations

The iCCA exome was sequenced, and inactivating mutations in multiple chromatin-remodeling genes (including *BAP1*, *ARID1A* and *PBRM1*) were found (Jiao et al., 2013). *ARID1A* has DNA binding activity, and it is a non-catalytic subunit of barrier-to-autointegration factor (BAF). BAP1 and PBRM1 bind to histones. These complexes are involved in chromatin remodelling, transcription regulation and DNA replication and repair (Hodges, Kirkland, & Crabtree, 2016).

A recent study has proposed a role for *ARID1A* in negative regulation of YAP/TAZ activity inside the nucleus. In the context of liver damage, *ARID1A* ablation led to iCCA development (Chang et al., 2018). In line with this, *BAP1* mutations pre-disposed CCA development (Pilarski et al., 2014) and in CCA cell-lines, *BAP1* tumour suppressor activity was related to increased ERK and c-Jun N-terminal kinases (JNK) activity. Loss of *PBRM1* was also reported to occur late in iCCA (Luchini et al., 2017).

## 1.5. Tumour microenvironment in CCA

Even though tumour cells are considered coordinators of tumour growth, the TME and its crosstalk with the CCA cells cannot be understated. CCA is histologically characterised as a high desmoplastic tumour. The abundant fibrotic stroma that surrounds and infiltrates the tumour is also known to modulate the progression and invasiveness of CCA (Fabris et al., 2019; Sirica & Gores, 2014). The CCA stroma consists of cancer-associated endothelial and lymphatic cells, CAFs and a complex group of inflammatory cells (macrophages, NK, neutrophils, and T cells) (Banales et al., 2020). In addition to this, the tumour stroma also contains an extensive network of ECM proteins (laminin, collagens, and fibronectin) (Govaere et al., 2016; Szendroi & Lapis, 1985). The next sections aim to summarise the current understanding of the role of the inflammatory cells, ECM and CAFs that occur in the CCA TME. Among these cells, CAFs have been the most extensively investigated cells (Banales et al., 2020).

### 1.5.1. Inflammatory cells

Through whole-exome and transcriptome sequencing it was uncovered that the subgroup of patients with significant characteristic elevation in the expression of immune checkpoint molecules had the poorest prognosis (Nakamura et al., 2015).

One type of inflammatory cells in the CCA TME that participate in the immune response are the M2-like tumour-associated macrophages which are known to stimulate Wnt signalling, affecting CCA progression and reducing patient outcome (Banales et al., 2020). Interestingly, in iCCA, poor disease-free survival is linked to high numbers of macrophages (Hasita et al., 2010); and in pCCA, high density of TAMs significantly showed tumour recurrence (Atanasov et al., 2015). Activated macrophages are also known to trigger cholangiocyte proliferation and transformation secreting cytokines such as IL-6, tumour necrosis factor-α (TNF-α), and TGF-β1 (Fabris, Sato, Alpini, & Strazzabosco, 2021). Another type of inflammatory cells is the myeloid-derived suppressor cell. These cells are known to be recruited in the TME by FAP-positive CAFs. In line with this, the levels of stromal FAP were evaluated in CCA, and high levels were associated with poor survival outcome (X. Yang et al., 2016). On the other hand, a better outcome was associated with CCA specimens that presented a high density of dendritic cells (CD83+) (Takagi et al., 2004). The current role of NK in CCA is not understood. However, some preliminary data in *in vitro* models have shown that cetuximab (anti-EGFR monoclonal antibody) increased CCA cell death via NK cells (Morisaki et al., 2012). Moreover, an *in vivo* study demonstrates that NK cells contain cytolytic activity against CCA and targeting NK cells showed a beneficial effect in patient quality of life (I. H. Jung et al., 2018).

Interestingly, the components of the adaptive immune response decrease during CCA progression (Goeppert et al., 2013). Higher population of CD4+ and CD8+ lymphocytes are associated with a better prognosis, lymph node metastases, and invasion (Fabris et al., 2021). A better prognosis has also been associated with presence of B cells (Banales et al., 2020). Current immunotherapy studies in CCA, showed that an anti-PD-1, named pembrolizumab, significant results to treat advanced CCA patients and is approved for a subgroup of hepatobiliary cancers (Alshari et al., 2019; Zhu et al., 2018). Durvalumab is another immunotherapy drug that showed increased patient survival (D. Y. Oh et al., 2022).

### 1.5.2. Extracellular matrix

The ECM is continuously remodelled by deposition of components, such as periostin (POSTN), tenascin C and osteopontin and an intensive secretion of metalloproteinases (MMP) (MMP1, MMP2, MMP3 and MMP9) (Fabris et al., 2019; Nissen, Karsdal, & Willumsen, 2019). Interestingly, overexpression of these 3 components is correlated with poor survival rates, an increase in tumour size and lymph node metastases (Fabris et al., 2021).

Periostin is found to be relevant in CCA, after demonstrating that by binding to integrin (ITG) α5β1 activates the PI3K/AKT pathway enhancing CCA proliferation and invasion (Utispan et al., 2012).

Although the knowledge of tenascin-C in CCA is limited, results based on other desmoplastic tumours showed that it accumulates in the ECM to help cell invasion and dissemination through MET- and EGFR- dependent mechanisms (De Wever et al., 2004).

Finally, the role of osteopontin has also been linked to immune responses and CCA progression (Fabris et al., 2021); however, further studies are required to elucidate its specific role. For instance, a recent study showed that low levels of osteopontin expression is associated with poor survival rates in iCCA (K. Q. Zhou et al., 2019). Nonetheless, a prior study showed that elevated expression of osteopontin in stromal cells is linked to increase invasion and metastasis (Laohaviroj, Chamgramol, Pairojkul, Mulvenna, & Sripa, 2016). An *in vitro* study in cell-lines demonstrated that osteopontin recruited mitogen-activated protein kinase (MAPK) 1 and activated MEK-MAPK1 pathway to mediate the phosphorylation of β-Catenin and nucleus accumulation, inducing the activation of Wnt signalling (Y. Zheng et al., 2018).

### 1.5.3. Tumour Stromal Cells and Cancer-associated Fibroblasts

The origin of CAFs in CCA remains unclear. However, some studies shown that they can originate from liver-resident hematopoietic stem cells (HSCs) (Okabe et al., 2009), portal fibroblasts (Dranoff & Wells, 2010), or bone marrow-derived circulating mesenchymal cells (Russo et al., 2006). They are characterised by expression of several markers, the most common ones being α-SMA, the mucin-like transmembrane glycoprotein podoplanin, and the cell surface metalloprotease CD10. CAFs are the major component in the CCA TME, and its expression correlates to poor patient

survival (Chuaysri et al., 2009). CAFs, in the context of iCCA, are a hugely heterogeneous population displaying distinctive phenotypic traits (Fabris, Andersen, & Fouassier, 2020).

CAFs play a significant role in CCA growth, progression, and treatment resistance. This hypothesis has been supported by a study that demonstrated that triggering CAF apoptosis with navitoclax results in a decrease in tumour burden and metastasis *in vivo* (Mertens et al., 2013). CAFs can also shape the TME as well as influencing tumour growth and invasion through releasing pro-oncogenic paracrine mediators. These include TGF-β1, hepatocyte growth factor (HGF), EGF, SDF-1, connective tissue growth factor (CTGF), ECM components, and MMPs (Sirica, 2011). Transcriptomic studies of the stromal component of CCA demonstrated that clinical outcome is negatively correlated with expression of profibrogenic and proinflammatory cytokines, TGF-β1 and TNF-α (Tanimura et al., 2005).

One of the most significant signalling pathways between CCA cells and CAFs is the HB-EGF/EGFR signalling pathway; in which there is an intense two-way communication by which CCA cells activated CAFs and in turn, CAFs sustain the invasive phenotype of cancer cells. CCA cells overexpress EGFR, which is then activated by HB-EGF released by CAFs. Once EGFR is activated, ERK 1/2 and STAT3 are phosphorylated leading to nuclear translocation of β-catenin, which unfolds a transcriptional program related in cell motility and invasion. Additionally, the activation of the receptor triggers TGF-β1 production by CCA cells, further enhances fibroblast activation and CAFs synthesis of HB-EGF (Claperon et al., 2013). Moreover, CAF-derived SDF-1 stimulates CCA cell invasion via ERK1/2 and AKT upon binding to its CXCR4. This effect is inhibited when using a CXCR4 inhibitor (Gentilini et al., 2012). Similarly, CCA cell behaviour is influenced by PDGF-β, which is secreted by CAFs. This ligand binds to the PDGFR-β receptor expressed by CCA cells making them resistant to apoptosis by activating HH signalling. This is supported by the fact that inhibiting the HH signalling pathway *in vivo*, apoptosis is induced, and tumour growth is decreased (Fingas et al., 2011). In addition, when PDGF-D is released by CCA cells, pro-lymphangiogenic functions are activated. This mechanism is mediated by the secretion of VEGF-A and VEGF-C (Cadamuro et al., 2019).

## 1.6. Cholangiocarcinoma experimental models

Human or animal primary cultures and established cell-lines have represented important *in vitro* models to understand the mechanisms behind cell biology, tissue morphology and the molecular basis of a certain diseases or drug response. Harrison *et al*., carried out the first cell culture in 1906 researching the origin of nerve fibres (RG., 1906). However, recently, new pre-clinical models have been developed with the aim to better mimic the patient tumour. In cancer research, choosing the most appropriate pre-clinical model is a key step to better understanding tumour development, progression, and metastasis, as well as discovering prognostic biomarkers, druggable targets and testing the effects of drugs on those targets. The different CCA experimental models are described in the following sections (Figure 1.5).

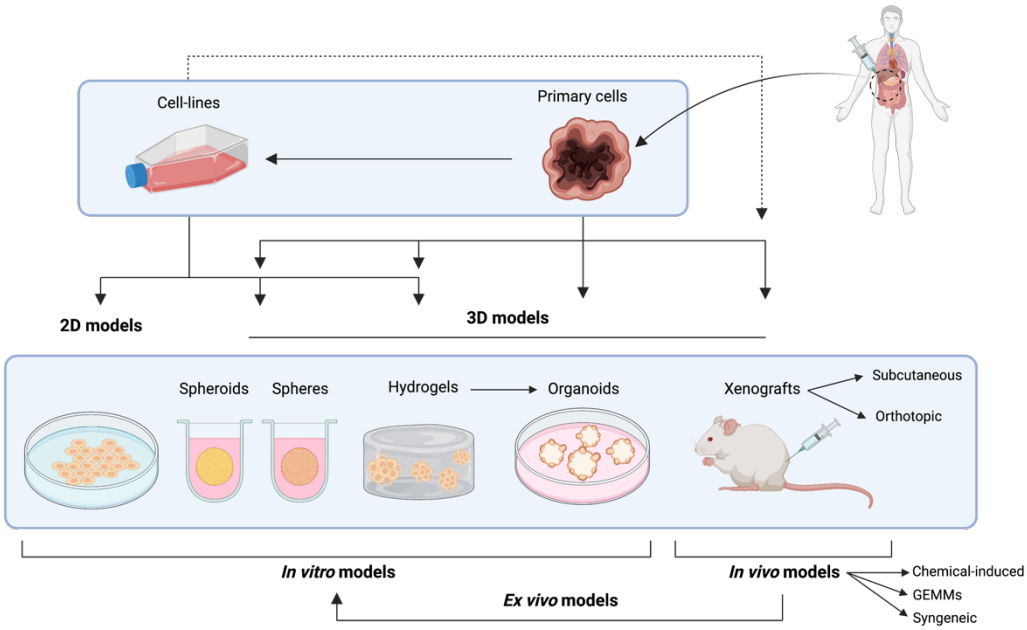



**Figure 1.5. Experimental models.** The upper section represents the primary cells derived from surgical human specimens, which can be used to establish an *in vitro* cell-line. From these cells, 2D and 3D models can be generated. 2D models can be generated from cell-lines (spheroids, spheres, or hydrogel-based models), or primary cells (spheroids, spheres, hydrogel-based models such as organoids, or xenografts models). All these models except the xenografts that is considered an *in vivo* model, are *in vitro* models. The xenografts models are subdivided in subcutaneous and orthotopic. Chemical-induced, GEMMs and Syngeneic models are also *in vivo* models that do not require human specimens. Cells extracted from *the in vivo* models can also be used to generate *ex vivo* models.

### 1.6.1. 2D models

Cell-lines are key tools for pre-clinical cancer research, but it remains unclear how well they represent patient tumour samples (Warren et al., 2021). The first established and characterised CCA cell-line was obtained from iCCA and named HChol-Y1 (Yamaguchi, Morioka, Ohkura, Hirohashi, & Kawai, 1985). Nowadays, there are several cell-lines described in the literature from which most have been biologically characterised, but the molecular characterisation has only been performed in a few (Massa et al., 2020).

The use of established cell-lines grown in 2D as a pre-clinical model for cancer research is usually associated with simple and low-cost maintenance as well as high reproducibility of experiments (Massa et al., 2020). However, 2D models have numerous limitations. Firstly, cells may lose their heterogeneity due to the selection for the sub-population of cells that can grow on plastic ultimately affecting the translation of pre-clinical data in a clinical context. Secondly, the necrotic core, which is present in the real tumour and known to affect cell signalling and drug response, is not present in 2D cultures. Finally, the 2D nature of the cultures do not represent the cell-cell, cell-ECM and cell-TME interactions present in the *in vivo* tumour (Massa et al., 2020).

The use of primary cell cultures instead of established cell-lines have overcome some of the limitations associated with the cell-lines (Massa et al., 2020). However, their biggest limitation is the lack of long-term culture. Additionally, working with primary cells is often more laborious and less efficient. This is particularly true in CCA, a highly desmoplastic tumours, where the overgrowth of stromal cells reduces the establishment efficiency (Ku et al., 2002). Nonetheless, the continuous advances in pre-clinical cancer research are providing new 3D models for a better translating knowledge to novel strategies in cancer.

### 1.6.2. 3D models

The 3D dimensional structure is an important tissue and organ characteristic; hence, the dimension in which cells are cultured *in vitro* for the study of cancer is of paramount importance (Baker & Chen, 2012). Moreover, cells in the real human are enveloped by an TME and ECM that contributes to tumour biology (Fitzgerald, Malhotra, Curtin, FJ, & CM, 2015). The development of 3D systems that integrate

these characteristics allows the study of the tumour in a more realistic environment as well as the ability to study the cell-TME and cell-ECM interactions (Massa et al., 2020).

Spheroids, spheres, and hydrogel-based models such as organoids are the most frequent used CCA 3D models.

#### 1.6.2.1. Spheroids and spheres

Suspension of cells from different origins such as cell-lines, patient-derived xenografts (PDXs) or primary cells can be grown in 3D forming spheroids (Białkowska, Komorowski, Bryszewska, & Miłowska, 2020). There are four major techniques used to induce spheroid formation *in vitro*. Firstly, agitation-based techniques, such as those based on gyratory shakers to let the cells aggregate into spheroids (Nunes, Barros, Costa, Moreira, & Correia, 2019). Secondly, hanging-drop techniques which rely on the formation of spheroids in small drops of cells in culture medium, which are suspended on a glass coverslip (Nunes et al., 2019). Thirdly, liquid overlay techniques where spheroids are formed by seeding the cells on top of non-adhesive surfaces, in a setting where the cells cannot bind to a surface and have to therefore attach to each other (Nunes et al., 2019). Finally, using microfluidics reactors, in which spheroids are formed in chambers within chips composed of microchannels (Nunes et al., 2019). These methods allow formation of floating spheroids characterised by the close cell-cell interaction of the cells. Desmosomes and dermal junctions reinforce cell-cell adhesion, which increases the formation of the ECM. The deposition of those proteins present in the ECM increases the spheroid density and a physical barrier is ultimately generated limiting the transport of nutrients into the spheroids (Zanoni et al., 2020). In CCA, the protein expression pattern during spheroid formation was explored using two established eCCA cell-lines (Mischiati et al., 2015).

Spheroids can also be generated from different cell suspensions forming a co-culture system. This type of culture was described in the 1970s as a system to examine communication between cells (Lawrence, Beers, & Gilula, 1978). Co-cultures allow the observation of intercellular interactions such as cell-cell, cell-TME and paracrine signalling by dissolved factors, ultimately resembling the *in vivo* situation (Kapalczynska et al., 2018). There are direct and indirect co-culture models. In the direct model, different types of cells are cultured together, whereas in the indirect a

physical barrier keeps them separated (Kapalczynska et al., 2018). Direct cultures provide a better outcome due to the possibility to observe all types of interactions previously described. The downside of co-culture systems is the inclusion of different variables (the degree of similarity and separation of cell populations, media used during culture, etc.), which must all be previously optimised (Kapalczynska et al., 2018). These practical limitations result in difficulties in conducting co-culture models. In CCA, a spheroid was established by co-culturing iCCA formed in syngeneic rat liver with varying numbers of CAFs from the same tumour type within a type I collagen matrix, which were confirmed to resemble the parental tumour (Campbell, Dumur, Lamour, Dewitt, & Sirica, 2012).

A different approach for generating clusters of cells without providing a substrate, is use of the sphere-forming assay. Sphere-formation consists of growing the cell in the absence of serum and incorporating growth factors known to stimulate cell proliferation (Ishiguro et al., 2017). The terms spheroid and sphere are not consistent throughout the literature, and this is critical to the rational use of spherical cancer models (Weiswald, Bellet, & Dangles-Marie, 2015). Spheres have allowed the characterisation of CSC and study of their role in tumour development as well as the resistance to chemotherapy in CCA (Cardinale et al., 2015). In CCA, spheres were formed from an eCCA gemcitabine resistant cell-line and iCCA cells from a patient with a gemcitabine resistant tumour (Kawamoto et al., 2018). Most recently, a study using spheres derived from iCCA and eCCA were used to compare features such as cell proliferation, sphere formation, migration and invasion (J. Yang et al., 2022). Spheres were also used to study the signalling between Numb and Notch signalling pathway in iCCA cells (Shu et al., 2021). In an indirect iCCA co-culture model, TAMs exposed to conditioned medium of CSC-enriched spheres, increased TAM recruitment and polarization (Raggi et al., 2017).

Protocols for the generation of spheroids and spheres are standardised. The main advantage of these models is the capacity to recapitulate the *in vivo* characteristics of intercellular communications, cell-ECM interaction, and cell-TME if co-cultures are conducted (A. M. K. Law et al., 2021). However, the size of spheroids and spheres can vary depending on the technique; and the cell-TME interaction is simple and static, as opposed to the *in vivo* tumour (A. M. K. Law et al., 2021).

#### 1.6.2.2. Hydrogel-based models

3D models can also be established by seeding cells in protein-based hydrogels such as collagen, Matrigel, Cultrex or fibrin (Y. Li & Kumacheva, 2018). Matrigel and Cultrex basement membrane extract (BME) are recognised as golden standard scaffolds for *in vitro* cancer cell growth. They are extracted from Engelbreth-Holm-Swarm mouse sarcoma tumours, and it contains laminin, type IV collagen, and entactin, in addition to other constituents such as proteoglycans and growth factors (Benton, Arnaoutova, George, Kleinman, & Koblinski, 2014). These hydrogels provide a broad range of chemical and mechanical signal to cells to influence cell proliferation, motility, matrix remodelling and immune escape (Di Modugno et al., 2019). However, their batch-to-batch variation often limit the isolation of the effect of a specific ECM property on cancer cell growth; as well experimental reproducibility (Y. Li & Kumacheva, 2018). Synthetic hydrogel scaffolds may overcome these limitations by providing control over hydrogel composition and properties (L. Gu & Mooney, 2016). In CCA, the most recent approach was the use of silk fibroin-gelatin/hyaluronic acid/heparan sulfate scaffolds to simulate the ECM that may serve as a CSC niche of CCA and reinforce stemness and EMT properties (Buhome, Wongwattanakul, Daduang, & Limpaiboon, 2022). The organoid is the most studied hydrogel-based model in CCA.

##### 1.6.2.2.1. Organoids

Organoids are derived from isolated organ progenitors or pluripotent stem cells that differentiate to form elements of organs exhibiting multiple cell types that self-organises to form a structure (Lancaster & Knoblich, 2014), as opposed to the spheroids, where self-organisation only occurs in some spheroids. They have the potential to be used as predictors for precision medicine response since they retain some of the important genetic and phenotypic characteristics of the original tissue and maintain the intratumoural heterogeneity (Ma et al., 2021). In CCA, a study confirmed that genetic aberrations were 80% maintained in organoid culture (Massa et al., 2020). Organoids require the use of Matrigel (Lancaster & Knoblich, 2014); hence, organoid formation efficiency is affected by the mechanical properties of the Matrigel, with values mimicking physiological organ stiffness (Sorrentino et al., 2020). However, the batch-to-batch effect of the Matrigel is a disadvantage in these models.

### 1.6.3. *In vivo* models

*In vivo* models are the most complex models, but they have the highest resemblance to the patient tumour. They aid our understanding of CCA cancer biology and are certainly a step on the way to a clinical trial. Of all the *in vivo* models, the most commonly used species is the mouse due to its easy manipulation, rate of reproductivity, and the possibility to genetically modify them. However, depending on the goals of the study, they can be limited. Overall, a review classified mice models (Massa et al., 2020) as following:

- Syngeneic models: these models have the advantage that they are immunocompetent, which is crucial for immunotherapy studies (E. Li, Lin, Chen, & Ou, 2019). In this model, mice are transplanted with tumour cells established in syngeneic inbred mouse strains (Bareham, Georgakopoulos, Matas-Cespedes, Curran, & Saeb-Parsy, 2021).
- Chemically induced models: these models are a good tool to study carcinogenesis as they mimic the early stages of cancer progression. In addition, they are useful to identify toxic compounds involved in carcinogenesis. Models are treated with compounds that induce DNA damage generating a tumour (Massa et al., 2020). In CCA, diethylnitrosamine, thioacetamide and dimethylnitrosamine have been shown to lead to tumour formation in mice, rats, and hamsters, respectively (Loeuillard, Fischbach, Gores, & Rizvi, 2019; Thamavit, Bhamarapravati, Sahaphong, Vajrasthira, & Angsubhakorn, 1978).
- Genetically-engineered models (GEMM): these models are used to study specific genomic alterations, as opposed to the random alterations that occur in the chemically induced models. GEMMs are subdivided into transgenic models and hydrodynamic transfected models (Loeuillard et al., 2019). Combining transgenic and chemically induced models could better clarify the mechanisms related to both tumour initiation and progression (Massa et al., 2020).

These models sometimes lack translation to the clinical setting due to the differences between human and mice tumour biology (Bareham et al., 2021).

- Xenografts models: these models recapitulate the genetic and epigenetic abnormalities of human tumours and therefore can predict the drug response of

a tumour in a human patient (Richmond & Su, 2008). They are generated by the transplantation of human cells, or patient-derived tissue into an immunodeficient mice. Xenografts models are subdivided in subcutaneous xenografts and orthotopic models (Day, Merlino, & Van Dyke, 2015).

PDX is a model used in the current study and therefore more detail is given in the following section.

#### 1.6.3.1. Patient-derived xenografts

These models are more likely to mimic human tumours and are currently being used to explore tumour biology and personalised drug testing (G. J. Yoshida, 2020). The implantation of human tumour fragments either derived from surgical specimens or biopsies is subcutaneous implanted (dorsal region) or orthotopic implanted to target organs (Hidalgo et al., 2014). It is recognised as a powerful and reliable model due to the ability to retain main traits of the tumour, surrounding stroma and tumour heterogeneity (Massa et al., 2020).

In CCA, there has been significant successful in generating PDX models from iCCA. The first PDX established was a KRAS-mutant that recapitulated the parental tumour from a genetic, immunogenetic, histologic and transcriptomic point of view (Cavalloni et al., 2016). This model was further used to test trabectedin and its ability to affect pathways involved in cholangiocarcinogenesis and cell adhesion (Peraldo Neia et al., 2016; Peraldo-Neia et al., 2014). A second iCCA PDX model, endogenously expressing the FGFR2-CCDC6 fusion protein was generated to study the ability of three FGFR inhibitors (Ponatinib, Dovitinig and BBGJ398) to affect FGFR signalling and ultimately inhibit tumour growth (Y. Wang et al., 2016). Another iCCA PDX from a patient with an *IDH* mutation was generated, and a multi-tyrosine kinase inhibitor (Dosatinib) was tested (Saha et al., 2016). A fourth iCCA-derived PDX was tested using a pan-FGFR inhibitor and this was associated with a decrease of size and necrosis (Kabashima et al., 2018). Interestingly, a study performed in both iCCA and eCCA PDX models, showed that a bromodomain and extra-domain inhibitor could supress tumour growth through the inhibition of c-Myc (P. L. Garcia et al., 2018). A recent study showed that Crenigacestat reduced tumour growth and switched Notch pathway to the same extend of gemcitabine in iCCA PDXs (Mancarella et al., 2020). The same PDX was used for a later study the determine the CD90 function (Mancarella

et al., 2022). Moreover, another PDX model was established to determine the effect of combination treatment of silencing the YTH domain family 2 and cisplatin in iCCA (C. S. Huang et al., 2022). Recently, a PDX was established for the study of invasive papillary CCA (Mwesige et al., 2022). The role of Niraparib in supressing tumour growth was also recently studied in a PDX model (Bezrookove et al., 2021). Finally, another recent study used PDXs to study the YAP/TAZ signalling pathway in promoting CCA (Qian et al., 2021). Nonetheless, it is important to be aware of some of the major limitations of the PDX models. Firstly, PDXs lack immune cells unless hosts are engrafted with a functional human immune system (Di Modugno et al., 2019). Additionally, the success of engraftment depends on the primary cells as well as the experience of the *in vivo* unit in doing such process. Another crucial limitation is the prolonged time needed for the generation of the model, especially if using it for personalised therapy (Massa et al., 2020).

### 1.6.4. *Ex vivo* models

Transition of cells from tumour xenografts to *in vitro* models involves direct transfer into 2D culture, which results in growth of a highly-selected subpopulation of cells that ultimately does not recapitulate tumour heterogeneity (Kapalczynska et al., 2018). Developing 3D *ex vivo* models from xenografts, could overcome the disadvantages of using established cell-lines; or avoid the use of large number of animals. An innovative *ex vivo* model was developed by embedding PDX cells admixed with stromal cells in a 3D tumour growth assay (3D-TGA) (Onion et al., 2016; Saunders et al., 2017). They established a novel pre-clinical model utilising tumour-derived ECM and incorporating patient-derived tumour-associated stromal cells (Onion et al., 2016).

## 1.7. Hypothesis and aims

The interaction between cancer cells and the supporting stroma may play a key role in CCA initiation, progression, and invasion. Mesenchymal cells appear to be one of the most prominent components of the TME, supporting growth and metastasis. An absolute pre-requisite to develop new cancer strategies is the comprehensive understanding of the biology underlying this crosstalk in a pre-clinical model that mimics the real tumour. Therefore, this project aims to investigate the role of the TME and, in particular, mesenchymal cells in driving CCA growth. Understanding this contribution to cancer progression could enable discovering new treatments using targeted therapies that are already available or identify new targets for drug development, with the ultimate goal to impact on CCA patient survival and quality of life.

Taken together, my **hypothesis** is that the mesenchymal cells present in the CCA TME are driving proliferation. Thus, this project **aimed** to:

1. Develop and characterise a cell-line-derived CCA spheroid model (Chapter 3).
2. Investigate the influence of the mesenchymal cells on CCA proliferation in a spheroid model (Chapter 4).
3. Investigate the influence on mesenchymal cells on PDX and PDX-derived spheroids (Chapter 5).
4. Identify active signalling pathways in the presence of mesenchymal cells (Chapter 6).

# Chapter 2. Material and Methods

## 2.1. Cell-lines

A panel of six CCA immortalised cell-lines and two human bone-marrow mesenchymal stem cells were used for this project. Four of the CCA cell-lines, KKU-M055, KKU-M156, KKU-M213 and HuCCA-1, were derived from tissue resected from Opisthorchis viverrini-related CCA (O-CCA); and two, RBE and TFK-1, were derived from tissue resected from non-Opisthorchis viverrini-related CCA (Non-O-CCA). Additional details of the cell-lines are given in Table 2.1. All cell-lines were obtained from Professor John Gordan, University of California, under a Material Transfer Agreement. Primary bone marrow-derived mesenchymal stem cells (hMSCs) were purchased from TCS Cellworks (Buckingham, UK), and the immortalised bone marrow-derived mesenchymal stem cells (iMSCs) were obtained through a collaboration with Dr James Dixon, School of Pharmacy, University of Nottingham. The CCA cell-lines and iMSCs were grown in high-glucose dulbecco's modified essential medium (DMEM) (Sigma, #D5671) supplemented with 1mM L-glutamine (Sigma, #G7513) and 10% (v/v) heat-inactivated fetal bovine serum (FBS) (Sigma, #F7524) (10% DMEM). The hMSCs were maintained in mesenchymal stem cell medium (MSCM) supplemented with FBS and mesenchymal stem cell growth supplement (ScienCell, Carlsbad, CA, USA). For the immortalised cell-lines, passages below 40 were used, while for MSCs, passage numbers 8 to 10 were used. All cell-lines were incubated in a 5% $CO_2$ air-humidified atmosphere at 37°C in a SANYO incubator (SANYO Electronics, Osaka, Japan). Mycoplasma tests were performed monthly to avoid using infected cells.

**Table 2.1. Cholangiocarcinoma cell-lines information.** The doubling time, anatomic site/classification, origin, genetic/molecular characteristics, and drug resistance are described for the panel of cell-lines used in this project. [1]Cell-lines with intrinsic chemotherapy resistance; [2]cell-lines with acquired chemotherapy resistance. *The Japanese Collection of Research Biosources found out that KKU-M156 were derived from KKU-M213 and became KKU-M213C.

| Cell-line | Doubling time | Anatomic Site/Classification | Origin | Genetic/ Molecular Alterations | Drug Resistance |
|---|---|---|---|---|---|
| **KKU-M055** | Not available | Intrahepatic (Opisthorchis viverrini-related) | Southeast Asian; Thai. Male (56 years). Primary tumour. | mMA2K1; high level mRNA FGFR1 | Not available |
| **KKU-M156 (KKU-M213C)** | 25.6 ± 0.2 hours | Intrahepatic (Opisthorchis viverrini-related) | *Derived from KKU-M213. Primary tumour. | Not available | [1]Cisplatin and Carboplatin |
| **KKU-M213 (KKU-M213A)** | 23.3 ± 0.8 hours | Intrahepatic (Opisthorchis viverrini-related) | Southeast Asian; Thai. Male (58 years). Primary tumour. | mKRAS; mTP53; mSMAD4 | Not available |
| **HuCCA-1** | ≈55 hours | Intrahepatic (Opisthorchis viverrini-related) | Southeast Asian; Thai. Male (54 years). Primary tumour. | Not available | [1]5-FU |
| **RBE** | Not available | Intrahepatic (Non-Opisthorchis viverrini-related) | Japanese. Female (64 years). Primary tumour. | mIDH1; mBIRC6; mMSH6; mMSH3; mKRAS | [2]FGFR inhibitors |
| **TFK-1** | ≈40 hours | Extrahepatic (distal) (Non-Opisthorchis viverrini-related) | Japanese. Male (63 years). Primary tumour. | mTP53; mMSH6; mFRFR3 | [2]Anti-EGFR Ab c; Mek inhibitors |

## 2.2. Routine culture of cell monolayer

### 2.2.1. Cell sub-culture

For maintenance, all cells were cultured in 75cm$^2$ flasks (Corning, #430641U). Light microscopy (Nikon Eclipse TS100) was used daily to monitor cell growth. Cells were passaged once they covered approximately 80-90% of the culture area. At passage, cells were washed with 5mL of pre-warmed phosphate-buffered saline (PBS) (Sigma, #806552) and detached from the plastic surface with 5mL of pre-warmed TrypLE Express (ThermoFisher, #12605028). Pre-warmed 10% DMEM was used to inhibit trypsin activity after 5 minutes of incubation at 37°C and the resulting suspension was centrifuged at 300g for 5 minutes in a Heraeus Megafuge 40R centrifuge (Thermo Fisher Scientific, Massachusetts, USA). The pellet was re-suspended in 10% DMEM. Cells were usually split at a ratio of 1:8 to 1:10.

### 2.2.2. Cell cryopreservation

Cells with low passage were cryopreserved when they were 80% confluent. Firstly, cells were detached according to the procedure explained for cell sub-culture (Chapter 2, Section 2.2.1). After centrifugation, cells were re-suspended in FBS containing dimethyl sulfoxide (DMSO) (Sigma, #D4540), resulting in 10% (v/v) final DMSO concentration. 1x10$^6$ cells/mL were added to a sterile cryogenic vial (Corning, #430659) labelled with the cell type, the passage number, and the date. The vials were immediately transferred to a Mr. Frosty cryofreezing container (VWR International, #479-3200) at -80°C to allow a slow and controlled temperature reduction. After 24h, vials were transferred to a box at the same temperature (-80°C).

### 2.2.3. Cell revival

To proceed with cell revival, cryogenic vials were thawed by swirling in a 37°C water bath (Fischer Scientific, Nickel Electro Clifton Unstirred Thermostatic Bath). The content was transferred to a falcon containing 10mL of pre-warmed 10% DMEM. The resulting suspension was then centrifuged at 300g for 5min. The pellet containing the cells was resuspended in 10mL of 10% DMEM and transferred into a 25cm$^2$ flask (Corning, #430168). The flask was placed in a 5% $CO_2$ air-humidified atmosphere at 37°C in a SANYO incubator. The following day, general conditions were monitored under the light microscope.

## 2.3. 3D i*n vitro* models

### 2.3.1. Generation of a luminescent cell population and puromycin selection

To generate luminescent cell-lines, CCA cells were lentivirally transduced with a pLVX-Puro Vector carrying the sequence of *Firefly luciferase* and a *Puromycin resistance gene* (Clontech, Takara Bio Company, Otsu, Japan). The enzyme firefly luciferase oxides the substrate D-luciferin in the presence of molecular $O_2$, magnesium, and adenosine triphosphate to produce yellow-green light at 560nm (Brennan, Lin, Huang, & Yang, 2018). A kill curve was performed to determine the optimal concentration of puromycin dihydrochloride (Sigma #P8833) to kill the non-transduced cells. $1\times10^4$ wild-type cells/mL were seeded in a 96-well plate and incubated 24 hours to allow cell attachment. The following day, a range of 0.5-8µg/mL puromycin was added to each well. Each condition was performed in 4 replicates and incubated for 72h. Following incubation, AlamarBlue assay (Chapter 2, Section 2.5.1). was used to assess the viability of the cells after treatment by measuring the absorbance at 570nm using a microplate reader (FLUOstar Omega, BMG Labtech). Cells resistant to the antibiotic treatment were seeded in 1:2 dilutions into a 96-well black plate with clear bottom (ThermoFischer, #165305) in triplicate wells and transferred to a 5% $CO_2$ air-humidified atmosphere at 37°C in a SANYO incubator. After 24h, 10µL of D-Luciferin (30mg/mL) (Caliper LifeSciences, Massachusetts, USA) was added to each well and the plate was incubated for 15 minutes at 37°C. The signal was determined using a luminometer microplate (FLUOstar Omega, BMG Labtech) and an *In Vivo* Bioluminescent Imaging (IVIS) (Xenogen, California, USA) (for more details of puromycin kill curves and standard curves of luminescence, see Chapter 4, Figure 4.2-Figure 4.5). In order to maintain the luminescent cell populations, cell-lines were weekly treated with puromycin for 72h.

### 2.3.2. Establishment of cell-line-derived spheroids for the direct co-culture system

Mouse-derived BME Cultrex PathClear purified from Engelbreth-Holm-Swarm tumours (Bio-techne, #3432-005-01) was defrosted overnight on ice at 4°C. Cells were detached according to the procedure explained for cell sub-culture (Chapter 2, Section 2.2.1). The pellet was then re-suspended in 10mL of pre-warmed 10% DMEM. Cells were counted using an automatic haemocytometer by staining with TrypanBlue

(Merck, #T8154) and calculations were carried to seed 1000 cells per well with the presence of 100µg/mL of BME. A constant volume of 200µL was added to each well in an ultra-low attachment (ULA) 96-well round bottom plate (Sigma #CLS3474). Cancer cells were cultured in mono- and co-culture with hMSCs or iMSCs at 3 ratios, 2:1, 1:2 and 1:1 (cancer cells:MSCs). Triplicates were carried out for each condition. Edge wells were filled with 10% DMEM. The plate was then centrifuged at 300g for 10 minutes and transferred to a 5% $CO_2$ air-humidified atmosphere at 37°C in a SANYO incubator. The assay was monitored daily using a brightfield microscope (Nikon Eclipse Ti, 4X objective).

### 2.3.3. Establishment of cell-line-derived spheroids for the indirect co-culture system

The same procedure for cell detachment and cell counting was used for the indirect co-culture system (Chapter 2, Section 2.3.2). Cells were counted and spheroids were formed from either 1000 cancer cells or 1000 iMSCs. BME was also defrosted overnight on ice at 4°C and added at a final concentration of 100µg/mL. A constant volume of 200µL was added to each well in an ULA 96-well plate. At day 3 of culture, a HTS Transwell®-96 Permeable Support with 0.4µm pore polycarbonate membrane (Corning, #3381) was added to the plate, and two iMSCs-derived spheroids were added to the transwell in 100µL of 10% DMEM reaching a final volume of 300µL per well. This pore size would allow the free circulation of soluble molecules through the membrane whilst cells would not be able to trespass it. The final ratio for the indirect system was 2:1 (cell-line-derived spheroids:iMSCs-derived spheroids).

## 2.4. 3D *ex vivo* models

### 2.4.1. Specimens and establishment of PDXs

CCA1, CCA2, CCA4, CCA5, CCA6, CCA7 and CCA11 tumours were obtained as fresh surgical material from tumour resections at Nottingham University Hospitals NHS Trust, collected with informed patient consent and National Research Ethics Service (NRES) approval (NRES REC 10/H0405/6) and used in accordance with NRES approval (NRES REC 08/H0403/37). Immunodeficient female $Rag2^{-/-}\ \gamma C^{-/-}$ (Rag2G, 8–10 weeks) (Jax lab, #014593) bred in-house under Home Office Project Licence P375A76F were used in this project. PDXs were generated by implantation of minced tumour fragments admixed with Matrigel (200µL/mouse) (BD Biosciences,

#356237) with or without hMSCs ($5\times10^5$/mouse) using an implant trochar (VetTech, UK) subcutaneously under local anaesthetic (EMLA Cream, Aspen Pharma, Ireland) in the mice under HO project license PPL 3003444. Mice were maintained in individually ventilated cages (Tecniplast UK) within a barriered unit illuminated by fluorescent lights set to give a 12-hour light-dark cycle, as recommended in the United Kingdom Home Office Animals (Scientific Procedures) Act 1986. The room was air-conditioned by a system designed to maintain an air temperature range of 21 ± 2°C and a humidity of 55% + 10%. Mice were housed in social groups during the procedure and provided with irradiated bedding and autoclaved nesting materials and environmental enrichment (Datesand, UK). Sterile irradiated 5V5R rodent diet (IPS Ltd, UK) and irradiated water (SLS, UK) was offered *ad libitum*. Tumours were measured weekly using Vernier calipers, and the volumes were calculated using the formula V = ab2/6, where a is the length and b is the width. Mice were also weighed weekly and given a daily health check by an experienced technician. NCRI guidelines for the welfare and use of animals in cancer research, LASA good practice guidelines and FELASA working group on pain and distress guidelines were also followed, as were the ARRIVE guidelines on the reporting of *in vivo* experiments. This work was carried out by the *in vivo* team in the Grabowska Lab. Upon reaching maximum growth as allowed under the NCRI guidelines (mean diameter 1.2cm), mice were killed by a Schedule 1 method (cervical dislocation), tumours were removed under aseptic conditions, minced, and passaged on into further donor mice (P1) or taken for banking and spheroid assays carried out in this project.

### 2.4.2. Dissociation of the PDX tumours

The dissociation of the PDXs received from the *in vivo* team was performed by following the standard protocol used in the Grabowska Lab (Onion et al., 2016). The fresh PDX tumours were enzymatically disaggregated in 10mL of pre-warmed Hanks' Balanced Salt Solution (HBSS) (Sigma #H8264) solution containing dispase (2.4U/ml; Invitrogen #17105041) and type II collagenase (100U/ml; Invitrogen #17101015) at 37°C at constant rotation in a Binder heating chamber (Fischer Scientific, #Series B). After 1h, disaggregated cells were removed and filtered in 10mL of pre-warmed 10% DMEM using a 70µm cell strainer (Corning #431751) to remove debris or clumps from samples and isolate single cells. Cells were then centrifuged at 300g for 5 minutes and resuspended in 10mL of 10% DMEM.

### 2.4.3. Establishment of PDX-derived spheroids

Spheroids were established using cells isolated from PDXs. Cells were manually counted using a Neubauer chamber and 1000 CCA cells were seeded alone for the spheroid mono-culture or mixed with MSCs (either iMSCs or hMSCs) in a 1:2 ratio (cancer cells:MSCs) for spheroid co-culture. Cells (alone or mixed) were seeded in a ULA 96-well plate in a total volume of 200µL per well. BME was included at a final concentration of 300µg/mL. After 10 minutes of centrifugation at 300g, plates were maintained in a 5% $CO_2$ air-humidified atmosphere at 37°C in a SANYO incubator. The media used for PDX spheroids formation was 10% DMEM. Triplicates were carried out for each condition. Edge wells were filled with 10% DMEM. The assay was monitored daily using brightfield microscopy.

## 2.5. Spheroid viability and proliferation

### 2.5.1. AlamarBlue Assay

The AlamarBlue assay incorporates a fluorometric growth indicator based on detection of cell metabolic activity (Rampersad, 2012). This assay was used to evaluate the metabolic activity of the 3D cultures. AlamarBlue (ThermoFisher, #DAL1025) was 1:5 diluted in 10% DMEM, and 50µL of the dilution was added to each well. Blank wells (no cells) were prepared using the same conditions but in the absence of cells. Plates were incubated for 1 hour in darkness inside the SANYO incubator in a 5% $CO_2$ air-humidified atmosphere at 37°C. Following incubation, the absorbance of the solution was measured at 570nm using the FLUOstar Omega microplate reader. Data was expressed as relative fluorescence (RFU).

### 2.5.2. PrestoBlue Assay

PrestoBlue assay functions as a cell viability indicator by using the reducing power of living cells (Sonnaert, Papantoniou, Luyten, & Schrooten, 2015). This assay was also used to evaluate the metabolic activity of the 3D cultures. 100µL of 10% DMEM was removed from each well and 10µL of PrestoBlue (ThermoFisher, #P50200) was added. Blank wells (no cells) were prepared using the same conditions. Plates were incubated for 30 minutes in darkness in a 5% $CO_2$ air-humidified atmosphere at 37°C in a SANYO incubator. Following incubation, the absorbance of the solution was

measured at 570nm using the FLUOstar Omega microplate reader. Data was expressed as RFU.

### 2.5.3. Live/dead staining

Live/dead staining was used to assess the viability of the cells forming the spheroids (Pal et al., 2020). The viable and dead cells were detected using Calcein Acetoxymethyl Ester (Ca-AM) (TermoFisher, #65-0853-39) and Propidium Iodide (PI) (TermoFisher, #00-6990-50), respectively. Ca-AM becomes green fluorescent (Ex/Em ~495 nm/~515 nm) upon cleavage by esterases. PI is a membrane impermeant red dye (Ex/Em ~530 nm/~635 nm) that is excluded from viable cells, but it binds to the double stranded DNA of the dead cells. In addition, Hoechst 33342 (ThermoFisher, #62249), a blue, fluorescent dye, was used to stain the nucleus of the cells. Spheroids were incubated with 10µM Ca-AM, 33µM of Hoechst and 5% (v/v) PI in 10% DMEM in a final volume of 100µL per well. Spheroids were incubated for 3 hours in a 5% $CO_2$ air-humidified atmosphere at 37°C in a SANYO incubator (for more details of live/dead staining optimisation, see Chapter 3, Section 3.2.2.1). Finally, fluorescent images of spheroids were captured using Nikon Eclipse TiE fluorescence microscopes. During imaging, the exposure time for fluorescence was kept constant.

Another live/dead staining method was used for the same purpose. This used dyes which were part of a commercial and already-optimised kit (ThermoFischer #L3224). Spheroids were washed twice with 100µL of pre-warmed PBS and incubated for 30 minutes in a solution of 40µM Ethidium homodimer (EthD-1) and 20µM Ca-AM in pre-warmed PBS. Ca-AM stained viable cells green and EthD-1 is a membrane-impermeable red fluorescent dye which binds to DNA of dead cells. The Nikon Eclipse TiE fluorescence microscope was used for cell imaging.

### 2.5.4. Luciferase assay

The luciferase assay was used to detect the bioluminescence signal of the luciferase-transduced cancer cells in co-culture with MSCs. Under light-proof conditions, 10µL of D-Luciferin (30mg/mL) was added to each well. After 15 minutes of incubation at 37°C, the bioluminescence signal was read at 485nm using the FLUOstar Omega luminometer reader. Data was expressed as relative luminescence (RLU).

### 2.5.5. Image analysis

ImageJ was applied to measure the area of spheroids by using a plugin application of ImageJ. The macro calculates the radius which facilitates in determining the area ($r$= √Aπ) and subsequently, the volume (V=43πr3) of the relevant spheroid.

## 2.6. Spheroid and PDX morphology

### 2.6.1. Embedding spheroids in a microarray

Spheroids were embedded in a microarray according to the published protocol (Ivanov & Grabowska, 2017). This methodology involves the use of a mold-making device (mold) that produces holes in an agarose gel to embed spheroids in the same plane for downstream processing and analysis (Ivanov & Grabowska, 2017). The plastic mold was first left at -20°C for 2 minutes. A 2% of low-gelling 2-hydroxyethyl agarose (Sigma, #SLBL3447V) solution (v/v) was prepared and 3mL of the solution was dispensed in a stainless-steel histology base mold. Consecutively, the plastic mold was placed on the top of the base mold containing the agarose and left at room temperature to allow gelling. The mold was then removed imprinting 66 wells in total. Each spheroid was transferred from the ULA 96-well plate to an individual eppendorf and washed with PBS solution twice. Spheroids were then fixed for 1 hour with 200µL of 4% paraformaldehyde (PFA) solution (Sigma, #P6148) in PBS (v/v) and washed twice again. The agarose bed was filled with spheroids and centrifuged 1minute at 100g. Agarose was slowly dispensed on the top of the array. The array was incubated overnight with diluted 1X Neutral Buffer Formalin (NBF) (ThermoFisher, #5700) in $dH_2O$. The sealed arrays were placed in a histological cassette and processed in a tissue processor (Leica TP1020) overnight. In the processor, the samples were dehydrated in a series of fresh alcohol solutions with increasing concentrations (one bath of 50%, 70%, and 90%, and four baths of 100% methanol, 1 hour each), cleared in xylene (three baths, 1 hour each), and infiltrated with molten paraffin (two baths, 2 hours each). During the infiltration process, the xylene is eliminated from the tissue by diffusion and molten wax is infiltrated. The wax, which has diffused or infiltrated into the tissue after replacing the clearing agent, gets deposited in the tissues (A. A. Shah et al., 2017). The agarose molds containing the spheroids were then embedded in paraffin the next day to create a block for sectioning.

### 2.6.2. Sectioning of the PDXs and spheroids

The block was trimmed using the microtome. First, it was trimmed using 20µm thickness, and once the wells of the array were visible on eye, the thickness was changed to 4µm. From that point, each section was placed on a pre-warmed water bath at 40-50°C and placed on a clean poly-L-lysine coated glass slides (ThermoFisher, #12372098). A light microscope was used to verify the presence of spheroids. If spheroids were observed, slides were kept and dried overnight at room temperature for further staining.

### 2.6.3. H&E Staining

Sections were then dewaxed in 3 baths of 100% xylenes (5 minutes incubation each) and rehydrated in 2 baths of 100% methanol (1 minute incubation each). Haematoxylin (ThermoFisher, #72804) and eosin (ThermoFisher, #LAMB/100-D) staining (H&E) was performed by 3 minutes of incubation in each dye. Sections were then dehydrated in 3 baths of 100% methanol (1 minute each) and cleared in 2 baths of 100% xylenes (3 minutes each) before cover-slipping (Corning, #13216778) with dibutyl phthalate (DPX) (ThermoFisher, #LAMB/DPX). Slides were then imaged using a Nikon's Eclipse E600 microscope.

### 2.6.4. Immunohistochemistry (IHC)

Slides were dewaxed in 3 100% xylene baths (5 minutes each) and rehydrated in 2 100% methanol baths (1 minute each). This was followed by running $dH_2O$ for 1 minute. Slides were then washed twice with PBS and immersed in a plastic rack with antigen retrieval in citrate buffer (10mM, pH = 6) or TRIS (10mM)/erthylenediamine tetraacetic acid (EDTA) (1mM) buffer (pH = 9.0), for 20 minutes using a JT366 microwave (98 °C). Sections were washed with PBS and the areas were lined with a solvent resistant PAP marker (Securline, #1400-20-PDC). Endogenous peroxidase activity was blocked in hydrogen peroxide ($H_2O_2$) (3% in PBS) for 10 minutes (30 minutes, 3% in $dH_2O$). Blocking was done in serum (20% vol/vol in PBS) from the species matching the species of the secondary antibody. Details of the primary antibodies and specific details of the methods used for each are given in Table 2.2. In general, primary antibody incubation of 30 minutes or 1 hour, was followed by incubation with the secondary antibody (30 minutes or 1 hour). For biotinylated secondary antibodies a signal amplification (30 minutes) with ABC Complex

(Vectastain, #PK-6100) was included. Diaminobenzidine (DAB) (Abcam, #ab64238) was used to visualize positive staining (10 minutes) and hematoxylin to counterstain (3 minutes). Slides were then dehydrated in 3 100% methanol baths (1 minute each) and cleared in and 2 100% xylene baths (3 minutes each) before cover-slipping with DPX. Slides were finally imaged using a Nikon's Eclipse E600 microscope.

**Table 2.2. List of antibodies (Ab) used in the IHC experiments.**

| Primary antibody | Dilution and incubation | Antigen retrieval | Secondary antibody | Dilution and incubation |
|---|---|---|---|---|
| Monoclonal mouse anti-human Ki-67 (Dako, #M7240) | 1:100 for 1 hour | Citric buffer | Polyclonal rabbit anti-mouse, Biotinylated (Dako, #E0354) | 1:200 for 30 minutes |
| Monoclonal mouse anti-human vimentin (Dako, #M0725) | 1:100 for 1 hour | Citric buffer | Polyclonal rabbit anti-mouse, Biotinylated (Dako, #E0354) | 1:200 for 30 minutes |
| Monoclonal mouse anti-human cytokeratin (CK) CK (Dako, #M7018) | 1:100 for 30 minutes | TRIS/EDTA buffer | Polyclonal rabbit anti-mouse (Dako, #P0260) | 1:200 for 1 hour |
| Monoclonal mouse anti-human CK19 (Dako, #M0888) | 1:100 for 30minutes | TRIS/EDTA buffer | Polyclonal rabbit anti-mouse (Dako, #P0260) | 1:200 for 1 hour |

#### 2.6.4.1. IHC quantification

##### 2.6.4.1.1. Ki-67

Positive expression was quantified in 5 arbitrary areas of each section by manually counting the positive cells and cancer cells and calculating the ratio of positively stained cancer cells over the total of cancer cells observed in each area. The average was calculated.

#### 2.6.4.1.2. Vimentin

The percentage of vimentin positive cells was quantified by assessing the percentage of positive cells in different areas of the whole section and normalised by the total number of cancer cells present in the corresponding area.

### 2.6.5. Immunofluorescence (IF)

Spheroids were collected from a ULA 96-well plate and fixed with 4% (v/v) PFA in PBS buffer (pH 7.2) (v/v) for 1 hour at room temperature. Washing buffer (WB) was prepared by adding 1mL of Triton X-100 and 2g of bovine serum albumin (BSA) to 1L of PBS. For blocking, spheroids were resuspended in cold (4°C) WB and transferred to a low-adherence 24-well plate and incubated at 4°C for 15 minutes. After, 200µL of WB with Ki-67 antibody (1:100, 2×concentration) was added to each well and incubated overnight at 4°C with mild rocking (60RPM on a horizontal shaker). Spheroids were washed 3 times with WB and incubated with secondary antibody (1:200, 2×concentration) overnight at 4°C with mild rocking/shaking. Spheroids were then washed and prepared for imaging. Fructose–glycerol clearing solution (50µL) was added at incubated with the spheroids for 20 minutes. Slide preparation was performed. A PAP pen was used to draw a rectangle in the middle of a slide and 3 layers of 1cm-long piece of sticky tape at both sides of the rectangle was placed. Spheroids were added to the middle of the rectangle. A coverslip was placed on top and gently pressure was applied both sides of the coverslip to firmly attach it to the double-sided sticky tape. Slides were then imaged using a confocal microscope (Zeiss 780). The IF procedure was carried out by the collaborator Dr Dan Booth. Amira was used for processing and analysing the data using the magic marker tool which allowed automatic segmentation of the stained structures. Amira is a user-friendly application that allows 2D-image slices to be digitally analysed, segmented, color-coded, and rendered for 3D reconstruction (Garza-Lopez et al., 2021).

### 2.6.6. Scanning Electron Microscopy (SEM)

Spheroids were collected from an ULA 96-well plate and fixed by incubation for 24 hours in 4% PFA in PBS buffer (pH 7.2) (v/v) for 1 hour at room temperature. Samples were washed in PBS and post-fixed by incubation with 2% osmium tetroxide for 1h. Spheroids were then fully dehydrated in a graded series of ethanol solutions, and dried in hexamethyldisilazane. Finally, samples were coated and observed under a scanning

electron microscope. The SEM procedure and imaging was carried out in the Faculty of Medicine, Khon Kaen (Thailand) by the collaborator Dr Sakaew Waraporn.

## 2.7. Bioinformatic analysis

### 2.7.1. RNA extraction

RNA was isolated according to the AllPrep DNA/RNA/Protein SOP (Qiagen #80004). Spheroids or PDX tissues were first lysed and homogenized in buffer RLT. The lysate was then passed through an AllPrep DNA spin column for the selective binding of genomic DNA and washed. Ethanol (Sigma #459836) was added to the flow-through from the AllPrep DNA spin column to provide appropriate binding conditions for RNA, and the sample was then applied to a RNeasy spin column, where total RNA binds to the membrane. Messenger RNA (mRNA) was finally eluted in RNase-free water. The NanoDrop (Thermo Scientific™ NanoDrop™ 2000/2000c Spectrophotometers) was then used to measure the absorbance and calculate the concentration of nucleic acids (260 nm) and purified proteins (280 nm). The RNA integrity number (RIN) was also assessed using the Agilent 2100 Bioanalyzer (TapeStation, housed within the DeepSeq facility, University of Nottingham). RNA was sent for sequencing (eukaryotic RNA-seq, Illumina PE150, 20M reads) (Novogene, Cambridge, UK).

### 2.7.2. Analysis

Sequences underwent quality trimming and genome alignment. This was carried out by Professor Nigel Mongan, University of Nottingham. The expression matrix was generated, filtered, and converted to Ensemble gene IDs, using Integrated Differential Expression and Pathway analysis (iDEP). The pre-processed data was then used for exploratory data analysis, with methods such as hierarchical clustering, heatmaps and principal component analysis (PCA). The identification of differential expressed genes (DEGs) was done with DESeq2 packages. Venn Diagrams were used to represent the overlap between genes expression. Volcano plots were used to represent gene expression. This was followed by enrichment analysis on the DEGs. Significant KEGG pathways were represented, and the percentage of overlapped genes was used to construct a hierarchical clustering tree. Fold-change values for all genes returned by DESeq2 were also used in pathway analysis using Gene Set Enrichment Analysis

(GSEA). The GSEA-based hallmarks were used to select and represent most significant hallmark.

## 2.8. Statistical analysis

GraphPad Prism Version 9.4.1 was used for statistical analysis. In the spheroid assays, two-way analysis of variance (ANOVA) test was applied to determine the difference of growth between mono-culture and co-cultures across the time-points. All error bars were shown as mean ± standard error of the mean (SEM). In all statistical comparisons, * = $p<0.05$, ** = $p<0.01$, *** = $p<0.001$ and **** = $p<0.0001$ was accepted as denoting the significance difference.

# Chapter 3. Development and characterisation of cell-line-derived CCA spheroids

## 3.1. Introduction

For decades, 2D culture of cell-lines have been a widely used pre-clinical model to study cancer due to the advantages they offer such as long-term expansion capacity, short replication doubling time, low maintenance costs, and high reproducibility (Habanjar, Diab-Assaf, Caldefie-Chezet, & Delort, 2021; Massa et al., 2020). However, cells grown as a monolayer in a culture flask or in a flat petri dish, are not representative of the real disease. Cells under these conditions have been forced to modify various complex biological factors promoting selection of a homogenous cell population capable of growing attached to a plastic surface (Massa et al., 2020). The function is altered as is the morphology, ultimately affecting the translation of pre-clinical data in a clinical context. In addition, the 2D nature of the cultures and the lack of TME means that they do not recapitulate the malignant microenvironment and the cell-stroma interactions (Kapalczynska et al., 2018). Moreover, cells in a monolayer have unlimited access to nutrients, oxygen, metabolites, and signal molecules which does not resemble the *in vivo* tumour mass whose availability to those elements varies due to its natural 3D architecture (Kapalczynska et al., 2018). These limitations highlight the need for representative *in vitro* tumour models to improve our understanding of tumour biology and progress drug discovery. Recently, more innovative *in vitro* models have been developed to improve these 2D culture of cell-lines. 3D models can recapitulate features of the native tumour such as the presence of tumour cell-TME and -ECM interactions and gradient distribution of chemical and biological factors (Pinto, Henriques, Silva, & Bousbaa, 2020); thus, they could be more promising models to recapitulate the *in vivo* tumour.

Spheroids are a type of 3D model where cells are grown as aggregates of cells having 3D cell-cell contact and grow in a more physiological environment that enhances production of ECM and stimulates inter-cellular communication (McMahon et al., 2012). Due to the 3D nature of spheroids, the access to nutrients, oxygen and the pH varies throughout the different layers. They form an outer proliferating layer, inner quiescent zone, and a potentially necrotic core, which ultimate resembles the physiological environment of an *in vivo* solid tumour (McMahon et al., 2012). Additionally, it has been shown that spheroids resemble the gene expression profiles of patient tumours more closely than those seen in 2D (Riffle, Pandey, Albert, & Hegde, 2017; Siva Sankar et al., 2017). Additionally, when evaluating biological

effects for the purpose of translating drugs to the clinic, 3D spheroids also reflect a better response than those in 2D cultures (Reynolds et al., 2017). These properties make them well-suited for characterising cancer biology; and therefore, they were used as a pre-clinical model in the present study in order to understand CCA biology.

Among all the available techniques to generate spheroids, the use of ULA-attachment plates to generate spheroids is an easy and well-established technique with no specialised equipment needed, for which a protocol had already been established in the Grabowska Lab for a number of tumours types (Pal et al., 2020). However, the morphology of spheroids is influenced by various factors, such as the cell type, cell density, culture method and media, and mechanical stress (Cheng, Tse, Jain, & Munn, 2009), and it is still challenging to produce spheroids from certain cell-lines (Ivascu & Kubbies, 2006). Nonetheless, various efforts can be made to overcome some challenges. For instance, if the cell-line expresses low intercellular junction proteins, there are several additives that can be added in the culture media such as Matrigel and other types of collagens that can contribute to support the compact and circular spheroid formation (Ivascu & Kubbies, 2006).

The work in this chapter aimed to establish and characterise cell-line-derived CCA spheroids which would be used in later chapters to further investigate the pathways activated in CCA as a result of the crosstalk between cancer cells and the TME. Cell-lines derived from related and non-related-fluke tumours (O-CCA and Non-O-CCA, respectively) were used to develop this model. Additionally, from the three subtypes that the CCAs are divided depending on their anatomical site of origin, five iCCA and one dCCA were used. In the first part of this chapter the steps to develop a 3D model using CCA cell-lines are described. Further characterisation of the viability and the morphology of the cancer cells when forming the spheroid are shown. The proliferation status is also characterised by Ki-67 IHC and IF staining, and the expression of CCA markers such as CK7 and CK19 is determined by IHC. Finally, the ultrastructure of those spheroids is assessed by SEM.

## 3.2. Results

### 3.2.1. Optimisation of seeding density for CCA spheroid formation

For initial evaluation and in order to assess the natural ability of CCA cells to form spheroids, one O-CCA cell-line (KKU-M055); and one non-O-CCA cell-line (TFK-1), were chosen. Both CCA cell-lines have previously been used in CCA research (Saijyo et al., 1995; Tepsiri et al., 2005) and were already available in the Grabowska and Bates Lab. The well-established method in the Grabowska Lab (Ivanov & Grabowska, 2017; Pal et al., 2020; Tchoryk et al., 2019) for the generation of spheroids was used (Chapter 2, Section 2.3.2). Initially, KKU-M055 were seeded at 6 different cell densities (1000 to 6000cells/well) with 4 technical replicates. During the centrifugation of the ULA 96- round bottom plate, all cells within the well were brought into close proximity at the bottom of the plate to allow interaction for initiation of the formation of a single spheroid, per well. The progressive growth was qualitatively monitored over a period of 7 days.

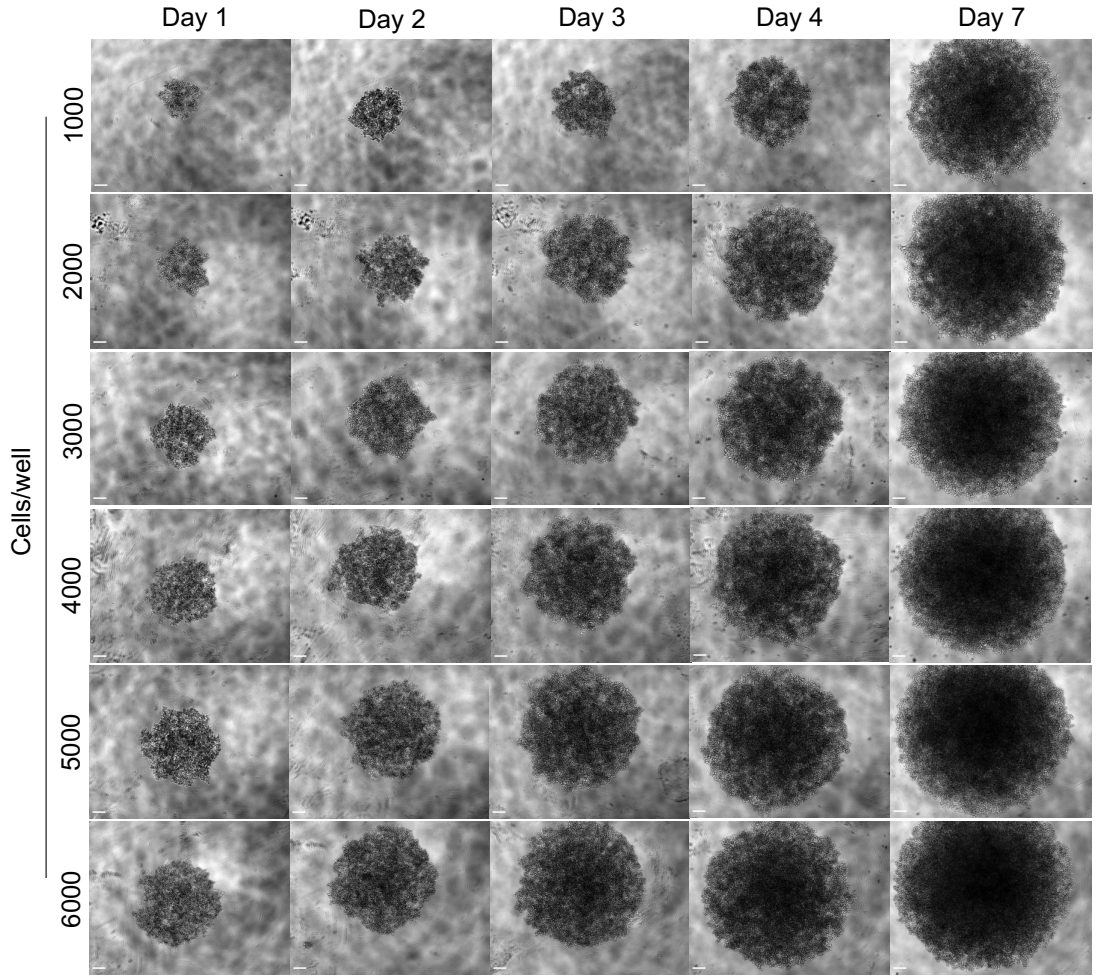



**Figure 3.1. KKU-M055 spheroid formation.** KKU-M055 cells were dispensed into a ULA 96-well round bottom plate at different densities (1000 to 6000cells/well). Progressive growth of the spheroid was monitored in 4 replicate wells on days 1, 2, 3, 4 and 7 using brightfield microscopy. Representative spheroids are shown (scale bars = 200µm).

Results showed that KKU-M055 cells were unable to form compact spheroids at any cell density during the period of 7 days. In addition, morphology was consistent across the range of seeding densities (Figure 3.1). To achieve a tighter spheroid, the same assay was performed using only the lowest cell density (1000cells/well) but adding a source of BME, at a non-gelling concentration (100µg/mL), which is known to promote cell-cell attachment within spheroids (Ivascu & Kubbies, 2006). Quantitative assessment of the area was substantiated using Fiji analysis software (Chapter 2, Section 2.5.5).

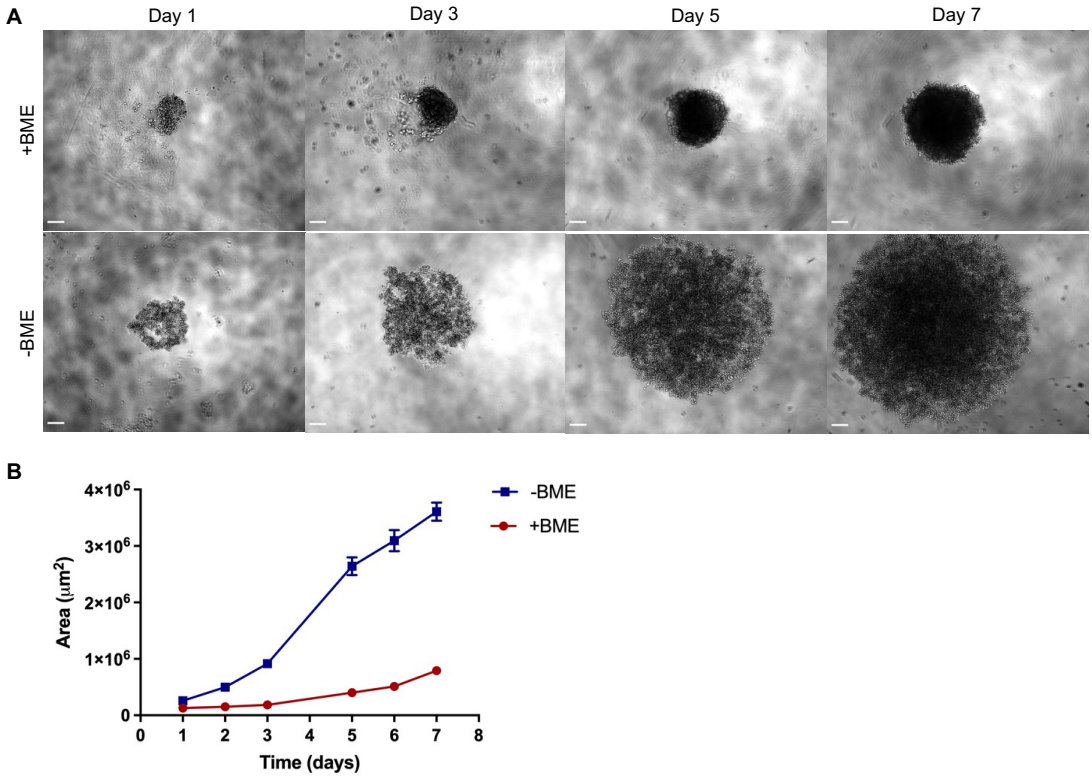



**Figure 3.2. KKU-M055 spheroid formation in the presence or absence of BME.** 1000 KKU-M055 cells per well were dispensed into a ULA 96-well round bottom plate with or without 100µg/mL of BME. Progressive growth of the spheroid was monitored in 4 replicate wells on days 1, 3, 5 and 7 using brightfield microscopy. Representative spheroids are shown (scale bars = 200µm) **(A)**. The area of the spheroid was determined in 4 technical replicates on days 1, 2, 3, 5, 6 and 7 using ImageJ Fiji (Mean ± SEM) **(B)**.

The presence of BME promoted cell-cell attachment, ultimately helping cells to form a more compact spheroid with a more defined border. Interestingly, after one day of culture, KKU-M055 cells formed a loosely-packed spheroid with a small difference between tested conditions. However, on day 3, KKU-M055 cells in the presence of BME became more tightly packed, forming round spheroids (Figure 3.2A); therefore, day 3 was noted as the first day of spheroid formation. The compact structure did not disintegrate by pipetting. A clear difference in area was found between conditions. The area of the spheroids was reduced by 50%. In the presence of BME, spheroid areas ranged from ~1x10$^6$µm$^2$ on day 3 to ~3.5x10$^6$µm$^2$ on day 7, whereas, in the absence of BME, spheroids reached areas from less than ~2x10$^5$µm$^2$ on day 3 to ~8x10$^5$µm$^2$ on day 7 (Figure 3.2B).

To investigate the impact of BME on CCA spheroid formation, TFK-1 cells were used to generate spheroids. TFK-1 cells were seeded in the ULA 96-well round bottom plate at 1000 cells/well with 4 technical replicates and in the presence or absence of a non-gelling BME concentration. The difference in spheroid-making capability was assessed.

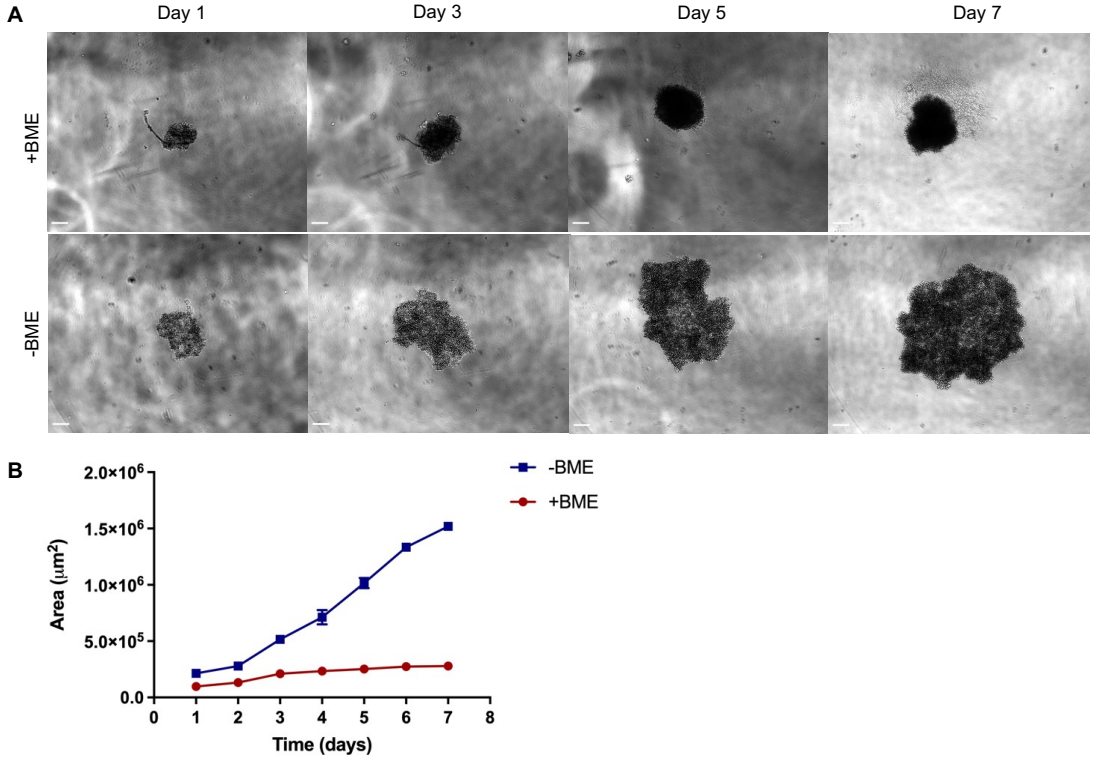



**Figure 3.3. TFK-1 spheroid formation in the presence or absence of BME.** 1000 TFK 1 cells were dispensed in each well into a ULA 96-well round bottom plate with or without 100µg/mL of BME. Progressive growth of the spheroid was monitored in 4 replicate wells on days 1, 3, 5 and 7. Representative spheroids are shown (scale bars = 200µm) **(A)**. The area of the spheroid was determined in 4 technical replicates on days 1, 2, 3, 5, 6 and 7 using ImageJ Fiji (Mean ± SEM) **(B)**.

TFK-1 cells formed compact spheroids in the presence of BME compared to the ones grown in absence of BME. However, both spheroids formed irregular edges (Figure 3.2A). Similar to the KKU-M055-derived spheroids, following quantification, the area was reduced by 50% in presence of BME. TFK-1-derived spheroids reached areas ranging from ~$5x10^5 µm^2$ on day 3 to ~$1.5x10^6 µm^2$ on day 7 in presence of BME; however, spheroids reached areas of less than ~$2x10^5 µm^2$ on day 3 to ~$3x10^5 µm^2$ in the absence of BME (Figure 3.3B).

### 3.2.2. Viability of the CCA cells in the spheroids

Once the optimal conditions to form CCA spheroid were chosen (1000 cells/well in presence of 100µg/mL of BME), and in order to investigate the accumulation and localization of live and dead cells and the formation of a potential necrotic core, CCA-derived spheroids were examined using live/dead staining (Chapter 2, Section 2.5.3). Additionally, the overall viability of the spheroids was determined using a metabolic assay, AlamarBlue (Chapter 2, Section 2.5.1). The live/dead staining was performed by adding a dye mixture to the spheroids. Ca-AM was used to measure metabolically active and viable cells (green staining). Hoechst was utilized to measure total cell count and nuclear shape (blue staining). PI was used to indicate a compromised cell membrane with subsequent binding to the nucleic acids (red staining). This protocol was previously optimised by a PhD student in the Grabowska Lab (Pal et al., 2020). The AlamarBlue assay was used to provide a quantitative indirect method to measure cell proliferation. AlamarBlue is a widely-used commercially available redox indicator dye that can evaluate metabolic activity and cellular health status (Eilenberger et al., 2018). The oxidised, blue, nonfluorescent AlamarBlue is reduced to a pink, fluorescent dye in the medium, by cell activity (O'Brien, Wilson, Orton, & Pognan, 2000). This can be further quantified using a plate reader. These bioassays were carried out for both KKU-M055 and TFK-1-derived spheroids in the presence or absence of BME at 3 different time-points.

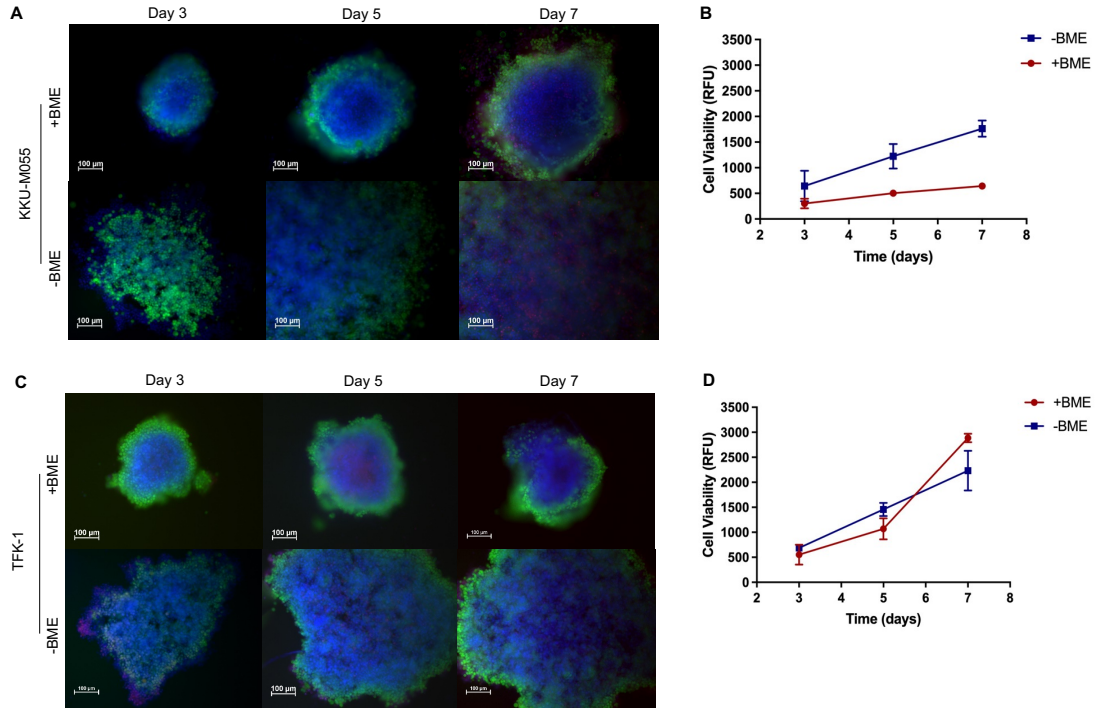



**Figure 3.4. KKU-M055 and TFK-1 spheroid viability.** 1000 KKU-M055 **(A)** and TFK-1 **(C)** cells were dispensed in each well into a ULA 96-well round bottom plate with or without 100µg/mL of BME. Live/dead staining was performed in 4 replicate wells after establishment in spheroid-shape on days 3, 5 and 7 using Hoechst 33342 (blue - nucleus staining), Ca-AM (green - live cells staining) and Propidium iodide (red - dead cells staining). Representative spheroids are shown. Progressive growth was monitored in 4 technical replicates wells on days 3, 5 and 7 using the Alamar Blue assay (Mean ± SEM) **(B** for KKU-M055 and **D** for TFK-1**)**.

PI-positive cells were found in KKU-M055-derived spheroids on both conditions tested on day 7. However, only a few dead cells were observed (Figure 3.4A). TFK-1-derived spheroids also showed only a few PI-positive cells (Figure 3.4C). KKU-M055 spheroids grown in the presence of BME gradually increased cell viability and remained spherical. Spheroids grown in the absence of BME did not stay spherical although cell viability still increased (Figure 3.4B). TFK-1 spheroids showed similar cell viability in both conditions tested (Figure 3.4D). Further optimisation of the live/dead staining was carried out.

### 3.2.2.1. Optimisation of the live/dead staining in the spheroid model

As it was unclear whether the absence of the necrotic core and dead cells was due to the lack of penetration of the PI into the spheroid, live/dead staining optimisation was performed. Spheroids were established according to the standard protocol (Chapter 2, Section 2.3.2). The staining was performed at day 7 to maximise the possibility of the presence of a necrotic core and 5 conditions were tested (Table 3.1).

**Table 3.1. Conditions tested for live/dead staining optimisation in the spheroid model.** 1000 KKU-M055 and TFK-1 cells per well were dispensed into a ULA 96-well round bottom plate. At day 7 of culture the following conditions were tested: the combination of 10µM of Calcein-AM (green - live cells staining) and 5µL of PI (red - dead cells staining) **(1)**; and a higher concentration, 15µM and 7.5µL of PI **(2)**, respectively; the combination of the 3 dyes at the same conditions **(3, 4)**. Finally, the combination of Calcein-AM and PI for a period of 2h and 33µM Hoechst (blue - nucleus staining) for 1h **(5)**.

| Condition | Calcein-AM (µM) | Hoechst (µM) | PI (µL) | Time (h) |
|---|---|---|---|---|
| **1** | 10 | X | 5 | 3 |
| **2** | 15 | X | 7.5 | 3 |
| **3** | 10 | 33 | 5 | 2 |
| **4** | 10 | 33 | 5 | 3 |
| **5** | 15 | 33 | 7.5 | 3 |

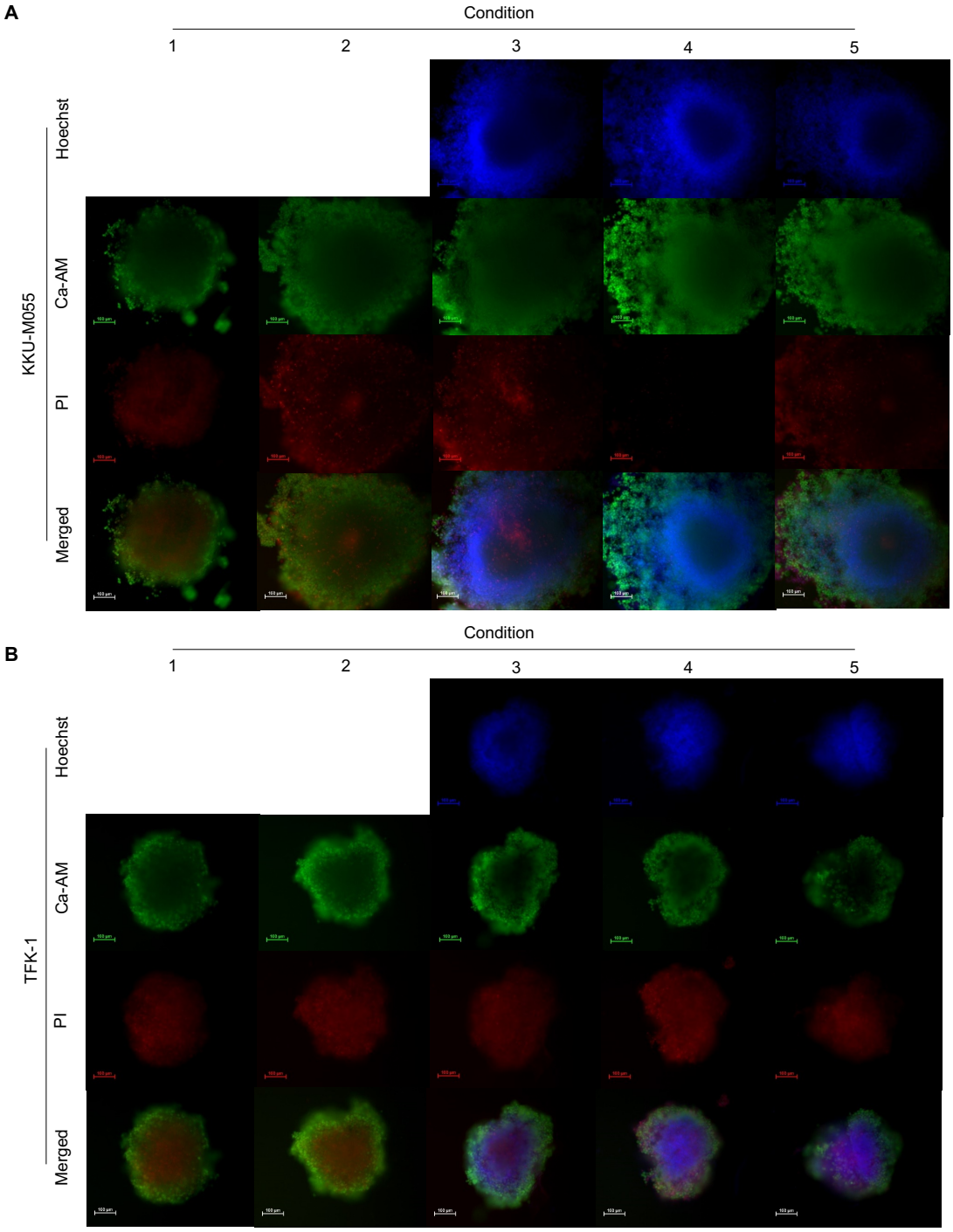



**Figure 3.5. Live/dead staining optimisation.** 1000 KKU-M055 **(A)** and TFK-1 cells **(B)** were dispensed into each well into a ULA 96-well round bottom plate with 100µg/mL of BME. Live/dead staining was monitored in 3 replicate wells on day 7. Five conditions were tested: the combination of 10µM of Ca-AM (green live/active cells staining) and 5µL of PI (red dead cells staining) (1); and a higher concentration, 15µM and 7.5 µL of PI (2), respectively; the combination of the 3 dyes at the same conditions (3, 4). Finally, the combination of Calcein-AM and PI for a period of 2 hours and 33µM Hoechst (blue nucleus staining) for 1 h (5). Representative spheroids are shown.

KKU-M055 spheroids consisted mostly of viable cells in all conditions (Figure 3.5A). The small number of individual dead cells were found in the 3 first conditions and located in the core of the spheroids. However, the intensity of the staining was low. These results were consistent with the first two conditions tested on the TFK-1 cell-line. TFK-1-derived spheroids also showed PI staining in the middle and edges on the last 3 conditions (Figure 3.5B).

### 3.2.3. Morphology of the CCA spheroids

After cell viability was assessed, spheroids were established for all the CCA cell-lines. This panel included 5 CCA cell-lines (4 O-CCA and 1 non-O-CCA). The cell viability and shape of the CCA-derived spheroids was determined by AlamarBlue assay and brightfield microscopy, respectively. The area was quantified using Fiji analysis software. Representative images of the morphology of the monolayers were also obtained by brightfield microscopy in order to assess individual cell morphology.

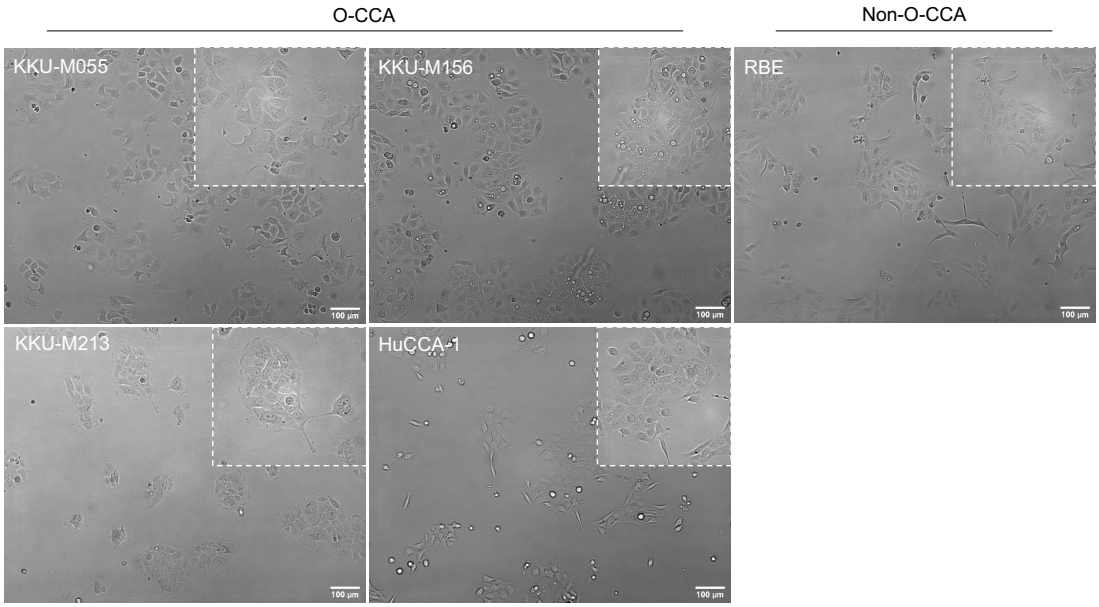



**Figure 3.6. Morphology of CCA cells cultured in 2D.** Five CCA cell-lines (KKU-M055, KKU-M156, KKU-M213, HuCCA-1 and RBE) were seeded in a 6-well plate in triplicates at $1x10^4$ cell density in each well. After 48h, the 2D morphology was assessed using brightfield microscopy.

Cells growing in 2D displayed different morphologies. At this stage, TFK-1 cells tested positive for mycoplasma; therefore, they were excluded from the panel whilst they underwent mycoplasma treatment. O-CCA cell-lines (KKU-M055, KKU-M156, KKU-M213 and HuCCA-1), showed epithelial-like morphology. RBE, displayed more mesenchymal features (Figure 3.6). Spheroids were then formed from those cell-lines.

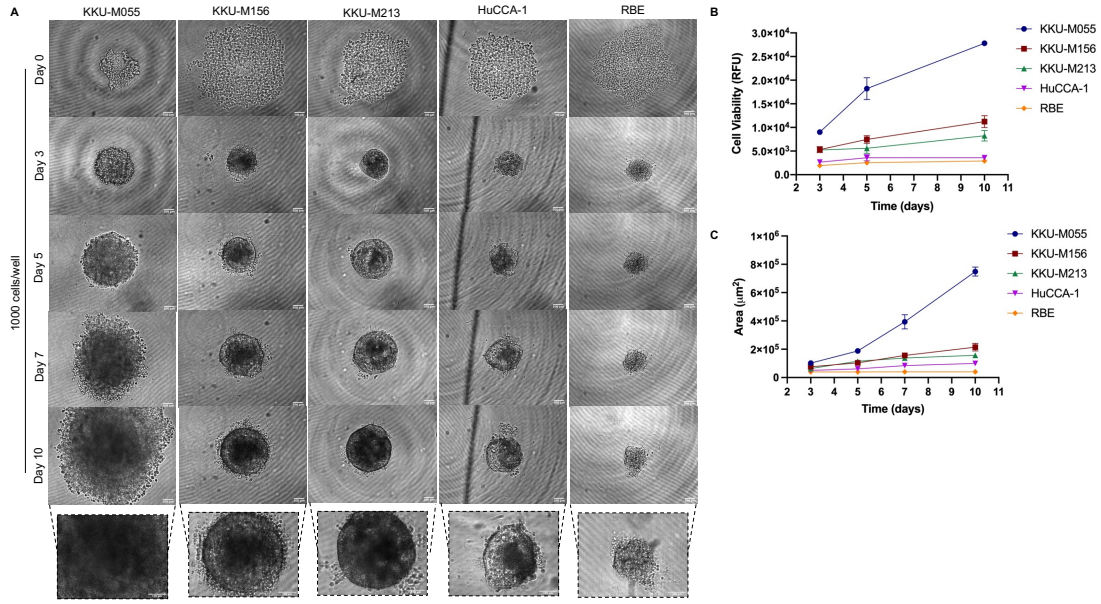



**Figure 3.7. Morphology of the CCA cell-line derived spheroids.** Five CCA cell-lines (KKU-M055, KKU-M156, KKU-M213, HuCCA-1 and RBE) were used for the generation of spheroids. 1000 cells were dispensed in each well into a ULA 96-well round bottom plate with 100µg/mL of BME. Progressive growth of the spheroid was monitored in 4 replicate wells on days 0, 3, 5, 7 and 10 using brightfield microscopy. Representative spheroids are shown (scale bars = 100µm) **(A)**. Cell viability was monitored in 4 replicate wells on days 3, 5 and 10 using the AlamarBlue assay (Mean ± SEM) **(B)**. The area of the spheroid was determined on days 3, 5, 7 and 10 using ImageJ Fiji (Mean ± SEM) **(C)**.

Differences between CCA cell-line-derived spheroids were observed at day 3 of culture and were more pronounced after 10 days. Starting at day 3, high compaction of cells was observed in almost all of the spheroids. KKU-M156 and KKU-M213 cell-lines generated uniform spheroids with a well-defined border until day 10, and a time-dependent cell viability and area increase. This was less noticeable in KKU-M055-derived spheroids. KKU-M055 cells generated round spheroids and maintained this appearance until day 5. After day 5, their borders became irregular ultimately forming compact aggregates and not spheroids albeit the viability and size increased over time. RBE spheroids formed compact spheroids, but the viability and size did not increase

over the period of culture. HuCCA-1-derived spheroids followed a similar tendency (Figure 3.7).

For more in-depth analysis, the spheroid-array methodology that was developed and optimised in the Grabowska Lab (Ivanov & Grabowska, 2017) was performed. This technique consists of a gel-based array that allows the embedding of fixed spheroids for downstream IHC. H&E was first used to stain the sections and assess the internal cell-line-derived spheroid morphology. CCA cells were grown as spheroids and they were fixed, paraffin embedded, sectioned, and stained (Chapter 2, Section 2.6.3) (technical replicates are in Appendix A, Figure A1 and Figure A2). Human CCA sections which were previously stained by a postdoctoral researcher in the Bates Lab, were also imaged to allow comparison.

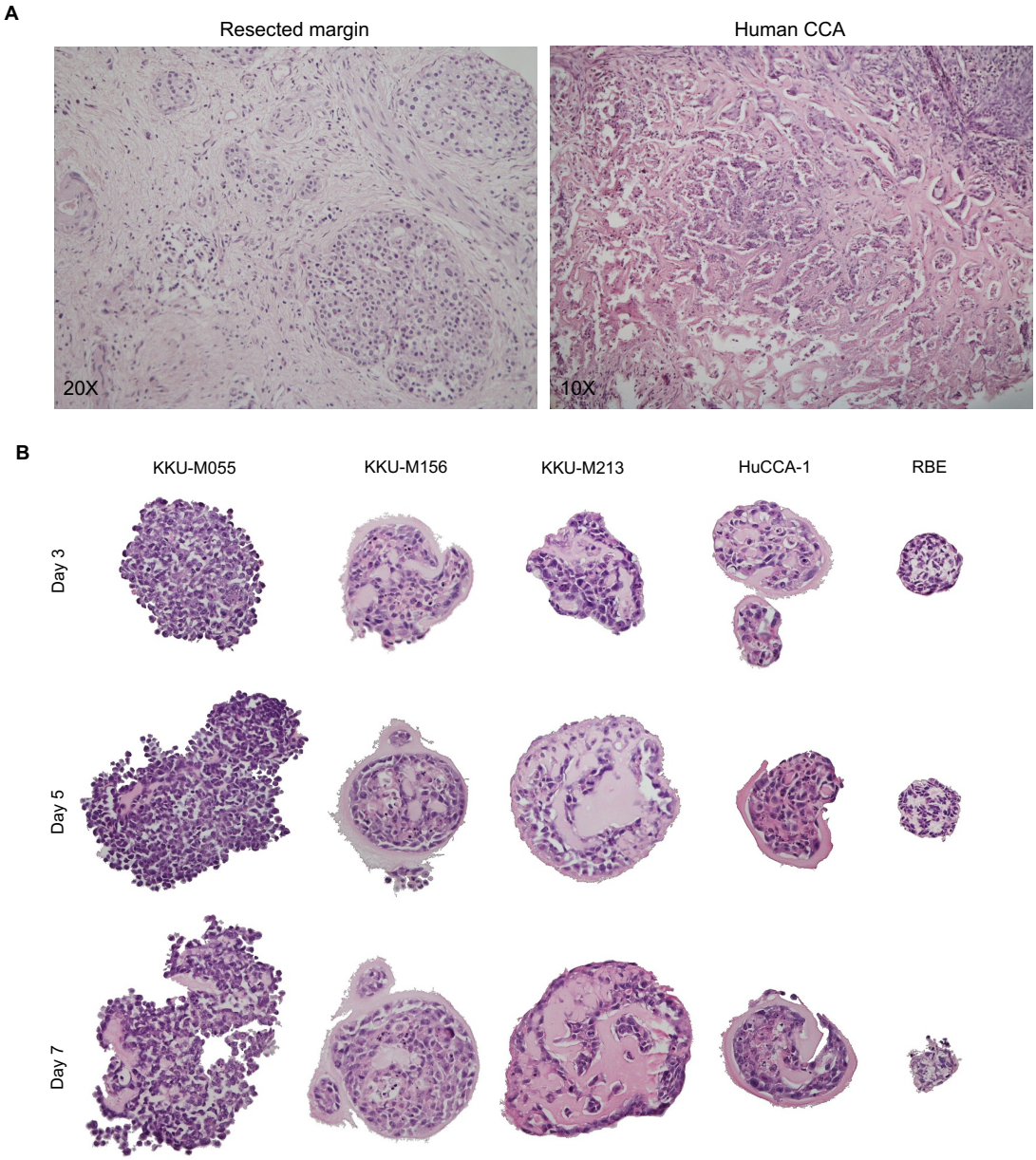



**Figure 3.8. H&E staining of human CCA tumour and CCA cell-line-derived spheroids.** H&E stain of surgically resected margin and human CCA tumour. Microscope objective = 20X and 10X **(A)**. 1000 cells per well were dispensed into a ULA 96-well round bottom plate from each of the 5 CCA cell-lines (KKU-M055, KKU-M156, KKU-M213, HuCCA-1 and RBE) with 100µg/mL of BME. CCA spheroids were fixed at day 3, 5 and 7 of culture, paraffin embedded, sectioned, and stained with H&E. Representative spheroids are shown (magnification: 20×) **(B)**.

H&E staining confirmed that spheroids consisted of cells displaying classical neoplastic features, such as nuclear pleomorphism; features that can be observed in the CCA tumour histology (Figure 3.8A). Interestingly, morphological differences between cell-line spheroids were observed. KKU-M156, KKU-M213 and HuCCA-1-derived spheroids increased in size and stayed uniformly spherical throughout the culture period. These spheroids presented internal material deposition. In the case of

RBE-derived spheroids, despite having a shape close to a perfect sphere at day 3, their size decreased over time and cellular structure and morphology was lost. KKU-M055-derived spheroids changed shape, and spheroids become disaggregated, losing structural integrity (Figure 3.8B).

### 3.2.4. Characterisation of the cellular proliferation of the CCA spheroids

To further characterise the panel of CCA spheroids, the spheroid-array was performed, and spheroids were immuno-stained for Ki-67 (Chapter 2, Section 2.6.4). Ki-67 protein is present in all phases of the cell cycle except G0 and is thus a marker for the growth fraction of a cell population (Riffle et al., 2017). Ki-67 is also a widely-used clinical marker in differentiating benign, from malignant intrahepatic biliary lesions (Tsokos, Krings, Yilmaz, Ferrell, & Gill, 2016). Ki-67 was quantified as percentage of positive cells against total cells (Chapter 2, Section 2.6.4.1.1) (technical replicates are in Appendix A, Figure A1 and Figure A2).

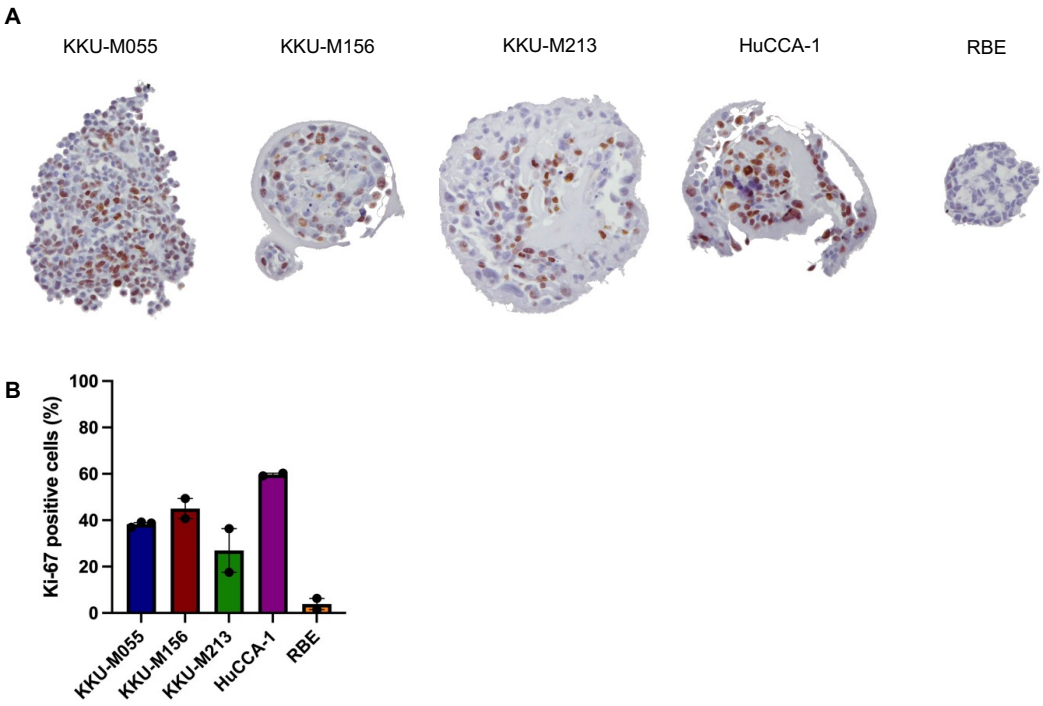



**Figure 3.9. Ki-67 staining of CCA cell-line-derived spheroids.** 1000 cells per well were dispensed into a ULA 96-well round bottom plate from each of the 5 CCA cell-lines (KKU-M055, KKU-M156, KKU-M213, HuCCA-1 and RBE) with 100µg/mL of BME. CCA spheroids were fixed at day 5 of culture, paraffin embedded, sectioned, and stained with Ki-67. Representative spheroids are shown (magnification: 20×) **(A)**. The number of Ki-67-positive cells was quantified by ImageJ software. The percentage of Ki-67 positive cells was normalized by the total number of cells and displayed as percentage of Ki-67 positive cells **(B)**.

The Ki-67 positive cells (dark brown nuclei) were distributed across the whole cross-section in the larger spheroids (KKU-M055, KKU-M156, KKU-M213 and HuCCA-1-derived spheroids). In contrast, the small RBE-derived spheroid had no expression of this marker (Figure 3.9A). Interestingly, HuCCA-1 had the highest percentage of proliferation, followed by KKU-M156, KKU-M055, KKU-M213 and RBE (Figure 3.9B).

Techniques such as the spheroid-array followed by IHC staining has allowed for the downstream CCA spheroid characterisation. Another commonly used technique to help characterising the spheroid is IF. While this technique has been extensively used for 2D culture, it required a refined method for 3D. Therefore, a procedure was followed from a Nature Protocol (Dekkers et al., 2019) in collaboration with Dr Dan Booth, an Associate Professor in the Biodiscovery Institute, University of Nottingham. Firstly, spheroids were collected at day 5, fixed, and immunolabelled for DAPI and Ki-67. Confocal microscopy was used to image the spheroids and Amira was used to visualise and interpret the results (Chapter 2, Section 2.6.5). To test this protocol, only one CCA cell-line was used to form spheroids (KKU-M213). Although the steps to perform IF, including mounting the slide, and imaging by confocal microscopy were performed by Dr Dan Booth. Amira was then conducted via the guidance of Dr Dan Booth. Using Amira's tools for image segmentation and geometry reconstruction, the 3D reconstruction of the spheroid was performed. Automatic, semi-automatic, and manual tools were used to mark the DAPI and Ki-67 positive cells.

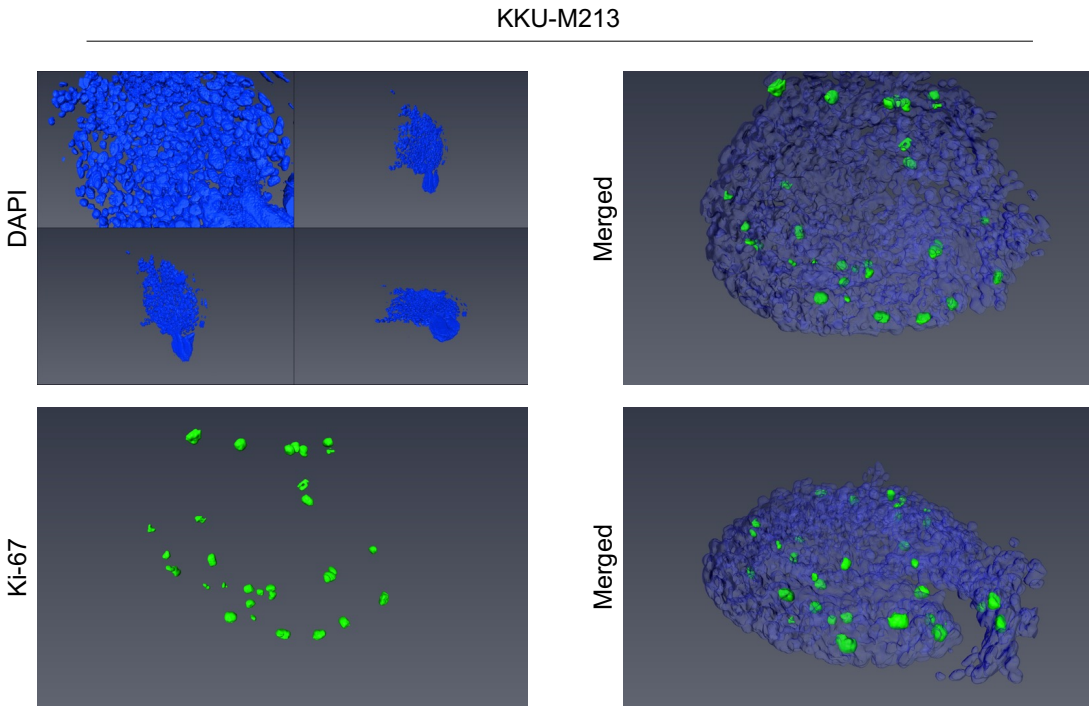



**Figure 3.10. Immunofluorescence staining of the KKU-M213-derived spheroids.** 1000 KKU-M213 cells per well were dispensed into a ULA 96-well round bottom plate with 100µg/mL of BME. At day 5, CCA spheroids were immunofluorescent stained for DAPI (blue) and Ki-67 (green). Spheroids were then imaged by confocal microscopy. Manual tools from Amira's software were used to mark the positive cells and perform the 3D reconstruction of the model.

Interestingly, the staining pattern correlated with the IHC results (Figure 3.9 and 3.10).

### 3.2.5. Expression of CK7 and CK19 in the CCA spheroids

CK7 and CK19 have been reported as useful immunohistochemical markers to distinguish CCA from HCC. Additionally, in CCA, high expression of these cytokeratins is correlated with tumour aggressiveness and poor survival (L. Z. Liu et al., 2018). Therefore, to evaluate whether the CCA spheroids are relevant models with CCA-related characteristics of the *in vivo* tumour, spheroids were stained with CK7 and CK19. Spheroids were grown and at day 5, the spheroid-array method was

performed and followed by IHC (Chapter 2, Section 2.6.4) (technical replicates are in Appendix A, Figure A1 and Figure A2).

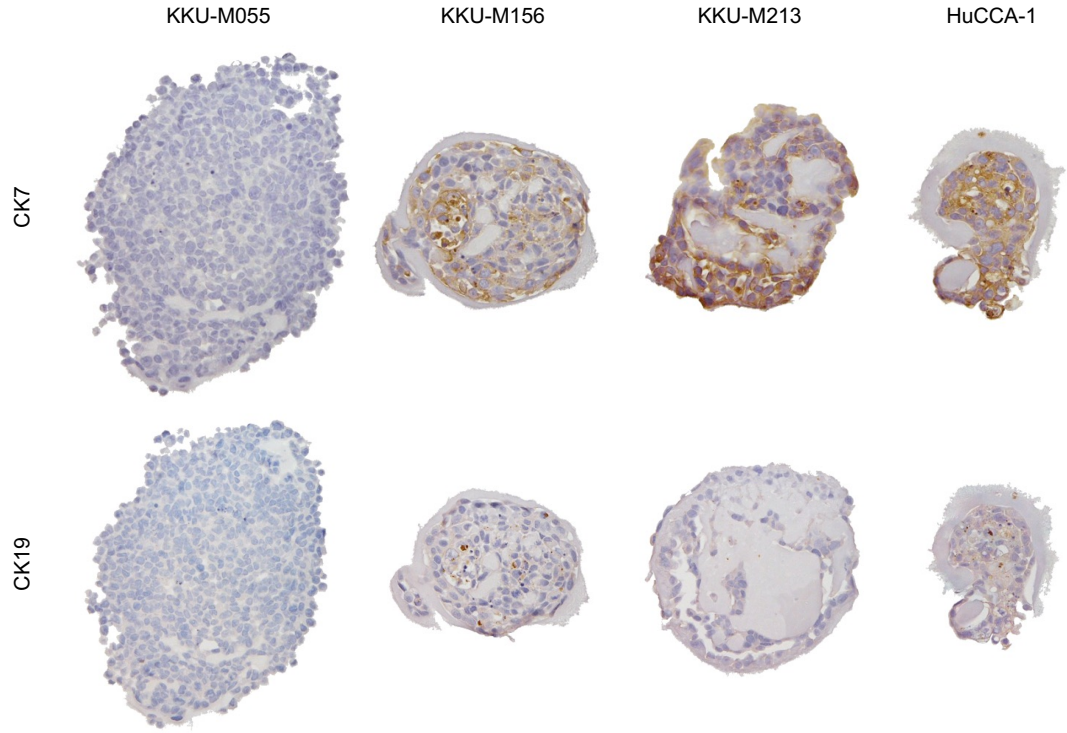



**Figure 3.11. CK7 and CK19 staining of CCA cell-line-derived spheroids.** 1000 cells per well were dispensed into a ULA 96-well round bottom plate from each of the 4 CCA cell-lines (KKU-M055, KKU-M156, KKU-M213 and HuCCA-1) with 100µg/mL of BME. CCA spheroids were fixed at day 5 of culture, paraffin embedded, sectioned, and stained with CK7 and CK19. Representative spheroids are shown (magnification: 20×).

In comparison to Ki-67 staining, the IHC protocol was well-established in the Grabowska Lab, however, the protocols for CK7 and CK19 staining were not yet optimised. Therefore, key variables such as the antigen retrieval buffer, the incubation time of both antibodies and the second antibody were optimised. These factors were based on the CK7 and CK19 antibody datasheet, and advice from peers with expertise in IHC techniques. Positive staining was present in the spheroids and the conditions were applied in the following chapters for CK7 and CK19 staining.

RBE cells formed small spheroids, and not enough sections were available to stain for those markers. CK7 was highly expressed in KKU-M156, KKU-M213 and HuCCA-1-derived spheroids; CK19 was also expressed, albeit notably less intense. The expression and distribution of those cytokeratins was on the cytoplasm of cells.

Interestingly, CK7 and CK19 expression was absent in the KKU-M055-derived spheroids (Figure 3.11).

### 3.2.6. Ultrastructural Characterisation of the CCA spheroids by SEM

In order to assess spheroid morphological parameters in more detail, SEM was performed. Electron microscopy is widely used to characterise cellular protrusions, integrity of cell–cell interactions and cellular membrane at nanoscale levels (Pinto et al., 2020). This work was carried out in collaboration with a visiting Assistant Professor, Dr Sakaew Waraporn in Khon Kaen University (Department of Anatomy, Faculty of Medicine).

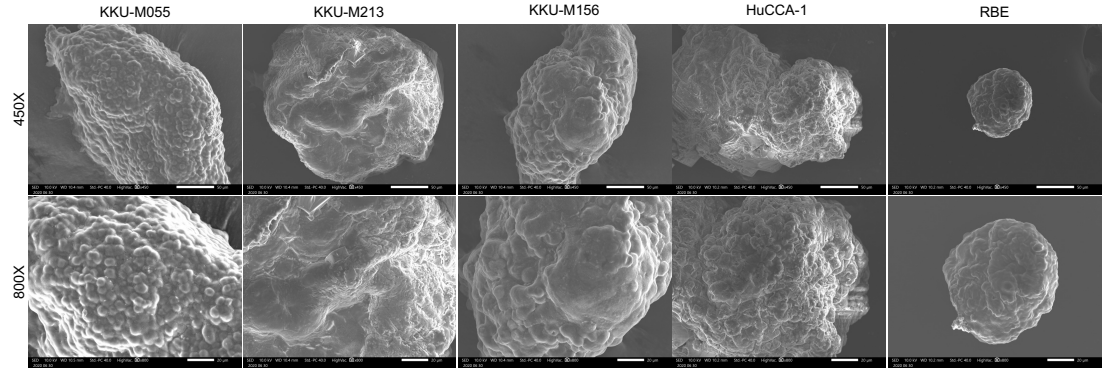



**Figure 3.12. SEM imaging of CCA-derived spheroids.** 1000 cells per well were dispensed into a ULA 96-well round bottom plate from each of the 5 CCA cell-lines (KKU-M055, KKU-M156, KKU-M213, HuCCA-1 and RBE) with 100µg/mL of BME. At day 5, spheroids processed for SEM. Spheroids were imaged at 450X (scale bar = 50µm) and then at 800X (scale bars = 20µm).

Interestingly, KKU-M213, KKU-M156 and RBE spheroids showed continuous smooth surfaces. It was difficult to distinguish individual cells demonstrating tight cell-cell interaction. In contrast, KKU-M055 and HuCCA-1-derived spheroids displayed cell-like round surfaces, this was more noticeable in the KKU-M055-derived spheroids (Figure 3.12).

## 3.3. Summary and Technical Discussion

CCA spheroid models were successfully established for 5 CCA cell-lines (KKU-M055, KKU-M156, KKU-M213, HuCCA-1 and RBE). Their growth, cell viability and proliferation were found to be cell-line-dependant. KKU-M055 showed the highest cell growth but least spheroid formation. KKU-M156, KKU-M213 and HuCCA-1-derived spheroids showed similar spheroid formation and similar rates of cell growth and proliferation. RBE formed spheroids, but they did not grow over time. Positive CK7 and CK19 expression was confirmed in the cell-line-derived spheroids except for KKU-M055. This in-depth characterisation of the pre-clinical CCA-derived spheroids was a key step to determine their ability to resemble aspects of the *in vivo* tumour and in the validity of their use in the current CCA research.

- **Spheroid formation**

Various cell culture techniques exist to generate *in vitro* spheroids in suspension (Chapter 1, Section 1.6.2.1) (Carlsson & Yuhas, 1984; Kelm, Timmins, Brown, Fussenegger, & Nielsen, 2003; Moscona, 1961; Santini & Rainaldi, 1999; R. M. Sutherland & Durand, 1984). However, the method presented in this project uses ULA coating surfaces that are hydrophilic, biologically inert, and non-degradable. This enables the rapid and highly reproducible formation of spheroids in a time-dependent manner (@CellCultureDish, 2020). This method was chosen since it was already established in the Grabowska Lab for the generation of spheroids from other cancer types, such as breast cancer (Riffle et al., 2017). Additionally, it has been demonstrated that tumour spheroids grown in ULA plates have equivalent growth rates and comparable gradients of proliferation (Vinci et al., 2012). Of the cell densities tested, 1000cells/well was chosen as the standard concentration for further experiments as it was more likely to avoid the generation of necrotic regions. Previous studies have shown that quiescent and necrotic regions become larger with bigger spheroids (Barisam, Saidi, Kashaninejad, & Nguyen, 2018). Additionally, adding a non-gelling concentration of BME to the culture medium prior to centrifugation induced spheroid formation most effectively. BME is a soluble form of basement membrane purified from Engelbreth-Holm-Swarm tumour and it contains laminin-111, collagen IV, heparan sulfate proteoglycan, entactin/nidogen, and several growth factors (Arnaoutova, George, Kleinman, & Benton, 2012). Indeed, the use of Matrigel in

spheroid formation has previously been shown to influence spheroid formation (Badea et al., 2019).

- **Spheroid cell viability and proliferation**

Live/dead staining, AlamarBlue and Ki-67 staining were the methods used to assess spheroid cell viability and proliferation. It is known that spheroids with a >500μm diameter form an organised structure compose of proliferating cells located in the outer zone, few mitosis-starved and poorly oxygenated cells in the intermediate zone, and necrosis in the central zone (Robert M. Sutherland et al., 2020). The results from the live/dead staining of CCA spheroids showed an absence of necrotic core. It was hypothesised that the spheroids do not form a necrotic core or that this method has a limitation when applying it to 3D models that have tight cell-cell contacts or high levels of matrix. Other techniques such as using readily optimised and commercial live/dead staining kits will be considered for characterising the spheroids in subsequent chapters. For instance, using the ethidium homodimer and Ca-AM from suppliers such as Fisher, which has shown to provide good results in 3D models (Ashworth et al., 2020).

Overall, similar results were obtained for both the AlamarBlue assay, and Ki-67. While most proliferating cells on spheroids derived from other cancer cells are seen on the spheroid surface (Pal et al., 2020), Ki-67 positive cells within the CCA spheroids had an alternate distribution. In concordance to the cell viability results, RBE-derived spheroids, did not express Ki-67; but the rest of the spheroids showed increased cell viability over time and high rate of proliferation.

AlamarBlue assay is a powerful method to assess cell viability. Several advantages have been reported (Nakayama, Caton, Nova, & Parandoosh, 1997; Nociari, Shalev, Benias, & Russo, 1998; O'Brien et al., 2000); however, it has its limitations. For instance, it only allows measurement of the metabolic activity of cells rather than the cell number (Rampersad, 2012). Metabolic pathways can be affected by the individual cell reducing ability and by agents affecting mitochondrial activity (Zachari et al., 2014). However, over the time measured, it can be assumed that higher metabolic activity is proportional to higher cell numbers. A more accurate method used to assess proliferation is Ki-67 staining. IHC and IF can be used to detect this protein in tissues and 3D models (Dekkers et al., 2019; Ivanov & Grabowska, 2017). With IHC, the

proteins are visualised with a coloured chromogen and viewed with a brightfield microscope. Whilst with IF, the proteins are visualised with a fluorochrome and viewed with a fluorescence microscope (Vinci et al., 2012). Each of these methods has advantages and disadvantages. One of the advantages of IHC is the permanent staining that can be achieved and therefore samples can be re-imaged after long-term storage. Additionally, tissue architecture and morphology can be easily interpreted in IHC stained slides. However, multiplex IF is a more accurate method if co-localisation is the outcome of the experiment. Nonetheless, the fluorescent signal fades over time. Additionally, it is important to add an isotype control to avoid false positives caused by autofluorescence (StageBio, 2018). Since the outcome of the experiment was to determine cell proliferation by Ki-67 staining, the IHC technique was found to be less time consuming and was therefore used for spheroid characterisation. The spheroid-array method and subsequent IHC requires high level expertise and although its applicability to examine morphology was demonstrated (Ivanov & Grabowska, 2017), having replicates of the conditions was challenging due to problems with array preparation and further sectioning. Therefore, Ki-67 quantification was performed over a low number of technical replicates.

- **Spheroid morphological characterisation**

The spheroid-array was used for spheroid morphological characterisation followed by H&E staining. Additionally, SEM was used to assess the ultrastructure of the models. CCA spheroid morphology and ultrastructure was cell-line-dependent. SEM is a technique that allows the characterisation of the cellular morphology. It can also provide information such as cell-cell interactions, organelle distribution and niches in which cells reside (Jaros, Petrov, Tesarova, & Hampl, 2017). While SEM cannot see features to the same resolution as transmission electron microscope (TEM), it is faster, less restrictive, and can sometimes be performed with limited or no sample preparation (T. Fischer, 2019). These advantages together with having the equipment for SEM available in the collaboration with Thailand, were the reasons for using SEM instead of TEM for assessing the ultrastructure.

Despite all the advantages presented in this chapter regarding the use of spheroids as a pre-clinical model to study CCA, mono-culture cell-line spheroids are not yet fully representative of *in vivo* tumours, since they lack the TME. Spheroids in which tumour

cells are co-cultured with mesenchymal cells, may better contribute to the understanding of the crosstalk between tumour and its TME.

# Chapter 4. The influence of Mesenchymal stem Cells on CCA proliferation in a spheroid model

## 4.1. Introduction

Malignancy of CCA is not only a consequence of cell transformation, but also a result of a complex and fluctuating interaction between cancer cells and supporting stroma in the TME. The presence of a well-grown fibrous stroma negatively correlates with CCA survival, and more recent studies have established its importance in maintaining tumorigenic identity of hepatobiliary tumours (Gentilini, Pastore, Marra, & Raggi, 2018). The highly desmoplastic TME consists of extracellular matrix and CCA stromal cells that are necessary for homeostatic maintenance, structural support, as well as activation of multiple signalling cascades involved in cancer (Adjei & Blanka, 2015; Albini & Sporn, 2007).

MSCs derived from the bone-marrow are multipotent stromal cells that can differentiate into a variety of cell types due to their capacities for self-renewal and proliferation. Under tumorigenic conditions and in response to chemokines and cytokines secreted by cancer cells, they can specifically migrate to primary and metastatic tumours and be 'educated' to proliferate and differentiate into components of the tumour stroma (Chen et al., 2019). Once the MSCs home to a cancer microenvironment, they differentiate and release a wide spectrum of chemokines and growth factors critical for the tumour progression (Ridge, Sullivan, & Glynn, 2017). Some studies showed that enhanced tumour proliferation and metastasis are potentially induced by MSCs (Scherzad et al., 2015). Although the role of MSCs in many cancers has been widely studied, the functional mechanisms underlying MSCs' effects on CCA progression are poorly understood. The few studies that have examined their role showed that iCCA has a large number of infiltrating MSCs (Haga et al., 2015; J. Liu, Han, Liu, & Qin, 2013) and that those MSCs or their conditioned media significantly increased CCA cells proliferation, metastatic potency and chemoresistance both *in vitro* and *in vivo* (Gan et al., 2021; W. Wang et al., 2015).

Given the crucial role of interaction between cancer cells and the supporting TME, the crosstalk between CCA cells and the MSCs was studied. The spheroid model established in the previous chapter was used for the generation of a co-culture CCA spheroid model. Spheroids are a useful model for studying tumour-stroma interactions, as they can be co-cultured with other cell types. Different strategies for generating co-culture spheroids exist, each allowing for a different degree of contact between the cell types (Vis, Ito, & Hofmann, 2020). Through contact, cells can communicate and

stimulate each other. Co-cultures can be divided into two types: direct and indirect. Direct co-cultures facilitate physical contact between the different cell types which allows for communication though their gap junctions and surface receptors (Vis et al., 2020). Indirect co-cultures incorporate a physical separation between cell types, such as the transwell system which incorporates a semi-permeable membrane, enabling signalling via the cell secretome (Vis et al., 2020). Conditioned medium is also an indirect system widely used. In this system the medium is first used for culturing one cell type and then transferred to the second cell type. The medium contains the cell secretome of the first cell type, which then affects the second cell type (Vis et al., 2020). Direct and indirect co-cultures have advantages and disadvantages. In direct co-cultures, intracellular interactions such as the cell-cell and cell-microenvironment interaction and paracrine signalling are present (Kapalczynska et al., 2018). However, contact-dependent and independent interactions cannot be differentiated and at least one cell population has to be labelled (Kapalczynska et al., 2018). In the transwell model, cell types can be separated for further characterisation, but only contact-independent interactions can be studied (Kapalczynska et al., 2018). Similarly, in the conditioned media, only contact-independent effects can be studied; however, the set-up is easy to achieve, well-established, and the simulated interaction is unidirectional (Kapalczynska et al., 2018; Whiteley et al., 2022). Nonetheless, all co-cultures require optimisation in terms of cell ratios and cell media components in order to allow for correct growth of both cell types (Abbott & Kaplan, 2015).

In the first part of this chapter the steps to develop luminescence CCA cell-lines are described in order to specifically track the growth of the cancer cells within co-cultures. The co-culture system is established by culturing CCA cells with MSCs, and the effect of cell proliferation by using different ratios are characterised. The difference between direct and indirect co-culture (transwell system) is also compared. These systems are illustrated in Figure 4.1. Finally, the model is characterised by Ki-67, Vimentin, CK7 and CK19 staining.

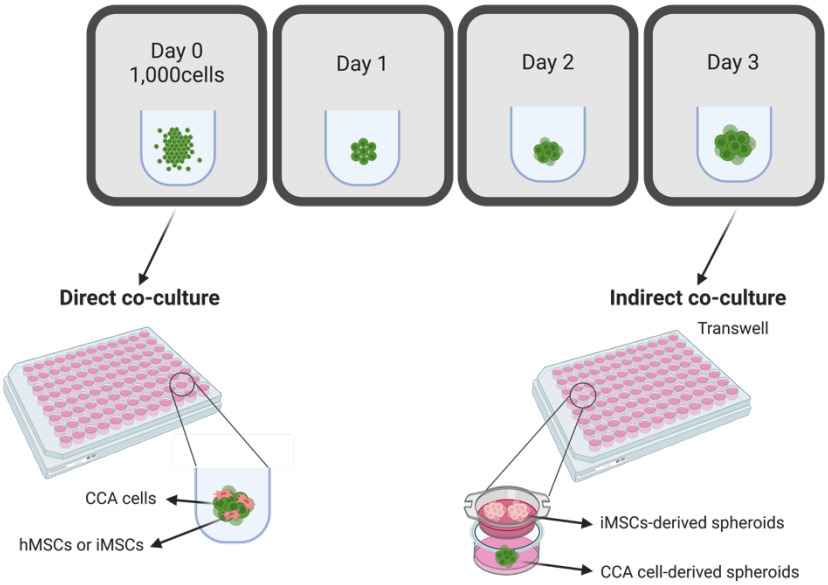



**Figure 4.1. Diagram of the direct and indirect co-culture of CCA and MSCs.** Direct co-cultures facilitate physical contact between the different cells. Indirect co-cultures incorporate a physical separation between cell types. The transwell system incorporates physical separation in the form of a transwell system using a semi-permeable membrane.

## 4.2. Results

### 4.2.1. Generation of stable CCA luciferase-transduced cell-lines

One of the primary challenges of the co-culture system is determining which cell receives, processes, and transmits signals. Therefore, in order to assess the growth and behaviour of the cancer cells within the co-culture, the population was transduced with a luminescent reporter. Bioluminescence (BL) has been widely used in the Grabowska Lab, especially in assessing the tumour behaviour following implantation in host animals, and tracking cancer cells in spheroid models derived from other types of cancer (Pal et al., 2020). The principal chemical reaction in BL involves a light-emitting molecule and an enzyme, called luciferin and luciferase, respectively. CCA cell-lines were transduced with a lentivirus to incorporate the firefly luciferase gene (Chapter 2, Section 2.3.1). This was carried out by Pam Collier, a research assistance in the Grabowska Lab. Lentivirus carries the firefly luciferase gene and the puromycin resistance gene driven by a cytomegalovirus promoter. This allows generation of firefly luciferase positive cells clones by puromycin selection. Thus, the first step towards the generation of a fully transduced population of cells, was to determine the concentration of puromycin required to kill non-transduced cells (Chapter 2, Section

2.3.1). This was accomplished by performing a kill curve where the cells were subjected to increasing amounts of antibiotic (0 to 8µg/mL) to determine the minimum concentration needed to kill all the cells over the course of 2 to 8 days. The concentration was determined for the 5 CCA cell-lines (KKU-M055, KKU-M156, KKU-M213, HuCCA-1 and RBE). $1\times10^4$ wild-type cells were seeded in a 96-well plate and incubated 24 hours to allow cell attachment. Four replicates were performed for each condition and incubated for 72h. AlamarBlue assay (Chapter 2, Section 2.5.1) was used to assess the viability of the cells after treatment.

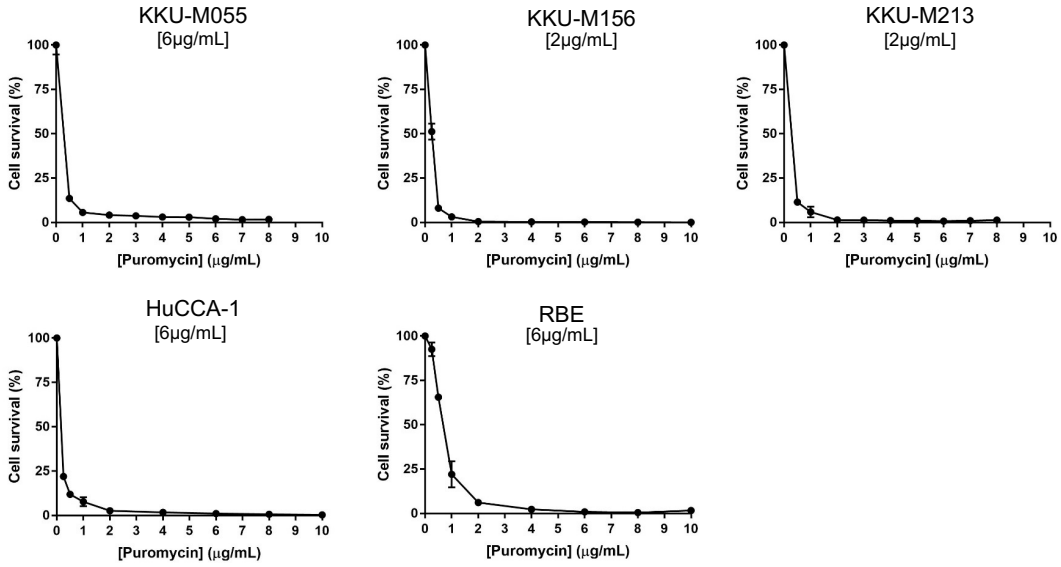



**Figure 4.2. Puromycin kill curves of CCA wild-type cells.** $1.0\times10^4$ of KKU-M055, KKU-M156, KKU-M213, HuCCA-1 and RBE wild-type cells were seeded in a 96-well plate for 24h. A range of puromycin concentrations (0 to 8µg/mL) was added in 4 replicates wells during 72h. Cell viability was determined using the AlamarBlue assay and cell survival was calculated relative to untreated cells (Mean ± SEM).

The concentration was found to be cell type dependent. KKU-M156 and KKU-M213 cells were killed when 2µg/mL of puromycin was used; however, a higher concentration, 6µg/mL was needed to kill all the KKU-M055, HuCCA-1 and RBE cells (Figure 4.2). After determining the concentration of puromycin required to kill non-transduced cells, the BL signal intensity was determined. This work was done in parallel to the mono-culture spheroid characterisation, and therefore TFK-1 cells were still included for luciferase transduction. It was after this work that the cell-line was excluded from any further work as it tested positive for mycoplasma. HuCCA-1 cells

also had an issue with sub-culturing, and they could not be included for luciferase transduction, though they tested negative for mycoplasma.

A series of cell densities of luciferase-transduced cells were prepared and seeded into a 96-well black plate with clear bottom in triplicate wells. At day 1 of culture the signal was measured after adding the substrate, D-luciferin, and incubating for 15 minutes (Chapter 2, Section 2.5.4). For high sensitivity and high resolution, an IVIS was used for reading the BL as well as a dedicated software integrated in a microplate reader (Chapter 2, Section 2.3.1). Results were compared to a positive control cell-line (MDA-MB-231), which had been successfully used multiple times for *in vivo* experiments. Additionally, for those cell-lines with a signal similar to the positive control, the signal was determined over the time in order to confirm the signal stability.

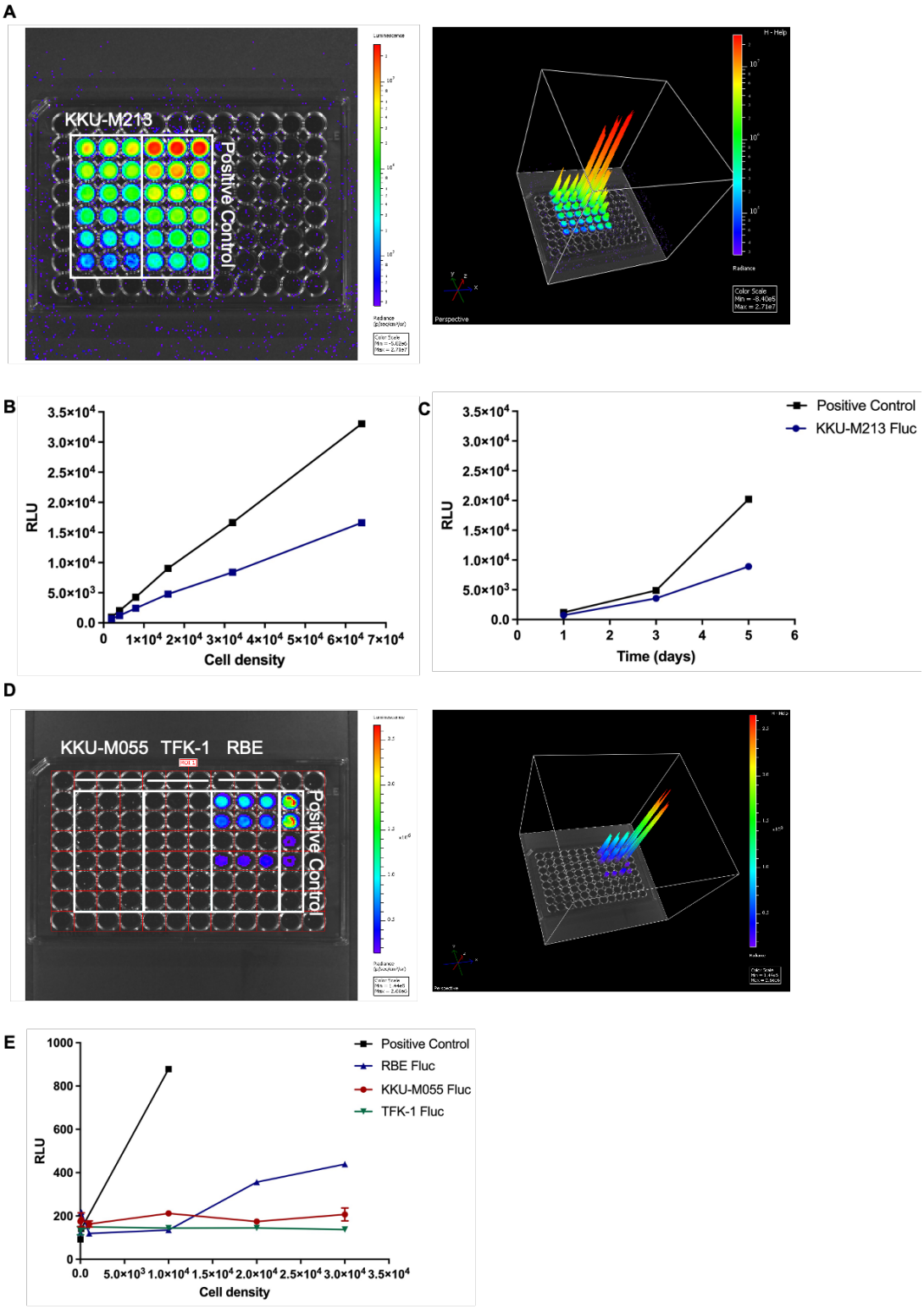



**Figure 4.3. First attempt to generate bioluminescent transduced CCA cells.** A range of KKU-M213, KKU-M055, TFK-1, RBE and MDA-MB-231 Fluc (positive control, PC) cell densities were seeded in a Corning Ultra-Web 96-well plates in triplicate wells. At day 1, the bioluminescence intensity was determined by adding D-luciferin and imaged in an *In Vivo* Imaging System **(A, D)** and read in a microplate reader (Mean ± SEM) **(C, E)**. Cell growth over time was also determined by adding D-luciferin at day 1, 3 and 5 **(B)**.

The BL intensity increased proportionally with increasing KKU-M213 cell numbers similar to the positive control (Figure 4.3A). RBE cells showed an attenuated signal compared to KKU-M213 cells. No signal was detected for the other cell-lines (Figure 4.3D and E). The stability of the luciferase activity in KKU-M213 was also confirmed (Figure 4.3C).

Transduction was repeated for RBE, TFK-1, KKU-M055 and KKU-M156 cells. Wild-type cells in 1:2 serial dilutions were seeded in a 96-well plate and incubated overnight for cell attachment and further lentiviral transduction. Once the transduction was done, cells were treated with puromycin according to the concentrations previously determined (Figure 4.2). Cells resistant to the antibiotic treatment were seeded into a 96-well black plate with clear bottom in triplicate wells.

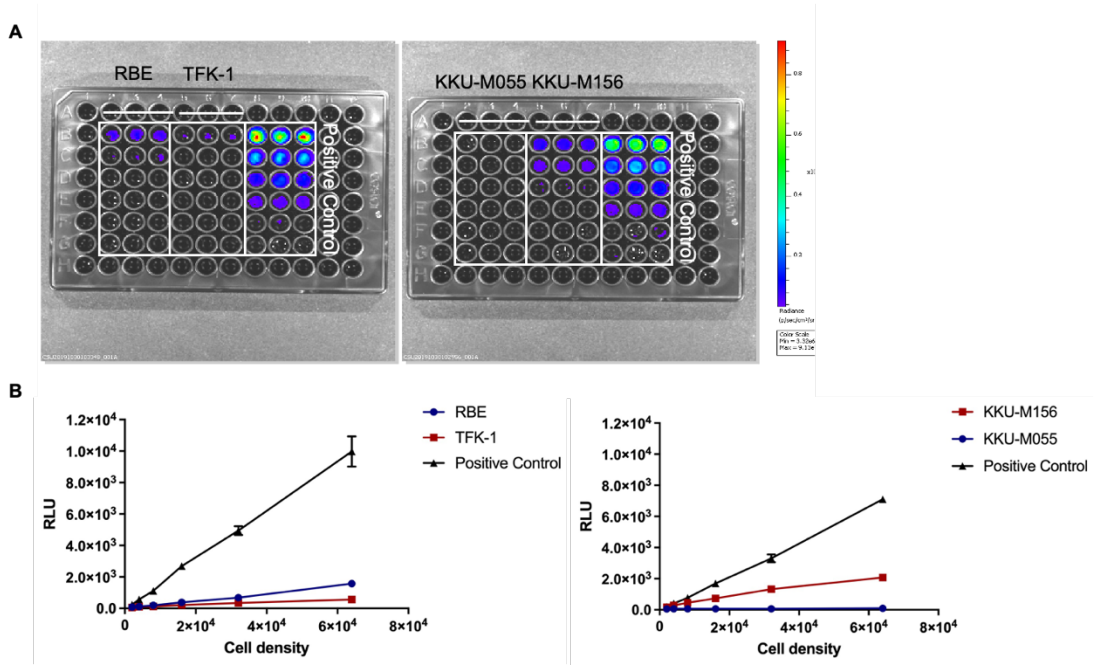



**Figure 4.4. Second attempt to generate bioluminescent transduced CCA cells.** A range of RBE, TFK-1, KKU-M055 and KKU-M156 and MDA-MB-231 Fluc (positive control, PC) cell densities were seeded in a Corning Ultra-Web 96-well plates in triplicate wells. At day 1, the bioluminescence intensity was determined by adding D-luciferin and imaged in an *In Vivo* Imaging System **(A)** and read in a microplate reader (Mean ± SEM) **(B)**.

Similar to the previous results, RBE and KKU-M156 cells showed an attenuated BL signal compared to the positive control. No signal was detected for the KKU-M055 cells (Figure 4.4A and B).

It is important to highlight that the BL intensity is cell-line dependent, and the positive control is a well-established cell-line for *in vivo* use. Therefore, $1\times10^4$ wild-type KKU-M055, KKU-M156 and RBE cells were seeded but this time the signal was compared to their corresponding wild-type cells instead of the positive control. After 24 hours the signal was measured after adding D-luciferin and incubating for 15min. The signal was read using the microplate reader (Chapter 2, Section 2.5.4).

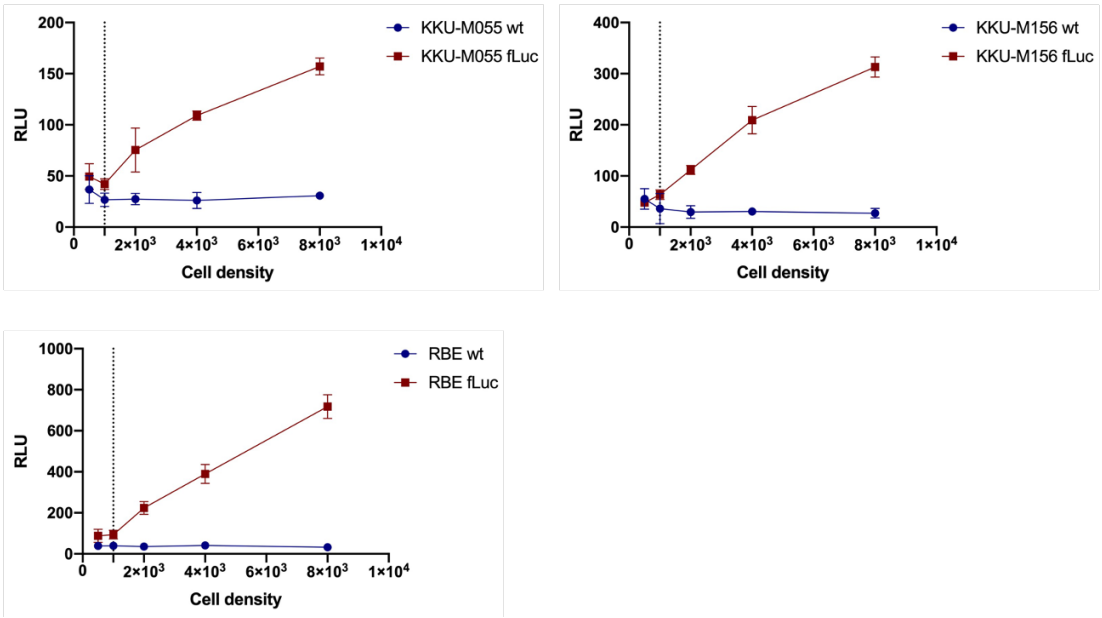



**Figure 4.5. Bioluminescent signal from transduced cells compared to their corresponding wild-type.** A range of KKU-M055, KKU-M156 and RBE densities were seeded in a Corning Ultra-Web 96-well plates in triplicate wells. At day 1, the bioluminescence intensity was determined by adding D-luciferin and read in a microplate reader. The dot line indicates the starting concentration.

Interestingly, when KKU-M055, KKU-M156 and RBE were compared to their corresponding wild-type, cells emitted BL signal. This signal increased when the cell density was increased (Figure 4.5). This result confirmed that the transduction was successful although the signal was weak relative to MDA-MB231-fluc cells, and therefore, they could be further used for the co-culture system although not for *in vivo* applications.

### 4.2.2. Effect of different co-culture ratios of CCA cells to hMSCs on CCA proliferation

Once cell-lines were confirmed to be luminescent, the next step was to establish the co-culture system by culturing them with hMSCs. Another challenge when co-culturing two types of cells is to keep a ratio between the two cell types that reflects the *in vivo* setting, considering the proliferation rate of each cell type and their characteristics when cultured *in vitro*. KKU-M213 cells and hMSCs were first used. Cell types were cultured alone (as mono-cultures) or at a cancer cell:hMSCs ratio of 2:1, 1:1 and 1:2 for 7 days. 1000cell/well was the starting cell density for all conditions. Both cell types were mixed together in each well and the plate was centrifuged for 10 minutes at 300g (Chapter 2, Section 2.3.2). The proliferation was determined every 2 days by adding D-luciferin and values were normalised to day 0. Qualitative assessment of the spheroid area was substantiated by quantitation in Fiji analysis software (Chapter 2, Section 2.5.5). This experiment was carried out in biological duplicates.

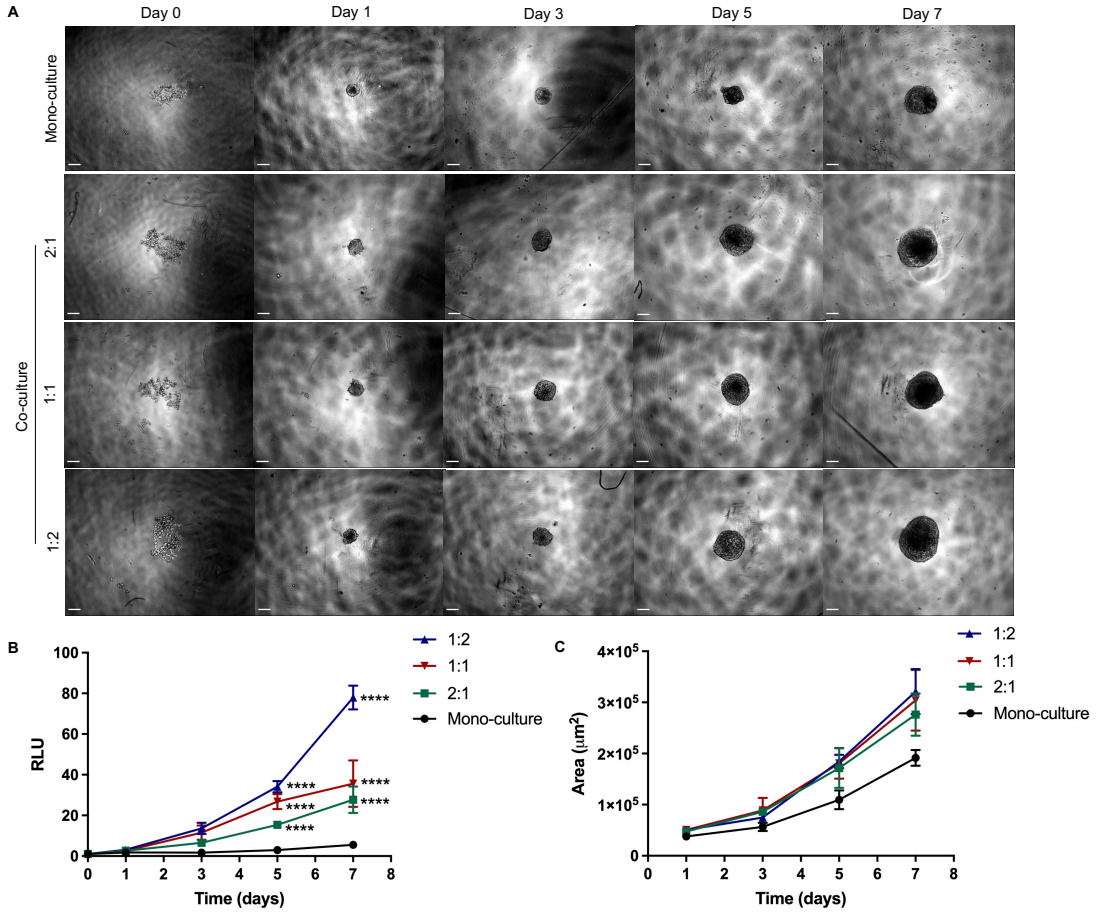



**Figure 4.6. Different ratios of KKU-M213 and hMSCs co-culture spheroids.** Cancer KKU-M213 cells were mono-cultured or co-cultured at a cancer cell:hMSCs ratio of 2:1, 1:2 and 1:1 into an ULA 96-well round bottom plate at a final cell density of 1000cells/well with 100µg/mL of BME. Spheroids were imaged at day 0, 1, 3, 5 and 7. Representative spheroids are shown (scale bars = 200µm) **(A)**. Progressive growth of the spheroid was monitored in triplicate wells by adding D-luciferin at day 1, 3, 5 and 7. Values were normalised to day 0 (Mean ± SEM). Co-cultures were compared to the mono-culture via two-way ANOVA (N=2) ****(p<0.0001) **(B)**. The area of the spheroid was determined in 4 replicate wells on days 1, 2, 3, 5, 6 and 7 using ImageJ Fiji (Mean ± SEM) **(C)**.

Spheroid growth rate, after day 3, was increased when in the hMSC co-cultures, as evidenced by the brightfield images (Figure 4.6A). Notably, a similar pattern of cell proliferation was observed in all the cell ratios. However, after day 3, the ratio that showed the highest proliferation was 1:2 (Figure 4.6B). At day 5 and 7, the signal of the mono-culture compared to the 2:1 ($p<0.0001$), 1:1 ($p<0.0001$) and 1:2 ( $p<0.0001$) co-culture ratios was significantly increased (Figure 4.6B).

To further characterise the KKU-M213 co-culture spheroid, spheroid-arrays were conducted (Chapter 2, Section 2.6.1). KKU-M213 cells were cultured at the same ratios, fixed, paraffin embedded and sectioned. Sections were H&E and Ki-67 stained.

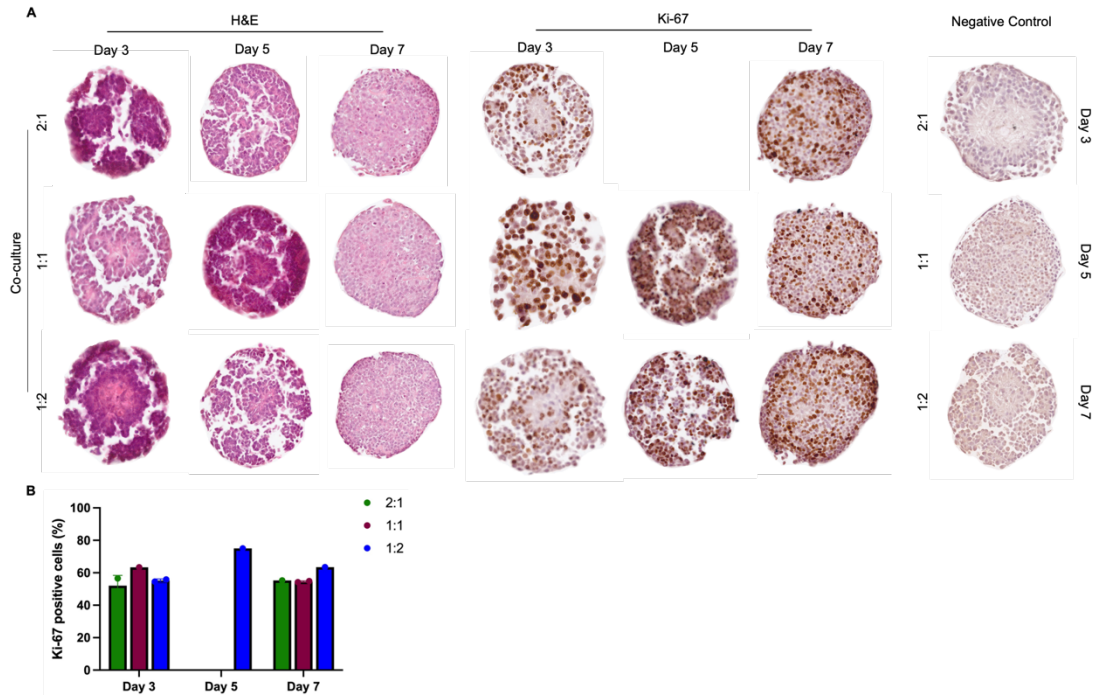



**Figure 4.7. Spheroid internal structure and morphology.** 1000 cells from KKU-M213 cells were hMSCs co-cultured at a ratio of 2:1, 1:1 1:2 (cancer cells:hMSCs) into an ULA 96-well round bottom plate with 100µg/mL of BME. CCA spheroids were fixed at day 5 of culture, paraffin embedded, sectioned, and stained with H&E and Ki-67. Representative spheroids are shown (microscope objective = 20X) **(A)**. Positive Ki-67 expression was quantified by manually counting the positive cells and cancer cells and calculating the ratio of positively stained cancer cells over the total of cancer cells on days 3, 5 and 7 **(B)**.

H&E results showed that spheroids became dense over time in the co-culture model with a compact internal structure at day 7, at all ratios tested. The Ki-67 positive cells (dark brown nuclei) were distributed across the whole cross-section. At day 3, Ki-67 staining seemed equal between spheroids with different cancer cell:hMSC ratios. However, higher expression of the marker was found in the 1:2 cancer cell:hMSC ratio at day 5 and 7, which correlates to the BL results (Figure 4.6 and 4.7).

### 4.2.3. Effect of hMSCs and iMSCs on CCA proliferation in a direct co-culture system

HMSCs are primary cells, and their *in vitro* lifespan is limited. Some issues were experienced whilst growing them in culture, which ultimately proved limiting. Therefore, an immortalised source of mesenchymal stem cells (iMSCs) was obtained from a collaboration with Dr James Dixon, (an Associate Professor in the Biodiscovery Institute, University of Nottingham) (Chapter 2, Section 2.1). These cells were grown

*in vitro* and the proliferation of the iMSCs and KKU-M213 co-cultures was determined. If iMSCs also enhanced proliferation, then these cells could be used alternatively during the study of the effect of MSCs on CCA proliferation.

KKU-M213 were cultured alone (as mono-cultures) or at a cancer cell:iMSCs or cancer cell:hMScs ratio of 1:2. 1000cell/well was the starting cell density for all conditions. The proliferation was determined every 2 days by adding D-luciferin, and values were normalised to day 0. Qualitative assessment of the area was substantiated by quantitation in Fiji analysis software. Three biological replicates were carried out.

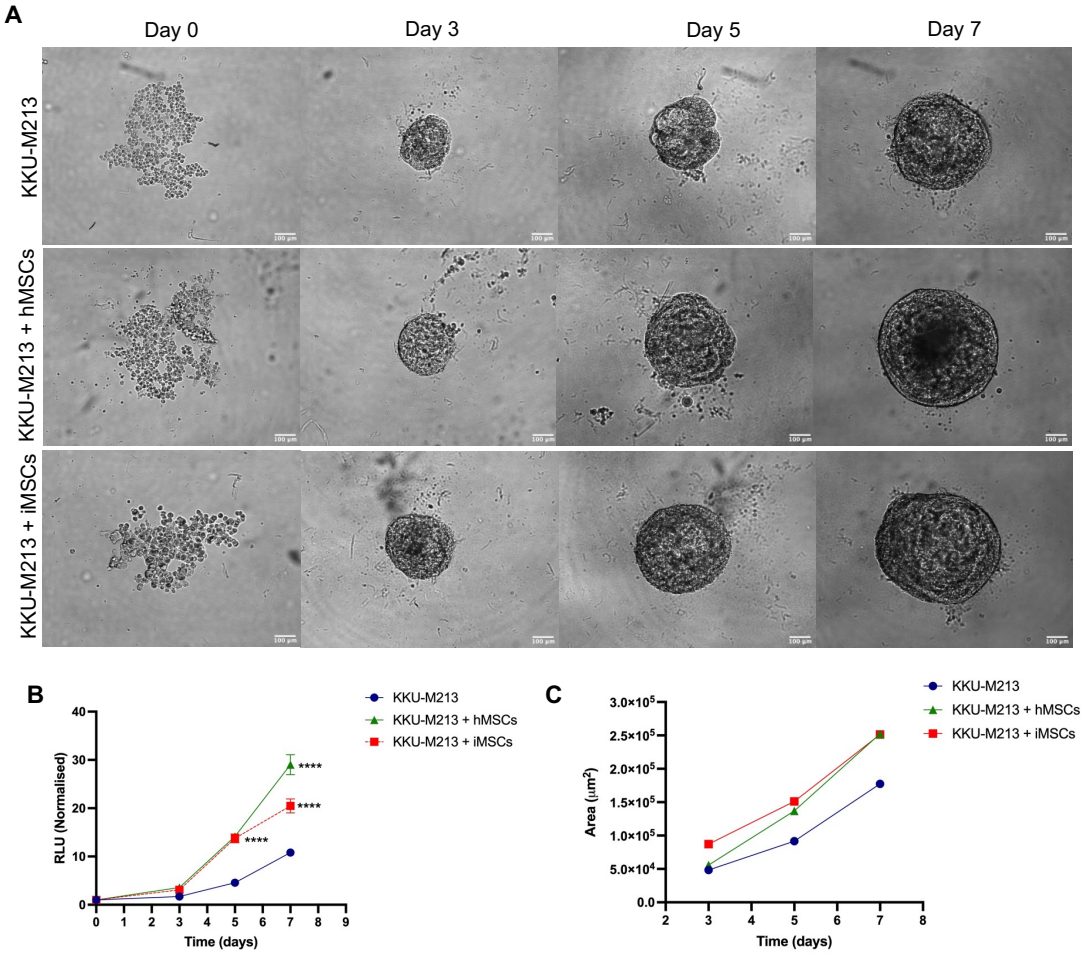



**Figure 4.8. Growth of KKU-M213 cells in co-culture with hMSCs or iMSCs.** Cancer KKU-M213 cells were mono-cultured or co-cultured at a cancer cell:hMSCs/iMSCs ratio of 1:2 into an ULA 96-well round bottom plate at a final cell density of 1000cells/well with 100µg/mL of BME. Spheroids were imaged at day 0, 3, 5 and 7 **(A)**. Progressive growth of the spheroid was monitored in triplicate wells by adding D-luciferin at day 0, 3, 5 and 7. Representative spheroids are shown. Values were normalised to day 0 (Mean ± SEM). Co-cultures were compared to the mono-culture via two-way ANOVA (N=2) ****($p<0.0001$) **(B)**. The area of the spheroid was determined in triplicate wells on days 3, 5 and 7 using ImageJ Fiji (Mean ± SEM) **(C)**.

Spheroid growth rate and area were significantly increased when co-cultured with both MSCs (Figure 4.8A). After day 3 and 5, the increase in area of both co-cultures was similar, though larger compared to the mono-culture (Figure 4.8C). At day 7, KKU-M213 co-culture spheroids with hMSCs and iMSCs reached a significantly larger area up to $2.5\times10^5\mu m^2$, compared to the KKU-M213 mono-culture spheroids which reached up to $1.6\times10^5\mu m^2$. Furthermore, the growth of the spheroids was significantly supported by both MSCs (Figure 4.8B). The addition of hMSCs and iMSCs significantly enhanced cell proliferation. At day 5, the difference between both co-cultures was almost identical ($p<0.0001$); however, at day 7, hMSCs ($p<0.0001$) enhanced KKU-M213 proliferation more than iMSCs ($p<0.0001$).

Selecting the ratio for the co-culture model that gives the best results in terms of proliferation; and confirming that the source of iMSCs also enhanced proliferation was achieved. The next step was to generate the co-cultures using the rest of the CCA cell-lines and compare their proliferation with the respective mono-cultures. Therefore, KKU-M055, KKU-M156, HuCCA-1 and RBE were grown as mono-cultures or at a cancer cell:iMSCs ratio of 1:2. Three biological replicates were carried out.

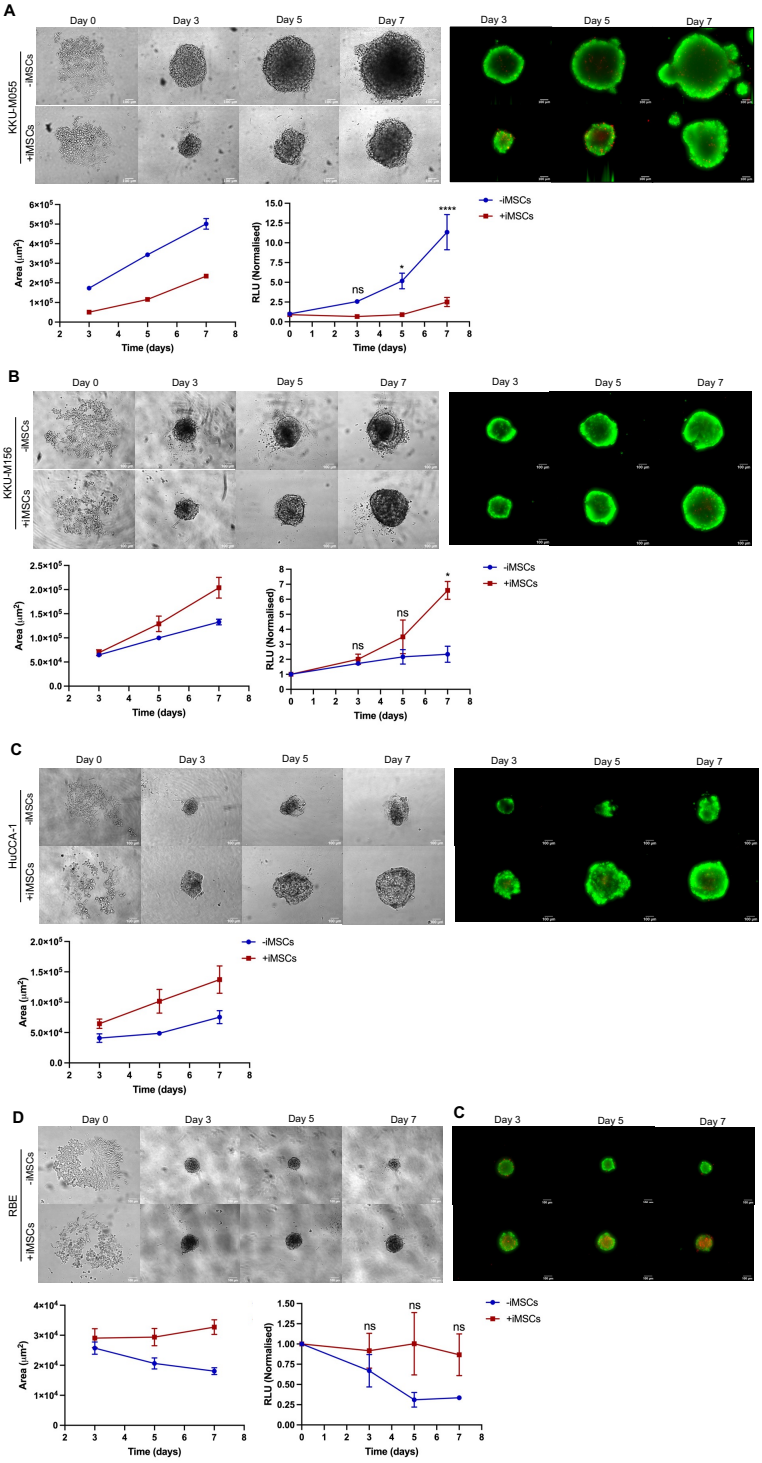



**Figure 4.9. Effect of iMSCs on CCA-derived spheroid proliferation in a direct co-culture system.** Cancer KKU-M055 **(A)**, KKU-M156 **(B)**, HuCCA-1 **(C)** and RBE **(D)** cells were mono-cultured and iMSCs co-cultured at 2:1 ratio (cancer cells:iMSCs) into an ULA 96-well round bottom plate at a final cell density of 1000cells/well with 100µg/mL of BME. Spheroids were imaged at day 0, 3, 5 and 7. Live/dead staining was monitored in triplicates after establishing in spheroid-shape on days 3, 5 and 7 using Ca-AM (green - live cells staining) and EthD-1 (red - dead cells staining). The area of the spheroid was determined in triplicate wells on days 3, 5 and 7 using ImageJ Fiji (Mean ± SEM). Progressive growth of the spheroid was monitored in triplicate wells by adding D-luciferin at day 0, 3, 5 and 7. Representative spheroids are shown (scale bars = 100µm). Values were normalised to day 0 (Mean ± SEM). Co-cultures were compared to the mono-culture via two-way ANOVA (N=2) ns($p>0.05$), *($p<0.05$) and ****($p<0.0001$).

All spheroids showed positive cell viability during the culture period apart from RBE. However, it was observed that spheroid growth and spheroid formation was supported in iMSCs co-culture in a cell-line dependent manner. Spheroid growth of KKU-M156, HuCCA-1 and RBE was strongly dependent on the addition of iMSCs, whereas the spheroid growth of KKU-M055 was higher in the mono-culture ($p=0.0151$ at day 5 and $p<0.0001$ at day 7). When looking at KKU-M055 co-culture spheroids, a clear and well-defined spheroid border was noticed compared to the mono-culture. This was also reflected in the spheroid growth and area (Figure 4.9A). Growth of KKU-M156-derived spheroids was similar to that of the KKU-M213-derived spheroids. The addition of iMSCs significantly supported KKU-M156 spheroid growth at day 7 ($p<0.0001$) and area (Figure 4.9B). Although RBE spheroid formation was strongly supported in iMSCs co-cultures, there was no significant difference in growth between mono- and co-culture spheroids. Interestingly, a necrotic core was formed when cells were in iMSCs co-cultures (Figure 4.9D). Finally, HuCCA-1-derived spheroids formed a slightly loose spheroid; however, co-culture spheroids form a compact spheroid with a well-defined border (Figure 4.9C). HuCCA-1 cells were not luminescent and therefore the RLU data was not available.

### 4.2.4. Effect of iMSCs on CCA proliferation in an indirect co-culture system

Although the direct co-culture system reflects the cell–cell interaction *in vivo* and is a promising approach to study the crosstalk between cancer cells and MSCs; one disadvantage is that the signalling of one cell to another cannot be easily evaluated. Therefore, this could be a limitation when interpreting data from techniques such as RNASeq. In indirect co-culture systems, where two or more cell types are physically separated and cultured under the same conditions, paracrine signalling can still occur and the effect of co-culture on growth and behaviour of one or both cell types can be assessed (Kapalczynska et al., 2018; Whiteley et al., 2022). To evaluate whether direct cell–cell interaction was important for the observed effects on cell growth in co-culture spheroids, an indirect co-culture model was optimised. The transwell co-culture system was chosen over the conditioned media approach.

KKU-M055, KKU-M156, KKU-M213 and RBE-derived spheroids were physically separated from iMSC-derived spheroids. HuCCA-1 cell-line was not included in the panel since it was not luminescent, and the results would not be comparable to the rest of the cell-lines. CCA and iMSCs spheroids were grown independently in a 96-well

ULA plate. At day 3, CCA spheroids were placed at the lower section of the transwell, whereas the iMSCs spheroids were cultured in the inserts (Figure 4.1) (Chapter 2, Section 2.3.3). In order to compare the outcome of this assay to the direct co-culture, the ratio cancer cells:iMSCs was maintained by placing one CCA-derived spheroid and two iMSCs-derived spheroids. Two biological replicates were performed.

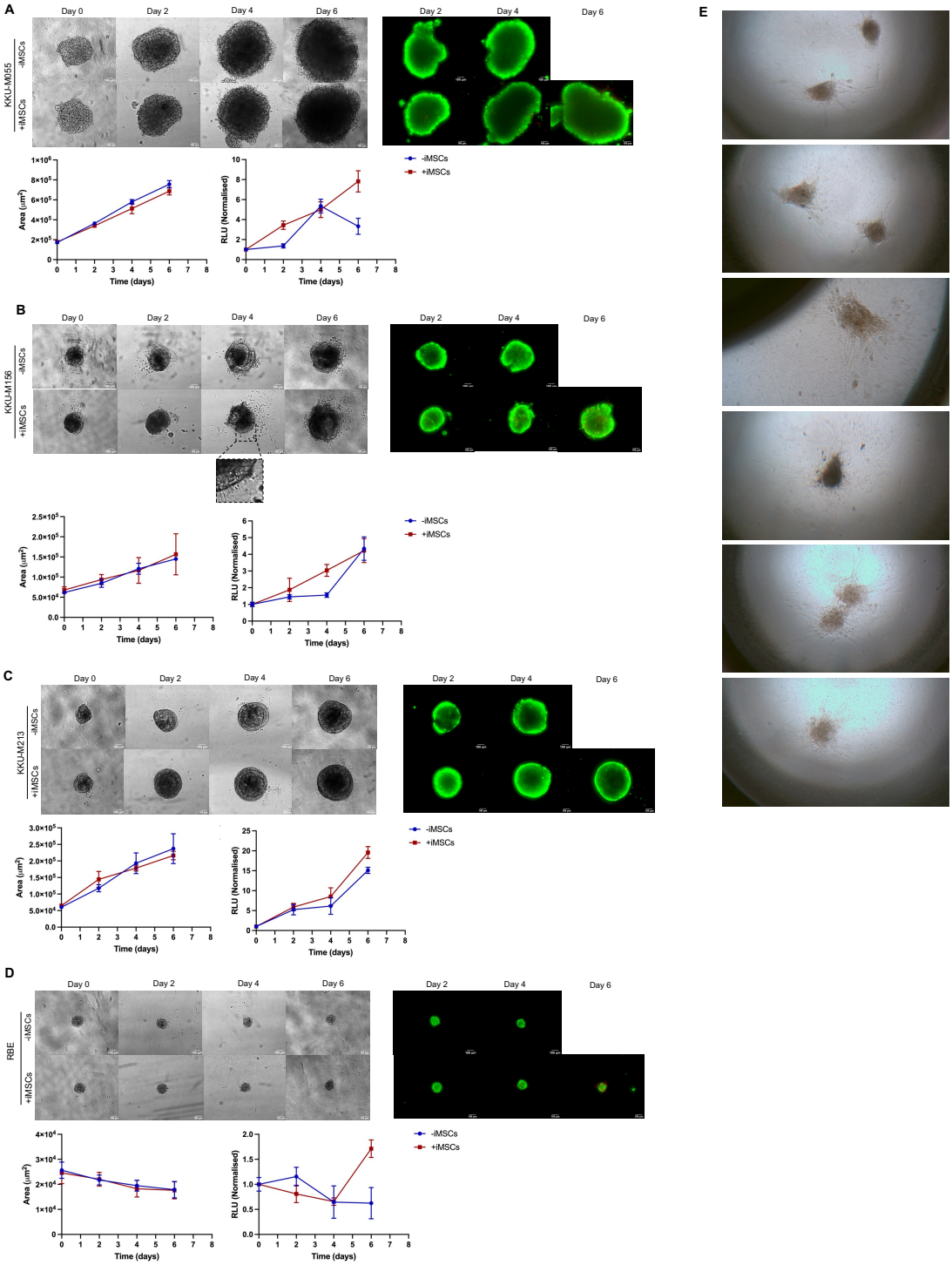



**Figure 4.10. Effect of iMSCs on CCA-derived spheroids in a co-culture transwell system.** Cancer KKU-M055 **(A)**, KKU-M156 **(B)**, HuCCA-1 **(C)** and RBE **(D)** cells were indirectly cultured in mono- and iMSCs co-culture at 1:2 ratio (cancer cells:iMSCs) into an ULA 96-well round bottom plate with 100µg/mL of BME. Spheroids were imaged at day 0, 3, 5 and 7. Live/dead staining was monitored in triplicates after establishing in spheroid-shape on days 3, 5 and 7 using Ca-AM (green - live cells staining) and EthD-1 (red - dead cells staining). The area of the spheroid was determined in triplicate wells on days 3, 5 and 7 using ImageJ Fiji (Mean ± SEM). Progressive growth of the spheroid was monitored in triplicate wells by adding D-Luciferin at day 0, 3, 5 and 7 (Mean ± SEM). Representative spheroids are shown (scale bars = 200µm). At day 5, the morphology of the iMSCs-derived spheroids on the transwell was assessed using a brightfield microscope **(E)**.

Spheroid area was not affected by iMSCs co-culture, and notably iMSCs did not impact cell proliferation in KKU-M156 and KKU-M213-derived spheroids (Figure 4.10B and C). Interestingly, KKU-M156 co-culture spheroids showed some spindles (Figure 4.10B). For KKU-M055 and RBE cells, iMSCs co-culture seemed to slightly increase proliferation after day 5, although the area remained the same (Figure 4.10A and D). The MSC-derived spheroids grown in the transwell setting were also imaged in the indirect system. Interestingly, the results showed the formation of a tube that adhered the spheroids to the transwell. In addition, some of the spheroids that were close to each other merged forming a single iMSC-derived spheroid that also formed tubes to attach to the transwell (Figure 4.10E).

In order to directly compare spheroid proliferation of cancer cells and iMSCs (direct or indirectly co-cultured), the ratio of the RLI signal and the area of mono-culture/co-culture was calculated.

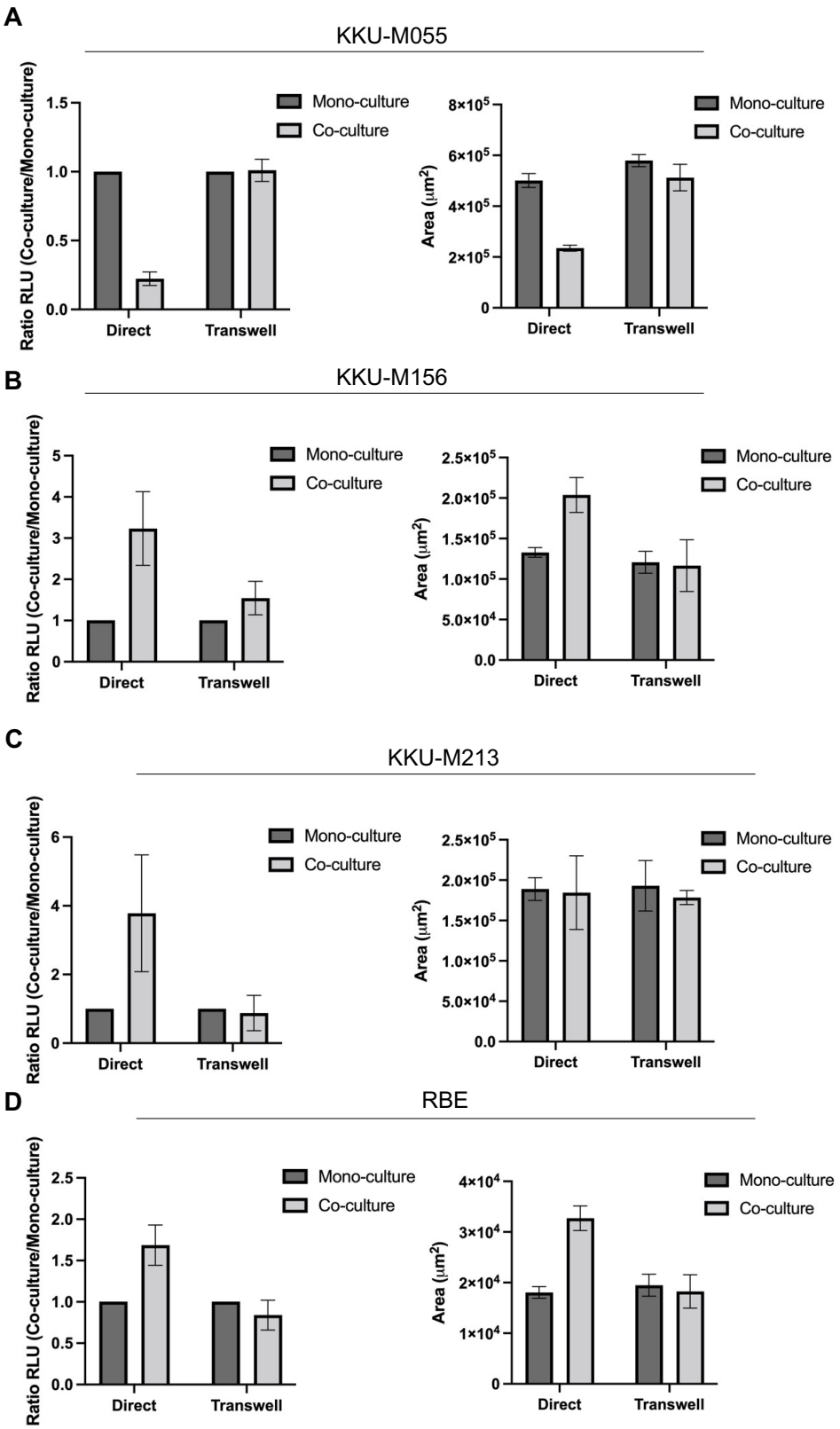



**Figure 4.11. Comparison between the direct and transwell system at day 5.** Cancer KKU-M055 **(A)**, KKU-M156 **(B)**, HuCCA-1 **(C)** and RBE **(D)** cells were mono-cultured and iMSCs co-cultured at 2:1 ratio (cancer cells:iMSCs). Progressive growth of the spheroid was monitored in triplicate wells by adding D-Luciferin at day 5. The area of the spheroid was determined in triplicate wells on days 3, 5 and 7 using ImageJ Fiji. Ratios were calculated by normalising to the matched mono-culture (Mean ± SEM).

The overall results from the direct co-culture showed that MSCs promoted proliferation of the KKU-M156, KKU-M213 and RBE cells. As previously shown, the MSCs had the opposite effect for KKU-M055 (Figure 4.10A and 4.11A). Alternatively, in the indirect co-culture, the growth of the KKU-M055, KKU-M213 and RBE, was the same as the mono-culture spheroids (Figure 4.11B-D). However, KKU-M156-derived spheroids showed a slightly higher proliferation compared to the mono-culture in the indirect system (Figure 4.11B). The ratio of the area showed similar results to the proliferation. Though, whilst a large increase in area was noticed on the direct system, no difference was found on the indirect system for any of the CCA-derived spheroids (Figure 4.11).

### 4.2.5. Morphology of the mono- and co-culture spheroids

The direct co-culture system was chosen to further investigate. The spheroid-array methodology was performed for a more in-depth analysis and characterisation of the model. The internal morphology between the mono-cultures and the co-cultures (with iMSCs) was compared by H&E staining. KKU-M055, KKU-M156, HuCCA-1 and RBE cells were grown as mono- and iMSCs co-culture, and at day 5 they were fixed. KKU-M213-derived spheroids were grown as mono- and iMSCs co-culture spheroids and fixed at day 3, 5 and 7. Additionally, KKU-M213 were co-cultured with hMSCs and fixed at day 5. All fixed spheroids were paraffin-embedded, sectioned and H&E stained (Chapter 2, Section 2.6.3) (technical replicates are in Appendix A, Figure A1 and Figure A2).

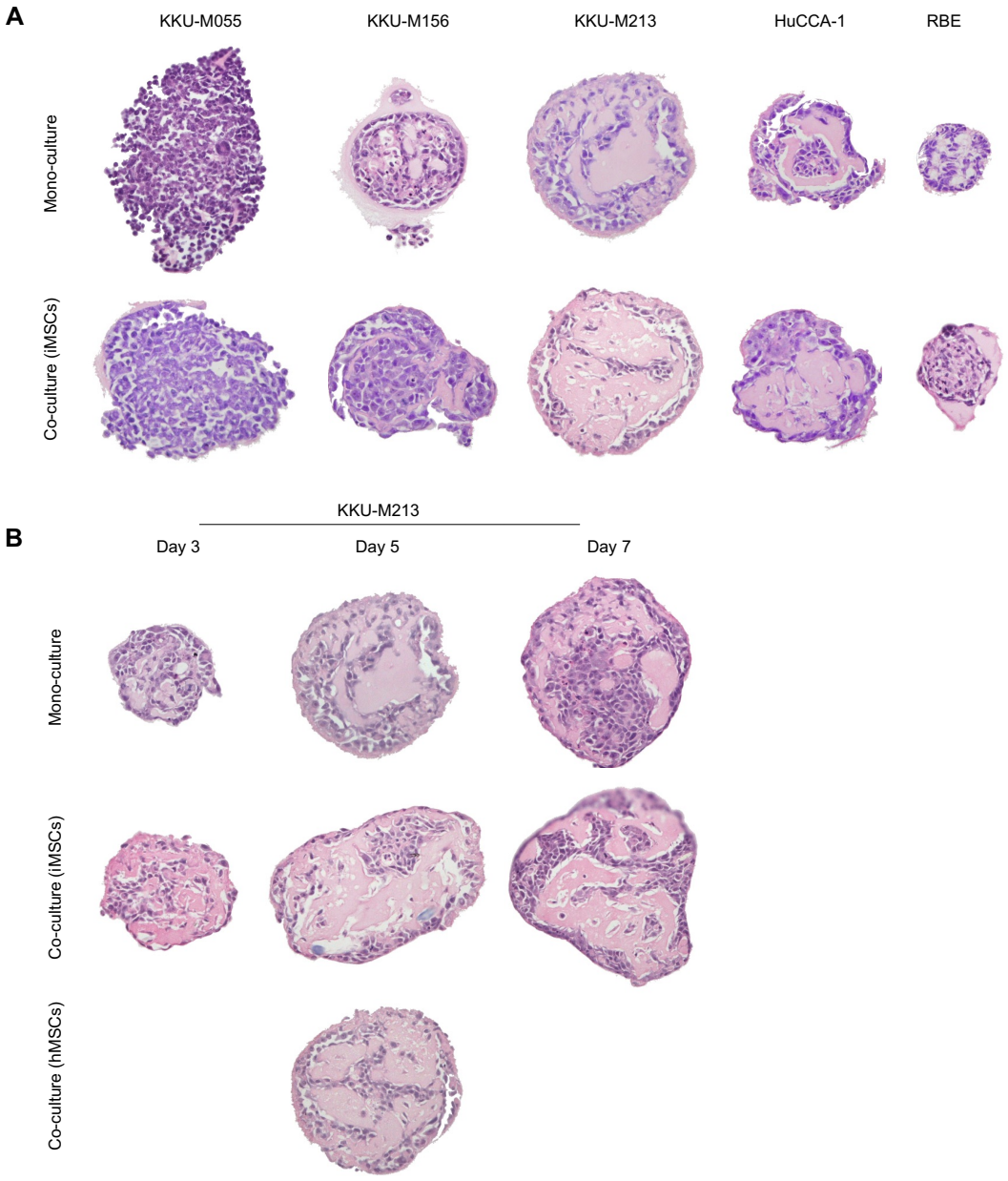



**Figure 4.12. Internal morphology of mono- and co-culture CCA spheroids.** 1000 cells from 5 CCA cell-lines (KKU-M055, KKU-M156, KKU-M213, HuCCA-1 and RBE) were mono-cultured or iMSCs co-cultured at a ratio of 1:2 (cancer cells:iMSCs or hMSCs) into an ULA 96-well round bottom plate with 100µg/mL of BME. CCA spheroids were fixed at day 5 of culture, paraffin embedded, sectioned, and stained with H&E **(A)**. KKU-M213 mono- and iMSCs co-cultures were fixed, paraffin embedded, sectioned and stained with H&E on day 3, 5 and 7. HMSCs and KKU-M213 co-cultures (ratio 1:2, cancer cells:hMSCs) were also fixed at day 5, paraffin embedded, sectioned, and stained with H&E **(B)**. At least 6 spheroids were embedded in the array from each condition. Representative spheroids are shown (microscope objective = 20X).

Interestingly, the internal structure of KKU-M055-derived spheroids was similar in both mono- and co-culture spheroids. However, the internal structures of the KKU-M213 and HuCCA-1 co-culture was different to the mono-cultures. Although the

mono-cultures formed internal structures with no cells inside them, these structures were more apparent in the co-culture spheroids. KKU-M156 mono-culture spheroids had a non-cellular, well-defined periphery. This structure was also present on the co-culture RBE spheroids (Figure 4.12A). The morphology of the cells within the spheroids was similar and therefore cancer cells could not be differentiated from iMSCs cells. A more detailed characterisation was performed for the KKU-M213-derived spheroids, where the H&E was performed at day 3, 5 and 7 after seeding. The H&E results of the hMSCs co-culture were also obtained for this cell-line. The results demonstrated that on day 5 and 7 the layer of cells was arranged close together and appeared densely packed in both mono- and co-culture spheroids, compared to day 3. Spheroids were larger in size when co-cultured with either type of MSC, and the presence of internal structures were more noticeable for the co-culture spheroids (similar to the KKU-M156 and HuCCA-1 cell-lines). No difference was found between the two types of co-culture in terms of histology (Figure 4.12B).

### 4.2.6. Characterisation of the cellular proliferation mono- and co-culture spheroids

To continue the comparison between mono- and co-culture spheroids, the expression of Ki-67 was determined. The previous conditions were used but spheroids were stained with Ki-67 (Chapter 2, Section 2.6.4) (technical replicates are in Appendix A, Figure A1 and Figure A2).

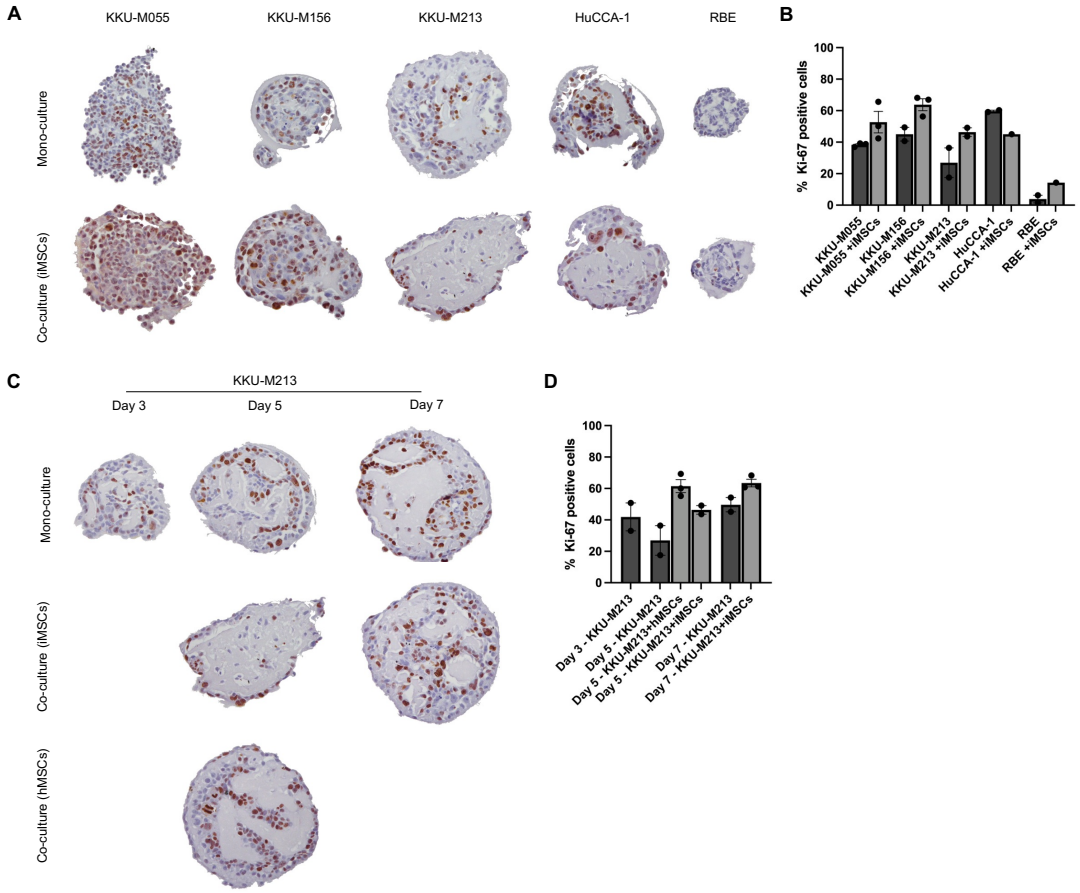



**Figure 4.13. Characterisation of the cellular proliferation of the CCA spheroids.** 1000 cells from 5 CCA cell-lines (KKU-M055, KKU-M156, KKU-M213, HuCCA-1 and RBE) were mono-cultured or iMSCs co-cultured at a ratio of 1:2 (cancer cells:iMSCs) into an ULA 96-well round bottom plate with 100µg/mL of BME. CCA spheroids were fixed at day 5 of culture, paraffin embedded, sectioned, and stained with Ki-67 **(A)**. KKU-M213 mono- and iMSCs co-cultures were fixed, paraffin embedded, sectioned and stained with Ki-67 on day 3, 5 and 7. HMSCs and KKU-M213 co-cultures (ratio 1:2, cancer cells:hMSCs) were also fixed at day 5, paraffin embedded, sectioned, and stained with Ki-67 **(C)**. At least 6 spheroids were embedded in the array from each condition. Representative spheroids are shown (microscope objective = 20X). Positive Ki-67 expression was quantified by manually counting the positive cells and cancer cells and calculating the ratio of positively stained cancer cells over the total of cancer cells on days 3, 5 and 7 **(B and D)**.

Overall, all spheroids expressed Ki-67, although these did not meet the expected criteria for different cell layers (proliferative, quiescent, and necrotic zones). Co-culture KKU-M055 spheroids contained more proliferating cells compared to the mono-cultures and similar results were found for the KKU-M156 and KKU-M213 spheroids. These results correlated with the RLU data for the KKU-M156 spheroids but not for the KKU-M055 (Chapter 4, Figure 4.9). Interestingly, the Ki-67 positive cells were found surrounding the internal structures. This was similar for the HuCCA-1-derived spheroids, although there was more expression of Ki-67 in the mono-cultures than co-cultures. Finally, the expression of Ki-67 in RBE-derived spheroids

was lower compared to the rest of the spheroids, but the expression was found to be higher on the co-cultures (Figure 4.13A and B). When looking at the results of the KKU-M213-derived spheroids over time, Ki-67 expression progressively increased. At day 5, Ki-67 was expressed substantially less in the co-cultures with iMSCs than hMSCs. However, co-cultures with iMSCs formed additional internal structures but this was not the case for all the replicates (Figure 4.13B and D).

### 4.2.7. Expression of Vimentin, CK7 and CK19 on the CCA spheroids

To complete the characterisation, the expression of a mesenchymal marker (vimentin) and the expression of both CCA markers (CK7 and CK19) was assessed in the mono- and co-culture spheroids. Vimentin is a protein normally expressed in cells of mesenchymal origin (Steinert & Roop, 1988). Therefore, this marker was chosen to localise the mesenchymal cells within the spheroids. However, it is important to understand that vimentin can also be expressed in epithelial cells undergoing EMT especially in pathological situations (Vuoriluoto et al., 2011). CK7 and CK19, previously used to confirm CCA histopathology in the mono-culture spheroids, were chosen to localise the CCA cells within the spheroids. Sections containing the spheroids were stained with Vimentin, CK7 and CK19 (Chapter 2, Section 2.6.4) (technical replicates are in Appendix A, Figure A1 and Figure A2).

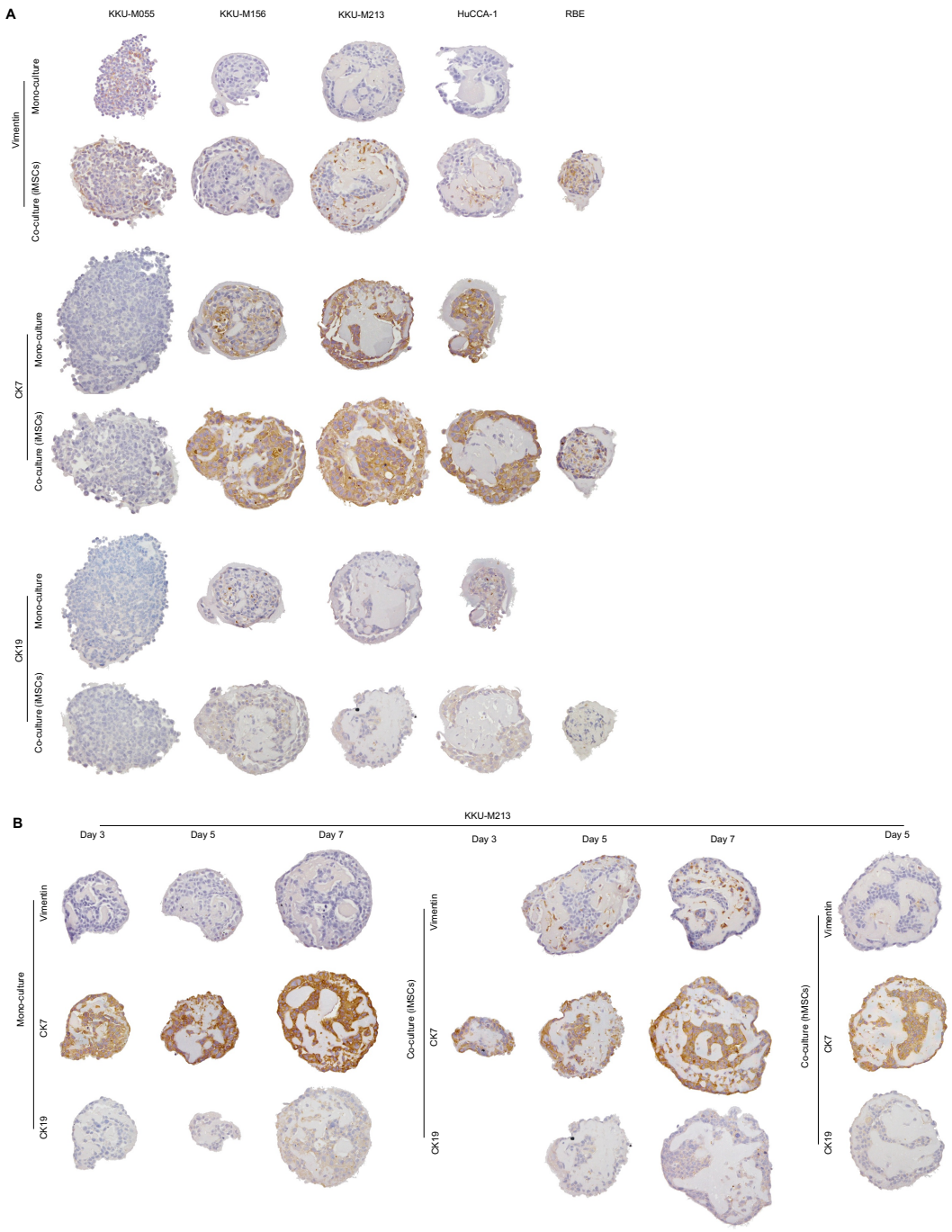



**Figure 4.14. Expression of Vimentin, CK7 and CK19 on CCA mono- and co-culture spheroids**. 1000 cells from 5 CCA cell-lines (KKU-M055, KKU-M156, KKU-M213, HuCCA-1 and RBE) were mono-cultured or iMSCs co-cultured at a ratio of 1:2 (cancer cells:iMSCs) into an ULA 96-well round bottom plate. CCA spheroids were fixed at day 5 of culture, paraffin embedded, sectioned, and stained with Vimentin, CK7 and CK19 **(A)**. KKU-M213 were fixed, paraffin embedded, sectioned and stained with Vimentin, CK7 and CK19 at day 3, 5 and 7. HMSCs and KKU-M213 co-cultures (ratio 1:2, cancer cells:hMSCs) were also fixed at day 5, paraffin embedded, sectioned, and stained with Vimentin, CK7 and CK19 **(B)**. Images represent mid sections through the spheroids. Representative spheroids are shown (microscope objective = 20X).

Apart from KKU-M055-derived mono-cultures which showed positive staining, Vimentin was only expressed in the co-culture spheroids. Interestingly, this cell-line was the only one not expressing the CCA markers, raising a question over the authenticity of this cell-line. Vimentin was expressed on the surrounding of the internal structures. Both mono- and co-culture KKU-M156, KKU-M213, HuCCA-1 and RBE-derived spheroids also expressed the CKs. CK7 was expressed in a higher degree than CK19 (Figure 4.14A). In the KKU-M213-derived spheroids, vimentin expression increased in the co-culture spheroids more intensely at day 7 compared to day 5. Additionally, the expression was found to be higher in the iMSCs co-culture compared to the hMSCs co-culture. Expression of CK7 was similar for all the conditions and had higher expression compared to CK19 (Figure 4.14B).

## 4.3. Summary and Technical Discussion

The lentiviral construct encoding for firefly luciferase gene was successfully expressed in CCA cells, which enabled tracking of growth of the cancer cells in the context of the co-cultures. The effect of this crosstalk in cell proliferation was investigated. It was found that CCA cancer cells either proliferated higher or were able to form tighter spheroids in the presence of MSCs. This effect was only found when the cells were directly co-cultured, displaying the importance of direct cell-cell communication in proliferation (Brucher & Jamall, 2014). The hepatobiliary nature of these models was also confirmed by the positive expression of CCA markers (CK7 and CK19).

- **Optimising the co-culture model**

In order to generate co-culture systems and track cell populations, cells have to be previously labelled. Two commonly used reporter genes, green fluorescent protein (GFP) and a bioluminescent reporter gene (luciferase), have been extensively used *in vivo* and *in vitro* (Choy et al., 2003). The acquisition of GFP signal relies on excitation by an external light source. Bioluminescence imaging, on the other hand, is based on the endogenous production of light by the expression of the enzyme luciferase (Choy et al., 2003). Bioluminescence was chosen over GFP since it was an established technique in the Grabowska Lab. Additionally, since BL does not require an excitation light source, it gives less background. The high intensity of the signal and ability of the signal to penetrate tissues are advantages for the *in vivo* experiments (Choy et al., 2003). Additionally, it has been shown that the bioluminescent luciferase imaging is more sensitive than GFP imaging (Choy et al., 2003). The BL intensity was found to be cell-line dependent. KKU-M213 showed the highest signal. The signal was similar to that in an already in-use breast cancer cell-line used to generate orthotopic xenografts models in the Grabowska Lab. Therefore, this could also be used for future *in vivo* experiments. The rest of the cell-lines had an attenuated signal. However, since cells were only intended to be used for *in vitro* purposes, the signal was considered sufficient.

Another important factor is the media in which the cell mixture grows. This is usually dependent on the cells within the co-culture model; for this model, DMEM was used. The MSCs growth media is designed to robustly support the standardised expansion of multipotent cells and therefore it could have impacted the growth of the cancer cells.

Additionally, the optimisation of the ratio is of paramount importance. Three ratios of tumour cells and MSCs were chosen. The 2:1 and 1:2 were proposed as the representation of a less and more stroma-rich tumour, whilst a 1:1 ratio was considerate moderate. The results that gave the highest proliferation rate was 1:2 (cancer cells:MSCs) and this correlates to the fact that CCA is a stroma-rich tumour (Brivio, Cadamuro, Strazzabosco, & Fabris, 2017).

- **Spheroid co-culture using iMSCs instead of hMSCs**

The availability of hMSCs was limited due to their slow growth. Additionally, primary cells have limited lifespan making experimental manipulation challenging (Hare, Collins, Cuddington, & Mossman, 2016). Therefore, immortalised MSCs were obtained from a collaboration in the University of Nottingham. This cell-line was transfected to force expression of hTERT to enable the cells to repress replicative senescence and overcome the growth crisis (Rambhatla, Chiu, Glickman, & Rowe-Rendleman, 2002). The effect of the iMSC co-cultures was first tested under the same conditions as the hMSC co-cultures. Cell proliferation was also significantly enhanced, hence confirming the use of iMSCs as an alternative for studying the crosstalk between cancer cells and MSCs on the spheroid models. Additionally, the effect of cancer cell proliferation was similar at day 5 using both MSCs and this time-point was chosen for assessing the morphology.

- **Spheroid proliferation in an indirect or direct system**

Choosing the right system to investigate the cell-stroma crosstalk is an important factor to consider. Both approaches have advantages and disadvantages that necessitate consideration (Chapter 1, Section 1.6.2.1); however, the model must be chosen based on a specific scientific question. Since the next steps were to perform RNASeq, it was thought that an indirect system would provide advantages due to having both cell types physically separated (Vis et al., 2020). From both indirect methods, the transwell system was chosen over the use of conditioned media as it enabled bidirectional signalling (cancer cell to MSCs and vice-versa). Interestingly, the cell proliferation was not affected in the iMSC indirect co-culture. KKU-M156 proliferation was the only cell-line that showed slightly higher proliferation in a transwell system. However, investigating the effect of the co-cultures in each cell-line in a direct and indirect system is an interesting question to explore in future research. In addition to this, the

protrusions from the cell surface, which was hypothesized to indicate an invasion effect of the KKU-M156 cells and iMSCs-derived spheroids is an interesting result but outside the scope of the current project.

- **Morphology of the mono- and co-culture spheroids**

The spheroid-array is an excellent technique and frequently used in this project for examining morphology and staining for expression markers by IHC. However, although 6 replicates were included per condition, some of them were lost during the step where agarose was added on the top or during sectioning. This limited obtaining representative sections from all conditions, especially for KKU-M213 and RBE mono-culture spheroids. This, however, can be improved by achieving a tighter control automating the transfer of spheroids from the culture plate to the arrays (Ivanov & Grabowska, 2017) or embed less spheroids per block. Cell-lines here formed loose aggregates (KKU-M055), irregularly shaped structures over time (RBE) and round spheroids with uniform density in their periphery (KKU-M156, KKU-M213 and HuCCA-1). This morphology was maintained in hMSCs or iMSCs co-culture. The markers vimentin, CK7 and CK19 were chosen according to the literature to stain mesenchymal (Satelli & Li, 2011) and CCA cells (L. Z. Liu et al., 2018), respectively.

The influence of MSCs on CCA proliferation in direct co-culture was demonstrated, using a spheroid model. These effects were observed in established models using standard cell-lines. The next step was to generate more relevant close-to-patient models such as patient-derived xenografts and PDX-derived spheroids. The crosstalk of the stroma and PDX cells was investigated in the following chapter.

# Chapter 5. The influence of Mesenchymal stem Cells on PDX and PDX-derived spheroids

## 5.1. Introduction

In every aspect of translational cancer research, from the biological aspects of the disease to the development of new treatments, the use of pre-clinical models is a key step. As previously shown, cell-line-derived spheroids are a useful model to study CCA. However, the main disadvantage of working with cell-lines is the loss of tumour heterogeneity due to the artificial selection, which could ultimately lead to clinical response discordance. During cell-line subculture, subpopulations adapted better for *in vitro* plastic environment are selected for and result in a relative homozygous population overtime (Sulaiman & Wang, 2017). Recently, there has been an increasing interest in the use of PDXs due to their potential to be a tool for personalised medicine (Ibarrola-Villava, Cervantes, & Bardelli, 2018; Kopper et al., 2019). The process of generating PDXs is based on the transfer of fresh tumour tissue (primary or metastatic) from the patient directly to an immunocompromised mouse (Siolas & Hannon, 2013). Depending on the cancer type, amount of tissue available, molecular properties, etc. the success rate of the PDX will vary. The *Ex Vivo* Cancer Pharmacology Centre, in Nottingham, has a dedicated unit to carry out *in vivo* work, which has great expertise in successfully generating PDXs (De Thaye et al., 2020; Onion et al., 2016; Pal et al., 2020). Since PDXs originate from patients, they can maintain the cellular and histological structure of the original tumour (Pompili, Porru, Caruso, Biroccio, & Leonetti, 2016). Through cytogenetic analysis it has been shown that it has a strong preservation of the overall genomic and gene expression profile matching the patient tumour. The clinical data of the response and resistance from patients also correlates to the PDX from which the patient has been derived (Pompili et al., 2016). All these advantages highlight the use of PDXs as more predictive pre-clinical model for studying cancer. Nonetheless, there are some disadvantages such as the cost and the potential mouse stromal cell infiltration after prolonged passage (Pompili et al., 2016). PDX-derived spheroids can be developed to replace aspects of the *in vivo* work and to support the replacement principle of the 3Rs (Replacement, Reduction and Refinement). Those models have gained considerable attraction in recent years due to the ease of culturing (Onion et al., 2016; Takahashi et al., 2021). Similar to PDXs, PDX-derived spheroids have always been grown in physiological environment, and therefore they are expected to enhance our understanding of cancer biology.

The work in this chapter aimed to characterise 7 CCA PDXs that were established by the *in vivo* unit from 7 anonymous donors. The histology of the PDXs was assessed by H&E and compared to the original tumour. The difference in growth in the presence or absence of MSCs was also determined by Ki-67 staining. Moreover, the expression of vimentin as a mesenchymal marker, and CK7 and CK19 as CCA markers was determined. Spheroids were then established and characterised from these 7 PDXs. This chapter intends to work towards the generation of well-established pre-clinical models for the CCA research community as well as elucidation of potential stroma-cell interactions in CCA in a more close-to-patient model.

## 5.2. Results

### 5.2.1. PDX characterisation

Tissues from 7 CCA patients were collected and grafted subcutaneously into RAG2G mice to grow and were maintained via *in vivo* passage. This work was carried out by the *in vivo* unit. To better comprehend the interaction between the stroma and cancer cells and avoid the cross-species interactions between human tumour and murine stromal cells which can mask the real signalling axes (Morton, Bird, Refaeli, & Jimeno, 2016; Pal et al., 2020), tumours were grafted with or without bone marrow-derived mesenchymal stem cells. Firstly, to determine how well each pair of PDXs reflected their original primary tumour, their histology was assessed and compared to their matched primary tumour. Samples of PDX tissue were received from the *in vivo* unit at early passage, and tissues were formalin-fixed and paraffin-embedded. Paraffin blocks were then sectioned for further IHC staining (Chapter 2, Section 2.6.4). The protocol established in the Grabowska Lab was followed for H&E and vimentin staining (Ivanov & Grabowska, 2017). CK7 and CK19, however, was used according to the previous optimised protocol (Chapter 2, Section 2.6.4).

#### 5.2.1.1. H&E Staining

Slides were first stained by H&E to examine the histology of PDX tumours and to further compare their architecture to that of the original donor tumours. H&E includes haematoxylin, which stains purplish blue cell nuclei; and eosin which stains the extracellular matrix and cytoplasm pink (Chan, 2014; A. H. Fischer, Jacobson, Rose, & Zeller, 2008). Histological assessment of H&E stained sections of human and PDX tumours was confirmed by Dr. Isioma Egbuniwe (Histopathology Specialty Registrar, Nottingham University Hospitals NHS Trust).

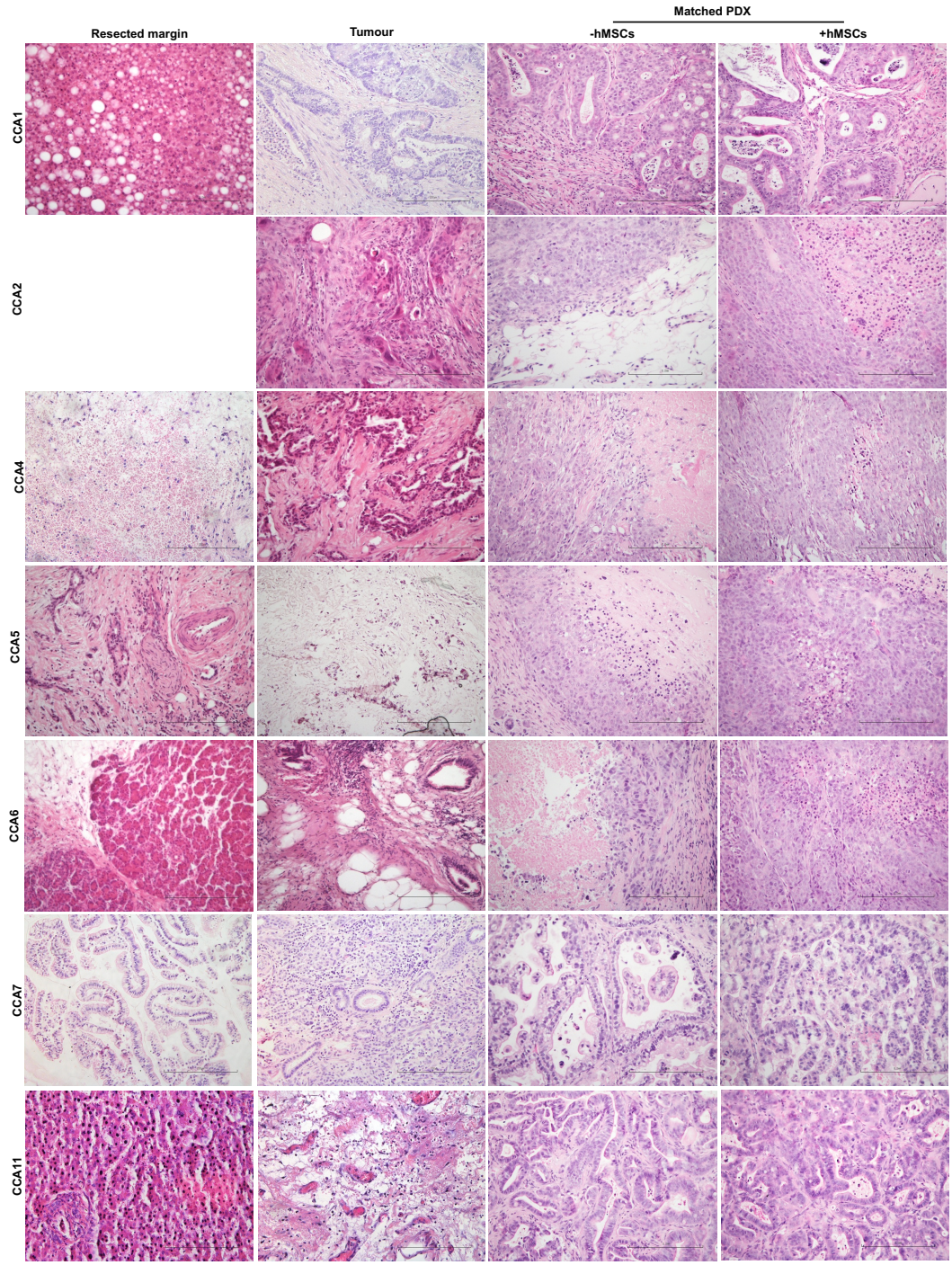



**Figure 5.1. H&E staining of CCA patient tumours and matched patient-derived xenograft in presence or absence of hMSCs.** Tissue from 7 CCA human tumours (CCA1, CCA2, CCA4, CCA5, CCA6 and CCA7) and from resected margins were collected. Tumour tissues were grafted subcutaneously into RAG2G mice to generate the matched PDX model in presence or absence of hMSCs. Samples from each resected margin, patient and matched PDX (+/-hMSCs) were paraffin embedded, sectioned, and stained with H&E. Representative stained sections are shown (magnification: 20×; scale bars = 200μm)

CCA tumours displayed varying histological patterns which were generally characterised by presence of infiltrative irregular glands lined by columnar-shaped

pleomorphic cells with eosinophilic cytoplasm. Overall, CCA1, CCA2, CCA4, CCA6 and CCA7 tumours appeared to be well to moderately differentiated adenocarcinomas and the remaining two tumours (CCA5 and CCA11) were poorly differentiated adenocarcinomas (Figure 5.1). The differentiation stage is strongly associated with tumour behaviour (Jogi, Vaapil, Johansson, & Pahlman, 2012). However, the clinical data of those patients was not accessible, and the histology could not be linked to their prognosis.

CCA1 and CCA7 PDXs formed gland-like structures similar to their matched tumour. CCA11 presented similar structures to CCA1 and CCA7, although not resembling the *in vivo* tumour. Similar, CCA4 and CCA6 did not resemble the original tumour; these PDX tissues mainly showed poor differentiation with a prominent fibro-desmoplastic stromal reaction. CCA5 matched the poorly differentiated tumour *in vivo*. Independent to their *in vivo* resemblance, two main groups of PDXs were observed. Group 1 that included CCA1, CCA7 and CCA11 which formed gland-like structures and therefore, they are classified as well differentiated adenocarcinomas and Group 2 that included CCA2, CCA4, CCA5 and CCA6 that are poor differentiated adenocarcinomas (Figure 5.1).

When comparing the architecture between PDXs grown in the presence or absence of hMSCs, cellular and tissue structure was relatively similar between both pairs in Group 2. However, in Group 1 the presence of MSCs affected the size and number of gland-like structures. CCA1 PDX grown in presence of hMSCs formed bigger gland-like structures compared to its corresponding PDX grown in absence of hMSCs. The opposite effect was observed in CCA7 PDX. CCA11 in presence of hMSCs appeared to have more gland-like structures. Therefore, the presence of hMSCs is affecting the histology of Group 1 in a PDX-dependent manner (Figure 5.1).

#### 5.2.1.2. Vimentin expression

To further characterise PDXs, the expression of vimentin was determined. Vimentin is found in the cytoplasm, where it functions to maintain the cyto-architecture and tissue integrity (Satelli & Li, 2011). In cancer, vimentin is a specific marker for cells of mesenchymal origin and epithelial cells that undergo EMT (C. Y. Liu, Lin, Tang, & Wang, 2015). Although it is difficult to distinguished positive cells between retained MSCs or epithelial cells undergoing EMT, the expression of vimentin is normally an

indicator of tumour diagnosis and prognosis (Satelli & Li, 2011). In iCCA, vimentin expression is associated with poor prognosis which could be attributed to aggressive tumour biology and poor survival after resection (Korita et al., 2010; Saentaweesuk et al., 2018). PDX samples in presence or absence of hMSCs were stained for vimentin (Chapter 2, Section 2.4.6). To assess the expression more objectively the percentage of vimentin positive cells was quantified by assessing the percentage of positive cells in different areas of the whole tissue and normalised by the total number of cancer cells present in the corresponding area (Chapter 2, Section 2.6.4.1.2). Due to the lack of slides, only one negative control with an isotype control antibody on the PDX+hMSCs tissues was included.

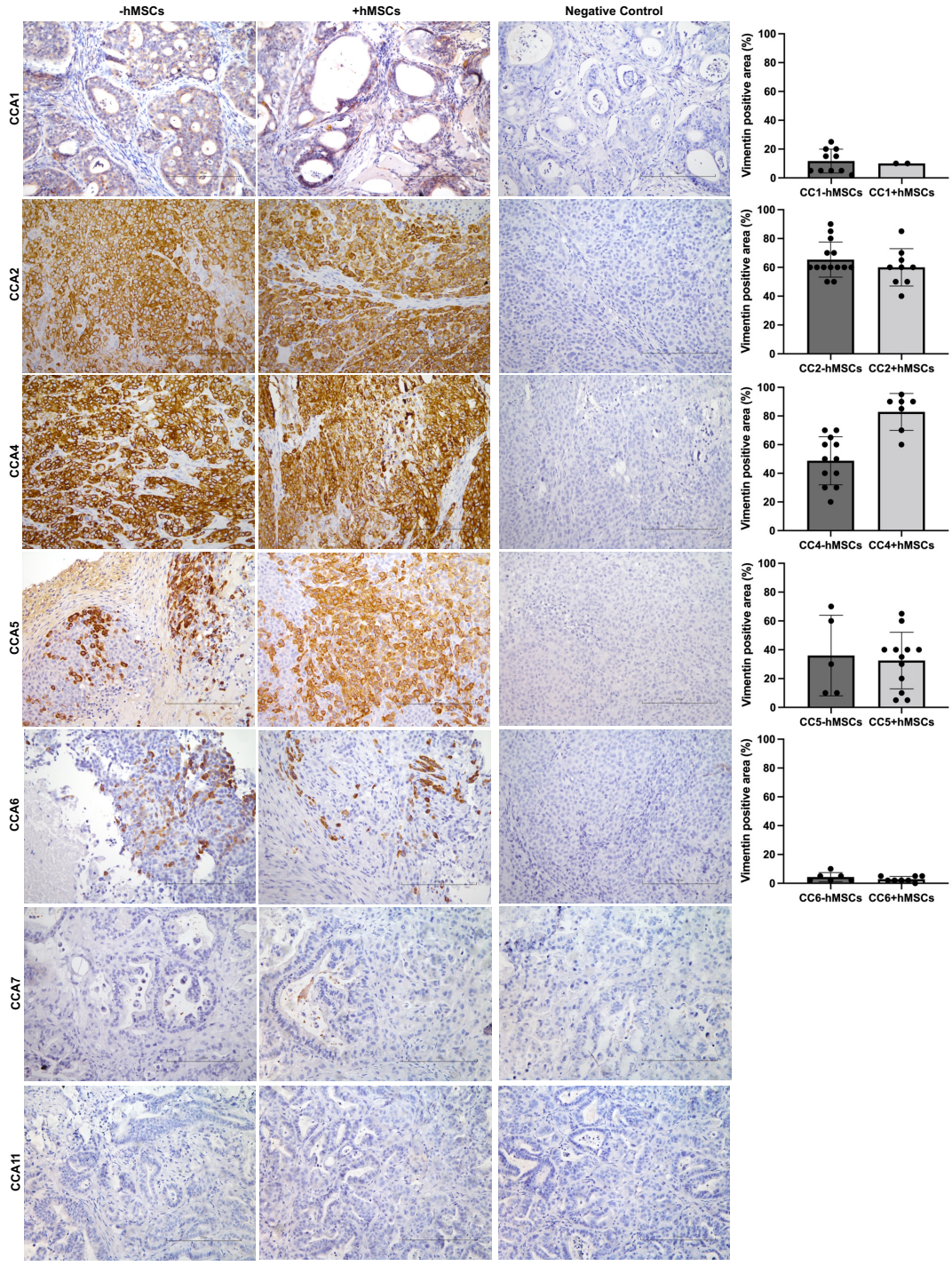



**Figure 5.2. Vimentin staining of CCA patient-derived xenograft in presence or absence of hMSCs.** Tissue from 7 CCA human tumours (CCA1, CCA2, CCA4, CCA5, CCA6 and CCA7) were grafted subcutaneously into RAG2G mice to generate the PDX model in presence or absence of hMSCs. PDX samples were paraffin embedded, sectioned, and stained with vimentin. One negative control with an isotype control antibody on the PDX+hMSCs tissues was included. Positive cells were quantified by assessing the percentage of positive cells in 5 different areas of the whole tissue and normalised by the total number of cancer cells present in the corresponding area (Mean ± SEM). Representative stained sections are shown (magnification: 20×; scale bars = 200µm).

Two main groups of PDXs were previously described, those well differentiated (Group 1: CCA1, CCA7 and CCA11) and those poor differentiated (Group 2: CCA2, CCA4, CCA5 and CCA6). Interestingly, only Group 2 was positive for vimentin with the exception of CCA1, although the expression was relatively low. Expression of vimentin varied between PDXs in Group 2, CCA4 and CCA2 showed the highest expression followed by CCA5 and CCA6. No difference was found in presence or absence of hMSCs for CCA2, CCA5 and CCA6. However, the presence of hMSCs increased vimentin expression in CCA4. Statistical analysis was not performed since these results are based on a N=1 (Figure 5.2).

#### 5.2.1.3. CK7 and CK19 expression

As the value of PDX models depends on their faithful representation of primary tumours (Ben-David et al., 2017), it is important to assess whether CCA PDXs retained their phenotypic characteristics throughout propagation. Therefore, the expression of two biliary markers, CK7 and CK19, was determined. CKs are intermediate filament proteins mainly expressed in epithelial cells. CKs are known to play a key role in maintaining epithelial barriers, regulating immune response, intracellular signalling involved in cell adhesion, proliferation, and differentiation (Frohwitter et al., 2016). Among them, CK7 and CK19 are expressed in various tissue types, such as liver bile ducts but absent in hepatocytes. Both markers have been reported as useful IHC markers to distinguish CCA from HCC. Additionally, apart from being an epithelial marker, abnormal expression of CK7 and CK19 had been reported as an important prognostic factor in various types of cancers (L. Z. Liu et al., 2018). Nonetheless, the prognostic significance of CK7 and CK19 had been rarely reported in CCA (L. Z. Liu et al., 2018). PDX samples were stained for CK7 and CK19 (Chapter 2, Section 2.6.4).

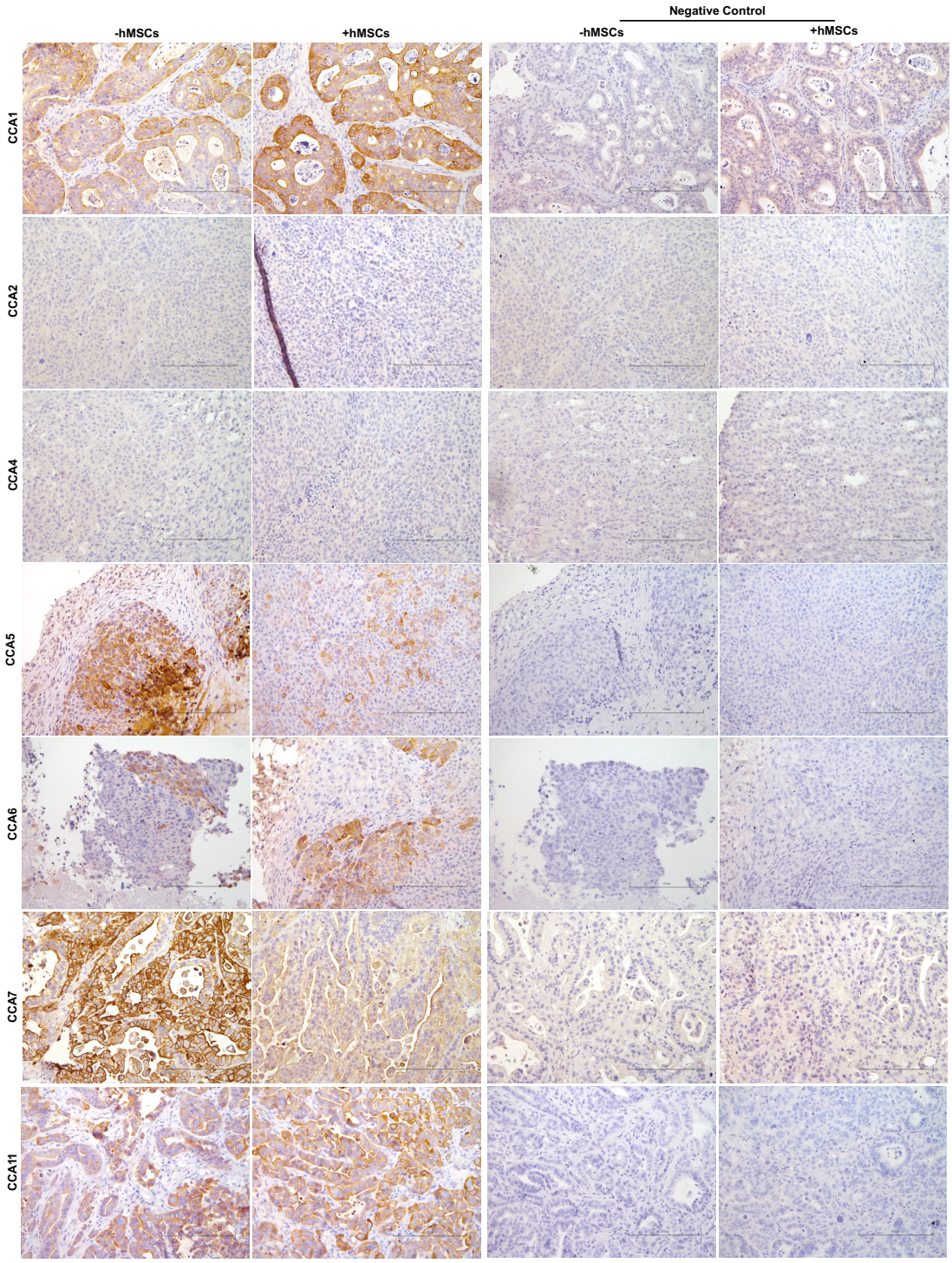



**Figure 5.3. CK7 staining of CCA patient-derived xenograft in presence or absence of hMSCs.** Tissue from 7 CCA human tumours (CCA1, CCA2, CCA4, CCA5, CCA6 and CCA7) were grafted subcutaneously into RAG2G mice to generate the PDX model in presence or absence of hMSCs. PDX samples were paraffin embedded, sectioned, and stained with CK7. Negative controls with an isotype control antibody were included per each condition. Representative stained sections are shown (magnification: 20×; scale bars = 200µm).

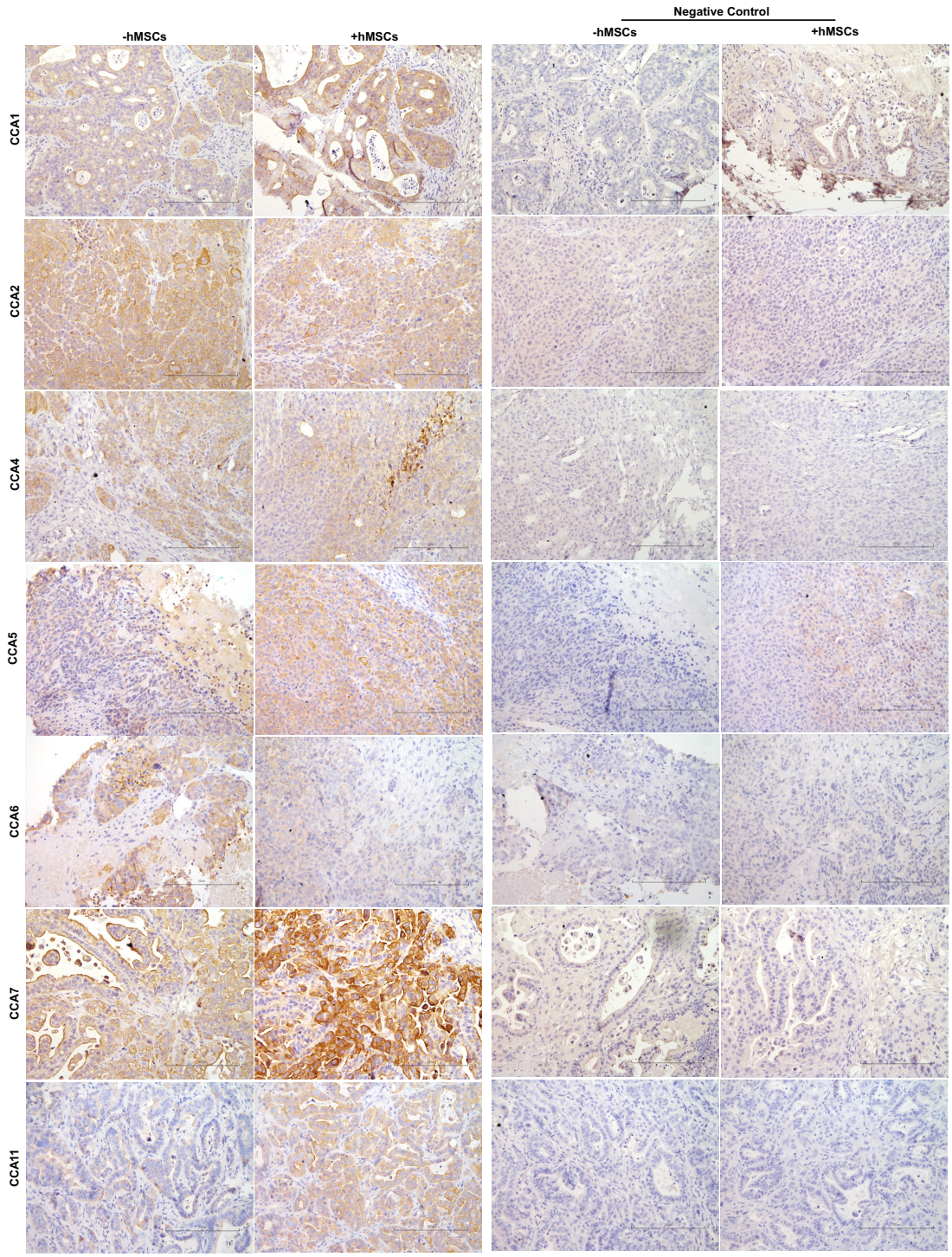



**Figure 5.4. CK19 staining of CCA patient-derived xenograft in presence or absence of hMSCs.** Tissue from 7 CCA human tumours (CCA1, CCA2, CCA4, CCA5, CCA6 and CCA7) were grafted subcutaneously into RAG2G mice to generate the PDX model in presence or absence of hMSCs. PDX samples were paraffin embedded, sectioned, and stained with CK19. Negative controls with an isotype control antibody were included per each condition. Representative stained sections are shown (magnification: 20×; scale bars = 200µm).

High-positive intensity was observed compared to the negative control sections, and therefore, accepted as a positive staining. Results were different for CK7 and CK19 staining. CK7 was notably more highly expressed in Group 1 (CCA1, CCA7 and CCA7), and from Group 2 only CCA5 and CCA6 showed positive staining. For Group 1, the expression was cytoplasmic and surrounding the gland-like structures (Figure 5.3). CK19, however, was expressed similarly in both groups (Figure 5.4). When looking at the difference of expression between the presence or absence of hMSCs, CK7 expression was generally similar between the pairs except for CCA1 and CCA7 in which expression was higher and lower in the presence of hMSCs, respectively. CK19, however, was generally highly expressed in the presence of hMSCs with the exception of CCA2 and CCA6. Although the expression was variable across the panel and conditions, overall, the results confirm the biliary phenotype of the PDXs.

### 5.2.2. PDX proliferation: Tumour volume and Ki-67 expression

Once the panel of PDXs was characterised and their biliary nature was confirmed, the effect of hMSCs in PDX growth was determined. Firstly, the tumour volume of the PDXs was used to determine the tumour growth rates. However, since this was a pilot study, each experiment was designed to evaluate a single PDX line, with 2 mice per group (absence or presence of hMSCs) (Figure 5.5). Tumour volume data was provided by the *in vivo* unit (Chapter 2, Section 2.4.1).

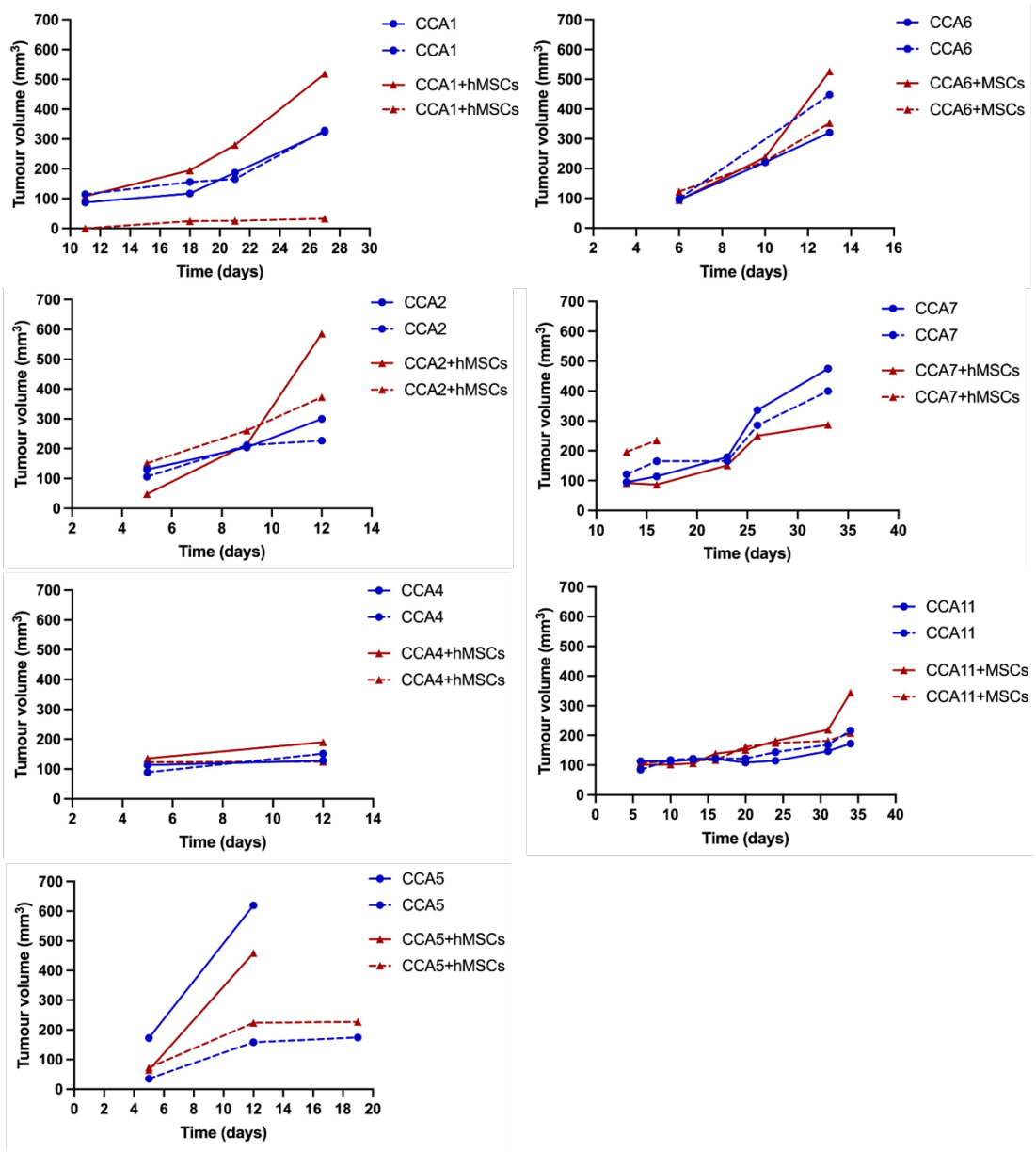



**Figure 5.5. Tumour growth rates of patient-derived xenograft in presence or absence of bone marrow-derived mesenchymal stem cells.** Tissue from 7 CCA human tumours (CCA1, CCA2, CCA4, CCA5, CCA6 and CCA7) were grafted subcutaneously into RAG2G mice to generate the PDX model. Each PDX line included 4 mice – 2 grown in absence of MSCs (depicted in blue), and 2 in presence of MSC (depicted in red). The first and second pair of mice are shown in a continue and discontinue line, respectively. Tumour volume was determined by serial caliper measurement and measured using the length and width.

One of the CCA1 mice did not grow after implantation; however, tumour growth curves from the first pair showed that the presence of hMSCs induced fastest tumour growth. Similar results were found for CCA2 and CCA6. CCA4 and CCA11 did not show significant tumour growth. CCA7 shown opposite results. Of note, one CC7 mouse was terminated at an early time-point of the study before it reached the max allowed volume. Finally, CCA5 showed controversial results in both pairs of PDXs.

For one mouse the presence of hMSCs increased tumour volume, this was the opposite for the other mouse (Figure 5.5).

The next step was to determine the difference of Ki-67 expression in PDXs in presence or absence of hMSCs. Ki-67 is present during all active phases of the cell cycle but is absent in resting cells. In CCA, high Ki-67 expression is associated with worse clinical outcome and a higher risk of relapse (Qiang et al., 2021). PDX samples were therefore stained for Ki-67 according to the protocol (Chapter 2, Section 2.6.4). At this point, due to the lack of sections for further staining and this being a well-established protocol, only one negative control was included (CCA1). Positive expression was quantified in five random areas of each section by manually counting the positive cells and cancer cells and calculating the ratio of positively stained cancer cells over the total of cancer cells observed in each area (Chapter 2, Section 2.6.4.1.1).

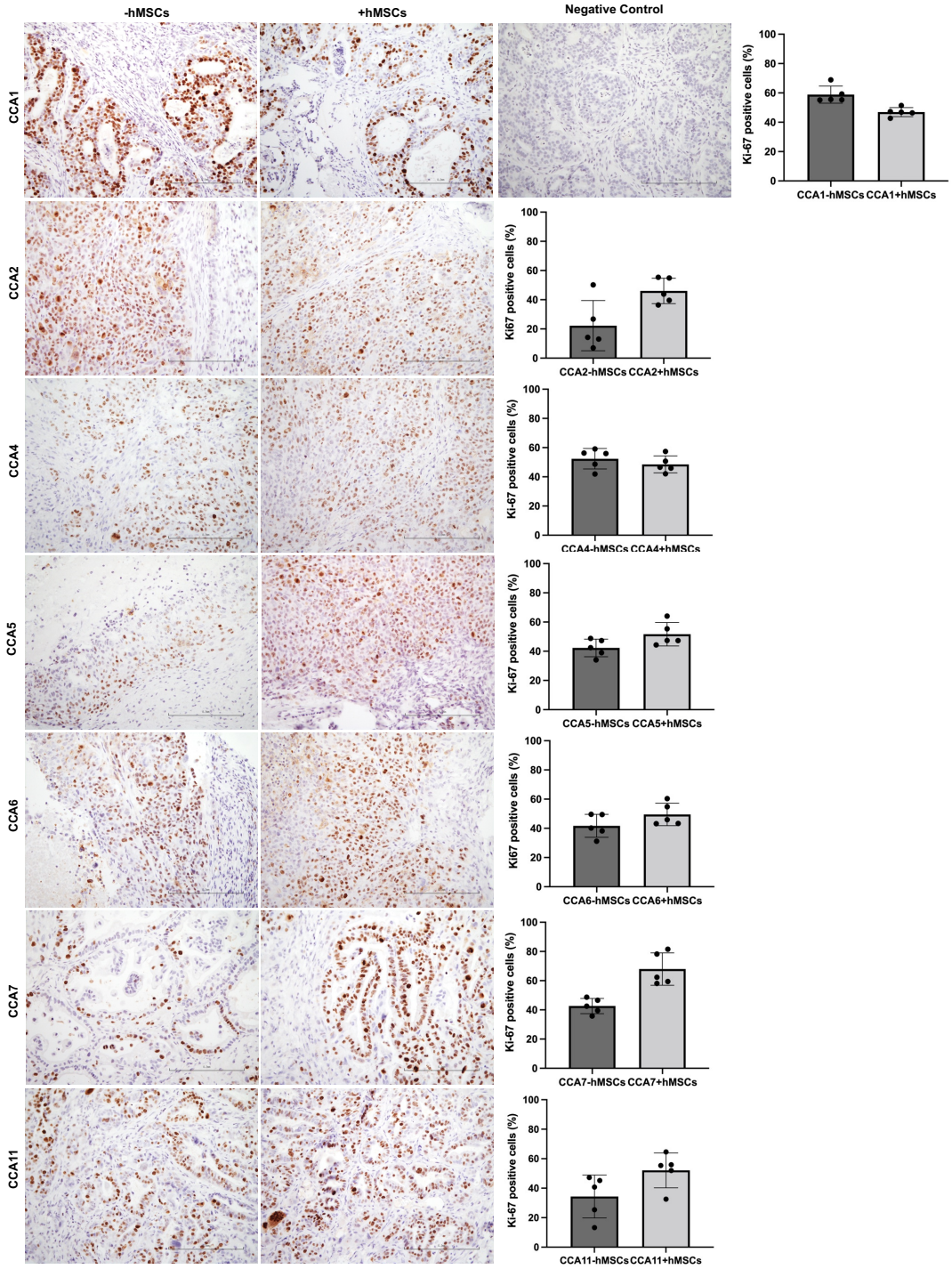



**Figure 5.6. Ki-67 staining of CCA patient-derived xenograft in presence or absence of hMSCs.** Tissue from 7 CCA human tumours (CCA1, CCA2, CCA4, CCA5, CCA6 and CCA7) were grafted subcutaneously into RAG2G mice to generate the PDX model in presence or absence of hMSCs. PDX samples were paraffin embedded, sectioned, and stained with Ki-67. One negative control with an isotype control antibody was included (CCA1). Positive expression was quantified in five areas of each section by manually counting the positive cells and cancer cells and calculating the ratio of positively stained cancer cells over the total of cancer cells observed in each area (Mean ± SEM, N=1). Representative stained sections are shown (magnification: 20×; scale bars = 200µm).

Interestingly, the majority of PDXs presented higher Ki-67 expression in the presence of hMSCs, except CCA1 and CCA4, which expression was similar in both conditions. Ki-67 was expressed in the nucleus and the positive cells in CCA1, CCA7 and CCA11 were found surrounding the gland-like structures. Statistical analysis was not performed since these results are based on a N=1 (Figure 5.6).

### 5.2.3. Generation of PDX-derived Spheroids

Although studies using PDX models continue to provide valuable information and remain important to cancer research in studying various types of tumours in more detail; economic and ethical issues related to animal research raise the need for the development of other suitable methods to maintain PDX cell cultures *ex vivo* (W. Zhang, Moore, & Ji, 2011). Spheroids derived from PDXs, could generate a complementary model to also depict biological and molecular mechanisms. Therefore, *ex vivo* PDX-derived spheroids were generated from the panel of 7 PDXs. Tissues were received fresh from an early passage from the *in vivo* unit. Tissues were enzymatically dissociated and plated in ULA 96-well plates following the protocol established in the Grabowska Lab (Pal et al., 2020). Due to the primary nature of the cells and the protocol being established for a different type of cancer, parameters such as the BME concentration required further optimisation. Therefore, CCA7 was initially used for optimisation. CCA7 PDX-derived cells were plated at 1000cells/well in 6 different concentrations (100-600μg/mL) and their progressive growth was qualitatively monitored over a period of 7 days using brightfield microscopy.

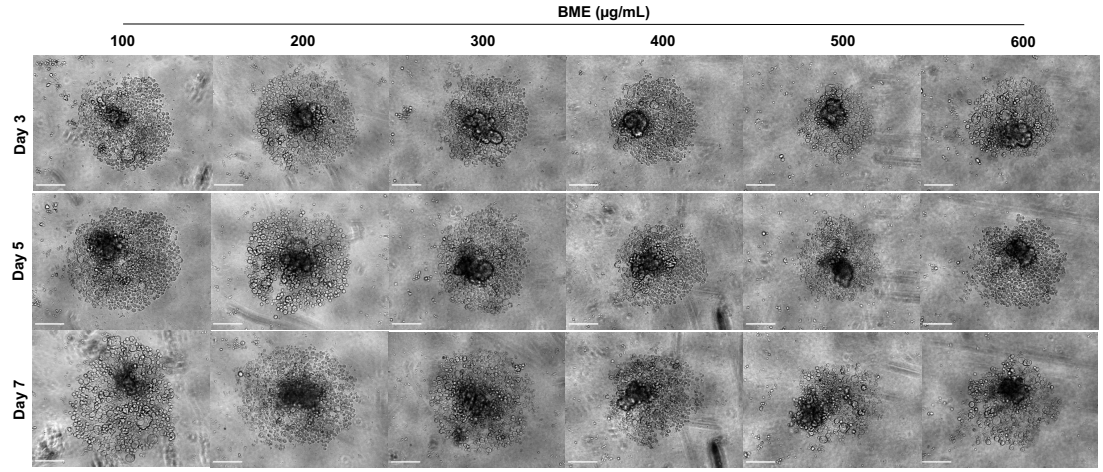



**Figure 5.7. CCA7 PDX-derived spheroids grown in a range of BME concentrations.** CCA7 tissue was enzymatically dissociated, and 1000 cells were dispensed in each well into a ULA 96-well round bottom plate. A range of BME concentrations was tested (100-600µg/mL). Progressive growth was monitored in triplicates wells on days 3, 5 and 7 using brightfield microscopy. Representative spheroids are shown (scale bars = 200µm).

A loose spheroid was formed in the middle of a poorly organized structure in all conditions. From the range of BME concentrations tested, the set of spheroids set up with 300µg/mL formed a more defined structure compared to the rest (Figure 5.11). Therefore, 300µg/mL was the concentration of BME used for the generation of the rest of CCA PDX-derived spheroids.

The next step was to grow spheroids from the rest of PDXs in presence or absence of MSCs in a direct co-culture system. Both hMSCs and iMSCs were used. Cells were cultured alone at a cancer cell:MSCs ratio of 1:2 for 7 days (Chapter 2, Section 2.4.3). The area of spheroids was determined using Fiji analysis software. Growth progression and cell viability were determined by brightfield images and PrestoBlue, respectively (Chapter 2, Section 2.5.2). The generation and characterisation of PDX-derived spheroids was performed one time per each PDX (N=1). PrestoBlue is a cell viability indicator, similar to AlamarBlue, that works under the principle of reducing power of living cells to quantitatively measure the proliferation of cells. Although AlamarBlue was the viability assay previous used, a postdoctoral researcher in the Grabowska Lab working with spheroid models had shown that PrestoBlue provided more consistent results compared to AlamarBlue. Additionally, a commercial live/dead staining was used to visualise the live and dead cells within spheroids. This assay works under the principle that live cells are distinguished by the presence of ubiquitous intracellular esterase activity, determined by the enzymatic conversion of the virtually

nonfluorescent cell-permeant calcein-AM to the intensely fluorescent calcein. The dye calcein is well retained within live cells, producing a uniform green fluorescence in live cells. EthD-1 enters cells with damaged membranes, and it is fluorescence upon binding to nucleic acids, thereby producing a red fluorescence in dead cells. The ability of the PDXs to form spheroids was different and related to which histology Group they belonged to. Group 1 (differentiated adenocarcinomas) required the MSC support to form spheroids (Figure 5.8), whereas Group 2 (undifferentiated adenocarcinomas) were capable of forming spheroids in mono-culture (Figure 5.9). Both groups will be described in detail in the following sections.

#### 5.2.3.1. Group 1: CCA1, CCA7 and CCA11

CCA1, CCA7 and CCA11 cells were derived from well differentiated adenocarcinomas.

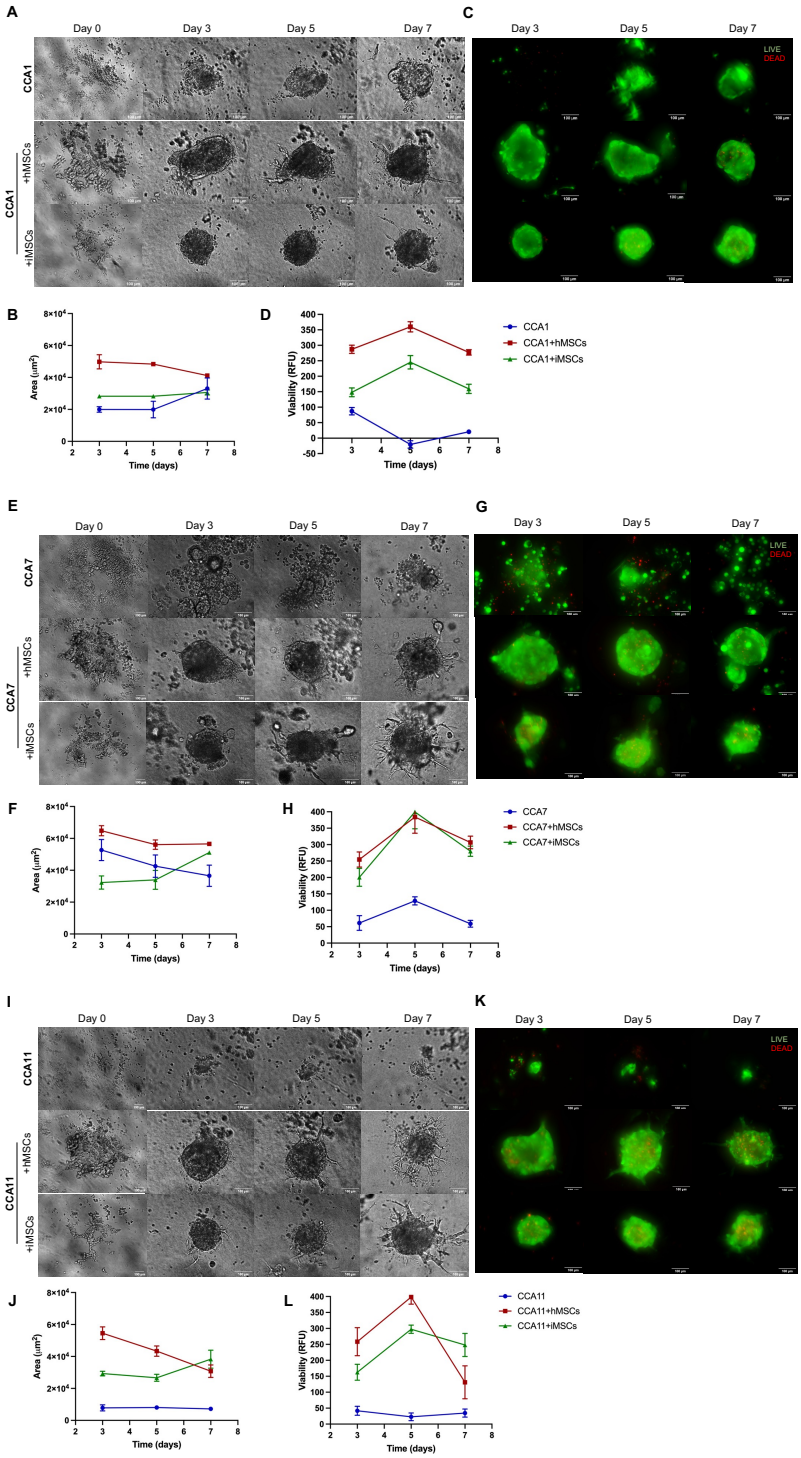



**Figure 5.8. CCA 1, 7 and 11 PDX-derived spheroids in presence or absence of hMSCs or iMSCs.** CCA tissues were enzymatically dissociated, and CCA PDX cells were mono- or co- cultured with hMSCs or iMSCs at 1:2 ratio (cancer cells:MSCs) with 300µg/mL. Spheroids were imaged at day 0, 3, 5 and 7 (**A, E** and **I** for CCA1, 7 and 11, respectively**)** using brightfield microscopy. Live/dead staining was monitored in triplicates after establishment in spheroid-shape on days 3, 5 and 7 using Ca-AM (green - live cells) and ethidium homodimer-1 (red - dead cells) (**C, G** and **K** for CCA1, 7 and 11, respectively). The area of the spheroid was determined in triplicates on days 3, 5 and 7 using ImageJ Fiji (**B, F** and **J** for CCA1, 7 and 11, respectively). Viability of the spheroid was monitored in triplicates at day 0, 3, 5 and 7 using PrestoBlue assay **(D, H** and **L** for CCA1, 7 and 11, respectively**)**. (Mean ± SEM, N=1). Representative spheroids are shown (scale bars = 200µm).

A notable difference was found in spheroid formation in the presence or absence of MSCs. The set of co-culture CCA1, CCA7 and CCA11 spheroids with hMSC stemmed from loosely connected cell clusters on day 0 and formed compact spheroids on day 3 which grew into larger spheroids over time. This rate of growth was similar for the set of spheroids co-culture with iMSCs. Interestingly, cell elongation was observed in the co-cultures, which were more visible in the CC7 and CC11 spheroids. Mono-culture CCA1, CCA7 and CCA11 spheroids formed a substantial less compact spheroid which was easy to disintegrate when pipetting (Figure 5.8A, E and I). Due to the instability of the mono-cultures, the majority of spheroids lost their 3D structure during the steps involved during live/dead staining. In general, the live/dead staining showed that all cells within the spheroids were viable. (Figure 5.8C, G and K). The difference on size was quantified and it was confirmed the set of both co-culture spheroids formed a larger spheroid compared to the mono-culture, being the one co-cultured with hMSCs the larger (Figure 5.8B, F and G). Cell viability was also measured using PrestoBlue. Cancer cells co-cultured with both MSCs showed an increase of cell viability with an unexpected rapid decreased after day 5. The viability of the cells in the mono-culture spheroids was lower, showing that PDXs cells from Group 1 require stromal support (Figure 5.8D, H and L).

#### 5.2.3.2. Group 2: CCA2, CCA4, CCA5 and CCA6

CCA2, CCA4, CCA5 and CCA6 cells were derived from poor differentiated adenocarcinomas.

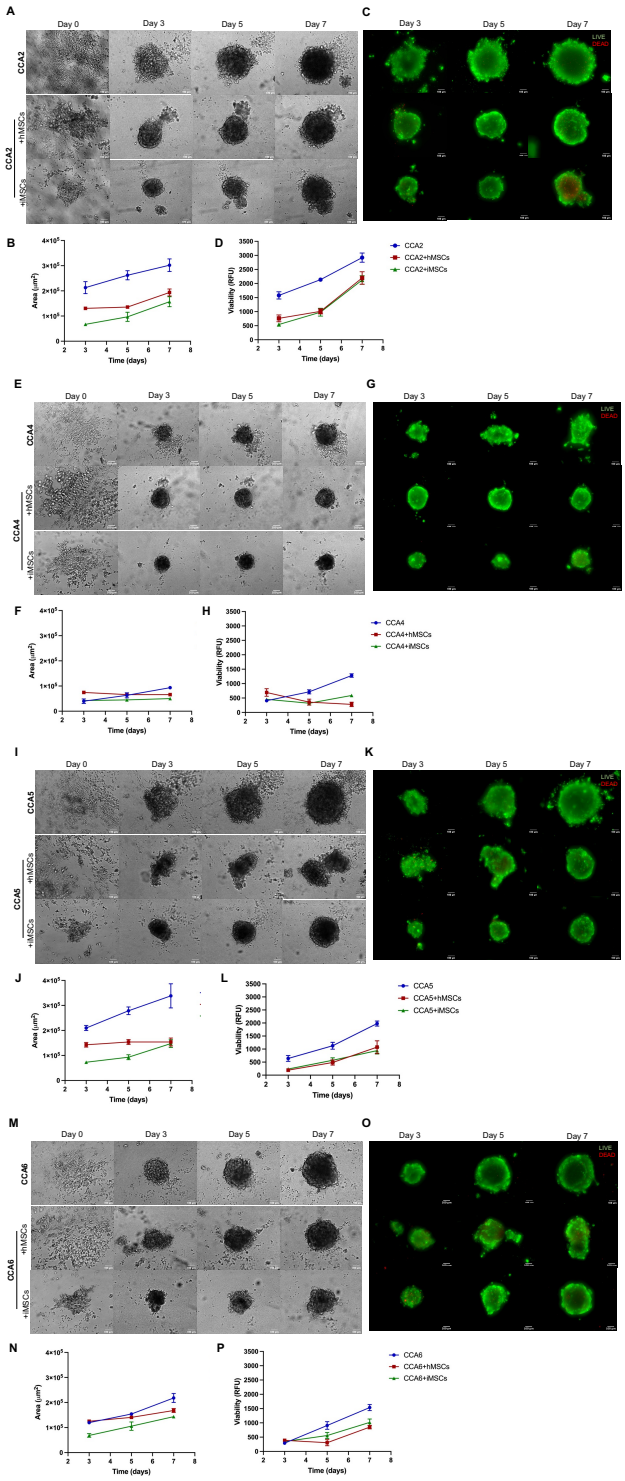



**Figure 5.9. CCA 2, 4, 5 and 6 PDX-derived spheroids in presence or absence of hMSCs or iMSCs.** CCA tissues were enzymatically dissociated, and CCA PDX cells were cultured in mono- or co-culture d with hMSCs or iMSCs at 1:2 ratio (cancer cells:MSCs) with 300µg/mL. Spheroids were imaged at day 0, 3, 5 and 7 **(A, E, I** and **M** for CCA2, 4, 5 and 6, respectively**)** using brightfield microscopy. Live/dead staining was monitored in triplicates after establishment in spheroid-shape on days 3, 5 and 7 using Ca-AM (green - live cells) and ethidium homodimer-1 (red - dead cells) **(C, G, K** and **O** for CCA2, 4, 5 and 6, respectively). The area of the spheroid was determined in triplicates on days 3, 5 and 7 using ImageJ Fiji **(B, F, J** and **N** for CCA2, 4, 5 and 6, respectively). Viability of the spheroid was monitored in triplicates at day 0, 3, 5 and 7 using PrestoBlue assay **(D, H, L** and **P** for CCA2, 4, 5 and 6, respectively**)**. (Mean ± SEM, N=1). Representative spheroids are shown (scale bars = 200µm).

PDX cells from Group 2 were capable of forming spheroids in presence or absence of MSCs. At day 0, cells with hMSCs formed a more visible cluster compared to the co-cultures with iMSCs and mono-cultures. Over time, cells formed a dense spheroid with defined edges in all conditions. Interestingly, the set of CCA4 mono-culture and co-culture spheroids formed a smaller spheroid compared to CCA2, CCA5 and CCA6 (Figure 5.9A, E, I and M). Overall, the live/dead staining showed that the cells were viable, except CCA2 in the presence of iMSCs at day 7 that showed cell death in the middle of the spheroid (Figure 5.9C, G, K and O). When assessing the area, CCA2 and CCA5-derived mono-culture spheroids were larger compared to the co-cultures. CCA4 and CCA6-derived spheroids formed a similar spheroid to the co-culture with hMSCs, but bigger than the co-culture with iMSCs (Figure 5.9B, F, J and N). Finally, in terms of viability, spheroids in mono-culture showed a higher viability compared to the co-cultures. Both co-cultures showed comparable cell viability (Figure 5.9D, H, L and P).

### 5.2.4. PDX-derived Spheroid characterisation

Once PDX cells were successfully grown as spheroids, the spheroid-array methodology was performed for a more in-depth analysis and characterisation. The internal morphology between the mono-cultures and the co-cultures was assessed by H&E staining. Vimentin, CK7 and CK19 as mesenchymal and epithelial biliary markers, respectively, were also used for characterisation.

#### 5.2.4.1. H&E staining

PDX-derived spheroid morphology was assessed by H&E staining. CCA PDX cells were grown as mono- and co-culture (with hMSCs and iMSCs) spheroids and at day 5 they were fixed. All fixed spheroids were followed by paraffin embedded, sectioned and H&E staining. Six spheroids were embedded in the array per condition (Chapter 2, Section 2.6.1). Technical replicates are in Appendix A, Figure A3 and Figure A4.

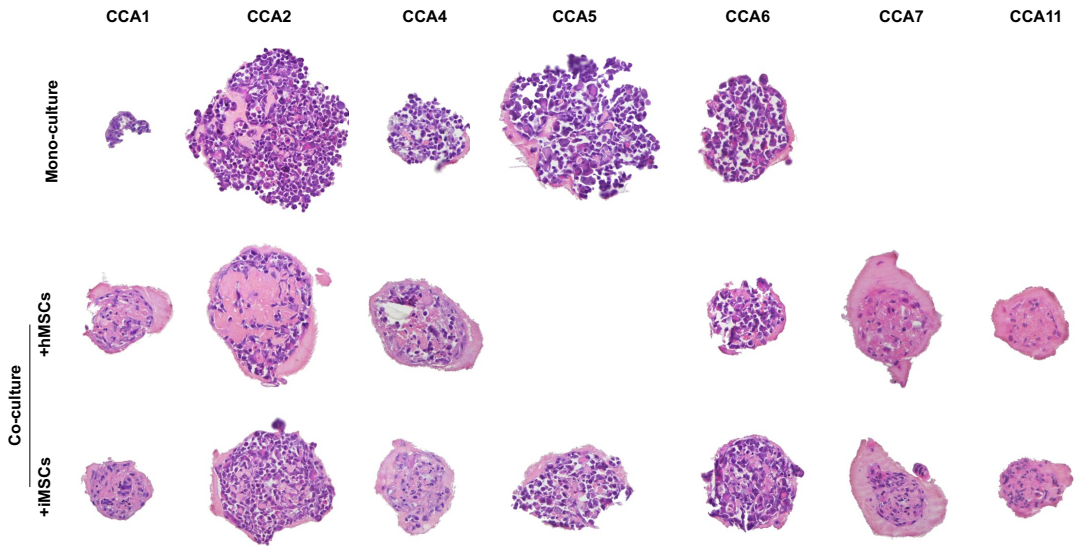



**Figure 5.10. H&E staining of CCA PDX-derived spheroids in presence or absence of hMSCs or iMSCs.** CCA tissues (CCA1, CCA2, CCA4, CCA5, CCA6, CCA7 and CCA11) were enzymatically dissociated, and PDX cells were cultured in mono- or co-culture with hMSCs and iMSCs at 1:2 ratio (cancer cells:MSCs) with 300µg/mL. CCA PDX-derived spheroids were fixed at day 5 of culture, paraffin embedded, sectioned, and stained with H&E. Representative spheroids are shown (magnification: 20×).

Problems were encountered with obtaining appropriate sections from all the spheroids in the panel because some disintegrated during collection and fixing, some were lost during sectioning and some because it was difficult to find a plane where all spheroids (which vary in size) were present. For instance, CCA7 and CCA11 mono-culture spheroids disintegrated whilst performing the spheroid-array methodology, which confirms the lack of denseness of the spheroids from Group 1. Interestingly, co-cultures from this group presented internal structures with high expression of eosin staining. Those structures were also found in the periphery of the spheroids. This was more apparent in the CCA7-derived spheroids. Regarding the PDXs derived from Group 2, the mono-culture spheroids were substantially bigger than the co-culture spheroids, a result that correlates with what was observed in the previous brightfield images (Figure 5.8 and 5.9). Interestingly, in the co-culture spheroids a ring was observed surrounding the spheroid. This peripheral structure, however, was smaller compared to the Group 1-derived spheroids. Mono-culture spheroids also had this structure although in less quantity. CCA2-derived spheroids co-cultured with hMSCs were the only set of spheroids that showed a high quantity of those internal structures (Figure 5.10).

### 5.2.4.2. Vimentin expression

To complete the characterisation of the model, the expression of vimentin was also determined (Chapter 2, Section 2.6.4). Technical replicates are in Appendix A, Figure A3 and Figure A4.

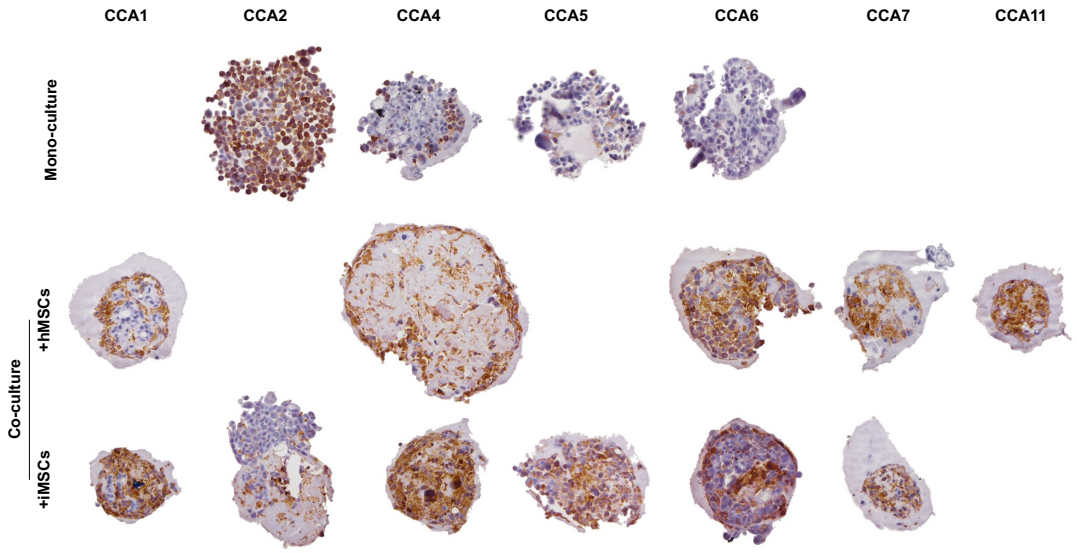



**Figure 5.11. Vimentin staining of CCA PDX-derived spheroids in presence or absence of hMSCs or iMSCs.** CCA tissues (CCA1, CCA2, CCA4, CCA5, CCA6, CCA7 and CCA11) were and enzymatically dissociated, and PDX cells were cultured in mono- or co-culture with hMSCs and iMSCs at 1:2 ratio (cancer cells:MSCs) with 300µg/mL. CCA PDX-derived spheroids were fixed at day 5 of culture, paraffin embedded, sectioned, and stained with Vimentin. Representative spheroids are shown (magnification: 20×).

Vimentin was expressed in all co-cultures, although to different degrees across the panel. CCA1 and CCA7 co-culture-derived spheroids, expressed vimentin in the regions surrounding the internal structures. This was not observed in the co-culture spheroids derived from Group 2. Overall, less vimentin expression was observed in the mono-culture spheroids from Group 2 than in the co-cultures. CCA2 expressed higher vimentin compared to CCA4, CCA5 and CCA6 (Figure 5.11).

### 5.2.4.3. CK7 and CK19 expression

The expression of CK7 and CK19 was also determined. Spheroids were grown and at day 5, the spheroid-array method was performed and followed by staining for CK7 and CK19 (Chapter 2, Section 2.6.4). Technical replicates are in Appendix A, Figure A3 and Figure A4.

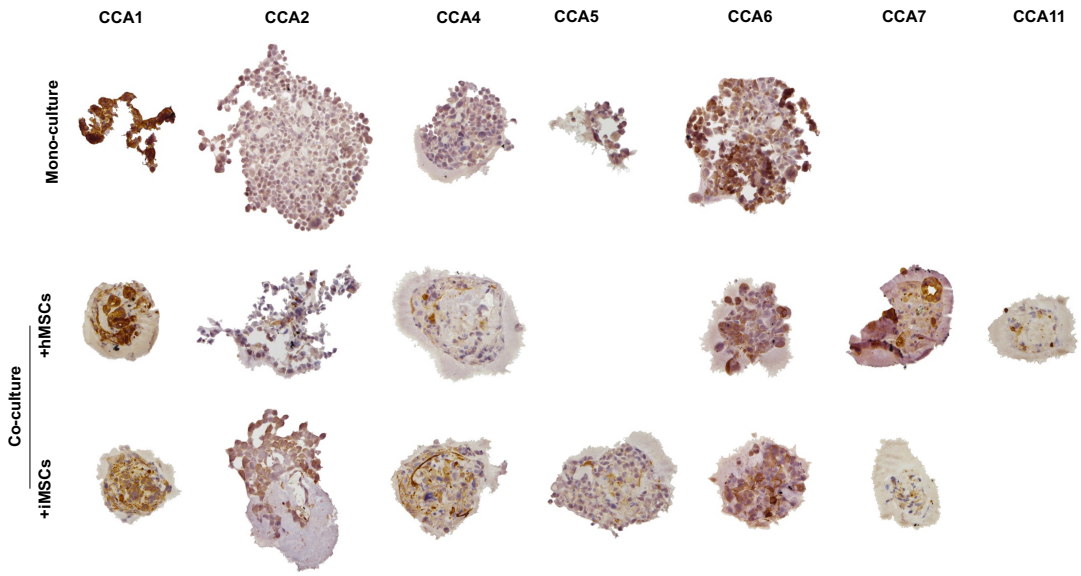



**Figure 5.12. CK7 staining of CCA PDX-derived spheroids in presence or absence of hMSCs or iMSCs.** CCA tissues (CCA1, CCA2, CCA4, CCA5, CCA6, CCA7 and CCA11) were enzymatically dissociated, and PDX cells were cultured in mono- or co-culture with hMSCs and iMSCs at 1:2 ratio (cancer cells:MSCs) with 300µg/mL. CCA PDX-derived spheroids were fixed at day 5 of culture, paraffin embedded, sectioned, and stained with CK7. Representative spheroids are shown (magnification: 20×).

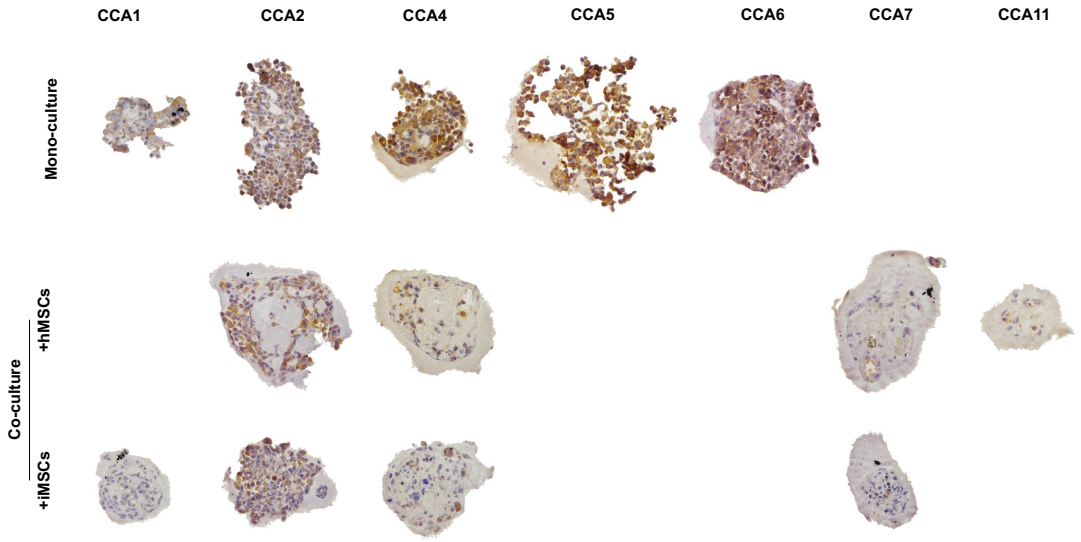



**Figure 5.13. CK19 staining of CCA PDX-derived spheroids in presence or absence of hMSCs or iMSCs.** CCA tissues (CCA1, CCA2, CCA4, CCA5, CCA6, CCA7 and CCA11) were enzymatically dissociated, and PDX cells were cultured in mono- or co-culture with hMSCs and iMSCs at 1:2 ratio (cancer cells:MSCs) with 300µg/mL. CCA PDX-derived spheroids were fixed at day 5 of culture, paraffin embedded, sectioned, and stained with CK7. Representative spheroids are shown (magnification: 20×).

Interestingly, the mono-culture CCA1-derived spheroid showed higher expression of CK7 compared the mono-cultures from Group 2, as observed with the PDX tissue. The majority of co-cultures showed CK7 staining. Especially notable was the staining in the CCA1 and CCA7 spheroids co-cultured with hMSCs, where the staining was observed in the internal structures (Figure 5.12). In the mono-culture spheroids, higher CK19 staining was observed in the Group 2-derived spheroids, compared to CC1 spheroid (only representative of Group 1). Expression was evenly distributed throughout the sections (Figure 5.13).

### 5.2.5. PDX-derived spheroid proliferation: Ki-67 expression

Once the majority of PDX-derived spheroids were characterised for H&E, Vimentin, CK7 and CK19 expression, the effect of MSCs on proliferation was assessed by Ki-67 expression. Positive expression was quantified by manually counting the positive cells and cancer cells and calculating the ratio of positively stained cancer cells over the total of cancer cells observed in each area (Chapter 2, Section 2.6.4.1.1). Technical replicates are in Appendix A, Figure A3 and Figure A4.

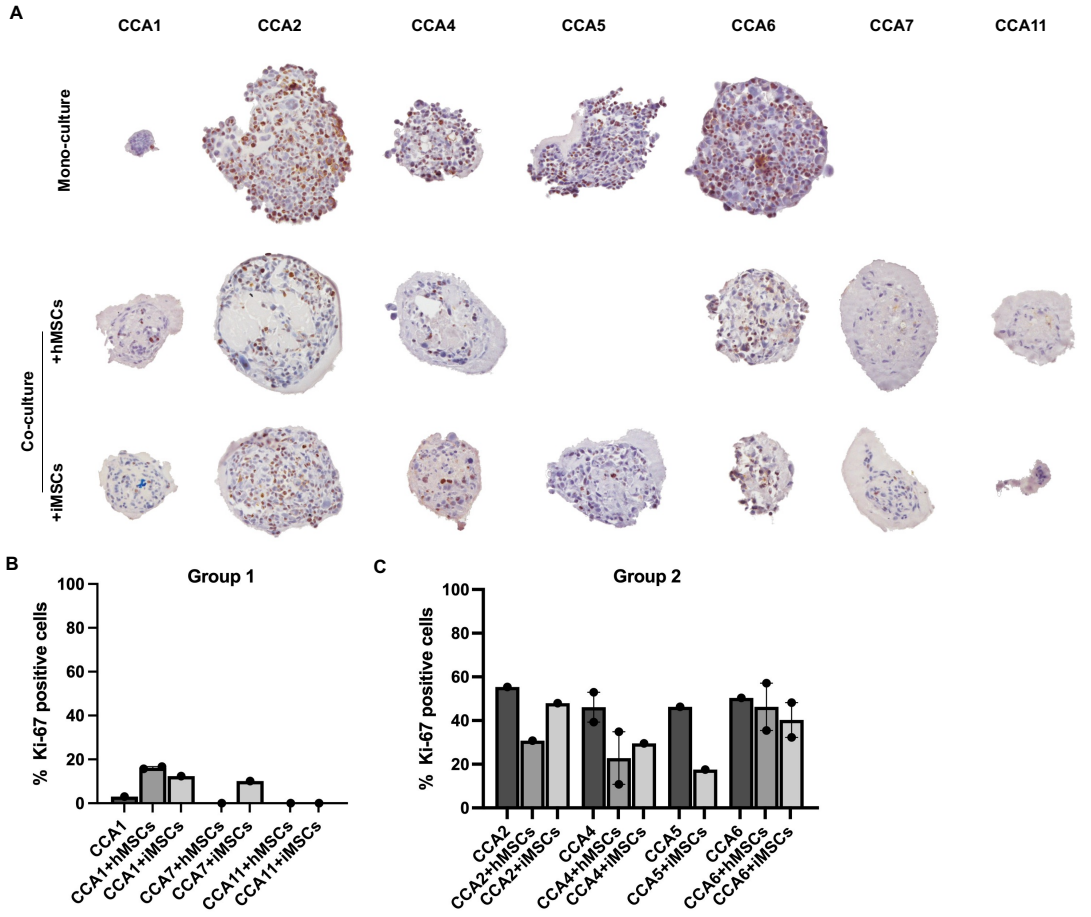



**Figure 5.14. Ki-67 staining of CCA PDX-derived spheroids in presence or absence of hMSCs or iMSCs.** CCA tissues (CCA1, CCA2, CCA4, CCA5, CCA6, CCA7 and CCA11) were enzymatically dissociated, and PDX cells were cultured in mono- or co-culture with hMSCs and iMSCs at 1:2 ratio (cancer cells:MSCs) with 300µg/mL. CCA PDX-derived spheroids were fixed at day 5 of culture, paraffin embedded, sectioned, and stained with Ki-67. Representative spheroids are shown (magnification: 20×) **(A)**. Positive expression was quantified by manually counting the positive cells and cancer cells and calculating the ratio of positively stained cancer cells over the total of cancer cells observed in each area for Group 1 **(B)** and Group 2 **(C)**.

The expression of Ki-67 was substantially lower in the spheroids derived from Group 1 (Figure 5.14A). As previously mentioned, problems were encountered with obtaining appropriate sections from representative spheroids which mainly affected Group 1-spheroids. However, enough sections were obtained for CCA1, and interestingly, Ki-67 expression was higher on the co-culture spheroids. Among both, the set of co-culture spheroids with hMSCs had higher Ki-67 staining compared to those co-cultured with iMSCs (Figure 5.14B). Spheroids from Group 2 showed the opposite result. CCA2, CCA4, CCA5 and CCA6 mono-culture spheroids expressed higher Ki-67 compared the co-culture spheroids. Moreover, co-culture spheroids for CCA1 and CCA4 showed slightly showed slightly higher Ki-67 expression in the

presence of iMSCs. On the contrary, CCA6 showed higher positive cells in the presence of hMSCs compared to iMSCs (Figure 5.14B).

## 5.3. Summary and Technical Discussion

CCA PDXs were successfully established from 7 CCA tumours (CCA1, CCA2, CCA4, CCA5, CCA6, CCA7 and CCA11). Their morphology was compared to their original tumour and found that the majority of PDXs resembled their matched tumour and were positive for the hepatobiliary markers (CK7 and CK19). Tumours were engrafted with or without hMSCs to generate PDXs, and although the morphology was similar between both conditions, the Ki-67 expression was higher in those engrafted with MSCs, apart from PDX CCA1 and CCA4. In addition, two PDX clusters were defined based on their morphology: Group 1 (well differentiated: CCA1, CCA7 and CCA11) and Group 2 (poor differenced: CCA2, CCA4, CCA5 and CCA6). This difference correlated with the Vimentin expression, which was higher in Group 2. Finally, the spheroid formation was dependent on the group they belong to. Group 1 required the stroma support to form spheroids, whereas Group 2 did not. The hepatobiliary nature of the PDX-derived spheroids was also confirmed by the positive staining of CK7 and CK19.

- **PDX Engraftment**

PDXs were generated and handled by the *in vivo* team, and therefore, there was limited control over the success of engraftment. However, from the tumour volume data it was noticed that the majority of PDX were successfully engrafted apart from a few that did not grow after implantation (Figure 5.5). There are some factors that influence the success rate of PDXs. Firstly, the characteristics of primary tumour, including the aggressiveness of tumour, histological type, and tumour cell percentage in the tissue. Secondly, the process for the generation of PDX. Thirdly, the size and number of tissues implanted. Fourthly, the location of implantation (J. Jung, Seol, & Chang, 2018). Hence, these factors could have influenced the lack of success rate in those specific PDXs.

- **Tumours and PDXs Morphological Characterisation**

The first step towards the characterisation of a PDX model is to determine their resemblance to the original tumour. Hence, confirm whether they reflect patients' tumours with regards to tumour heterogeneity, histopathology, gene expression, and mutations, and treatment response. The morphology was indeed compared by H&E, and not all the PDXs resembled the tumour histology. It should be emphasised that in

this study the histology of the tumour tissue was from a separate core from that implanted into the mice. Therefore, the differences in histology in some of the PDXs could also be due to different sample portion. This was an important factor discussed in a study that characterised breast PDXs (J. Yu et al., 2017).

IHC was performed manually. There are many critical steps in performing IHC such as antigen retrieval, selection and preparation of antibody and reagents, incubation, washing, and counterstaining; therefore, using automated IHC machines instead can generate more reliable and reproducible results (S. W. Kim, Roh, & Park, 2016). However, since this is a research study, manual staining was prioritised in order to have more flexibility on a possible optimization of a specific antigen-antibody reaction if needed.

Quantification of IHC also needed to be carefully planned since it was a subjective assessment (Cregger, Berger, & Rimm, 2006). CK7 and CK19 expression levels were not quantified since the reason for this staining was to confirm the hepatobiliary nature of the samples. Vimentin, a cytoplasmic protein (Danielsson, Peterson, Caldeira Araujo, Lautenschlager, & Gad, 2018), was quantified by an assessment of the proportion of positive cells (Danielsson et al., 2018). This consisted of assessing the relative percentage of positive cells in relation to the total number of cells in the whole section. However, the limitation of this method is that it did not show the intensity of the IHC staining. Assessing the intensity of the staining and scoring it from 0 to 3 (0, negative; 1, weak positive; 2, moderate positive; and 3, strong positive) could provide important information regarding the difference in the level of protein expression (S. W. Kim et al., 2016). For Ki-67, since it is a nuclear protein (L. T. Li, Jiang, Chen, & Zheng, 2015), positive cells were individually counted, and the percentage of positive cells was calculated over the total number of tumour cells. To avoid bias, the average of five random areas was calculated. Quantifying and scoring these results by more than one researcher will be considered for future work when the staining of the tumour samples and the replicates of the PDX is performed. Normally, manual quantification is subjective and is prone to observer variability that limits reproducibility and statistical confidence (Feuchtinger et al., 2015). Therefore, digital image analysis techniques that offer an objective approach will also be considered to improve the accuracy of these results (Feuchtinger et al., 2015).

Negative and positive controls are known to support the presence or absence of a probed molecule. Positive controls in IHC protocols are specimens containing the target molecule in its known location. On the other hand, negative controls, are to demonstrate that the reaction visualised is due to the interaction of the epitope of the target molecule and the paratope of the antibody (Hewitt, Baskin, Frevert, Stahl, & Rosa-Molinar, 2014). In this study only negative controls were included in the IHC protocol, since both vimentin and Ki-67 were antibodies previously tested and confirmed to work in the Grabowska Lab (Ivanov & Grabowska, 2017). Even though negative controls were included in the protocol, there were not enough sections to have a negative control per each pair of PDX and therefore the negative controls were selected according to the following judgment: for vimentin, the matched PDX with MSCs was used for each pair of PDX. Vimentin is a mesenchymal marker (C. Y. Liu et al., 2015), and although both conditions of PDXs expressed vimentin, it was first hypothesised to only be present in the PDXs with MSCs. For Ki-67, since the staining of all the slides was performed on the same day and it was an antibody highly used in the Grabowska Lab (Ivanov & Grabowska, 2017), only one slide was used as a negative control. For the CK7 and CK19 markers, since they were not previously used, a negative control per each condition of PDX was included.

- **Spheroid formation from PDX cells and morphology assessment**

As the maintenance of PDX raises ethical and economic concerns (Domenici et al., 2021), it was determined whether it was possible to maintain CCA cells in 3D culture, deriving these cells from PDX explants. The protocol used for the generation of this model was similar to the one for the cell-line-derived spheroids; however, an extra step was needed for the generation of the model, the disassociation of the PDX tissue. There are three main dissociation techniques based on chemical, mechanical and enzymatic processes. Chemical dissociation involves the sequestration of cations implicated in the conservation of the intracellular 3D structure and is achieved by exposing the tissue to reagents that degrade the intercellular connections (Castell & Gómez-Lechón, 2009). Mechanical dissociation involves the homogenization of the solid tumour sample by manual mincing (Cunningham, 2010). Finally, the enzymatic dissociation takes advantage of the action of enzymes with different targets (Ljung et al., 1989). In this study, the tissue was enzymatically disaggregated using specific selection of enzymes, concentrations and exposure times optimised by the Grabowska Lab to

generate the best cell yield (Pal et al., 2020). Nonetheless, *ex vivo* material cannot be totally dissociated into single cells. Therefore, a strainer was used to facilitate the selection of aggregates, which has been shown to help in previous studies (Morales & Alpaugh, 2009).

Finally, one of the biggest challenges was to assess proliferation in the co-cultures of PDX cells and MSCs (either iMSCs or hMSCs) since the PDX cells were not luminescent neither fluorescent labelled. Therefore, the results referred to the viability of the mixed cells. The use of cell dyes is an excellent choice to track dynamics in a mixed co-culture (S. Chung, Kim, Seo, Kim, & Lee, 2017). Therefore, using a GFP or a luciferase reporter gene to label the PDX cells previous to performing the co-culture will be considered for future work.

The spheroid-array technique was used for the assessment of the morphology of the PDX-derived spheroids. The printed holes on the agarose had a paraboloid shape served to arrange spheroids in the same plane (Ivanov & Grabowska, 2017). However, and, similar to the cell-line arrays, during the addition of the agarose layer, some of the spheroids lost their initial position, and therefore, this limited obtaining representative sections from all conditions.

PDXs and PDX-derived spheroids were successfully generated and characterised. The next step was to elucidate potential pathways involved in the crosstalk of the mesenchymal cells and the CCA cells. The transcriptome of these models in the different setups were sequenced and results are described in the following chapter.

# Chapter 6. Identification of active signalling pathways in co-cultures of cancer cells and MSCs

## 6.1. Introduction

Gene expression is defined as the process by which cells are able to decode the information within their genetic material to generate products such as RNA and ultimately proteins, necessary for the correct cellular function. The set of all RNA transcripts is referred to as the transcriptome (Z. Wang, Gerstein, & Snyder, 2009). Of the 3 main types of RNA, mRNA, transfer RNA (tRNA), and ribosomal RNA (rRNA), the mRNA is read and translated into the string of amino acids that make up the synthesised protein (Clancy, 2008). Each cell in a multicellular organism contains the same genetic material. If the genotype of a cell is analysed, it not only contains the code for it specific function, but also the information to perform other functions. Certain sections of the genome are introns, which are fragments that do not codify for proteins although having a key role in cell regulation. The exome includes all those regions that encode for the proteins involved in cellular function. The difference in expression between cells of different types is called differential expression (Eghbalnia, Wilfinger, Mackey, & Chomczynski, 2020).

Due to the advanced Next Generation Sequencing (NGS) technology, the entire transcriptome can be analysed by RNA Sequencing (RNASeq). This approach provides information on the expression levels of the transcripts (Singh, Singh, Chaudhary, Mehla, & Kumar, 2012). Although the expression level of mRNA only explains a fraction of variation in protein abundance, the abundance of mRNA is often an excellent proxy for the presence of a protein (Vogel & Marcotte, 2012). Therefore, understanding the transcriptome is often used as a surrogate for protein information, which can ultimately help researchers to understand cell biology. RNASeq has made important contributions in various fields, especially cancer research, including studies on differential gene expression analysis and cancer biomarkers, cancer heterogeneity and evolution, cancer drug resistance, cancer microenvironment and immunotherapy (M. Hong et al., 2020). In CCA, the transcriptomic landscape and the interplay between malignant cells and niche cells remains poorly understood. There are only a few studies that try to reveal those cellular interactions (Fabris et al., 2020). One of the latest studies indicated the presence of three CAF subtypes in the stroma, being the vascular CAFs the most prominent ones, which could secrete high levels of IL-6 to modulate tumour epigenetic alterations and promote progression (M. Zhang et al., 2020).

RNAseq consists of four key steps: total RNA extraction, library construction, sequencing, and data analysis (Y. Wang et al., 2020). During isolation, the RNA is extracted from the biological sample. The quality of RNA is typically measured using an Agilent Bioanalyzer, which produces a RIN between 1 and 10 with 10 being the least degradation, and therefore the highest quality samples. The RNA quality will dictate the production of the library for sequencing. The construction of libraries involves isolating the mRNA, reverse-transcribing the mRNA to cDNA, fragmenting, or amplifying primed cDNA molecules, and ligating sequencing adaptors. mRNA molecules are the most frequently studied RNA species because they encode proteins (Kukurba & Montgomery, 2015). After, the sequencing takes place, this is a sequencing-by-synthesis method to sequence tens of millions of sequence clusters in parallel. There are dedicated companies that can perform the library production and sequencing. Typically, after the sequencing FASTQ files are obtained. Those contain the reads (sequences that have been read) as well as the quality associated to every read base. During the data analysis stage, these sequences undergo quality trimming and genome alignment. This produces the counts table, that contains the number of reads associated to every gene, that can be further explored via bioinformatics tools (Kukurba & Montgomery, 2015).

In previous chapters, pre-clinical spheroids models to study CCA were developed from both cell-lines and PDX cells. These models were grown in the presence of MSCs, which significantly enhanced spheroid formation and proliferation. Given the ability of MSCs to directly interact with cancer cells and modulate their function, the transcriptome of those models was studied in order to elucidate the signalling pathways activated in the presence of MSCs. However, since the effect on proliferation was only significant in the direct co-culture system, investigating the crosstalk between two cell populations without physical separation was more complexed. The work in this chapter aimed to plan an experimental design for RNASeq. An exploratory analysis and determination of the DEGs and enriched pathways in the presence of MSCs in the cell-line-derived spheroid model was then performed. This analysis was also performed for the PDXs. Both models were compared to the human CCA tumours.

This analysis was done in collaboration with Prof Nigel Mongan, a bioinformatician in the University of Nottingham; and Prof Jesper Anderson, a bioinformatician in Biotech Research and Innovation Centre at the University of Copenhagen, Denmark,

with whom a short-term scientific mission was supported by the European Cholangiocarcinoma Network, but not performed due to the COVID-19 breakdown. Cristina Rusu, a junior bioinformatician in University of Valencia, also helped in guiding this analysis.

## 6.2. Results

### 6.2.1. Experimental design and data pre-processing

An experimental design was carefully planned. Three different categories of cells were included (Figure 6.1):

1. A panel of 7 CCA tumours (CCA1, CCA2, CCA4, CCA5, CCA6, CCA7 and CCA11).
2. A panel of 7 PDXs in which those patients' tumours had been implanted into a mouse in the presence or absence of hMSCs. A single sample was included per PDX and condition. At this stage PDX-derived spheroid were not yet optimised, and therefore, those models were not included for sequencing.
3. Cell-line-derived spheroids grown in presence or absence of MSCs. Both MSCs (iMSCs (immortalised) and hMSCs (primary)) were used for the generation of the co-culture model, and a ratio of 1:2 (cancer cells:MSCs) was used. Biological triplicates were included per condition. The cell-line from which the spheroids were generated was KKU-M213.

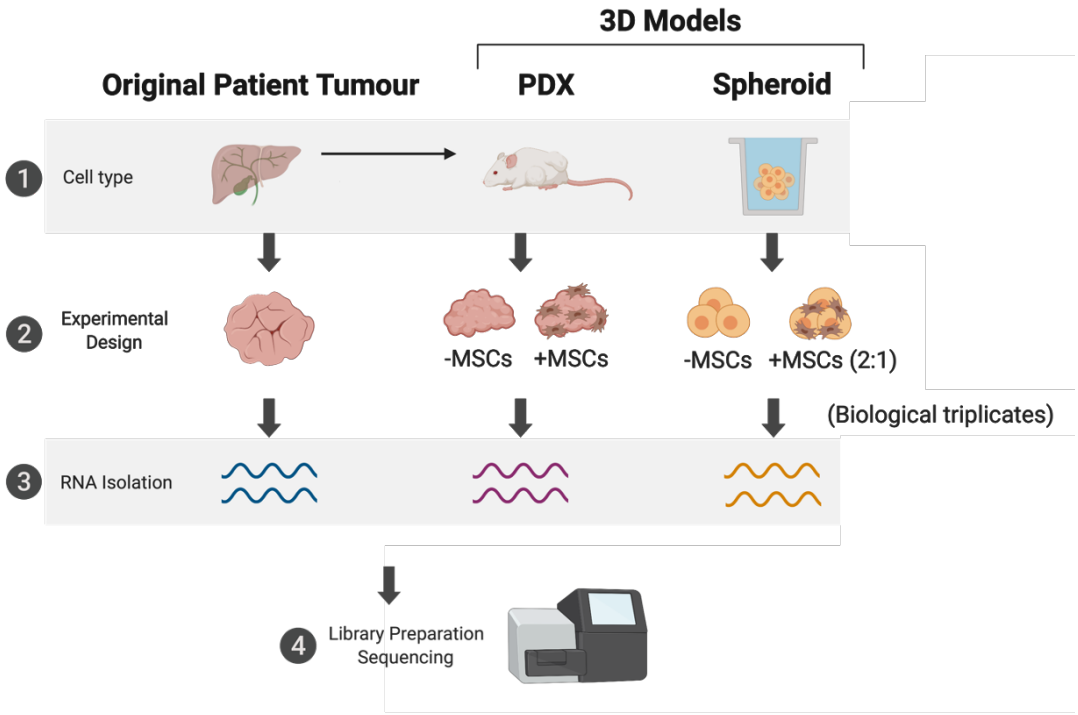



**Figure 6.1. Experimental design for RNASeq analysis.** 30 samples (original patient tumours, their matched PDXs in the presence or absence of hMSCs and triplicates of KKU-M213-derived spheroids in the presence or absence of both iMSCs or hMSCs) were collected (**1** and **2**). RNA was isolated of those samples using Qiagen Allprep kit (**3**). RNA was then sent for further library preparation and sequencing (**4**).

A total of 30 biological samples was collected for further RNA extraction. RNA was isolated using a Qiagen Allprep kit (Chapter 2, Section 2.7.1). The quality of the RNA was analysed, and the majority of samples showed a RIN higher than 6 (Appendix A, Table 1A). Samples were sent for cDNA library preparation and sequencing to a dedicated facility in Cambridge, Novogene (UK). The FASTQ data of all the samples was received and processed by Prof Nigel Mongan, who performed the quality control, alignment to the human genome and generated a count data table. The data was analysed using two approaches, R and iDEP. A pipeline for R was established with the help of Elena Cristina Rusu. However, the analysis and figures for this chapter were generated using iDEP, a more user-friendly approach, which encompasses many useful R and Bioconductor packages, vast annotation databases, and related web services (Ge, Son, & Yao, 2018). Both analyses provided reproducible results.

### 6.2.2. Activated pathways in the CCA co-culture spheroids

The dataset corresponding to the cell-line-derived spheroids was first studied in order to determine potential pathways activated by the presence of MSCs. Three biological

replicates of spheroids grown in absence or presence of both MSCs (hMSCs or iMSCs) were included in the analysis. The input for the analysis was the gene-level expression matrix (provided from Prof Nigel Mongan) and the experimental design.

#### 6.2.2.1. Pre-processing and Exploratory analysis

Once the data was processed, the software recognised the human species as the best match. The low expressed genes were removed from further analysis, to avoid noise for the downstream analyses (minimum 0.5 counts per million (CPM) in at least one sample). The CPMs were calculated by normalizing the read counts by the total counts per sample. From 60676 genes in 9 samples, 17711 genes passed filter and 17688 were converted to Ensembl gene IDs. The remaining 23 genes were kept in the data using original gene IDs. To perform the exploratory analysis (clustering analysis and PCA) the counts were transformed using rlog. This approach effectively reduces mean-dependent variance (Love, Huber, & Anders, 2014).

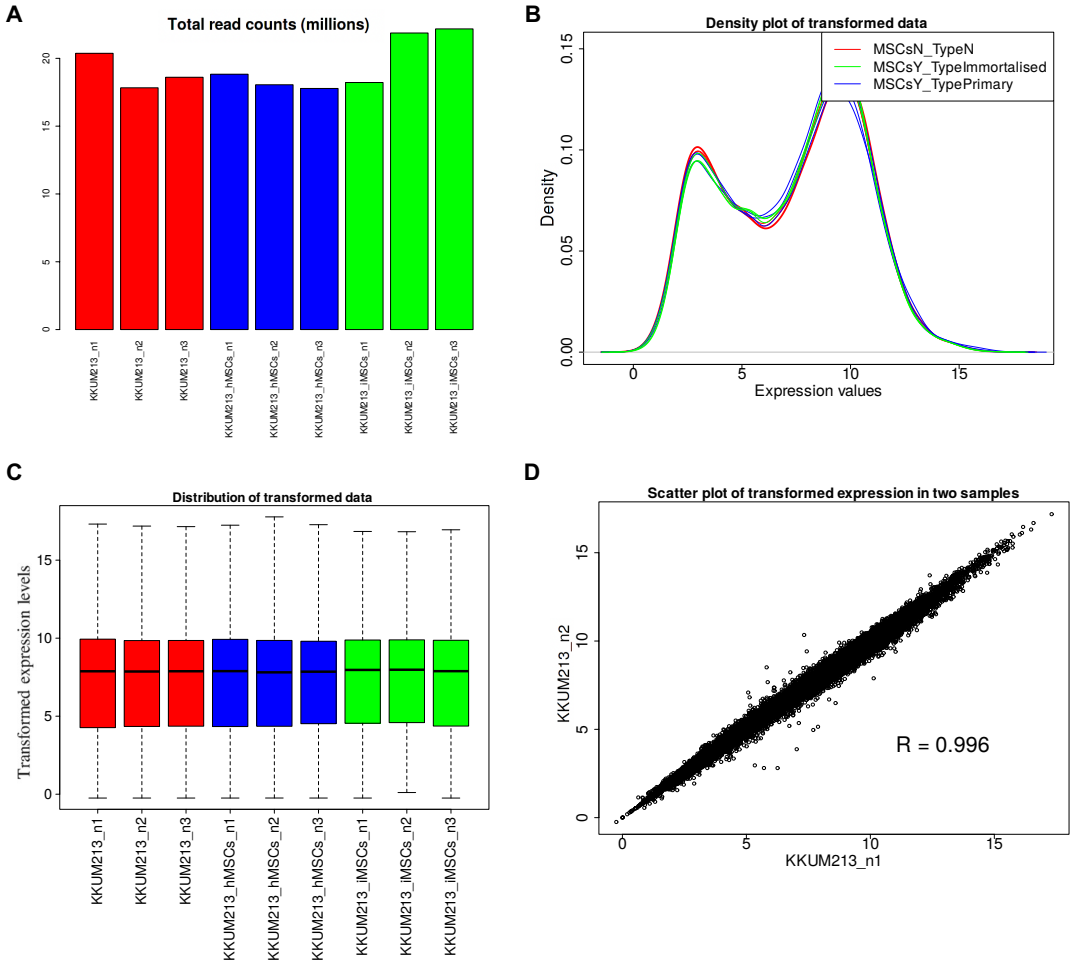



**Figure 6.2. Diagnostic plots of the KKU-M213-derived spheroids.** Counts data and experimental design were used to generate the total read counts per library **(A)**, the density plot to show the distribution of transformed data **(B)**, the boxplot of transformed data **(C)** and the scatter plot of KKU-M213_n1 and KKU-M213_n2 (one representative example) **(D)**. These graphs were generated using IDEP.

The results showed some small variation in library sizes, confirming the absence of a strong bias in sequencing depth (Figure 6.2A). Distribution of the transformed data was also determined (Figure 6.2B and C) and variation among replicates was confirmed to be small (Figure 6.2D).

Hierarchical clustering with a heatmap was used to provide a holistic view of the data. Using the transformed data, iDEP ranked all genes by standard deviation across all samples, the data was then centered by subtracting the average expression level for each gene. The top 1000 most variable genes were used in hierarchical clustering as well as the top 50, from which the name was indicated.

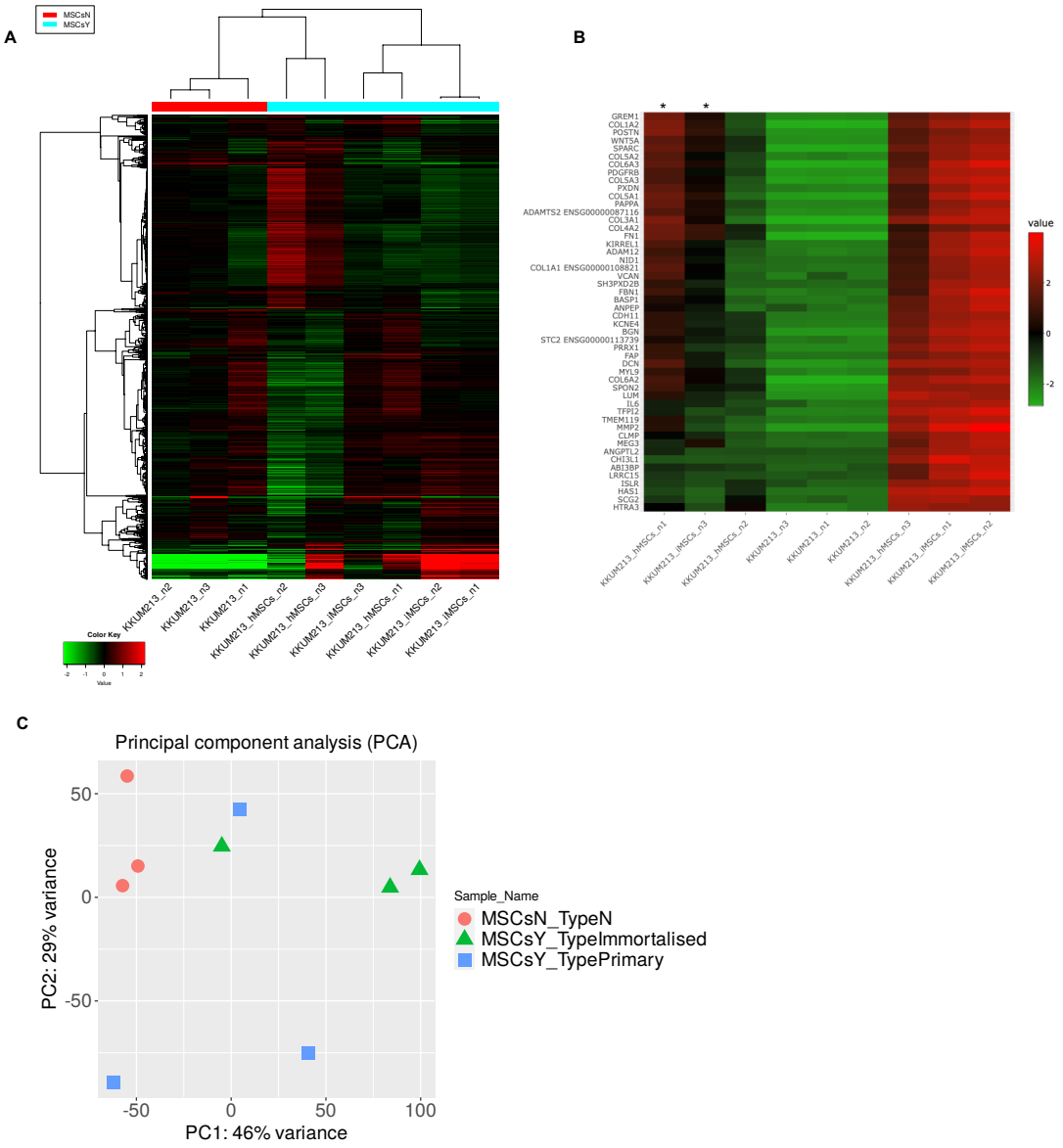


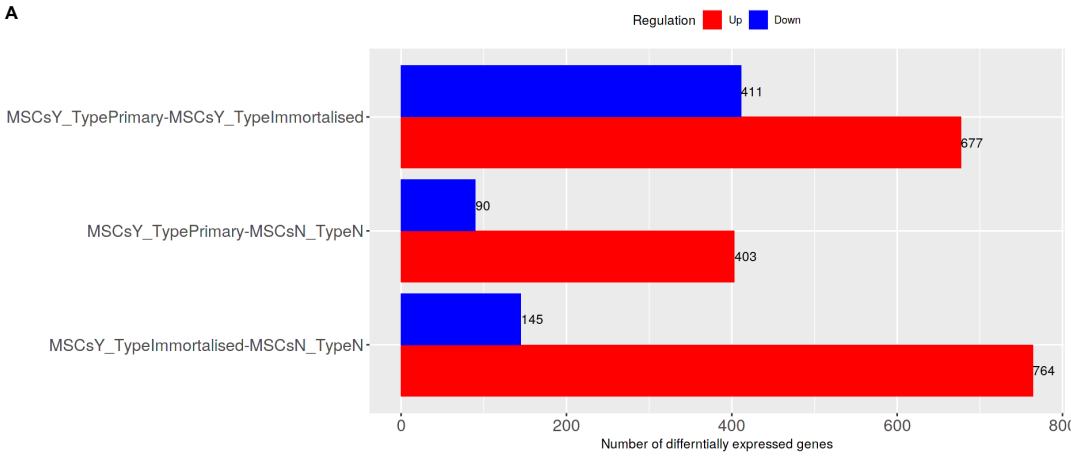

**Figure 6.3. Exploratory analysis for the KKU-M213-derived spheroids.** The gene expression of genes in the presence or absence (TypeN) of iMSCs (TypeImmortalised) or hMSCs (TypePrimary) was explored by generating Hierarchical clustering of all the genes **(A)** and 50 most variable genes **(B)** and PCA analyses **(C)**. These plots were generated using IDEP.

Results suggested that the presence of MSCs induced a change in the expression of hundreds of genes (Figure 6.3A and B). Variations among technical replicates are minimal for the mono-culture spheroids; however, co-cultures n1 and n3 with hMSCs and iMSCs, respectively, had the higher variance within the triplicates (indicated with * in Figure 6.3B). The PCA plot confirmed a difference between the mono- and co-culture spheroids, along the first principal component that explained 46% of the

variance and the second principal component that explained 29% of the variance (Figure 6.3C).

#### 6.2.2.2. Differentially expressed genes and enriched pathways

Once the data was explored, differentially expressed genes identified by the presence of both MSCs were identified using the DESeq2 package. A pairwise-comparison was performed using a model where the comparison was first dependent on the interaction between cancer cells and MSCs, but it also captured the additional effects of MSCs type (Expression ~ Type + MSCs). The false discovery rate (FDR), also called adjusted p-value, cutoff was set as 0.1 (10% chances that the genes are defined as differentially expressed) and the minimum fold change as 2 (ratio between conditions to be equal or higher than 2). These were the default parameters.




| Comparisons | Up | Down |
|---|---|---|
| MSCsY_TypePrimary-MSCsY_TypeImmortalised | 677 | 411 |
| MSCsY_TypePrimary-MSCsN_TypeN | 403 | 90 |
| MSCsY_TypeImmortalised-MSCsN_TypeN | 764 | 145 |

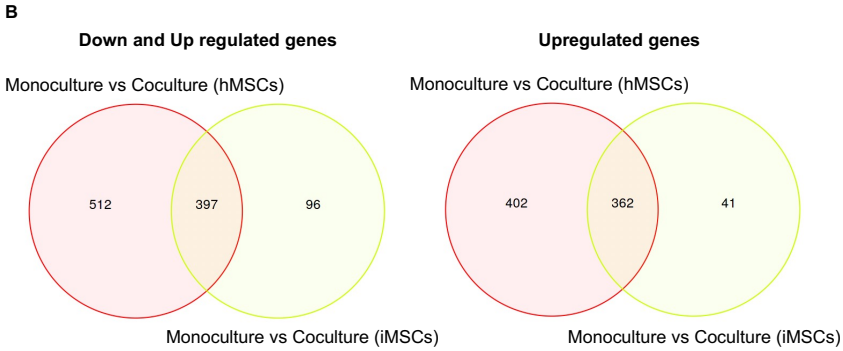



**Figure 6.4. DEGs genes identified by DESeq2 for the KKU-M213-derived spheroids.** The number of differentially expressed genes between the mono-culture and the co-cultures spheroids with either hMSCs or iMSCs cells was determined **(A)**. A Ven Diagram to illustrate the overlap between the expressed genes in the presence of MSCs was generated as well as the overlap between the upregulated genes **(B)**. These graphs were generated using IDEP.

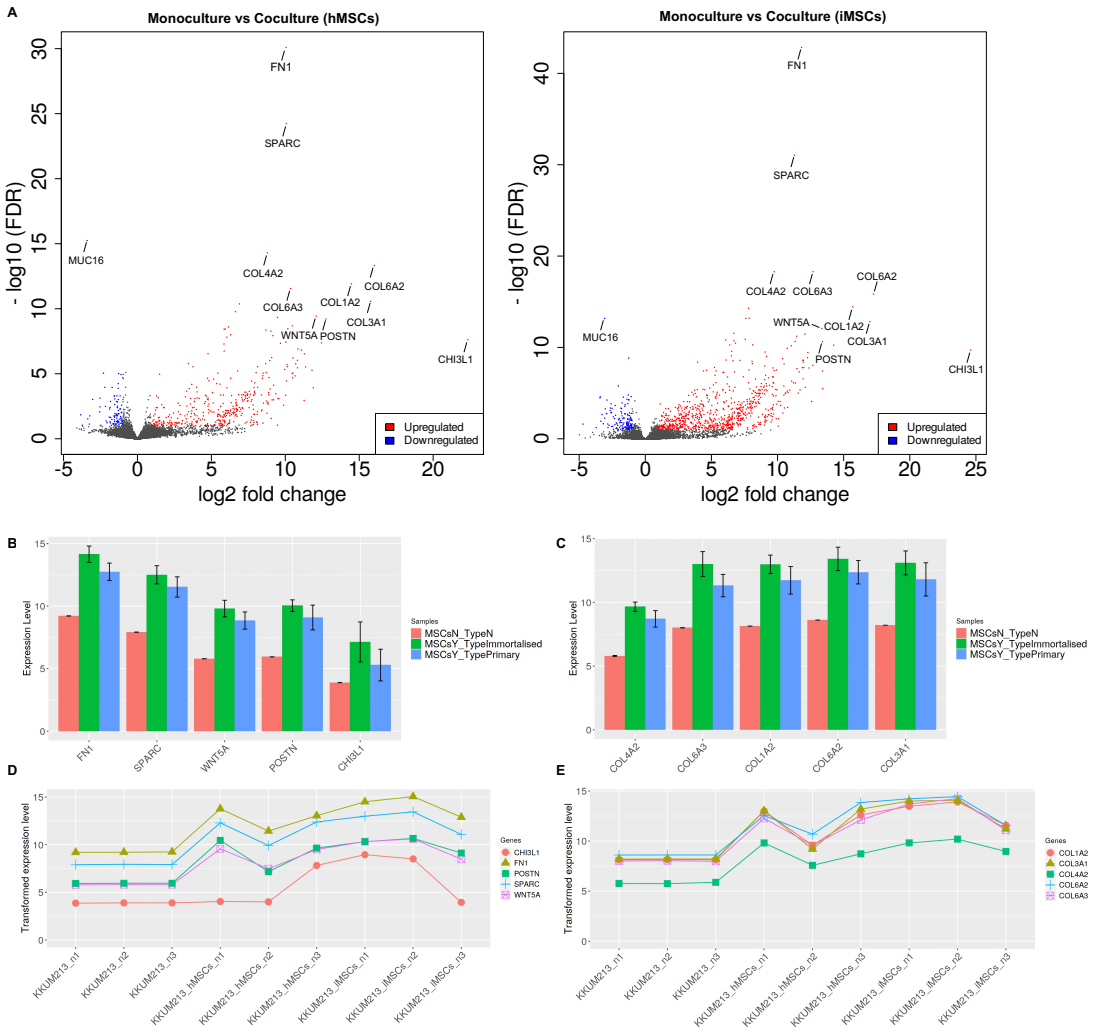



**Figure 6.5. Summary plots for differential expression analysis using DESeq2 for the KKU-M213-derived spheroids.** The differential expressed genes between mono-culture and co-culture with hMSCs or iMSCs were separated based on their FDR and fold change in a Volcano plot. The upregulated and downregulated genes were despite in red and blue, respectively **(A)**. For FN1, SPARC, WNT5A, POSTN and CHI3L1 **(B)** and the family of COL **(C)** the average expression level was determined. The expression level was also determined per sample for FN1, SPARC, WNT5A, POSTN and CHI3L1 **(D)** and the family of COL **(E).** These graphs were generated using IDEP.

With the DESeq2 package, 403 upregulated and 90 downregulated genes were identified in the presence of hMSCs, and 764 upregulated and 145 downregulated in the presence of iMSCs (Figure 6.4A). Of those genes, 397 were shared between both comparisons, of which 362 were upregulated. Interestingly, a variety of genes were also found to be upregulated and downregulated comparing both co-culture models. (Figure 6.4B).

This data was also represented as a volcano plot, where the most upregulated genes were towards the right, the most downregulated genes were towards the left, and the most statistically significant genes were towards the top. The top upregulated genes ranked by the absolute values of fold-change, identified the expression of FN1, SPARC, a family of collagens (COL), WNT5A1, POSTN and CHI3L1 in the presence of MSCs (Figure 6.5A). Of those genes, the individual expression level was determined per group (Figure 6.5B and C) and per sample (Figure 6.5C and D). The upregulated genes were then subjected to enrichment analysis based on the distance between the terms by the percentage of overlapped genes.

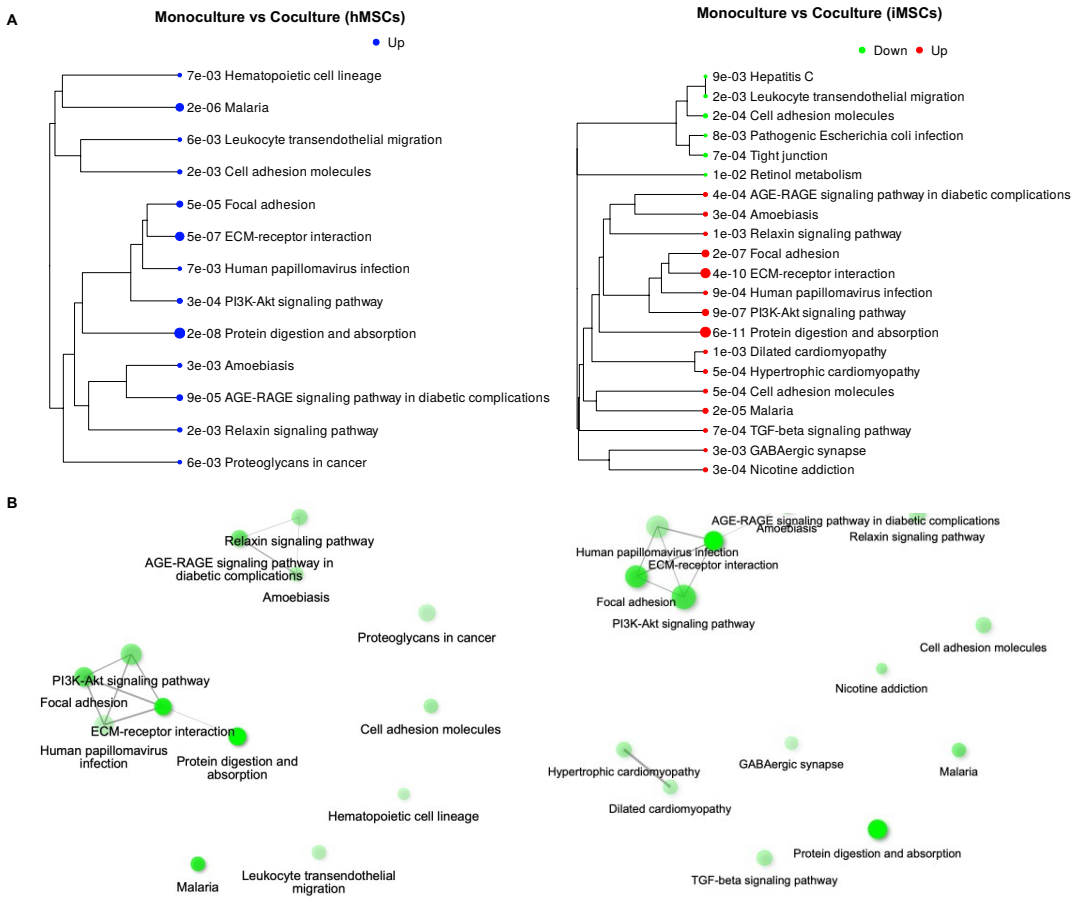



**Figure 6.6. Overrepresentation analysis of KEGG pathways for the KKU-M213-derived spheroids.** The distance between the KEGG pathways and the percentage of overlapped genes was the used to construct a hierarchical clustering tree **(A)** and a network of KEGG pathways **(B)** for the comparison of DEGs between mono- and co-culture spheroids with both hMSCs or iMSCs. The upregulated enriched pathways are depicted in blue for the co-culture with hMSCs and green and red for the downregulated and upregulated enriched pathways for iMSCs co-culture, respectively. The area of circle in the graph represents the fold-change value. The network nodes represented the proteins, and the edges represented the predicted functional associations. These graphs were generated using IDEP.

This enrichment analysis investigated the fraction of those genes that are in a specific KEGG pathway. The hierarchical clustering tree and network show that the enriched terms were similar in both comparisons (mono-culture vs co-culture either with iMSCs or hMSCs). However, no significant down-regulated pathways were shown in the presence of hMSCs. The 2 most significant KEGG pathways enriched in DEGs were Protein digestion and absorption (FDR=1.5e-08 for the comparison mono-culture vs co-culture with hMSCs and FDR=6.0e-11 for the comparison mono-culture vs co-culture with iMSCs) and ECM-receptor interaction (FDR=4.9e-07 for the comparison mono-culture compared vs with hMSCs and FDR=4.2e-10 for the comparison mono-culture vs co-culture with iMSCs). Of those significant pathways in both sets of genes, the one that included the majority of the upregulated genes was PI3K-Akt signalling pathway (20 and 35 genes in the co-culture with hMSCs or iMSCs, respectively) (Figure 5.6A). Additionally, the network of KEGG pathways predicted a functional association between the upregulated pathways in both comparison (Figure 5.6B).

#### 6.2.2.3. Pathway analysis (GSEA)

A GSEA (Subramanian et al., 2005) was conducted in the pre-ranked mode using a recent algorithm based on the fgsea package (Sergushichev, 2016). This approach estimated a p-value by permuting the genes in a gene set, leading to randomly assigned gene sets of the same size. Instead of using selected DEGs that are sensitive to arbitrary cutoffs, pathway analysis used the fold-change values of all genes to identify coherently altered pathways (Ge et al., 2018). Genes with FDR>1 were removed before pathway analysis, a filter of FDR=0.2 was included as a cutoff and a minimal and maximal gene set of 5 and 2000, respectively, was selected.

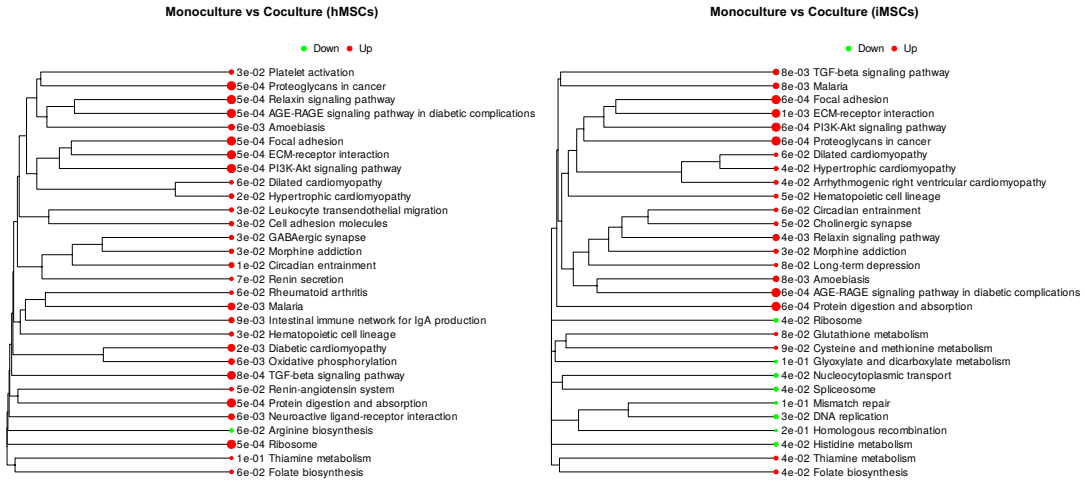



**Figure 6.7. Gene set enrichment analysis for the KKU-M213-derived spheroids.** The GSEA-based KEGG-enrichment plots of representative gene sets from activated pathway were determined for the comparison between mono- and co-culture spheroids with hMSCs (left) or iMSCs (right). The vertical items are the names of KEGG terms, and the downregulated and upregulated pathways are represented in green and red, respectively. the length of horizontal graph represents the gene ratio. The area of circle in the graph represents the fold-change value. These graphs were generated using IDEP.

Results showed similar enriched pathways to the previous analysis. Protein digestion and absorption (FDR= 4.6e-04 for the comparison mono-culture vs co-culture with hMSCs and FDR= 9.8e-04 for the comparison mono-culture vs co-culture with hMSCs), ECM-receptor interaction (FDR=4.6e-04 for the comparison mono-culture vs co-culture with hMSCs and FDR=5.8e-04 for the comparison mono-culture vs co-culture with iMSCs) and PI3K-Akt signalling pathway (FDR=4.6e-04 for the comparison mono-culture vs co-culture with hMSCs and FDR=5.8e-04 for the comparison mono-culture vs co-culture with iMSCs) were the most significant upregulated pathways (Figure 6.7). In order to gain further insights, the gene sets database for pathway analysis was changed and Hallmarks.MSigDB gene sets was used instead. Hallmark gene sets summarise and represent specific well-defined biological processes. These gene sets were generated by a computational methodology based on identifying overlaps between gene sets in other MSigDB collections (32880 gene sets) and retaining genes that display coordinate expression (Liberzon et al., 2015).

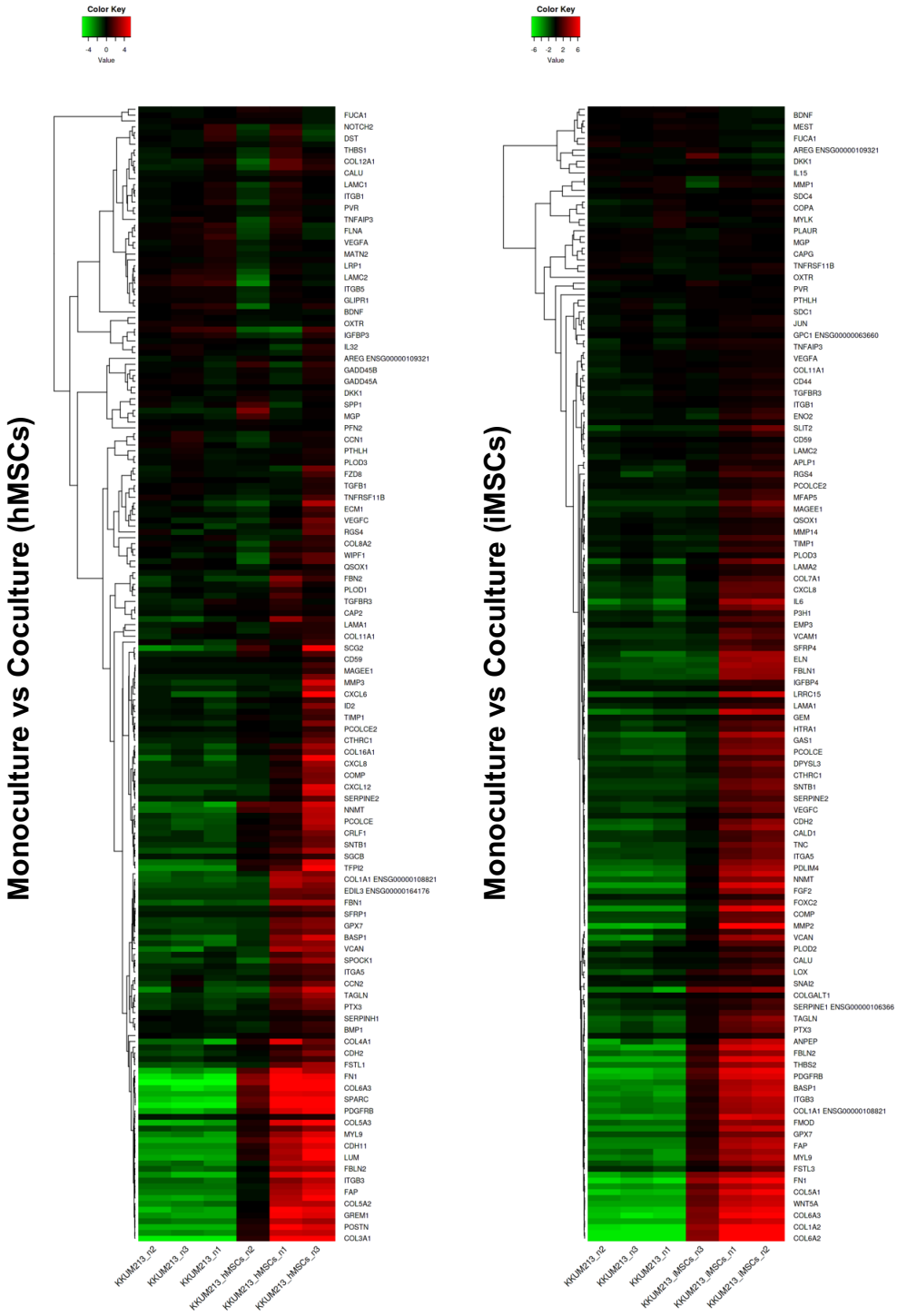



**Figure 6.8. Heatmap of the EMT pathway**. The GSEA-based Hallmark-enrichment plots selected the EMT as the most significant pathway for both comparisons (mono-culture compared to co-culture with either hMSCs (left) or iMSCs (right)). The vertical items are the names of genes. The area of circle in the graph represents the fold-change value. These graphs were generated using IDEP.

The most significant Hallmark pathway was EMT for both comparisons (FDR= 1.7e-04 for the comparison mono-culture vs co-culture with hMSCs and FDR=2.5e-04 for

the comparison mono-culture vs co-culture with iMSCs). Interestingly, the heatmap for the expression of genes showed FN1 and the family of COL as the most differentially expressed genes in co-culture with MSCs. SPARC was also present as the most upregulated gene in the presence of hMSCs (Figure 6.8).

### 6.2.3. Bioinformatic analysis of the PDXs

Once the analysis for the spheroid model was completed, the same steps were carried out to determine potential upregulated pathways in the co-culture spheroids with hMSCs. 7 PDXs (CCA1, CCA2, CCA4, CCA5, CCA6, CCA7 and CCA11) were included; each PDX was included as a single biological replicate in absence or presence of hMSCs. The input for the analysis was the gene-level expression matrix (provided by Prof Nigel Mongan) and the experimental design, which defined how the samples related to the experimental conditions.

#### 6.2.3.1. Pre-processing and Exploratory analysis

Once the data was processed, the software recognised the human species as the best match. The low expressed genes were removed from further analysis, to avoid noise for the downstream analyses (0.5 CPM in at least one sample). From a total of 60676 in 14 samples, 22907 genes passed filter and 22866 were converted to Ensembl gene IDs. The remaining 41 genes were kept in the data using original gene IDs.

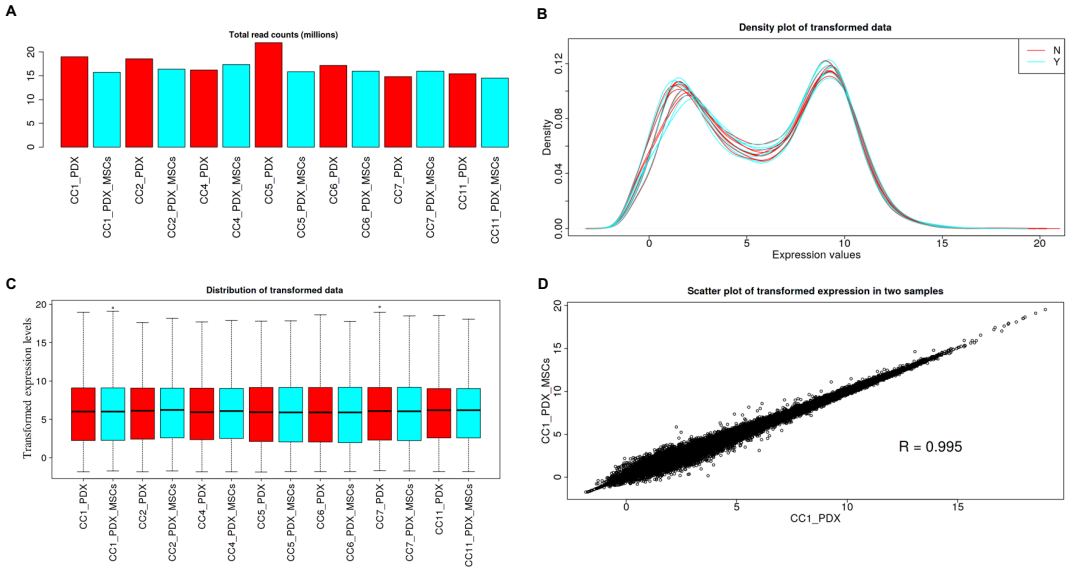



**Figure 6.9. Diagnostic plots of PDXs.** Counts data and experimental design were used to generate the total read counts per library **(A)**, the density plot to show the distribution of transformed data **(B)**, the boxplot of transformed data **(C)** and the scatter plot of CC1_PDX and CC1_PDX_MSCs **(D)**. These graphs were generated using IDEP.

The bar plot of total read counts and the distribution of transformed data confirmed minimal variation in library sizes (Figure 6.9A and B). Minimal variation among replicates was also confirmed (representative figure, Figure 6.9D). The data was further explored by generating the heatmaps and the PCA plot.

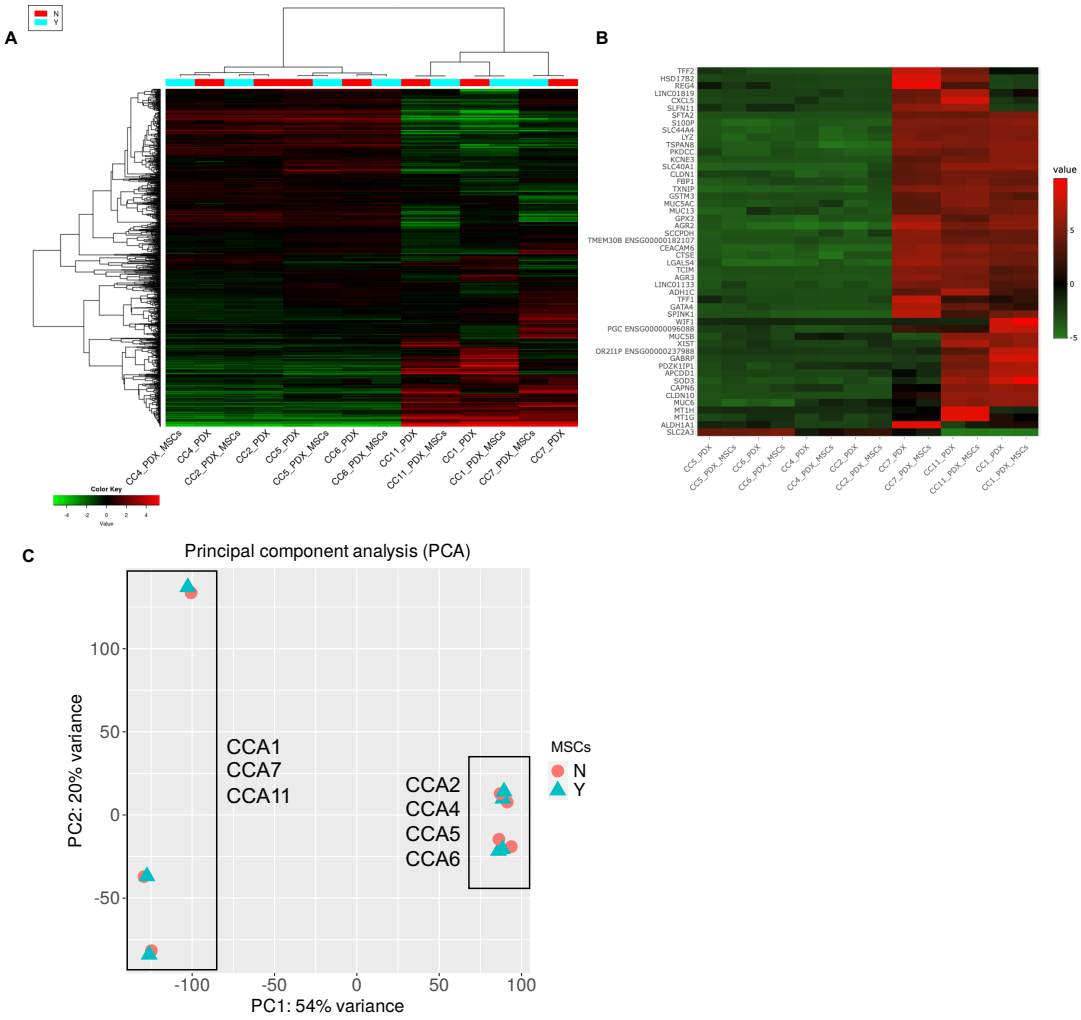



**Figure 6.10. Exploratory analysis for the PDXs.** The gene expression of genes in the presence and absence of MSCs was explored by generating Hierarchical clustering of all the genes **(A)** and 50 most variable genes **(B)** and PCA analyses **(C)**. These plots were generated using IDEP.

The top 1000 and 50 most variable genes were used in hierarchical clustering. Interestingly, samples were clustered in two groups independent of the presence of MSCs. The first group clustered was CCA1, CCA7 and CCA11. The second group was CCA2, CCA4, CCA5 and CCA6 (Figure 6.10A and B). Interestingly, these results correlate to the difference in histology and spheroid formation observed in the previous chapter. These PDXs grouped together despite the presence of MSCs. Group 2 clustered together with a 54% variance from Group 1. Group 1 was distributed across the second principal component with a variance of 20% (Figure 6.10C). The variability between tumours was larger than the variability derived from the presence or absence of MSCs. Therefore, it was difficult to observe any effect due to the MSCs. In order to assess whether there was any effect due to the MSC presence, the original tumour

condition was treated as a batch effect and removed it[1] (using the package limma (Ritchie et al., 2015)) and recreated the PCAs.

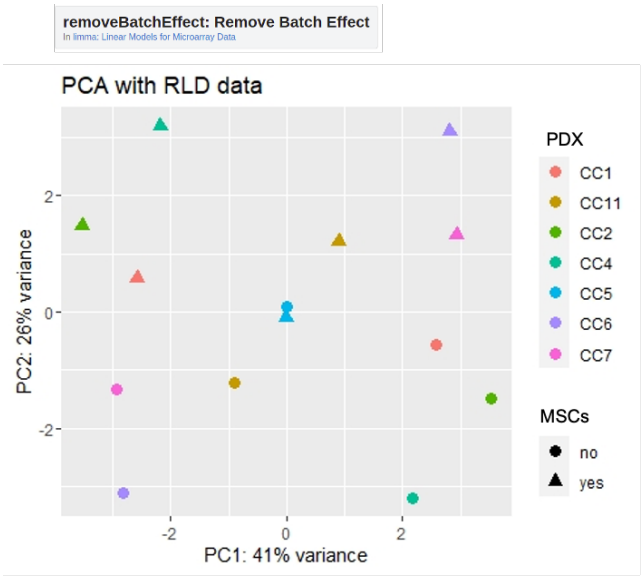



**Figure 6.11. PCA plot of the PDXs after removing batch effect.** Data was normalised removing the tumour effect and the samples were plotted to determine the variance between samples and conditions. This plot was generated using IDEP.

This result showed that there is some effect due to the MSC, since the samples can be separated according to their presence. After removing the batch effect, the samples in presence or absence of MSCs were on the top and bottom of the PCA2, respectively, with a 26% of variance. However, the highest variance was found on PCA1 with a 41% variance (Figure 6.11).

#### 6.2.3.2. Differentially expressed genes and GSEA

Once the data was explored, differentially expressed genes in the co-cultures with MSCs were determined. A pairwise-comparison was performed using a model where the comparison was first dependent on the interaction between cancer cells and MSCs, but it also captured the additional effects of MSCs type (Expression ~ Type + MSCs). The FDR cutoff was set as 0.1 and the minimum fold change as 2.

No genes were found to be significant, and therefore no enriched pathways were found to be activated in the MSCs co-cultures. Even though no genes were found to be

[1] Limma's removebacheffect function fits a linear model to the data, including both regular treatments and possible batch effects, and then removes the component due to the batch effects.

significant on this analysis, there was an evident difference between the 2 Groups of PDXs which would be interesting to explore but beyond the aims of the current project.

### 6.2.4. 3D CCA models

In order to explore the models in more detail, all samples were run to generate a PCA plot including the tumours from which PDXs were derived.

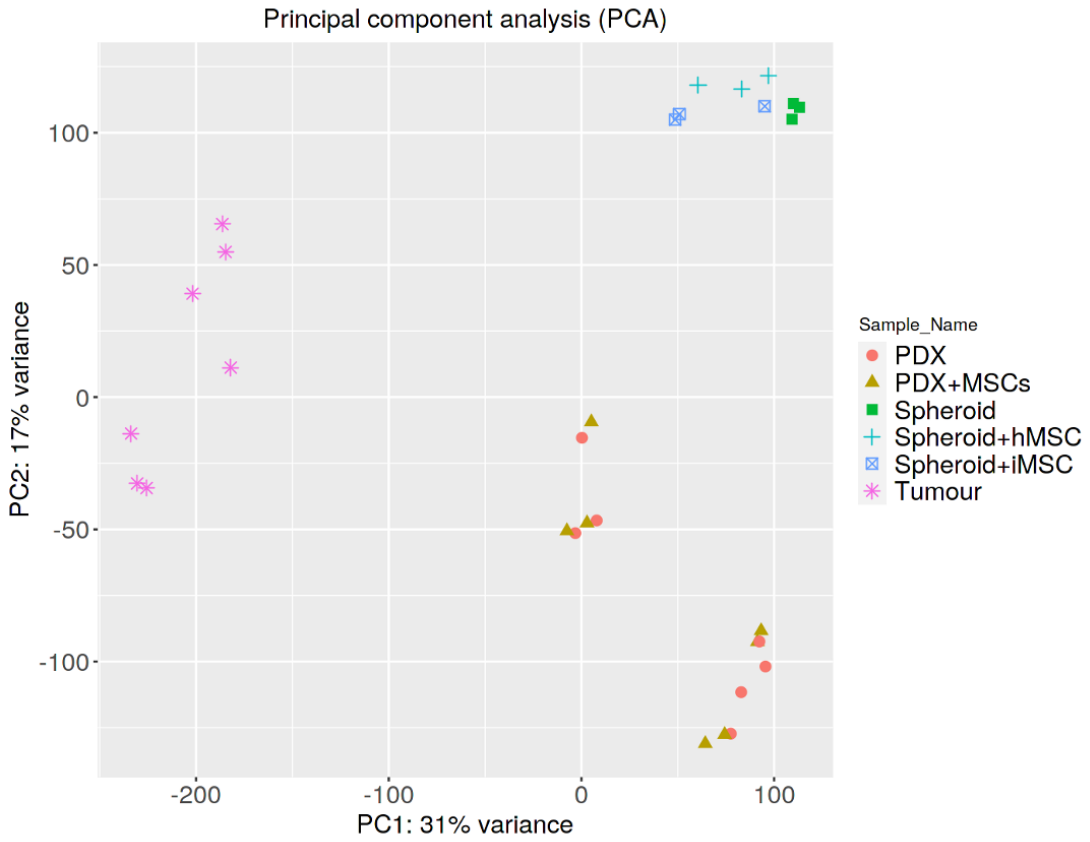



**Figure 6.12. PCA plots of 3D CCA models.** PDXs in the presence or absence of hMSCs, spheroids in the presence or absence of either hMSC or iMSCs and CCA tumours were sequenced and plotted in a PCA. This plot was generated using IDEP.

There was a considerable transcriptomic distance between the tumours and corresponding PDXs, explaining almost the 31% of variance. Group 1 PDXs were closer to the tumours than those in Group 2. Group 2 PDXs were at the same distance to the tumours as cell-line-derived spheroids. Interestingly, co-cultures spheroids were closer to the tumours than the mono-cultures (Figure 6.12).

## 6.3. Summary and Technical Discussion

A bioinformatic analysis of the transcriptome of the different models developed on previous chapters was performed. For the cell-line-derived spheroids the top upregulated genes were FN1, SPARC, a family of COL, WNT5A1, POSTN and CHI3L1. Additionally, two pathways were identified as upregulated, the ECM-receptor interaction and the PI3K-AKT pathway, which could be driving the enhanced proliferation in the co-cultures. In the PDXs, the exploratory analysis, clustered the PDXs in two groups, the same groups that were defined based on their morphology.

The analysis was done using R and iDEP, although iDEP was used to generate all the figures in this chapter. R is a powerful and widely used tool to identify DEGs and altered pathways by using established packages (Huber et al., 2015). However, these packages can be time-consuming, and sometimes out of reach for researchers with no experience in coding (Ge et al., 2018). iDEP is a web application that connects 63 R/Bioconductor packages, and the main advantage was that it was user-friendly, and it did not require coding experience (Ge et al., 2018). Similar to iDEP, there are applications such as START App (shiny transcriptome analysis resource tool) that performs similar analysis (Nelson, Sklenar, Barnes, & Minnier, 2017), among others. However, iDEP contains more packages for analysing the RNASEq compared to the rest of applications (Ge et al., 2018). Therefore, and together with being recommended in a bioinformatic course, were the reasons for the ultimate choice of this software.

- **Quality of the RNA**

The quality of the RNA was assessed by both Nanodrop and RIN analysis. The RIN results from some of the samples were low, especially those derived from human tumours. It is known that low-quality RNA can substantially affect the sequencing results and lead to erroneous biological conclusions (Kukurba & Montgomery, 2015). However, the internal quality checks (QC) performed by Novogene confirmed acceptable QC and the sequencing was therefore performed. The low quality of the tumours was hypothesised to be due to being old samples that were stored for a long time in -80ºC. A limited number of studies have sought to identify factors that may contribute to RNA quality outcomes using human pancreas tissue (Philips et al., 2017). Some of them include storying it in RNAlater (a medium that inhibits RNAse activity) (Philips et al., 2017).

- **Exploratory analysis**

The data was separated in two datasets, the cell-line derived spheroids (mono- and co-cultures) and the PDXs. However, and before analysing the data, an exploratory analysis was performed for both datasets. The exploratory analysis is a fundamental step to visualise, plot and manipulate the data to assess its quality (Data, Komorowski, Marshall, Salciccioli, & Crutain, 2016). Firstly, a total read-count plot was generated. This confirmed that in both datasets, the differential expressed genes are biologically differential and not due to a higher count of a particular sample (Evans, Hardin, & Stoebel, 2018). The data was then transformed and plotted in a density plot and boxplot. In RNASeq analysis, it is important to use transformed data in order to stabilise the variance across mean values (K. A. Johnson & Krishnan, 2022).

- **DESEq analysis**

In the cell-line-derived spheroids, the PCA plot showed a variability between the iMSCs co-cultures and hMSCs co-cultures, and therefore the analysis was performed separately. The low counts were first filtered since they were not expressed at a biologically meaningful level in any condition. In addition, transcripts having read count (within 0-10 rage) are considered artifacts in the literature (Bourgon, Gentleman, & Huber, 2010). From a statistical point of view, removing low count genes allows the mean-variance relationship in the data to be estimated with greater reliability (C. W. Law et al., 2016). Additionally, the default FDR and fold change cut-off values were used to screen out differentially expressed genes (Ge et al., 2018). FDR was set as 0.1 (10% of the genes are not false positive). The fold change was set as 2. Applying a fold change cut-off, in addition to the FDR, meant that those genes that were significant through being consistent between replicates but not in absolute sense, were also removed.

There are different packages to perform the analysis of RNASeq such as limma, EdgeR and DESeq2 (S. Liu et al., 2021). The package used in this study was DESeq2 since it was recommended by the bioinformaticians that helped conducting the analysis. These three packages are similar although having different steps among the processes of the analysis. For instance, a linear model is used for statistics in limma, whereas the negative binomial distribution is used in EdgeR and DESeq2. Additionally, EdgeR and

limma require normalised RNASeq count data, whilst DESeq2 do not (S. Liu et al., 2021).

For the cell-line-derived dataset, the top differential expressed genes were FN1, SPARC, a family of COL, WNT5A1, POSTN and CHI3L1. Techniques such as qPCR could be used to validate these targets (Coenye, 2021). Nonetheless, a recent study suggested that RNASeq data was robust enough to not require validation by qPCR and/or other approaches (Coenye, 2021).

For the dataset of the PDXs, a normalisation to remove the batch effect was performed using the limma package. It was hypothesised that the variability between PDX samples (e.g between CCA1 PDX and CCA2 PDX) was higher than the condition tested (presence or absence of MSCs). This function is known to remove unwanted batch effects fitting a linear model to the data, that includes both batches and the condition tested and then removes the component related to the batch effect (rdrr.io, 2020). However, even after removing the batch effect, no significant genes were found (Figure 6.11). This data needs further investigation.

- **Pathway enrichment and Gene set enrichment analysis**

Both pathway enrichment and gene set enrichment analysis were used to identify potential significant pathways based on the DEGs. For the pathway enrichment, the list of DEGs was used as an input to determine the up- or down-regulated pathways (ADVAITA). GSEA, however, analysed all genes based on their differential expression rank, and searched for pathways whose genes were enriched at the top or bottom of the ranked gene list (Reimand et al., 2019). Several established pathway enrichment analysis methods are available, and the choice of which to use depends on the type of gene list. GSEA was indeed recommended for RNASeq data (Reimand et al., 2019).

In both analyses, ECM-receptor signalling pathway was an enriched pathway, meaning that the top-most differentially expressed genes were involved in this pathway, ultimately suggesting that the ECM-receptor interaction is affected by the presence of MSCs. Similarly, the PI3K-AKT pathway was also enriched containing the majority of differentially expressed genes. Despite the wide application of these tools in transcriptome analysis, there are biases and false positives in these pathway analysis results that should be considered (Yan, Chi, Chang, & Tian, 2020). It has been

shown that unrelated pathways can be significantly enriched by pathway analysis due to shared genes in the pathways (Donato et al., 2013). The network nodes were generated to improve the rationality and interpretation of this data. However, based upon prior knowledge of these pathways, it has been shown that ECM can activate PI3K-AKT signalling pathway (Nallanthighal, Heiserman, & Cheon, 2019), and therefore, it was hypothesised that the enhanced proliferation of the co-culture models could be driven by these pathways. The KEGG and Hallmarks collection of genes were used for this study. However, other established collection of genes can also be used for a specific biological process, location and disease (ADVAITA). The analysis of the co-cultures is complex by the fact that the MSCs are present in one of the samples and therefore some of the signals are probably coming from them. However, this had to be done in this setting because the indirect co-culture was not effective (Chapter 4, Figure 4.10).

The results from a bioinformatic analysis on RNASeq data should be carefully interpreted, since there are many combinations of methods and gene set databases available to use. This study was guided by two bioinformaticians that confirmed the rationale of the analysis. Based on that, both ECM-receptor interaction and PI3K-AKT signalling pathway were proposed as potential pathways that may be driving cell proliferation in the MSCs co-culture cell-line models. The PDX dataset required further investigation, and was included in a bigger study in the Grabowska Lab.

# Chapter 7. Discussion, Conclusions and Future directions

## 7.1. Discussion

In this study, pre-clinical CCA spheroid models that may better represent *in vivo* biology and the tumour microenvironment components, were successfully developed using standard cell-lines or primary CCA cells expanded as PDXs, and co-cultured with a source of immortalised or primary MSCs to model the influence of the TME. Cell proliferation was found to be significantly promoted by the influence of both MSCs in the cell-line derived spheroids. Importantly, this effect was only found in the direct co-culture model. The potential mechanisms underlying this proliferation involved the ECM-receptor and PI3K-AKT signalling pathways. PDX models maintained the hepatobiliary nature and were classified into two groups based on the morphology, Group 1 (well differentiated) and Group 2 (poor differentiated). In the PDX-derived spheroids, it was noted that the presence of stromal support enhanced the formation of spheroids in Group 1.

- **CCA cell-lines successfully form 3D spheroids with distinct morphologies**

All five of the CCA cell-lines that were used successfully formed spheroids. Additionally, these cell-lines spanned two of the three subtypes of CCA (Banales et al., 2020). KKU-M055 (Tepsiri et al., 2005), KKU-M156 (Tepsiri et al., 2005), KKU-M213 (Obchoei et al., 2011), HuCCA-1 (Sirisinha et al., 1991) and RBE (Enjoji, Sakai, Nawata, Kajiyama, & Tsuneyoshi, 1997) belong to the iCCA type, and TFK-1 (Saijyo et al., 1995) belong to the dCCA type. Many studies show that iCCA incidence and mortality are increasing, while eCCA is declining worldwide (Blechacz, 2017; Gentilini et al., 2018). Additionally, the cell-lines that formed spheroids included cells derived from Opisthorchis Viverrini-driven cancer (KKU-M055, KKU-156, KKU-M213 and HuCCA-1), and cells derived from non-Opisthorchis Viverrini-driven cancer (TFK-1 and RBE). ICCA driven by infection with Opisthorchis viverrini, a liver fluke, is endemic in Far East and Southeast Asia and although historically seen as an uncommon cancer in the West, non-fluke-associated malignancy has increased in incidence in the UK, Europe, and the United States over the last four decades (J. W. Valle, Kelley, Nervi, Oh, & Zhu, 2021; Younger et al., 2022).

A model was generated that incorporated mesenchymal stem cells. This was relevant because CCA is highly desmoplastic (Sripa & Pairojkul, 2008) and MSCs are known to enter and form a component of tumour stroma (Quante et al., 2011). ICCA patients

with presence of MSCs in the TME are known to induce chemoresistance in CCA cells through production of IL-6, and subsequent activation of autophagy by regulating the AMPK/mTOR signalling pathway (Gan et al., 2021). In addition, in the Grabowska Lab it had been demonstrated that co-culturing cancer cells with MSCs enhance proliferation of breast cancer cells (Pal et al., 2020). However, and to the best of our knowledge, the role of MSCs in CCA remained unknown prior to the current study.

MSCs are known to differentiate to CAFs (Quante et al., 2011). Given the heterogeneity of CAFs, subpopulations of these cells should be characterised in detail. Although the characterisation of the MSCs to CAFs was not performed, this is something interesting to consider for future work. In fact, presence of different fibroblast subpopulations and the effect of the cancer type has been reported to influence the net outcome (Barrett & Puré, 2020). A solution for the issues concerning the heterogeneity of CAFs could be profiling CAF populations at the single cell level as well as performing IF or IHC (H. Huang et al., 2022; Lorsakul, 2017; Wong et al., 2019; M. Yu et al., 2020). A study based on single-cell RNA sequencing in CCA patients segregated two CAF subpopulations, inflammatory and growth factor-enriched, myofibroblastic (Affo et al., 2021). In addition to the CAFs, the immune cells are also an important component of the CCA TME. Generating a model to better understand the mechanisms implicated in the tripartite interplay of tumour cells and the main elements of the CCA TME could be something to consider for further investigation. Indeed, a triple co-culture spheroid has been developed and characterised for pancreatic cancer (Lazzari et al., 2018). They described the model as a pertinent and easy-to-handle tool, which could be introduced in routine pre-clinical screening for pancreatic cancer treatment.

This project therefore introduced a 3D *in vitro* model in which CCA cell-lines cells were co-cultured with MSCs to mimic the stroma-tumour interaction. The common approach in cancer research is to use animal models. Nonetheless, there are many concerns regarding the manipulation of animals under certain experimental conditions (Hoarau-Véchot, Rafii, Touboul, & Pasquier, 2018). Additionally, many experimental animals are immunocompromised and do not offer the same stroma-tumour interaction, which prevents the direct translation of novel research to clinic. The lack of human tumour in mouse models is also a factor that affects the lack of translation. Obtaining concordance between experimental animal models and clinical trials still

remains challenging, the average rate of concordant results reaches 8% (Cekanova & Rathore, 2014).

Among all the 3D models, the Grabowska Lab had already expertise in the use of spheroids (Ivanov & Grabowska, 2017; Pal et al., 2020), and together with the advantages they offer, they were selected as the 3D *in vitro* model for this study. First of all, it is important to define spheroid as it can sometimes overlap with organoid depending on previous literature. Organoids are generally recognised as an *in vitro* "miniorgan" or complex tissue-like structure with multiple cell types grown in the presence of a matrix (Prior, Inacio, & Huch, 2019). In this study, spheroids are referred to as "cell aggregates". Spheroids are often generated from immortalised cell-lines (Sato et al., 2021). Some of the advantages of using spheroid over other 3D models are that they are easy to handle and high reproducible (Y. Fang & Eglen, 2017; Habanjar et al., 2021). Additionally, they allow better cell-cell contact, with increased intercellular communication, and more uniform distribution of receptors and adhesion molecules over the cell surface (Knight & Przyborski, 2015). A scaffold-free method using ULA plates was chosen for the generation of spheroids. With this technique, a large number of spheroids can be simultaneously generated on the same plate, facilitating the reproducibility of the model and enabling the monitoring of spheroid formation and growth (Pinto et al., 2020). Scaffold and scaffold-free techniques can be used for spheroid formation. For scaffold-based approaches, 3D cell culture is done by seeding the cells on a porous matrix (Langer & Vacanti, 1993). The concept of a scaffold-free technique, however, is characterised by two processes, first the self-organisation of cells without the need of applying external forces and second the self-assembly depending on cell natural features (Alghuwainem, Alshareeda, & Alsowayan, 2019). A notable benefit of this method is the easily manipulation for the downstream applications. Additionally, due to the high initial cell seeding density, cell proliferation is not a key factor to start the model (Alghuwainem et al., 2019).

Spheroids have been extensively used and characterise in other types of cancer. However, in CCA, these models have not yet been highly explored. A few examples where this model was developed is using SK-ChA-1 and Mz-ChA-1 cell-lines to generate spheroids by a rotatory culture system that inhibited CCA cells adhering on the bottom surface (Mischiati et al., 2015). In another study, spheroids were established from iCCA cell lines (SG231, HUCCT1, CCLP1, and CCA4) in

anchoring-independent conditions (Raggi et al., 2017). TFK-1 cells were also used to generate spheroids using ULA plates (Kawamoto et al., 2018).

In this study, KKU-M156, KKU-M213, HuCCA-1 and RBE cell-lines showed high efficiency of spheroid formation, whereas KKU-M055 showed low efficiency. It is known that even for the same tumour type, the efficiency of spheroid formation is cell-line dependent (Han, Kwon, & Kim, 2021). The process of spheroid formation has been described as an initial aggregation of cells initiated by integrin-mediated attachment to ECM molecules, and then cells are aggregated compactly by E-cadherin mediation (H. Lu & Stenzel, 2018). This is consistent with our results, KKU-M055 were the only mono-culture spheroids that expressed Vimentin (Chapter 4, Figure 4.14). Vimentin, is a hallmark of EMT, involved in cell shape maintenance, motility, and directional migration (B. Zhou et al., 2021), and associated with reduced E-cadherin expression *in vitro* (B. Zhou et al., 2021). In the presence of BME, the KKU-M055 generated more defined 3D spheroids (Chapter 3, Figure 3.2). Adding reconstituted BME in the media is known to contribute to compact spheroids. Different additives are suggested to support spheroid formation such as Matrigel, Geltrex and Colagen (Han et al., 2021).

CCA cell-lines in mono-culture formed different size spheroids even under the same conditions. For instance, KKU-M055 formed the biggest spheroids and RBE the smallest. In fact, the low ability of the KKU-M055 to form compact spheroids could have contributed to this result. Spheroid size is mainly determined by cell type and seeding density and it is a critical factor related to tumour biology and drug screening. The heterogeneous cell layers depend on the spheroid size, and the access of oxygen and nutrients inside the spheroid becomes more difficult as the spheroid becomes larger (Han et al., 2021). Therefore, spheroid size is an important factor to control and optimise. Spheroids, however, were only used to explore cell biology, the difference on size was acceptable. If the outcome was drug screening, this is something that would have required further optimisation. The degree of drug penetration is known to be affected, compact spheroids are known to be more resistant to drugs than aggregated cells, and smaller spheroids are more sensitive to both treatments such as chemotherapy and radiotherapy. Additionally, the presence of hypoxic cells in larger spheroids may increase resistance to the therapy (Han et al., 2021).

Spheroids were characterised by assessing cell viability, and live/dead staining and AlamarBlue were used. It is well known that large spheroids display an inner layer of necrotic cells, a peri-necrotic zone of apoptotic cells surrounded by a middle layer of quiescent viable cells, and an outer layer of highly proliferative and migratory cells (Nath & Devi, 2016). This was not consistent with our results (Chapter 3, Figure 3.4). However, the differences in compactness of spheroids could lead to issues with dye penetration and ultimately inaccurate conclusions. A commercial kit for assessing the live/dead staining was proposed for future assays. In regard to AlamarBlue, results were consistent with the size (Chapter 3, Figure 3.7) since the strong fluorescence signal was found in the large spheroids.

Spheroids showed a similar histological appearance to human CCA (Chapter 3, Figure 3.8). The internal structures found in the spheroids were hypothesised to be ECM produced by cancer cells after cell-cell interaction. Alcian Blue staining may be an appropriate method to elucidate if there is presence of mucins and ECM components in the spheroids. KKU-M055 and RBE showed a different morphology compared to the rest of the spheroids. In fact, KKU-M055 expressed low levels of CK7 and CK19, and the authenticity of the cell-line was questioned. Short tandem repeat profiling should be carried out on this cell-line to verify the identity. For the RBE cell-line, although the Non-O-CCA nature should be considered, it was hypothesised that they suffered mechanical stress due to quick compactness. This is consistent to a previous study that has shown that the growth of spheroid in a confined rigid environment inhibits its own growth (Helmlinger, Netti, Lichtenbeld, Melder, & Jain, 1997). Additionally, other studies support this statement by showing that a compressive stress applied on spheroid grown is linked to a decrease in cell division (Delarue et al., 2013; F. Montel et al., 2011; F. D. Montel, M.; Elgeti, J.; Vignjevic, D.; Cappello, G.; Prost, J., 2019).

- **Mesenchymal stem cells enhanced cell-line proliferation in a direct co-culture system**

The interaction between cancer cells and mesenchymal stem cells was investigated in spheroids in a co-cultured system. A source of primary or immortalised MSCs was used. Both cells were human, and bone-marrow derived, the difference was that the immortalised cells when through a process of immortalisation. Mesenchymal-stem cells are important components of the TME and can specifically migrate to primary

tumours and metastatic tumours and proliferate and differentiate into components of the tumour stroma (Ljujic et al., 2013; Uchibori et al., 2013). There are numerous studies that have demonstrated that MSCs play an important role in various types of cancer such as gastric cancer, ovarian cancer and leukemia (Z. W. Gu, He, Wang, Tian, & Di, 2019; He et al., 2019; J. A. Kim et al., 2015). Additionally, in gastric cancer it has been demonstrated that at least 20% of CAFs originate from bone marrow mesenchymal stem cells (Quante et al., 2011). In iCCA, it was revealed that there was also a large number of MSCs infiltrating cells (Gan et al., 2021), but their role remains still unknown.

To the best of our knowledge, this is the first study investigating the crosstalk between the CCA cancer cells and MSCs in 3D models. The study of the interaction between cancer cells and stroma cells has previously been studied in 2D co-culture systems in CCA (Fabris et al., 2000; Holt et al., 2009; Massani et al., 2013). One study used conditioned medium from CSC-enriched spheroids to expose tumour associated macrophages (Raggi et al., 2017); and differently, a type I collagen matrix to co-culture model cells derived from iCCA formed in syngeneic rat liver with different clonal α-SMA-positive CAFs (Campbell et al., 2012).

We demonstrated a significant higher cancer cell proliferation in the hMSCs and iMSCs co-cultures, except for KKU-M055 and RBE co-culture spheroids (Chapter 4, Figure 4.9). For the RBE spheroids, the mechanical stress seemed to affect the growth of the cells in a 3D environment and the co-culture made no difference. For the KKU-M055 and MSCs co-culture, cell viability and spheroid size were higher in the mono-culture spheroid. However, when Ki-67 was quantified, the expression was higher in the MSCs co-cultures. Ki-67 is a more accurate method to quantify proliferation since metabolic assays may not accurately represent changes in cell growth (Quent, Loessner, Friis, Reichert, & Hutmacher, 2010). This effect was only found in the direct system. It is known that communication between cancer cells and MSCs can be indirect or direct. Indirect communication involves the exchange of extracellular vesicles (exosomes, microvesicles, etc.) and soluble molecules (cytokines, chemokines, growth factors, etc.). Direct communication, on the other hand, involves membrane protein interactions such as integrin and/or notch signalling, gap junctional intercellular communication, etc (Melzer, von der Ohe, & Hass, 2018). Such crosstalk affects tumour progression or can induces differentiation of MSC. This also

contributes to ECM restructure and EMT (Melzer et al., 2018). This result suggests the need of a direct contact to enhance cell proliferation. In fact, direct co-cultures are more likely to mimic the *in vivo* environment (Vis et al., 2020). However, the idea to investigate the indirect co-culture system was to facilitate the manipulation of the two cell types for further applications where they have to be independently studied.

An interesting effect was the invasive phenotype noticed in the MSC-derived spheroids in the indirect co-culture system (Chapter 4, Figure 4.10). In fact, studying the MSCs-derived spheroids it is something that has been performed in other studies and difference between their behaviour in 2D and 3D has been proofed. For instance, the secretion of exosomes seemed to significantly increase when they were cultured in spheroid form compared to 2D (M. Kim, Yun, Park, Choi, & Min, 2018; Thippabhotla, Zhong, & He, 2019). The effect of MSCs on cancer cell invasion it is something that has also not been explored in this study. The Grabowska Lab has established techniques to investigate invasion in spheroids (Pal et al., 2020), which could be used for assessing CCA invasion in the presence of MSCs in future studies.

Based on the morphology, it was noticed that the presence of MSCs enhanced the internal structures that were hypothesised to be ECM (Chapter 4, Figure 4.12). In breast cancer, MSCs play a critical role in ECM remodelling (Maffey et al., 2017). Therefore, it was hypothesised that mesenchymal stem cells in contact with the cancer cells may develop tumour-associated functionalities thereby promoting cell proliferation and generating ECM components. In fact, the role of the ECM components has been associated in promoting iCCA progression, therapeutic resistance, and immunosuppression (Brivio et al., 2017; Cadamuro et al., 2018; Fabris et al., 2019; Sirica, 2011; Sirica, Strazzabosco, & Cadamuro, 2021; Vaquero, Aoudjehane, & Fouassier, 2020).

The spheroid co-culture model was also characterised using Vimentin, CK7 and CK19. Initially, vimentin expression was intended to be used as a mesenchymal marker to localise the MSCs in the co-culture, and although the positive staining was only found in the co-cultures it could not be differentiated whether the positive cells were the MSCs or cancer cells that underwent EMT after being in contact with the MSCs. One approach that could confirm this is the use of a luciferase IHC marker that could stain the luminescent cancer cells. Both CCA markers were expressed in the spheroid co-cultures apart from the KKU-M055 spheroids. Using the spheroid-array technique as

a means to characterise the potential differentiation of MSCs to CAFs, it is something that could be further explored. For instance, look at the expression of two important CAF markers, α-SMA and fibroblast protein activation (Kawamoto et al., 2018).

- **PDX-derived cells successfully form 3D spheroids and were classified into two groups based on their morphology**

The cell-line-derived spheroids were demonstrated to be a suitable *in vitro* model to study the crosstalk between the MSCs and the cancer cells. However, PDXs and PDX-derived spheroids models were developed as they are known to be closer-to-the patient that the cell-line-derived spheroids (Pal et al., 2020). Cell-lines are a powerful tool and offer several advantages. They are cost effective, easy to use, provide an unlimited supply of material and do not require ethical approval (Kaur & Dufour, 2012). However, cell-lines do not completely resemble primary cells. They are manipulated to proliferate indefinitely which may have altered their phenotype, native functions, and their responsiveness to stimuli. Serial passage of cell-lines can further cause genotypic and phenotypic variation over an extended period of time (Kaur & Dufour, 2012).

First, PDXs had been successfully generated from human CCA biopsies by the *in vivo* team in the Grabowska Lab. Although not all the PDXs morphologically resembled the histology of their original tumour in terms of differentiation, the hepatobiliary markers CK7 and CK19 (L. Z. Liu et al., 2018) were highly expressed in the PDXs, confirming that the components of the CCA tumours are still maintained in the PDXs. A previous study using CCA PDXs investigated whether the histological morphology was maintained during passages, and although they confirmed that PDXs preserved histological features during passages (Y. Gao et al., 2021), this is something that could be investigated in these PDXs.

The expression of CK7 and CK19 was not determined in the human samples due to lack of tissue. CK7 and CK19 are standard markers in the clinic to characterise CCA. In fact, CK7/CK19 index was a prognostic factor for iCCA patients' survival (L. Z. Liu et al., 2018). With access to the clinicopathological data of the tumours, the index could be calculated and associated with their survival. Additionally, this index could then be compared to the PDXs from which they were derived. Indeed, obtaining this data would provide an important piece in the validation of this model.

The morphology of the PDXs remained the same in the presence or absence of MSCs. Unpublished data in the Grabowska Lab, showed that human MSCs were lost when they were engrafted with breast cancer cells in PDX models. Therefore, the replacement of the human stroma by murine stroma was hypothesised to be the reason for the maintained morphology. In fact, previous studies have been published supporting this statement (Blomme et al., 2018; Pearson et al., 2016). To assess this, primers for human or mouse MSCs could be generated to perform qPCR and assess the percentage of human and mouse MSCs on those samples. This is indeed something that is currently being carried out in the Grabowska Lab.

Ki-67 expression was higher in PDXs which had been co-implanted with hMSCs. In CCA patients, upregulation of Ki-67 has been shown to be associated with advanced stage disease, poor prognosis, and decreased survival rates (Horie, Endo, Kawasaki, & Terada, 2000; Iguchi et al., 2009; Schiffman et al., 2014). However, this needs further confirmation in biological replicates.

PDXs generated in this study were classified into well or poorly differentiated adenocarcinomas. Tumour differentiation status has also previously shown to have significant effect on prognosis (Ebata et al., 2003; Rea et al., 2004). Prognosis is poorer on low differentiated tumours than on high differentiated ones (Mao et al., 2015). Vimentin expression is often related to poor prognosis and low differentiation (M. J. Gu & Choi, 2014; Handra-Luca et al., 2011; Tadokoro et al., 2016). This correlated with the findings of this study; low differentiated PDXs expressed higher vimentin than those well differentiated (Chapter 5, Figure 5.2).

PDX models in many ways represent a major progress in pre-clinical cancer research but need to be viewed within the context of the associated challenges. Challenges include the immense resources that are needed to establish as well as maintain the tumour banks; the lack of current standardised criteria for assessing histological, stromal, and genetic drift from the original tumour; and the numerous biological challenges of using immunocompromised animal models. For studying drug responses, PDXs models also need to be viewed as complementary to other pre-clinical models with a well-defined genetic background (Tentler et al., 2012). Taken together, and since the goal of the project was to investigate the crosstalk between the cancer cells and stromal cells, spheroid models were formed using PDXs cells. The majority of studies refer the 3D models derived from primary cells as organoids or tumoroids.

However, organoids require a scaffold-based system to grow, here the 3D models were grown in suspension and therefore still called spheroids. There is strong evidence that models using primary cells maintain the histological features, expression profile, and genomic landscape of their matched primary tissues (Maier et al., 2021), making them suitable for translational studies. It has previously been shown that organoids can be generated from CCA in the presence of BME (Broutier et al., 2017) or needle biopsies (Nuciforo et al., 2018). Using a scaffold-free technique, spheroids can also be generated from undifferentiated and well-differentiated primary eCCA cells to investigate tumour biology (Mischiati et al., 2015). In this system, phenotypical changes were observed in terms E-cadherin and vimentin expression (Mischiati et al., 2015).

In this project, mono- and co-cultures of primary cells and primary human MSCs or immortalised human MSCs were successfully generated (Chapter 5, Figure 5.8 and 5.9). A different pattern of aggregation was noticed between those from Group 1 (well differentiated) and Group 2 (poor differentiated). First, in line with the characterisation steps, the biliary phenotype of these models was confirmed by the positive CKs expression (Chapter 5, Figure 5.12 and Figure 5.13). The different pattern of aggregation correlated to what the post-doctoral researcher in the Grabowska Lab found with cells from other types of PDXs (breast, lung, prostate and colorectal). Some PDXs formed tight spheroids, and others formed loose spheroids. The hypothesis was that some of the PDXs may resembled different subtypes of tumours, or that there was a selection of a clonal population due to the *in vitro* process; or cells experimented a process of transformation in their plasticity. This work can by extended by doing a similar approach to an already published study (Georgopoulou et al., 2021), where they characterised single-cell phenotypes of PDXs and correlating these with the genomic and transcriptomic profiles of the PDX-derived models (Georgopoulou et al., 2021). Differently, another hypothesis that may explain the lack of spheroid formation in Group 1 is that the apoptosis activation upon dissociation caused ROCK-dependent actomyosin hyperactivation, which is triggered by the loss of E-cadherin (Ohgushi et al., 2010). This can be resolve by treating the cells with ROCK inhibitor. Indeed, this has been shown to help cells survive in the 3D culture after dissociation (Ramasamy, Yu, Selden, Hodgson, & Cui, 2013).

The difference between the tight and loose group of PDX-derived spheroids is something that is currently being explored in the Grabowska Lab.

- **Primary human and immortalised MSCs supported Group 1 PDX-derived spheroids**

Co-cultured spheroids were successfully produced from primary cells passaged as PDXs and human or immortalised MSCs. This allowed for the observation of potential biological changes, contributing to the fundamental investigation into the possible phenotypic and behavioural changes that may occur when MSCs and CCA cells interact. Since the cell-cell interaction was proven to be necessary for cell proliferation in the cancer cell-line-derived spheroids, the direct system was also used.

The presence of hMSCs enhanced the production of what structures was hypothesised to consist of ECM, similar to what was observed in the cancer cell-line-derived spheroids. In contrast to what others have seen in spheroids from co-cultured cells, there was not distinct localisation of cancer and stromal cells based on the markers used to stain the samples in this study. In other studies, using co-cultures of cancer cells and fibroblast, the cancer cells were shown to be primarily localised to the periphery of the spheroid, whilst the fibroblast cells in the core (Amann et al., 2014; Herter et al., 2017).

The presence of hMSCs supported spheroid formation in Group 1 (spheroids derived from well-differentiated PDXs). Consistent with these findings, Ki-67 was higher in CCA1 co-culture spheroids (Chapter 5, Figure 5.14). Many controversies have been reported concerning the use of MSCs in cancer, some reporting the inhibition of the tumour invasiveness and metastasis (D. Gao et al., 2018; Serhal et al., 2019), and others reporting an increase in tumorigenicity (Melzer, von der Ohe, & Hass, 2019; J. Zhou et al., 2018). For instance, an *in vitro* study exploring the role of MSCs derived from various sources on different types of ovarian cells, proofed that MSCs had an anti-proliferative effect and antiapoptotic on ovarian cancer (Khalil et al., 2019). In contrast, in colorectal cancer, MSCs increased carcinogenic potential through cross direct co-culture (I. R. Oh, Raymundo, Kim, & Kim, 2020). In this study, the presence of MSCs enhanced spheroid formation and it was hypothesised that MSCs could be supporting spheroid formation by secreting matrix proteins. This correlates to what has been seen i.e. that the cross-talk between cancer cells and the surrounding stroma

promotes tumour progression and creates a dynamic extracellular matrix (Ridge et al., 2017).

- **ECM-receptor and PI3K-AKT signalling pathways may be driving cell proliferation in CCA**

Given the enhanced spheroid formation and proliferation in the co-cultures of cancer cells and MSCs, the crosstalk was further explored using transcriptomic techniques. It is important to interpret the results carefully since the readouts are complex due to the presence of multiple cell populations.

The cell-line derived spheroids were first studied. The PCA plot showed that the mono-culture spheroids were similar within the biological replicates (Chapter 6, Figure 6.3). However, this was not the same for the hMSCs or iMSCs co-cultures. It is important to point out that the phenotypic reprogramming of stem cells is dependent on the cellular environment (Pittenger et al., 2019). Therefore, it is not surprising that co-cultures including these cells were slightly more variable, since the time of when the samples were collected was different as well as the passage of the cells.

This study identified a number of upregulated genes that were common in both comparisons (mono-culture vs co-culture with either hMSCs or iMSCs), which were ECM-related genes. Growing evidence highlighted the importance of ECM proteins in the progression of iCCA (Carpino et al., 2019). Therefore, it was not surprising that, ECM proteins appeared upregulated in the presence of MSCs. As a result of the direct co-culture, these genes may be expressed by the MSCs as opposed to being expressed in the cancer cells. Among the ECM-related genes, POSTN, COLs and FN1 appeared to be upregulated in MSCs co-cultures. POSTN overexpression in iCCA, has been found to correlate with shorted survival times of patients (Baril et al., 2007) and COL3A1 to promote iCCA cell migration (Carpino et al., 2019). FN1 is another ECM component that has been reported to be a main driver of tumour progression in different type of cancers by different mechanisms including the increase of growth factors signalling via integrin clustering (Levental et al., 2009; Petersen, Ronnov-Jessen, Howlett, & Bissell, 1992). In fact, the establishment of a nascent metastatic niche happens by the activation of resident stromal cells that produce FN1 which sustains the recruitment of hematopoietic bone marrow progenitor cells (Kaplan et al., 2005). SPARC was another upregulated gene in the MSC co-culture. SPARC binds to

several integral components of the ECM and exhibits an anti-adhesive effect that includes disruption of focal adhesions and therefore cell spreading and mobility (Murphy-Ullrich, 2001; Nagaraju & Sharma, 2011). Additionally, its cooperation with FN1 is known to be critical for full activation of fibroblasts (S. Yoshida et al., 2021). In the wake of these facts, it is conceivable that ECM proteins could be potential targets for new treatments in CCA.

Apart from ECM-related genes, genes such as CHI3L1 and WNT5A were also found to be upregulated in the co-cultures. In CCA, CH3L1 is known to be a CAF-derived factor to recruit macrophages thereby creating an immunosuppressive environment that benefits CCA (M. Zhou et al., 2021). WNT5A, a Wnt ligand associated with non-canonical Wnt signalling, is upregulated in biliary injury (Wilson et al., 2020). In fact, conditioned media from MSCs has been found to upregulate the Wnt/ß-catenin signalling pathway in CCA cells (W. Wang et al., 2015).

Besides measuring gene expression at the genome-scale level, other approaches can be used to measure the expression levels of a smaller subset of genes. This can include qRT-PCR, or the construction of eGFP reporters with the gene coding for the transcript of interest (Wilson et al., 2020). Therefore, it would be of interest to validate some of these targets using these techniques. Additionally, being able to determine if the signal came from the cancer cells or the MSCs would provide an important piece in the validation of this model and understanding of the crosstalk. One potential solution to overcome this is to sort the cancer and MSC cells before analysing them. A previous study employed flow cytometry to separate RFP- and GFP-tagged cells in trypsinized spheroids (C. R. Hong et al., 2018). However, a student in the Grabowska Lab found that cell dissociation and sorting procedures impacted the cell membrane leading to changes in the receptors' status. To avoid this interference, other approaches such as single cell RNASeq (scRNASeq) can also be considered. ScRNASeq offers an unprecedented opportunity and has demonstrated its utility in dissecting intra-tumour heterogeneity at a single cell resolution in different types of cancer, such as primary glioblastoma and colorectal cancer (X. Li & Wang, 2021). Another alternative is the spatial transcriptomics, that aims to count the number of transcripts of a gene at distinct spatial locations in a tissue (Williams, Lee, Asatsuma, Vento-Tormo, & Haque, 2022).

The top pathways affected by genes that were upregulated in co-culture involved the ECM-receptor interaction and PI3K-AKT signalling pathways (Chapter 6, Figure 6.6

and Figure 6.7). In line with this, a study integrating the RNA expression of iCCA and normal biliary epithelial cells from Expression Omnibus (GEO) and The Cancer Genome Atlas (TCGA) databases showed the ECM-receptor interaction as one enriched significant pathway (Xiao et al., 2022). In CCA, PI3K-AKT signalling pathway is also highly activated (Dokduang et al., 2013), and it is correlated with tumour metastasis and poor prognosis (Yothaisong et al., 2013). PI3K-AKT signalling pathway is known to have essential roles in cell-cycle progression, survival, migration, and cell growth (Pompura & Dominguez-Villar, 2018), and may explain the enhanced cell proliferation.

The link between the ECM-receptor interaction and PI3K-AKT pathways has already been described in cancer. ECM reorganisation and stiffness is reported to be determined by changes in collagen cross-linking, which drives tumour progression through PI3K-AKT activation mediated by integrin receptors (Levental et al., 2009; Ng & Brugge, 2009). Additionally, SPARC was reported to interact with integrin and the incorporation of SPARC-integrin-FN1-mediated activation of AKT to help cancer cells to migrate or invade into adjacent stroma (S. Yoshida et al., 2021). In CCA, particularly, PI3K-AKT signalling it is also known to be activated by POSTN which interacts with integrin α5 expressed by CCA cells, ultimately stimulating tumour cell proliferation and invasion (Utispan et al., 2012). Nonetheless, the molecular mechanism of how these pathways may be linked together to enhance cell proliferation in CCA needs further investigation.

A hallmark that was affected was the EMT pathway. The involvement of EMT-like processes in CCAs has been proposed and supported by evidence of disruption in epithelial cell-cell junctions to promote mesenchymal features (Sawanyawisuth, Sashida, & Sheng, 2021). COL, ITGs and SPARC belong to the EMT gene signature (L. Wu, Amjad, Yun, Mani, & de Perrot, 2022), and these genes were indeed upregulated in the MSCs co-cultures. Integrin complexes enable cancer cells to receive signals from ECM proteins which are essential in the initiation and progression of EMT (Lamouille, Xu, & Derynck, 2014). Collagen and SPARC are two ECM proteins that are known to mediate the interactions between the ECM and the cancer cells (Frisbie, Buckanovich, & Coffman, 2022; S. Yoshida et al., 2021).

Taken all together, it was hypothesised that in the co-culture system, the mesenchymal stem cells secrete ECM proteins (such as collagen, SPARC, POSTN, etc.) that bind to

the integrins expressed by the CCA cells which consecutively activate the PI3K-AKT signalling pathway to promote cell proliferation (Figure 7.1).

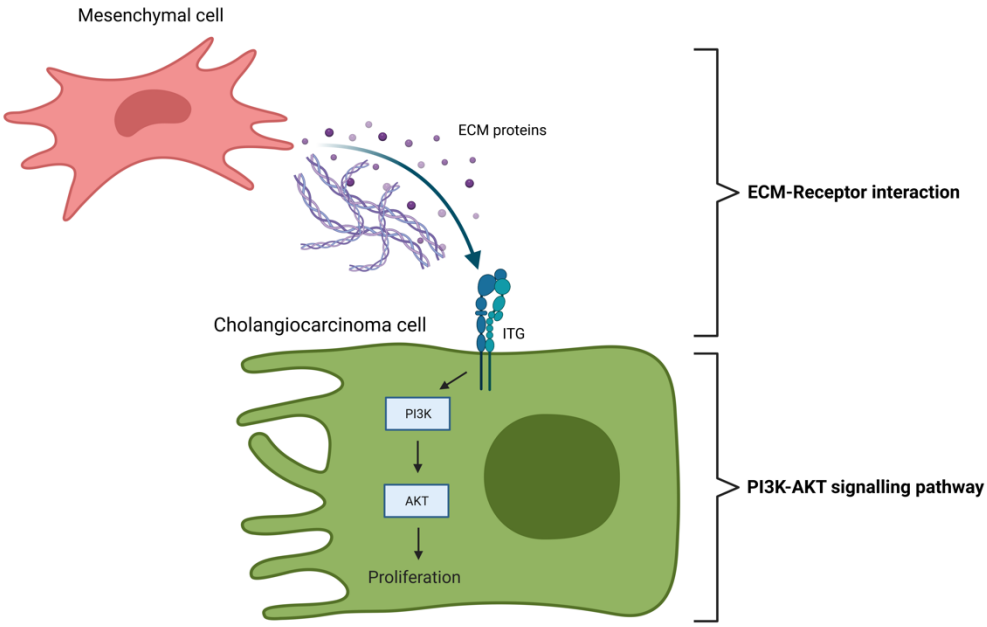



**Figure 7.1. Schematic pathway hypothesis of the biological effects of the mesenchymal cells in CCA proliferation.** Mesenchymal cells present in the tumour microenvironment secrete ECM proteins such as collagen, SPARC and POSTN that bind to the integrins (ITG) expressed by the cancer cells (ECM-receptor interaction), which further activates the PI3K-AKT signalling pathway resulting in an enhanced cell proliferation in the cancer cells.

To test the significance of these pathways in cell proliferation, already available treatments could be used to determine whether cell proliferation is reduced. Some drug assays have already been performed in CCA to target PI3K-AKT signalling pathway. For instance, combined targeting of mTOR and AKT using RAD001 and MK-2206 small molecule inhibitors showed significant antitumour effects *in vitro* and in pre-clinical models (Ewald et al., 2013; Yothaisong et al., 2013); and combined used of sorafenib and everolimus to inhibit AKT/mTOR pathway and ERK, respectively, resulted in CCA cell proliferation inhibition (Yokoi et al., 2018). Celecoxib was also found to inhibit the proliferation of CCA cells and to induce cell death *in vitro* and *in vivo* by reducing pAKT levels (Z. Zhang, Lai, & Sirica, 2004). Although the ECM has not yet been targeted in CCA, one of the most successful cases is the application of TKIs in non-small cell lung cancer with EGFR mutation (Goldberg et al., 2020) and chronic myeloid leukemia (Jabbour & Kantarjian, 2012), which is partially mediated by the blockage of the signal transduction stimulated by receptors of the ECM.

- **PDXs were classified in two groups based on their transcriptome**

PDXs were studied next. The PCA plot showed no difference between the presence or absence of MSCs (Chapter 6, Figure 6.10). In fact, the loss of human tumour stroma, which is replaced by mouse stroma, is a concern regarding the PDXs models (Blomme et al., 2018; Invrea et al., 2020). The heterogeneity among PDX samples may explain this clustering. However, PDXs were clustered based on the previously defined groups (well or poor differentiated). It is not surprising that the transcriptome also matches the difference on morphology. In prostate cancer, the relationship between genetic and morphological heterogeneity has been previously suggested (Singh et al., 2002).

The understanding of the transcriptome of the PDXs and its effect on spheroid formation are now being investigated in a bigger project in the Grabowska Lab where other types of PDXs are also included. Some of the proposed experiments were to investigate the transcriptomic data and identify a set of genes that may define the tight and loose group of PDXs. Additionally, gene variants will be determined and linked to the potential formation of the groups. Additionally, some spatial transcriptomic data is also being considered. Spatial transcriptomics is a rapidly growing field that promises to comprehensively characterise tissue organization and architecture at the single-cell or subcellular resolution. Such information provides a solid foundation for mechanistic understanding of many biological processes (Dries et al., 2021).

When the transcriptome of the 3D models (cell-line-derived spheroids and PDXs) was plotted in a PCA together with the transcriptome of the CCA tumours, the cell-line-derived co-cultures and PDXs Group 1 had less variability compared to the mono-cultures (Chapter 6, Figure 6.12). This was expected since the addition of MSCs may be resembling the tumour TME. Group 1 of PDXs had less variability than Group 2, this will need further validation. In line with this, inclusion of additional samples e.g. resected margin as controls, could help in the understanding of these results.

Taken all together, it can be concluded that there is no perfect model; each can be useful and appropriate, depending on the research question being investigated. However, it is of paramount importance to do a detailed characterisation, especially given the recent importance of the different stages of cancer.

## 7.2. Future work

This project has made an important contribution in the generation of useful 3D models to study the interaction between the MSCs and CCA cancer cells. However, ongoing analysis will allow the models to be interrogated to understand this crosstalk and its clinical relevance. Hence, the following work is proposed to continue the current study.

Cell-line derived spheroids:

- Generate spheroid-arrays from biological replicates to confirm the staining results (vimentin, Ki-67, CK7 and CK19) and use ECM markers to confirm whether the internal structures are indeed ECM. Some ECM markers to use could be the upregulated genes in the RNASeq data (COL, POSTN and FN1).
- Characterise immunohistologically the potential differentiation of the MSCs to CAFs and characterise the population of CAFs. In CCA, myofibrotic CAFs showed α-SMA and low IL-6. Inflammatory CAFs showed low α-SMA and high IL-6. Finally, antigen-presenting CAFs showed high expression of MHC II family genes (Geng et al., 2021). These markers can be used to evaluate the potential differentiation of MSCs after being co-cultured with the cancer cells.
- Optimise the flow cytometry technique to gain better sample quality or perform single-cell transcriptomics. This approach could help to characterise the effect of the cancer cells on the MSCs as well as the effect of the MSCs on the cancer cells.

PDXs and PDX-derived spheroids:

- Section human tissues and stain them for vimentin, Ki-67, CK7 and CK19. Their expression can then be correlated with their matched PDXs to confirm their resemblance.
- Due to the high heterogeneity between the PDXs, biological replicates can be generated and further sequenced. This will allow a detailed study of the transcriptome, and perhaps a better understanding on the difference between the well and poor differentiate PDXs.
- Sequence PDX-derived spheroids in biological replicates and compare them to the PDXs and original tumours from which they were derived.

Overall:

- Validate some of the significant targets (COLs, SPARC and ITGs.) hypothesised to be driving proliferation and spheroid formation by qRT-PCR, IHC or IF.
- Include the TCGA data for CCA and visualise the tumours in the context of the TCGA data. It is important to point out that the method used for RNA extraction may affect the transcriptome, and therefore a small difference is expected between the TCGA tumours and the tumours in this project. Accessing the TCGA data will also allowed to include resected margin, which is something that was not available for the current project.
- Test existing drugs used to treat other types of cancer, to target both ECM-receptor interaction and PI3K-AKT signalling pathways in the 3D CCA spheroids and determine whether it inhibits cell proliferation.

## 7.3. Conclusions

To restore stromal cell-driven signalling, a co-culture model incorporating CCA together with MSCs, using either CCA cell-lines or CCA isolated from patient-derived xenografts was established. Using these models, an enhanced proliferation in the co-culture models compared with the mono-cultures was shown. The results should be carefully interpreted on spheroid size, metabolic assays, and live/dead staining in co-culture models where the readouts are more complicated due to the presence of multiple cell populations. Thus, we confirmed effects on proliferation using a proliferative marker, Ki-67.

The enhanced proliferation observed when the co-culture spheroids involved ECM-receptor interaction and PI3K-AKT signalling pathways, suggesting that the phenotypic changes may occur via activation of PI3K signalling after the ECM-receptor interaction. Future studies may further elucidate the complex interactions between the multiple signalling pathways involved in stromal cell-driven phenotypic changes in CCA that result in disease progression.

Models such as the one described here are important in allowing the study of tumour biology as well as reducing the use of animals to investigate complicated interactions. They also allow *in vitro* investigation using PDX cells and therefore, more close-to-patient models, which will allow more robust and clinically relevant identification of novel drug treatments and drug screening.

# Appendix A.

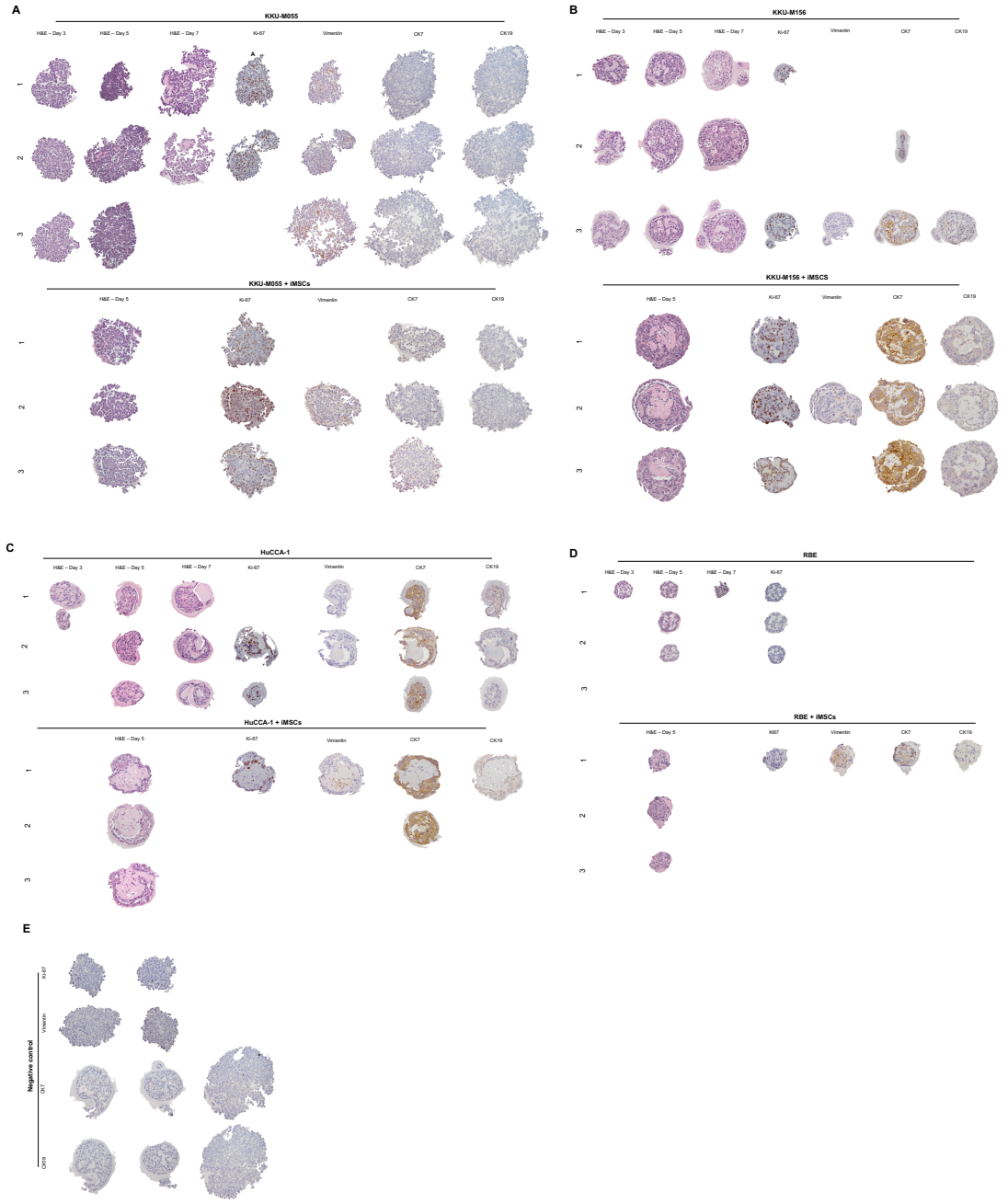



**Figure A1. Technical replicates of the cell-line derived spheroids in the spheroid-array.** 1000 cells from 4 CCA cell-lines (KKU-M055 **(A)**, KKU-M156 **(B)**, HuCCA-1 **(C)** and RBE **(D)** were mono-cultured or iMSCs co-cultured at a ratio of 1:2 (cancer cell:iMSCs) into an ULA 96-well round bottom plate with 100µg/mL of BME. CCA spheroids were fixed at day 5 of culture, paraffin embedded, sectioned, and stained with H&E, Ki-67, Vimentin, CK7 and CK19. The numbers indicate the technical replicates. Negative controls **(E)** (magnification: 20×).

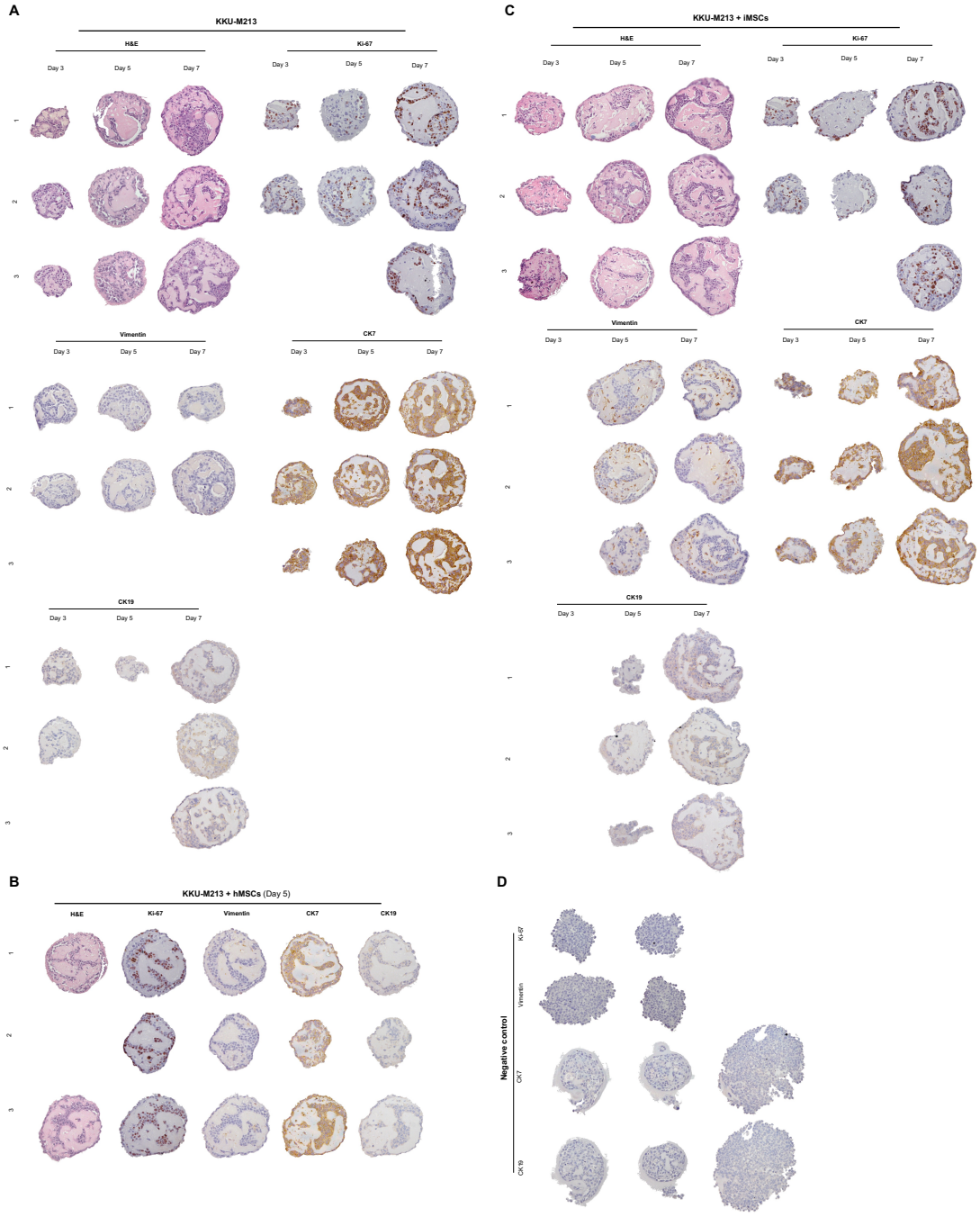



**Figure A2. Technical replicates of KKU-M213-derived spheroids in the spheroid-array.** 1000 KKU-M213 cells were mono-cultured **(A)**, hMSCs co-cultured **(B)** or iMSCs co-cultured **(C)** at a ratio of 1:2 (cancer cell:MSCs) into an ULA 96-well round bottom plate with 100µg/mL of BME. CCA spheroids were fixed at day 3, 5 and 7 of culture, paraffin embedded, sectioned, and stained with H&E, Ki-67, Vimentin, CK7 and CK19. The numbers indicate the technical replicates. Negative controls **(D)** (magnification: 20×).

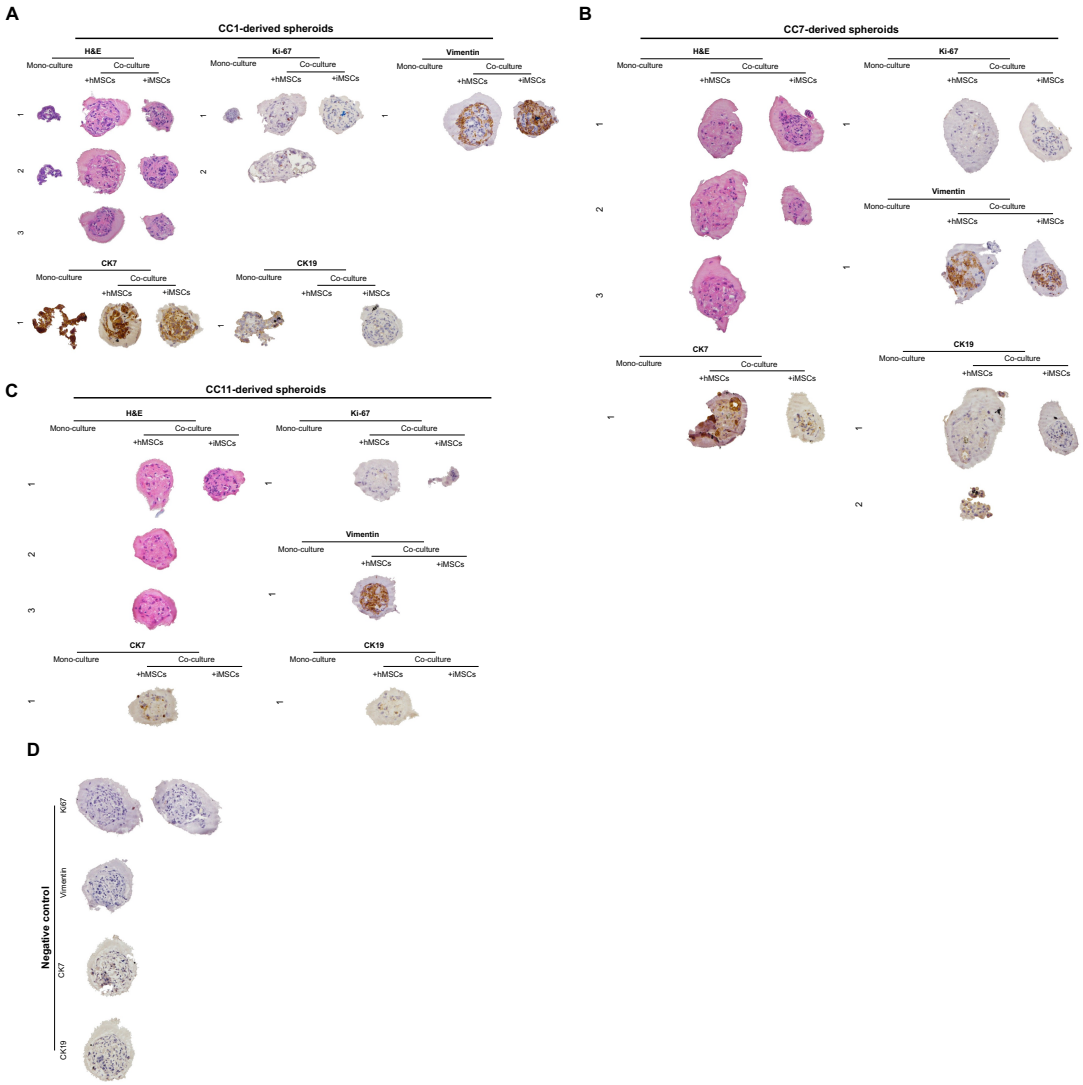



**Figure A3. Technical replicates of Group 1 PDX-derived spheroids in the spheroid-array.** CCA tissues (CCA1 **(A)**, CCA7 **(B)** and CCA11 **(C)**) were mechanically and enzymatically dissociated, and PDX cells were cultured in mono- or co-culture with hMSCs and iMSCs at 2:1 ratio (cancer cells:MSCs) with 300µg/mL. CCA PDX-derived spheroids were fixed at day 5 of culture, paraffin embedded, sectioned, and stained with H&E, Ki-67, Vimentin, CK7 and CK19. The numbers indicate the technical replicates. Negative controls **(D)** (magnification: 20×).

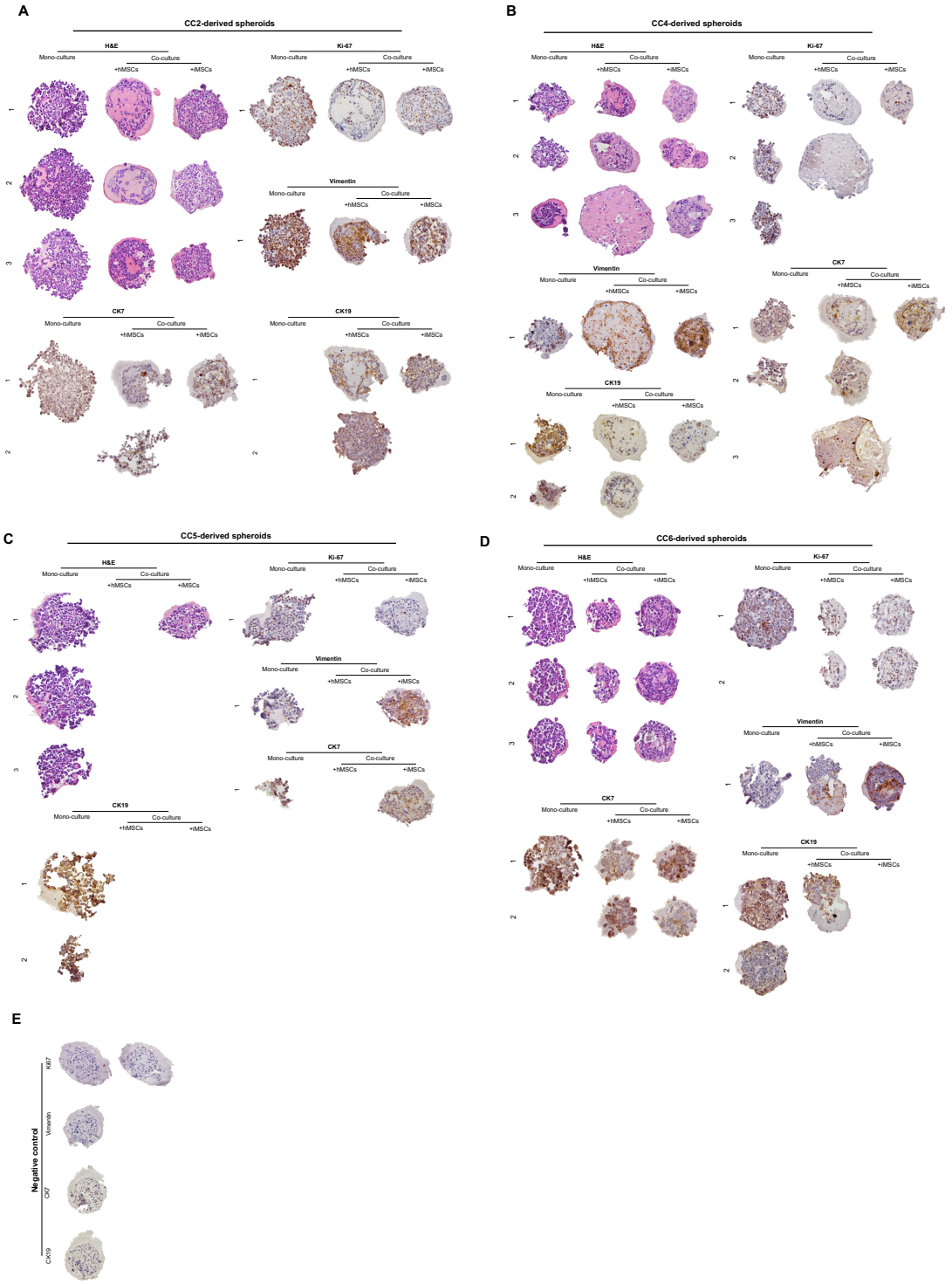



**Figure A4. Technical replicates of Group 2 PDX-derived spheroids in the spheroid-array.** CCA tissues (CCA2 **(A)**, CCA4 **(B)**, CCA5 **(C)** and CC6 **(D)**) were mechanically and enzymatically dissociated, and PDX cells were cultured in mono- or co-culture with hMSCs and iMSCs at 2:1 ratio (cancer cells:MSCs) with 300µg/mL. CCA PDX-derived spheroids were fixed at day 5 of culture, paraffin embedded, sectioned, and stained with H&E, Ki-67, Vimentin, CK7 and CK19. The numbers indicate the technical replicates. Negative controls **(E)** (magnification: 20×).

**Table A1. Summary of the concentration, purity (A260/A280 and A260/A230 ratios) and RIN of the RNA samples isolated for RNASeq.** RNA was isolated using a Qiagen Allprep kit (Chapter 2, Section 2.7.1).

| Sample | Conc. (ng/µl) | A260/A280 | A260/A230 | RIN |
|---|---|---|---|---|
| CC1 - Tumour | 31.6 | 2.7 | 0.18 | 6.7 |
| PDX CC1 -MSCs | 1856.1 | 2.07 | 2.2 | 6.2 |
| PDX CC1 +MSCs | 1442.1 | 2.08 | 1.49 | 5.6 |
| CC2 - Tumour | 898.1 | 2.09 | 1.71 | 1.9 |
| PDX CC2 -MSC | 2661.5 | 2.05 | 1.82 | 8.8 |
| PDX CC2 +MSC | 1074.9 | 2.11 | 1.19 | 8.9 |
| CC4 - Tumour | 6.1 | 2.33 | 0.22 | 2.1 |
| PDX CC4 -MSC | 2330.6 | 2.08 | 1.88 | 8.8 |
| PDX CC4 +MSC | 2828.4 | 2.1 | 1.78 | 8.7 |
| CC5 - Tumour | 15.3 | 2.34 | 0.4 | 6.1 |
| PDX CC5 -MSC | 689.6 | 2.08 | 1.83 | 9.2 |
| PDX CC5 +MSCs | 739.4 | 2.04 | 1.55 | 9 |
| CC6 - Tumour | 1220.9 | 2.07 | 2.16 | 6.2 |
| PDX CC6 -MSCs | 305.6 | 2.06 | 1.16 | 9.3 |
| PDX CC6 +MSCs | 1779.3 | 2.07 | 2.09 | 9.1 |
| CC7 - Tumour | 541.2 | 2.08 | 1.54 | 8.2 |
| PDX CC7 -MSCs | 209.2 | 2.07 | 1.02 | 6.4 |
| PDX CC7 +MSCs | 820.9 | 2.07 | 1.22 | 7.1 |
| CC11 - Tumour | 35.9 | 2.16 | 0.18 | 1.6 |
| PDX CC11 -MSC | 965.1 | 2.11 | 1.43 | 8.4 |
| PDX CC11 +MSC | 891.2 | 2.11 | 1.74 | 8.6 |
| KKUM213 n1 | 21.5 | 2.29 | 1.18 | 9.7 |
| KKUM213 n2 | 10.8 | 3.05 | 0.02 | 10 |
| KKUM213 n3 | 56.7 | 2.14 | 0.46 | 10 |
| KKUM213+hMSCs n1 | 130.3 | 2.16 | 0.25 | 10 |
| KKUM213+hMSCs n2 | 63.7 | 2.13 | 0.91 | 10 |
| KKUM213+hMSCs n3 | 157.6 | 2.13 | 0.91 | 10 |
| KKUM213+iMSCs n1 | 119.3 | 2.12 | 1.79 | 10 |
| KKUM213+iMSCs n2 | 122.1 | 2.11 | 0.84 | 10 |
| KKUM213+iMSCs n3 | 141 | 2.13 | 0.54 | 10 |

# Achievements

- **Publications**

  - **Sueca-Comes, M**., Rusu, E. C., Grabowska, A. M., & Bates, D. O. (2022). Looking Under the Lamppost: The Search for New Cancer Targets in the Human Kinome. *Pharmacological Reviews*, 74(4), 1134-1143. doi: https://doi.org/10.1124/pharmrev.121.000410

- **Oral presentations**

  - Medicine & Health Science Faculty Postgraduate Research Forum. Nottingham, UK, 2019 – Best '2 minutes of Impact' presentation.
  - CCA-UK Annual Meeting. Nottingham, UK, 2019.
  - N-Trans Sandpit: Opportunities and Skills Development in Applying for Funding. Nottingham, UK, 2020 – Best Non-Clinical Fellowship Application and Best 3 minutes Elevator Speech.
  - Cancer Research Nottingham Symposium. Virtual, UK, 2020.
  - Sue Watson Event. Virtual, UK, 2021. – Best Presentation (First Prize).

- **Poster presentations**

  - Annual Division of Cancer and Stem Cells Meeting. Nottingham, UK, 2019. – Best Poster Prize.
  - BACR Tumour Microenvironment Meeting. Nottingham, UK, 2019. – Poster Prize Commendation.
  - Cancer Research Nottingham Symposium. Nottingham, UK, 2019.
  - BACR Student Virtual Conference. UK, 2021.
  - AMMF Virtual European Conference. UK, 2021
  - EACR Virtual Conference: Goodbye Flat Biology. UK, 2021.

- **Funded Training Courses**

  - Biomolecular Skills School – University of Nottingham and Research Complex at Harwell, UK, 2019.
  - Novel Experimental CCA Models: from Ex-vivo Patient-Derived Organoids to In-vivo Animal Models – University of Glasgow, Beatson Institute for Cancer

Research UK, 2020. *Cancelled due to COVID-19 and re-scheduled virtually in 2021.*

- **Grants**

  - Short term scientific mission (STSM) – Biotech Research and Innovation Centre (BRIC), Copenhagen, Denmark. 2020-04-01 to 2020-04-20. *Cancelled due to COVID-19.*

# COVID Statement

The abrupt closure of the University in response to the COVID-19 pandemic in March to August 2020, had various repercussions on my research work. Lockdown was particularly disruptive for our lab group because it occurred shortly after we moved buildings. Before this, I had the next experiments planned out so that I could get all the data I needed and start writing up everything for my thesis and finish my PhD by the 30/09/2021. However, according to the circumstances I had to conduct a contingency plan. During this period, I performed a bioinformatic study regarding the Cancer Kinome in collaboration with Elena Cristina Rusu which has recently been accepted for publication in Pharmacological Reviews (Sueca-Comes, 2022). Additionally, I learned the basics of Amira, a software platform for 3D and 4D data visualization, processing, and analysis. Due to the disruptions that occurred during the lockdown, an additional 6-week funded extension was granted by the University of Nottingham. However, this was not enough to compensate for some of the time lost in the lab. This meant that I was unable to perform the drug testing, which is now considered a future plan.

# References


@CellCultureDish. (2020, 2020-06-09). Spheroid Models: Getting Started and Culture Tips - Cell Culture Dish. Retrieved from https://cellculturedish.com/spheroid-models-getting-started-and-culture-tips/

Abbott, R. D., & Kaplan, D. L. (2015). Strategies for improving the physiological relevance of human engineered tissues. *Trends Biotechnol, 33*(7), 401-407. doi:10.1016/j.tibtech.2015.04.003

Aboulkheyr Es, H., Zhand, S., Thiery, J. P., & Warkiani, M. E. (2020). Pirfenidone reduces immune-suppressive capacity of cancer-associated fibroblasts through targeting CCL17 and TNF-beta. *Integr Biol (Camb), 12*(7), 188-197. doi:10.1093/intbio/zyaa014

Adjei, I. M., & Blanka, S. (2015). Modulation of the tumor microenvironment for cancer treatment: a biomaterials approach. *J Funct Biomater, 6*(1), 81-103. doi:10.3390/jfb6010081

ADVAITA. Pathway Analysis vs Gene Set Analysis: What is the Difference and When Should I Use Each? Retrieved from https://advaitabio.com/ipathwayguide/pathway-analysis-vs-gene-set-analysis/

Affo, S., Nair, A., Brundu, F., Ravichandra, A., Bhattacharjee, S., Matsuda, M., . . . Schwabe, R. F. (2021). Promotion of cholangiocarcinoma growth by diverse cancer-associated fibroblast subpopulations. *Cancer Cell, 39*(6), 883. doi:10.1016/j.ccell.2021.05.010

Al-Bahrani, R., Nagamori, S., Leng, R., Petryk, A., & Sergi, C. (2015). Differential Expression of Sonic Hedgehog Protein in Human Hepatocellular Carcinoma and Intrahepatic Cholangiocarcinoma. *Pathol Oncol Res, 21*(4), 901-908. doi:10.1007/s12253-015-9918-7

Albini, A., & Sporn, M. B. (2007). The tumour microenvironment as a target for chemoprevention. In *Nat Rev Cancer* (Vol. 7, pp. 139-147). England.

Alghuwainem, A., Alshareeda, A. T., & Alsowayan, B. (2019). Scaffold-Free 3-D Cell Sheet Technique Bridges the Gap between 2-D Cell Culture and Animal Models. *Int J Mol Sci, 20*(19). doi:10.3390/ijms20194926

Alshari, O. M., Dawaymeh, T. A., Tashtush, N. A., Aleshawi, A. J., Al Manasra, A. R. A., & Obeidat, K. A. (2019). Completely resolved advanced biliary tract cancer after treatment by pembrolizumab: a report of two cases. *Onco Targets Ther, 12*, 5293-5298. doi:10.2147/OTT.S197559

Amann, A., Zwierzina, M., Gamerith, G., Bitsche, M., Huber, J. M., Vogel, G. F., . . . Zwierzina, H. (2014). Development of an innovative 3D cell culture system to study tumour--stroma interactions in non-small cell lung cancer cells. *PLoS One, 9*(3), e92511. doi:10.1371/journal.pone.0092511

Arai, Y., Totoki, Y., Hosoda, F., Shirota, T., Hama, N., Nakamura, H., . . . Shibata, T. (2014). Fibroblast growth factor receptor 2 tyrosine kinase fusions define a unique molecular subtype of cholangiocarcinoma. *Hepatology, 59*(4), 1427-1434. doi:10.1002/hep.26890

Arnaoutova, I., George, J., Kleinman, H. K., & Benton, G. (2012). Basement membrane matrix (BME) has multiple uses with stem cells. *Stem Cell Rev Rep, 8*(1), 163-169. doi:10.1007/s12015-011-9278-y

Ashworth, J. C., Thompson, J. L., James, J. R., Slater, C. E., Pijuan-Galito, S., Lis-Slimak, K., . . . Merry, C. L. R. (2020). Peptide gels of fully-defined composition and mechanics for probing cell-cell and cell-matrix interactions in vitro. *Matrix Biol, 85-86*, 15-33. doi:10.1016/j.matbio.2019.06.009

Atanasov, G., Hau, H. M., Dietel, C., Benzing, C., Krenzien, F., Brandl, A., . . . Jonas, S. (2015). Prognostic significance of macrophage invasion in hilar cholangiocarcinoma. *BMC Cancer, 15*, 790. doi:10.1186/s12885-015-1795-7

Badea, M. A., Balas, M., Hermenean, A., Ciceu, A., Herman, H., Ionita, D., & Dinischiotu, A. (2019). Influence of Matrigel on Single- and Multiple-Spheroid Cultures in Breast Cancer Research. *SLAS Discov, 24*(5), 563-578. doi:10.1177/2472555219834698

Baghban, R., Roshangar, L., Jahanban-Esfahlan, R., Seidi, K., Ebrahimi-Kalan, A., Jaymand, M., . . . Zare, P. (2020). Tumor microenvironment complexity and therapeutic implications at a glance. *Cell Commun Signal, 18*(1), 59. doi:10.1186/s12964-020-0530-4

Baker, B. M., & Chen, C. S. (2012). Deconstructing the third dimension: how 3D culture microenvironments alter cellular cues. *J Cell Sci, 125*(Pt 13), 3015-3024. doi:10.1242/jcs.079509

Banales, J. M., Cardinale, V., Carpino, G., Marzioni, M., Andersen, J. B., Invernizzi, P., . . . Alvaro, D. (2016). Expert consensus document: Cholangiocarcinoma: current knowledge and future perspectives consensus statement from the European Network for the Study of Cholangiocarcinoma (ENS-CCA). *Nat Rev Gastroenterol Hepatol, 13*(5), 261-280. doi:10.1038/nrgastro.2016.51

Banales, J. M., Marin, J. J. G., Lamarca, A., Rodrigues, P. M., Khan, S. A., Roberts, L. R., . . . Gores, G. J. (2020). Cholangiocarcinoma 2020: the next horizon in mechanisms and management. *Nat Rev Gastroenterol Hepatol, 17*(9), 557-588. doi:10.1038/s41575-020-0310-z

Bareham, B., Georgakopoulos, N., Matas-Cespedes, A., Curran, M., & Saeb-Parsy, K. (2021). Modeling human tumor-immune environments in vivo for the preclinical assessment of immunotherapies. *Cancer Immunol Immunother, 70*(10), 2737-2750. doi:10.1007/s00262-021-02897-5

Baril, P., Gangeswaran, R., Mahon, P. C., Caulee, K., Kocher, H. M., Harada, T., . . . Lemoine, N. R. (2007). Periostin promotes invasiveness and resistance of pancreatic cancer cells to hypoxia-induced cell death: role of the beta4 integrin and the PI3k pathway. *Oncogene, 26*(14), 2082-2094. doi:10.1038/sj.onc.1210009

Barisam, M., Saidi, M. S., Kashaninejad, N., & Nguyen, N. T. (2018). Prediction of Necrotic Core and Hypoxic Zone of Multicellular Spheroids in a Microbioreactor with a U-Shaped Barrier. *Micromachines (Basel), 9*(3). doi:10.3390/mi9030094

Barrett, R. L., & Puré, E. (2020). Cancer-associated fibroblasts and their influence on tumor immunity and immunotherapy. *Elife, 9*. doi:10.7554/eLife.57243

Ben-David, U., Ha, G., Tseng, Y. Y., Greenwald, N. F., Oh, C., Shih, J., . . . Golub, T. R. (2017). Patient-derived xenografts undergo mouse-specific tumor evolution. *Nat Genet, 49*(11), 1567-1575. doi:10.1038/ng.3967

Benton, G., Arnaoutova, I., George, J., Kleinman, H. K., & Koblinski, J. (2014). Matrigel: from discovery and ECM mimicry to assays and models for cancer research. *Adv Drug Deliv Rev, 79-80*, 3-18. doi:10.1016/j.addr.2014.06.005

Berdasco, M., & Esteller, M. (2010). Aberrant epigenetic landscape in cancer: how cellular identity goes awry. *Dev Cell, 19*(5), 698-711. doi:10.1016/j.devcel.2010.10.005

Berx, G., & van Roy, F. (2009). Involvement of members of the cadherin superfamily in cancer. *Cold Spring Harb Perspect Biol, 1*(6), a003129. doi:10.1101/cshperspect.a003129

Bezrookove, V., Patino, J. M., Nosrati, M., Desprez, P. Y., McAllister, S., Soroceanu, L., . . . Dar, A. A. (2021). Niraparib Suppresses Cholangiocarcinoma Tumor Growth by Inducing Oxidative and Replication Stress. *Cancers (Basel), 13*(17). doi:10.3390/cancers13174405

Białkowska, K., Komorowski, P., Bryszewska, M., & Miłowska, K. (2020). Spheroids as a Type of Three-Dimensional Cell Cultures-Examples of Methods of Preparation and the Most Important Application. *Int J Mol Sci, 21*(17). doi:10.3390/ijms21176225

Blechacz, B. (2017). Cholangiocarcinoma: Current Knowledge and New Developments. *Gut Liver, 11*(1), 13-26. doi:10.5009/gnl15568

Blechacz, B., & Gores, G. J. (2008). Cholangiocarcinoma: advances in pathogenesis, diagnosis, and treatment. *Hepatology, 48*(1), 308-321. doi:10.1002/hep.22310

Blomme, A., Van Simaeys, G., Doumont, G., Costanza, B., Bellier, J., Otaka, Y., . . . Turtoi, A. (2018). Murine stroma adopts a human-like metabolic phenotype in the PDX model of colorectal cancer and liver metastases. *Oncogene, 37*(9), 1237-1250. doi:10.1038/s41388-017-0018-x

Bonnans, C., Chou, J., & Werb, Z. (2014). Remodelling the extracellular matrix in development and disease. *Nat Rev Mol Cell Biol, 15*(12), 786-801. doi:10.1038/nrm3904

Boulter, L., Guest, R. V., Kendall, T. J., Wilson, D. H., Wojtacha, D., Robson, A. J., . . . Forbes, S. J. (2015). WNT signaling drives cholangiocarcinoma growth and can be pharmacologically inhibited. *J Clin Invest, 125*(3), 1269-1285. doi:10.1172/JCI76452

Bourgon, R., Gentleman, R., & Huber, W. (2010). Independent filtering increases detection power for high-throughput experiments. *Proc Natl Acad Sci U S A, 107*(21), 9546-9551. doi:10.1073/pnas.0914005107

Brennan, T. V., Lin, L., Huang, X., & Yang, Y. (2018). Generation of Luciferase-expressing Tumor Cell Lines. *Bio Protoc, 8*(8). doi:10.21769/BioProtoc.2817

Brivio, S., Cadamuro, M., Strazzabosco, M., & Fabris, L. (2017). Tumor reactive stroma in cholangiocarcinoma: The fuel behind cancer aggressiveness. *World J Hepatol, 9*(9), 455-468. doi:10.4254/wjh.v9.i9.455

Broutier, L., Mastrogiovanni, G., Verstegen, M. M., Francies, H. E., Gavarro, L. M., Bradshaw, C. R., . . . Huch, M. (2017). Human primary liver cancer-derived organoid cultures for disease modeling and drug screening. *Nat Med, 23*(12), 1424-1435. doi:10.1038/nm.4438

Brucher, B. L., & Jamall, I. S. (2014). Cell-cell communication in the tumor microenvironment, carcinogenesis, and anticancer treatment. *Cell Physiol Biochem, 34*(2), 213-243. doi:10.1159/000362978

Bruno, S., Grange, C., Deregibus, M. C., Calogero, R. A., Saviozzi, S., Collino, F., . . . Camussi, G. (2009). Mesenchymal stem cell-derived microvesicles protect against acute tubular injury. *J Am Soc Nephrol, 20*(5), 1053-1067. doi:10.1681/ASN.2008070798

Buhome, O., Wongwattanakul, M., Daduang, J., & Limpaiboon, T. (2022). 3D Silk Fibroin-Gelatin/Hyaluronic Acid/Heparan Sulfate Scaffold Enhances Expression of Stemness and EMT Markers in Cholangiocarcinoma. *In Vivo, 36*(3), 1155-1167. doi:10.21873/invivo.12815

Cadamuro, M., Brivio, S., Mertens, J., Vismara, M., Moncsek, A., Milani, C., . . . Fabris, L. (2019). Platelet-derived growth factor-D enables liver myofibroblasts to promote tumor lymphangiogenesis in cholangiocarcinoma. *J Hepatol, 70*(4), 700-709. doi:10.1016/j.jhep.2018.12.004

Cadamuro, M., Stecca, T., Brivio, S., Mariotti, V., Fiorotto, R., Spirli, C., . . . Fabris, L. (2018). The deleterious interplay between tumor epithelia and stroma in cholangiocarcinoma. *Biochim Biophys Acta Mol Basis Dis, 1864*(4 Pt B), 1435-1443. doi:10.1016/j.bbadis.2017.07.028

Campbell, D. J., Dumur, C. I., Lamour, N. F., Dewitt, J. L., & Sirica, A. E. (2012). Novel organotypic culture model of cholangiocarcinoma progression. *Hepatol Res, 42*(11), 1119-1130. doi:10.1111/j.1872-034X.2012.01026.x

Cardinale, V., Renzi, A., Carpino, G., Torrice, A., Bragazzi, M. C., Giuliante, F., . . . Alvaro, D. (2015). Profiles of cancer stem cell subpopulations in cholangiocarcinomas. *Am J Pathol, 185*(6), 1724-1739. doi:10.1016/j.ajpath.2015.02.010

Carlsson, J., & Yuhas, J. M. (1984). Liquid-overlay culture of cellular spheroids. *Recent Results Cancer Res, 95*, 1-23. doi:10.1007/978-3-642-82340-4_1

Carpino, G., Overi, D., Melandro, F., Grimaldi, A., Cardinale, V., Di Matteo, S., . . . Mancone, C. (2019). Matrisome analysis of intrahepatic cholangiocarcinoma unveils a peculiar cancer-associated extracellular matrix structure. *Clin Proteomics, 16*, 37. doi:10.1186/s12014-019-9257-x

Castell, J. V., & Gómez-Lechón, M. J. (2009). Liver cell culture techniques. *Methods Mol Biol, 481*, 35-46. doi:10.1007/978-1-59745-201-4_4

Cavalloni, G., Peraldo-Neia, C., Sassi, F., Chiorino, G., Sarotto, I., Aglietta, M., & Leone, F. (2016). Establishment of a patient-derived intrahepatic cholangiocarcinoma xenograft model with KRAS mutation. *BMC Cancer, 16*, 90. doi:10.1186/s12885-016-2136-1

Cekanova, M., & Rathore, K. (2014). Animal models and therapeutic molecular targets of cancer: utility and limitations. *Drug Des Devel Ther, 8*, 1911-1921. doi:10.2147/dddt.s49584

Chan, J. K. (2014). The wonderful colors of the hematoxylin-eosin stain in diagnostic surgical pathology. *Int J Surg Pathol, 22*(1), 12-32. doi:10.1177/1066896913517939

Chang, L., Azzolin, L., Di Biagio, D., Zanconato, F., Battilana, G., Lucon Xiccato, R., . . . Piccolo, S. (2018). The SWI/SNF complex is a mechanoregulated inhibitor of YAP and TAZ. *Nature, 563*(7730), 265-269. doi:10.1038/s41586-018-0658-1

Che, L., Fan, B., Pilo, M. G., Xu, Z., Liu, Y., Cigliano, A., . . . Chen, X. (2016). Jagged 1 is a major Notch ligand along cholangiocarcinoma development in mice and humans. *Oncogenesis, 5*(12), e274. doi:10.1038/oncsis.2016.73

Chen, Z., Guo, P., Xie, X., Yu, H., Wang, Y., & Chen, G. (2019). The role of tumour microenvironment: a new vision for cholangiocarcinoma. *J Cell Mol Med, 23*(1), 59-69. doi:10.1111/jcmm.13953

Cheng, G., Tse, J., Jain, R. K., & Munn, L. L. (2009). Micro-environmental mechanical stress controls tumor spheroid size and morphology by suppressing proliferation and inducing apoptosis in cancer cells. *PLoS One, 4*(2), e4632. doi:10.1371/journal.pone.0004632

Choy, G., O'Connor, S., Diehn, F. E., Costouros, N., Alexander, H. R., Choyke, P., & Libutti, S. K. (2003). Comparison of noninvasive fluorescent and bioluminescent small animal optical imaging. *Biotechniques, 35*(5), 1022-1026, 1028-1030. doi:10.2144/03355rr02

Chuaysri, C., Thuwajit, P., Paupairoj, A., Chau-In, S., Suthiphongchai, T., & Thuwajit, C. (2009). Alpha-smooth muscle actin-positive fibroblasts promote biliary cell

proliferation and correlate with poor survival in cholangiocarcinoma. *Oncol Rep, 21*(4), 957-969. doi:10.3892/or_00000309

Chung, J. Y., Hong, S. M., Choi, B. Y., Cho, H., Yu, E., & Hewitt, S. M. (2009). The expression of phospho-AKT, phospho-mTOR, and PTEN in extrahepatic cholangiocarcinoma. *Clin Cancer Res, 15*(2), 660-667. doi:10.1158/1078-0432.CCR-08-1084

Chung, S., Kim, S. H., Seo, Y., Kim, S. K., & Lee, J. Y. (2017). Quantitative analysis of cell proliferation by a dye dilution assay: Application to cell lines and cocultures. *Cytometry A, 91*(7), 704-712. doi:10.1002/cyto.a.23105

Clancy, S. B., W. (2008). Translation: DNA to mRNA to Protein. *Nature Education, 1*(1), 101.

Claperon, A., Guedj, N., Mergey, M., Vignjevic, D., Desbois-Mouthon, C., Boissan, M., . . . Fouassier, L. (2012). Loss of EBP50 stimulates EGFR activity to induce EMT phenotypic features in biliary cancer cells. *Oncogene, 31*(11), 1376-1388. doi:10.1038/onc.2011.334

Claperon, A., Mergey, M., Aoudjehane, L., Ho-Bouldoires, T. H., Wendum, D., Prignon, A., . . . Fouassier, L. (2013). Hepatic myofibroblasts promote the progression of human cholangiocarcinoma through activation of epidermal growth factor receptor. *Hepatology, 58*(6), 2001-2011. doi:10.1002/hep.26585

Claperon, A., Mergey, M., Nguyen Ho-Bouldoires, T. H., Vignjevic, D., Wendum, D., Chretien, Y., . . . Fouassier, L. (2014). EGF/EGFR axis contributes to the progression of cholangiocarcinoma through the induction of an epithelial-mesenchymal transition. *J Hepatol, 61*(2), 325-332. doi:10.1016/j.jhep.2014.03.033

Clements, O., Eliahoo, J., Kim, J. U., Taylor-Robinson, S. D., & Khan, S. A. (2020). Risk factors for intrahepatic and extrahepatic cholangiocarcinoma: A systematic review and meta-analysis. *J Hepatol, 72*(1), 95-103. doi:10.1016/j.jhep.2019.09.007

Coenye, T. (2021). Do results obtained with RNA-sequencing require independent verification? In *Biofilm* (Vol. 3, pp. 100043).

Cregger, M., Berger, A. J., & Rimm, D. L. (2006). Immunohistochemistry and quantitative analysis of protein expression. *Arch Pathol Lab Med, 130*(7), 1026-1030. doi:10.5858/2006-130-1026-IAQAOP

Cunningham, R. E. (2010). Tissue disaggregation. *Methods Mol Biol, 588*, 327-330. doi:10.1007/978-1-59745-324-0_32

Dang, L., & Su, S. M. (2017). Isocitrate Dehydrogenase Mutation and (R)-2-Hydroxyglutarate: From Basic Discovery to Therapeutics Development. *Annu Rev Biochem, 86*, 305-331. doi:10.1146/annurev-biochem-061516-044732

Danielsson, F., Peterson, M. K., Caldeira Araujo, H., Lautenschlager, F., & Gad, A. K. B. (2018). Vimentin Diversity in Health and Disease. *Cells, 7*(10). doi:10.3390/cells7100147

Dankner, M., Rose, A. A. N., Rajkumar, S., Siegel, P. M., & Watson, I. R. (2018). Classifying BRAF alterations in cancer: new rational therapeutic strategies for actionable mutations. *Oncogene, 37*(24), 3183-3199. doi:10.1038/s41388-018-0171-x

Data, M. I. T. C., Komorowski, M., Marshall, D. C., Salciccioli, J. D., & Crutain, Y. (2016). Exploratory Data Analysis. In *Secondary Analysis of Electronic Health Records* (pp. 185-203). Cham (CH): Springer

Day, C. P., Merlino, G., & Van Dyke, T. (2015). Preclinical mouse cancer models: a maze of opportunities and challenges. *Cell, 163*(1), 39-53. doi:10.1016/j.cell.2015.08.068

De Thaye, E., Van de Vijver, K., Van der Meulen, J., Taminau, J., Wagemans, G., Denys, H., . . . De Wever, O. (2020). Establishment and characterization of a cell line and patient-derived xenograft (PDX) from peritoneal metastasis of low-grade serous ovarian carcinoma. *Sci Rep, 10*(1), 6688. doi:10.1038/s41598-020-63738-6

De Wever, O., Nguyen, Q. D., Van Hoorde, L., Bracke, M., Bruyneel, E., Gespach, C., & Mareel, M. (2004). Tenascin-C and SF/HGF produced by myofibroblasts in vitro provide convergent pro-invasive signals to human colon cancer cells through RhoA and Rac. *FASEB J, 18*(9), 1016-1018. doi:10.1096/fj.03-1110fje

Dekkers, J. F., Alieva, M., Wellens, L. M., Ariese, H. C. R., Jamieson, P. R., Vonk, A. M., . . . Rios, A. C. (2019). High-resolution 3D imaging of fixed and cleared organoids. *Nat Protoc, 14*(6), 1756-1771. doi:10.1038/s41596-019-0160-8

Delarue, M., Montel, F., Caen, O., Elgeti, J., Siaugue, J. M., Vignjevic, D., . . . Cappello, G. (2013). Mechanical control of cell flow in multicellular spheroids. *Phys Rev Lett, 110*(13), 138103. doi:10.1103/PhysRevLett.110.138103

Deoliveira, M. L., Schulick, R. D., Nimura, Y., Rosen, C., Gores, G., Neuhaus, P., & Clavien, P. A. (2011). New staging system and a registry for perihilar cholangiocarcinoma. *Hepatology, 53*(4), 1363-1371. doi:10.1002/hep.24227

Di Modugno, F., Colosi, C., Trono, P., Antonacci, G., Ruocco, G., & Nistico, P. (2019). 3D models in the new era of immune oncology: focus on T cells, CAF and ECM. *J Exp Clin Cancer Res, 38*(1), 117. doi:10.1186/s13046-019-1086-2

Dokduang, H., Juntana, S., Techasen, A., Namwat, N., Yongvanit, P., Khuntikeo, N., . . . Loilome, W. (2013). Survey of activated kinase proteins reveals potential targets for cholangiocarcinoma treatment. *Tumour Biol, 34*(6), 3519-3528. doi:10.1007/s13277-013-0930-9

Domenici, G., Eduardo, R., Castillo-Ecija, H., Orive, G., Montero Carcaboso, Á., & Brito, C. (2021). PDX-Derived Ewing's Sarcoma Cells Retain High Viability and Disease Phenotype in Alginate Encapsulated Spheroid Cultures. *Cancers (Basel), 13*(4). doi:10.3390/cancers13040879

Donato, M., Xu, Z., Tomoiaga, A., Granneman, J. G., Mackenzie, R. G., Bao, R., . . . Draghici, S. (2013). Analysis and correction of crosstalk effects in pathway analysis. *Genome Res, 23*(11), 1885-1893. doi:10.1101/gr.153551.112

Dranoff, J. A., & Wells, R. G. (2010). Portal fibroblasts: Underappreciated mediators of biliary fibrosis. *Hepatology, 51*(4), 1438-1444. doi:10.1002/hep.23405

Dries, R., Chen, J., Del Rossi, N., Khan, M. M., Sistig, A., & Yuan, G. C. (2021). Advances in spatial transcriptomic data analysis. *Genome Res, 31*(10), 1706-1718. doi:10.1101/gr.275224.121

Drilon, A., Laetsch, T. W., Kummar, S., DuBois, S. G., Lassen, U. N., Demetri, G. D., . . . Hyman, D. M. (2018). Efficacy of Larotrectinib in TRK Fusion-Positive Cancers in Adults and Children. *N Engl J Med, 378*(8), 731-739. doi:10.1056/NEJMoa1714448

Drilon, A., Siena, S., Ou, S. I., Patel, M., Ahn, M. J., Lee, J., . . . De Braud, F. G. (2017). Safety and Antitumor Activity of the Multitargeted Pan-TRK, ROS1, and ALK Inhibitor Entrectinib: Combined Results from Two Phase I Trials (ALKA-372-001 and STARTRK-1). *Cancer Discov, 7*(4), 400-409. doi:10.1158/2159-8290.CD-16-1237

Du, R., Lu, K. V., Petritsch, C., Liu, P., Ganss, R., Passegue, E., . . . Bergers, G. (2008). HIF1alpha induces the recruitment of bone marrow-derived vascular modulatory cells to regulate tumor angiogenesis and invasion. *Cancer Cell, 13*(3), 206-220. doi:10.1016/j.ccr.2008.01.034

Ebata, T., Nagino, M., Kamiya, J., Uesaka, K., Nagasaka, T., & Nimura, Y. (2003). Hepatectomy with portal vein resection for hilar cholangiocarcinoma: audit of 52 consecutive cases. *Ann Surg, 238*(5), 720-727. doi:10.1097/01.sla.0000094437.68038.a3

Eghbalnia, H. R., Wilfinger, W. W., Mackey, K., & Chomczynski, P. (2020). Coordinated analysis of exon and intron data reveals novel differential gene expression changes. *Sci Rep, 10*(1), 15669. doi:10.1038/s41598-020-72482-w

Eilenberger, C., Kratz, S. R. A., Rothbauer, M., Ehmoser, E. K., Ertl, P., & Kupcu, S. (2018). Optimized alamarBlue assay protocol for drug dose-response determination of 3D tumor spheroids. *MethodsX, 5*, 781-787. doi:10.1016/j.mex.2018.07.011

Endo, I., Gonen, M., Yopp, A. C., Dalal, K. M., Zhou, Q., Klimstra, D., . . . Jarnagin, W. R. (2008). Intrahepatic cholangiocarcinoma: rising frequency, improved survival, and determinants of outcome after resection. *Ann Surg, 248*(1), 84-96. doi:10.1097/SLA.0b013e318176c4d3

Enjoji, M., Sakai, H., Nawata, H., Kajiyama, K., & Tsuneyoshi, M. (1997). Sarcomatous and adenocarcinoma cell lines from the same nodule of cholangiocarcinoma. *In Vitro Cell Dev Biol Anim, 33*(9), 681-683. doi:10.1007/s11626-997-0125-z

Erdogan, B., Ao, M., White, L. M., Means, A. L., Brewer, B. M., Yang, L., . . . Webb, D. J. (2017). Cancer-associated fibroblasts promote directional cancer cell migration by aligning fibronectin. *J Cell Biol, 216*(11), 3799-3816. doi:10.1083/jcb.201704053

Evans, C., Hardin, J., & Stoebel, D. M. (2018). Selecting between-sample RNA-Seq normalization methods from the perspective of their assumptions. *Brief Bioinform, 19*(5), 776-792. doi:10.1093/bib/bbx008

Ewald, F., Grabinski, N., Grottke, A., Windhorst, S., Nörz, D., Carstensen, L., . . . Jücker, M. (2013). Combined targeting of AKT and mTOR using MK-2206 and RAD001 is synergistic in the treatment of cholangiocarcinoma. *Int J Cancer, 133*(9), 2065-2076. doi:10.1002/ijc.28214

Fabris, L., Andersen, J. B., & Fouassier, L. (2020). Intrahepatic cholangiocarcinoma: A single-cell resolution unraveling the complexity of the tumor microenvironment. *J Hepatol, 73*(5), 1007-1009. doi:10.1016/j.jhep.2020.07.017

Fabris, L., Perugorria, M. J., Mertens, J., Bjorkstrom, N. K., Cramer, T., Lleo, A., . . . Strazzabosco, M. (2019). The tumour microenvironment and immune milieu of cholangiocarcinoma. *Liver Int, 39 Suppl 1*, 63-78. doi:10.1111/liv.14098

Fabris, L., Sato, K., Alpini, G., & Strazzabosco, M. (2021). The Tumor Microenvironment in Cholangiocarcinoma Progression. *Hepatology, 73 Suppl 1*, 75-85. doi:10.1002/hep.31410

Fabris, L., Strazzabosco, M., Crosby, H. A., Ballardini, G., Hubscher, S. G., Kelly, D. A., . . . Joplin, R. (2000). Characterization and isolation of ductular cells coexpressing neural cell adhesion molecule and Bcl-2 from primary cholangiopathies and ductal plate malformations. *Am J Pathol, 156*(5), 1599-1612. doi:10.1016/S0002-9440(10)65032-8

Fan, B., Malato, Y., Calvisi, D. F., Naqvi, S., Razumilava, N., Ribback, S., . . . Willenbring, H. (2012). Cholangiocarcinomas can originate from hepatocytes in mice. *J Clin Invest, 122*(8), 2911-2915. doi:10.1172/jci63212

Fang, T., Lv, H., Lv, G., Li, T., Wang, C., Han, Q., . . . Wang, H. (2018). Tumor-derived exosomal miR-1247-3p induces cancer-associated fibroblast activation to foster lung metastasis of liver cancer. *Nat Commun, 9*(1), 191. doi:10.1038/s41467-017-02583-0

Fang, Y., & Eglen, R. M. (2017). Three-Dimensional Cell Cultures in Drug Discovery and Development. *SLAS Discov, 22*(5), 456-472. doi:10.1177/1087057117696795

Feuchtinger, A., Stiehler, T., Jütting, U., Marjanovic, G., Luber, B., Langer, R., & Walch, A. (2015). Image analysis of immunohistochemistry is superior to visual scoring as shown for patient outcome of esophageal adenocarcinoma. *Histochem Cell Biol, 143*(1), 1-9. doi:10.1007/s00418-014-1258-2

Fingas, C. D., Bronk, S. F., Werneburg, N. W., Mott, J. L., Guicciardi, M. E., Cazanave, S. C., . . . Gores, G. J. (2011). Myofibroblast-derived PDGF-BB promotes Hedgehog survival signaling in cholangiocarcinoma cells. *Hepatology, 54*(6), 2076-2088. doi:10.1002/hep.24588

Fischer, A. H., Jacobson, K. A., Rose, J., & Zeller, R. (2008). Hematoxylin and eosin staining of tissue and cell sections. *CSH Protoc, 2008*, pdb prot4986. doi:10.1101/pdb.prot4986

Fischer, T. (2019). Transmission (TEM) vs. Scanning (SEM) Electron Microscopes: What's the Difference? Retrieved from https://www.thermofisher.com/blog/materials/tem-vs-sem-whats-the-difference/

Fitzgerald, K. A., Malhotra, M., Curtin, C. M., FJ, O. B., & CM, O. D. (2015). Life in 3D is never flat: 3D models to optimise drug delivery. *J Control Release, 215*, 39-54. doi:10.1016/j.jconrel.2015.07.020

Fouassier, L., Marzioni, M., Afonso, M. B., Dooley, S., Gaston, K., Giannelli, G., . . . Coulouarn, C. (2019). Signalling networks in cholangiocarcinoma: Molecular pathogenesis, targeted therapies and drug resistance. *Liver Int, 39 Suppl 1*, 43-62. doi:10.1111/liv.14102

Francis, H., DeMorrow, S., Venter, J., Onori, P., White, M., Gaudio, E., . . . Alpini, G. (2012). Inhibition of histidine decarboxylase ablates the autocrine tumorigenic effects of histamine in human cholangiocarcinoma. *Gut, 61*(5), 753-764. doi:10.1136/gutjnl-2011-300007

Francis, H., Meng, F., Gaudio, E., & Alpini, G. (2012). Histamine regulation of biliary proliferation. *J Hepatol, 56*(5), 1204-1206. doi:10.1016/j.jhep.2011.09.023

Frisbie, L., Buckanovich, R. J., & Coffman, L. (2022). Carcinoma-Associated Mesenchymal Stem/Stromal Cells: Architects of the Pro-tumorigenic Tumor Microenvironment. *Stem Cells, 40*(8), 705-715. doi:10.1093/stmcls/sxac036

Frohwitter, G., Buerger, H., PJ, V. A. N. D., Korsching, E., Kleinheinz, J., & Fillies, T. (2016). Cytokeratin and protein expression patterns in squamous cell carcinoma of the oral cavity provide evidence for two distinct pathogenetic pathways. *Oncol Lett, 12*(1), 107-113. doi:10.3892/ol.2016.4588

Gan, L., Shen, H., Li, X., Han, Z., Jing, Y., Yang, X., . . . Xia, Y. (2021). Mesenchymal stem cells promote chemoresistance by activating autophagy in intrahepatic cholangiocarcinoma. *Oncol Rep, 45*(1), 107-118. doi:10.3892/or.2020.7838

Gao, D., Mittal, V., Ban, Y., Lourenco, A. R., Yomtoubian, S., & Lee, S. (2018). Metastatic tumor cells - genotypes and phenotypes. *Front Biol (Beijing), 13*(4), 277-286. doi:10.1007/s11515-018-1513-3

Gao, Y., Zhou, R., Huang, J. F., Hu, B., Cheng, J. W., Huang, X. W., . . . Yang, X. R. (2021). Patient-Derived Xenograft Models for Intrahepatic Cholangiocarcinoma and Their Application in Guiding Personalized Medicine. *Front Oncol, 11*, 704042. doi:10.3389/fonc.2021.704042

Garcia, M. G., Bayo, J., Bolontrade, M. F., Sganga, L., Malvicini, M., Alaniz, L., . . . Mazzolini, G. (2011). Hepatocellular carcinoma cells and their fibrotic microenvironment modulate bone marrow-derived mesenchymal stromal cell migration in vitro and in vivo. *Mol Pharm, 8*(5), 1538-1548. doi:10.1021/mp200137c

Garcia, P. L., Miller, A. L., Gamblin, T. L., Council, L. N., Christein, J. D., Arnoletti, J. P., . . . Yoon, K. J. (2018). JQ1 Induces DNA Damage and Apoptosis, and Inhibits Tumor Growth in a Patient-Derived Xenograft Model of Cholangiocarcinoma. *Mol Cancer Ther, 17*(1), 107-118. doi:10.1158/1535-7163.MCT-16-0922

Garza-Lopez, E., Vue, Z., Katti, P., Neikirk, K., Biete, M., Lam, J., . . . Hinton, A., Jr. (2021). Protocols for Generating Surfaces and Measuring 3D Organelle Morphology Using Amira. *Cells, 11*(1). doi:10.3390/cells11010065

Gautheron, J., Vucur, M., Reisinger, F., Cardenas, D. V., Roderburg, C., Koppe, C., . . . Luedde, T. (2014). A positive feedback loop between RIP3 and JNK controls non-alcoholic steatohepatitis. *EMBO Mol Med, 6*(8), 1062-1074. doi:10.15252/emmm.201403856

Ge, S. X., Son, E. W., & Yao, R. (2018). iDEP: an integrated web application for differential expression and pathway analysis of RNA-Seq data. *BMC Bioinformatics, 19*(1), 534. doi:10.1186/s12859-018-2486-6

Geng, X., Chen, H., Zhao, L., Hu, J., Yang, W., Li, G., . . . Sun, B. (2021). Cancer-Associated Fibroblast (CAF) Heterogeneity and Targeting Therapy of CAFs in Pancreatic Cancer. *Front Cell Dev Biol, 9*, 655152. doi:10.3389/fcell.2021.655152

Gentilini, A., Pastore, M., Marra, F., & Raggi, C. (2018). The Role of Stroma in Cholangiocarcinoma: The Intriguing Interplay between Fibroblastic Component, Immune Cell Subsets and Tumor Epithelium. *Int J Mol Sci, 19*(10). doi:10.3390/ijms19102885

Gentilini, A., Rombouts, K., Galastri, S., Caligiuri, A., Mingarelli, E., Mello, T., . . . Pinzani, M. (2012). Role of the stromal-derived factor-1 (SDF-1)-CXCR4 axis in the interaction between hepatic stellate cells and cholangiocarcinoma. *J Hepatol, 57*(4), 813-820. doi:10.1016/j.jhep.2012.06.012

Georgopoulou, D., Callari, M., Rueda, O. M., Shea, A., Martin, A., Giovannetti, A., . . . Consortium, I. (2021). Landscapes of cellular phenotypic diversity in breast cancer xenografts and their impact on drug response. *Nature Communications*.

Gilkes, D. M., Bajpai, S., Chaturvedi, P., Wirtz, D., & Semenza, G. L. (2013). Hypoxia-inducible factor 1 (HIF-1) promotes extracellular matrix remodeling under hypoxic conditions by inducing P4HA1, P4HA2, and PLOD2 expression in fibroblasts. *J Biol Chem, 288*(15), 10819-10829. doi:10.1074/jbc.M112.442939

Goeppert, B., Frauenschuh, L., Renner, M., Roessler, S., Stenzinger, A., Klauschen, F., . . . Capper, D. (2014). BRAF V600E-specific immunohistochemistry reveals low mutation rates in biliary tract cancer and restriction to intrahepatic

cholangiocarcinoma. *Mod Pathol, 27*(7), 1028-1034. doi:10.1038/modpathol.2013.206

Goeppert, B., Frauenschuh, L., Zucknick, M., Stenzinger, A., Andrulis, M., Klauschen, F., . . . Weichert, W. (2013). Prognostic impact of tumour-infiltrating immune cells on biliary tract cancer. *Br J Cancer, 109*(10), 2665-2674. doi:10.1038/bjc.2013.610

Goldberg, S. B., Redman, M. W., Lilenbaum, R., Politi, K., Stinchcombe, T. E., Horn, L., . . . Gandara, D. R. (2020). Randomized Trial of Afatinib Plus Cetuximab Versus Afatinib Alone for First-Line Treatment of EGFR-Mutant Non-Small-Cell Lung Cancer: Final Results From SWOG S1403. *J Clin Oncol, 38*(34), 4076-4085. doi:10.1200/JCO.20.01149

Govaere, O., Wouters, J., Petz, M., Vandewynckel, Y. P., Van den Eynde, K., Van den Broeck, A., . . . Roskams, T. (2016). Laminin-332 sustains chemoresistance and quiescence as part of the human hepatic cancer stem cell niche. *J Hepatol, 64*(3), 609-617. doi:10.1016/j.jhep.2015.11.011

Gu, L., & Mooney, D. J. (2016). Biomaterials and emerging anticancer therapeutics: engineering the microenvironment. *Nat Rev Cancer, 16*(1), 56-66. doi:10.1038/nrc.2015.3

Gu, M. J., & Choi, J. H. (2014). Epithelial-mesenchymal transition phenotypes are associated with patient survival in intrahepatic cholangiocarcinoma. *J Clin Pathol, 67*(3), 229-234. doi:10.1136/jclinpath-2013-201806

Gu, Z. W., He, Y. F., Wang, W. J., Tian, Q., & Di, W. (2019). MiR-1180 from bone marrow-derived mesenchymal stem cells induces glycolysis and chemoresistance in ovarian cancer cells by upregulating the Wnt signaling pathway. *J Zhejiang Univ Sci B, 20*(3), 219-237. doi:10.1631/jzus.B1800190

Guedj, N., Zhan, Q., Perigny, M., Rautou, P. E., Degos, F., Belghiti, J., . . . Paradis, V. (2009). Comparative protein expression profiles of hilar and peripheral hepatic cholangiocarcinomas. *J Hepatol, 51*(1), 93-101. doi:10.1016/j.jhep.2009.03.017

Guest, R. V., Boulter, L., Dwyer, B. J., Kendall, T. J., Man, T. Y., Minnis-Lyons, S. E., . . . Forbes, S. J. (2016). Notch3 drives development and progression of cholangiocarcinoma. *Proc Natl Acad Sci U S A, 113*(43), 12250-12255. doi:10.1073/pnas.1600067113

Guo, X., Oshima, H., Kitmura, T., Taketo, M. M., & Oshima, M. (2008). Stromal fibroblasts activated by tumor cells promote angiogenesis in mouse gastric cancer. *J Biol Chem, 283*(28), 19864-19871. doi:10.1074/jbc.M800798200

Habanjar, O., Diab-Assaf, M., Caldefie-Chezet, F., & Delort, L. (2021). 3D Cell Culture Systems: Tumor Application, Advantages, and Disadvantages. *Int J Mol Sci, 22*(22). doi:10.3390/ijms222212200

Haga, H., Yan, I. K., Takahashi, K., Wood, J., Zubair, A., & Patel, T. (2015). Tumour cell-derived extracellular vesicles interact with mesenchymal stem cells to modulate the microenvironment and enhance cholangiocarcinoma growth. *J Extracell Vesicles, 4*, 24900. doi:10.3402/jev.v4.24900

Han, S. J., Kwon, S., & Kim, K. S. (2021). Challenges of applying multicellular tumor spheroids in preclinical phase. *Cancer Cell Int, 21*(1), 152. doi:10.1186/s12935-021-01853-8

Hanahan, D. (2022). Hallmarks of Cancer: New Dimensions. *Cancer Discov, 12*(1), 31-46. doi:10.1158/2159-8290.CD-21-1059

Hanahan, D., & Coussens, L. M. (2012). Accessories to the crime: functions of cells recruited to the tumor microenvironment. *Cancer Cell, 21*(3), 309-322. doi:10.1016/j.ccr.2012.02.022

Hanahan, D., & Weinberg, R. A. (2000). The hallmarks of cancer. *Cell, 100*(1), 57-70. doi:10.1016/s0092-8674(00)81683-9

Hanahan, D., & Weinberg, R. A. (2011). Hallmarks of cancer: the next generation. *Cell, 144*(5), 646-674. doi:10.1016/j.cell.2011.02.013

Handra-Luca, A., Hong, S. M., Walter, K., Wolfgang, C., Hruban, R., & Goggins, M. (2011). Tumour epithelial vimentin expression and outcome of pancreatic ductal adenocarcinomas. *Br J Cancer, 104*(8), 1296-1302. doi:10.1038/bjc.2011.93

Hare, D., Collins, S., Cuddington, B., & Mossman, K. (2016). The Importance of Physiologically Relevant Cell Lines for Studying Virus-Host Interactions. *Viruses, 8*(11). doi:10.3390/v8110297

Hasita, H., Komohara, Y., Okabe, H., Masuda, T., Ohnishi, K., Lei, X. F., . . . Takeya, M. (2010). Significance of alternatively activated macrophages in patients with intrahepatic cholangiocarcinoma. *Cancer Sci, 101*(8), 1913-1919. doi:10.1111/j.1349-7006.2010.01614.x

Hass, R. (2020). Role of MSC in the Tumor Microenvironment. *Cancers (Basel), 12*(8). doi:10.3390/cancers12082107

He, W., Liang, B., Wang, C., Li, S., Zhao, Y., Huang, Q., . . . Shi, M. (2019). MSC-regulated lncRNA MACC1-AS1 promotes stemness and chemoresistance through fatty acid oxidation in gastric cancer. *Oncogene, 38*, 4637–4654. doi:10.1038/s41388-019-0747-0

Helmlinger, G., Netti, P. A., Lichtenbeld, H. C., Melder, R. J., & Jain, R. K. (1997). Solid stress inhibits the growth of multicellular tumor spheroids. *Nat Biotechnol, 15*(8), 778-783. doi:10.1038/nbt0897-778

Herter, S., Morra, L., Schlenker, R., Sulcova, J., Fahrni, L., Waldhauer, I., . . . Bacac, M. (2017). A novel three-dimensional heterotypic spheroid model for the assessment of the activity of cancer immunotherapy agents. *Cancer Immunol Immunother, 66*(1), 129-140. doi:10.1007/s00262-016-1927-1

Hewitt, S. M., Baskin, D. G., Frevert, C. W., Stahl, W. L., & Rosa-Molinar, E. (2014). Controls for immunohistochemistry: the Histochemical Society's standards of practice for validation of immunohistochemical assays. *J Histochem Cytochem, 62*(10), 693-697. doi:10.1369/0022155414545224

Hidalgo, M., Amant, F., Biankin, A. V., Budinska, E., Byrne, A. T., Caldas, C., . . . Villanueva, A. (2014). Patient-derived xenograft models: an emerging platform for translational cancer research. *Cancer Discov, 4*(9), 998-1013. doi:10.1158/2159-8290.CD-14-0001

Hoarau-Véchot, J., Rafii, A., Touboul, C., & Pasquier, J. (2018). Halfway between 2D and Animal Models: Are 3D Cultures the Ideal Tool to Study Cancer-Microenvironment Interactions? *Int J Mol Sci, 19*(1). doi:10.3390/ijms19010181

Hodges, C., Kirkland, J. G., & Crabtree, G. R. (2016). The Many Roles of BAF (mSWI/SNF) and PBAF Complexes in Cancer. *Cold Spring Harb Perspect Med, 6*(8). doi:10.1101/cshperspect.a026930

Holt, A. P., Haughton, E. L., Lalor, P. F., Filer, A., Buckley, C. D., & Adams, D. H. (2009). Liver myofibroblasts regulate infiltration and positioning of lymphocytes in human liver. *Gastroenterology, 136*(2), 705-714. doi:10.1053/j.gastro.2008.10.020

Hong, C. R., Bogle, G., Wang, J., Patel, K., Pruijn, F. B., Wilson, W. R., & Hicks, K. O. (2018). Bystander Effects of Hypoxia-Activated Prodrugs: Agent-Based Modeling Using Three Dimensional Cell Cultures. *Front Pharmacol, 9*, 1013. doi:10.3389/fphar.2018.01013

Hong, M., Tao, S., Zhang, L., Diao, L. T., Huang, X., Huang, S., . . . Zhang, H. (2020). RNA sequencing: new technologies and applications in cancer research. *J Hematol Oncol, 13*(1), 166. doi:10.1186/s13045-020-01005-x

Horie, S., Endo, K., Kawasaki, H., & Terada, T. (2000). Overexpression of MDM2 protein in intrahepatic cholangiocarcinoma: relationship with p53 overexpression, Ki-67 labeling, and clinicopathological features. *Virchows Arch, 437*(1), 25-30. doi:10.1007/s004280000201

Huang, C. S., Zhu, Y. Q., Xu, Q. C., Chen, S., Huang, Y., Zhao, G., . . . Yin, X. Y. (2022). YTHDF2 promotes intrahepatic cholangiocarcinoma progression and desensitises cisplatin treatment by increasing CDKN1B mRNA degradation. *Clin Transl Med, 12*(6), e848. doi:10.1002/ctm2.848

Huang, H., Wang, Z., Zhang, Y., Pradhan, R. N., Ganguly, D., Chandra, R., . . . Brekken, R. A. (2022). Mesothelial cell-derived antigen-presenting cancer-associated fibroblasts induce expansion of regulatory T cells in pancreatic cancer. *Cancer Cell, 40*(6), 656-673 e657. doi:10.1016/j.ccell.2022.04.011

Huber, W., Carey, V. J., Gentleman, R., Anders, S., Carlson, M., Carvalho, B. S., . . . Morgan, M. (2015). Orchestrating high-throughput genomic analysis with Bioconductor. *Nat Methods, 12*(2), 115-121. doi:10.1038/nmeth.3252

Ibarrola-Villava, M., Cervantes, A., & Bardelli, A. (2018). Preclinical models for precision oncology. *Biochim Biophys Acta Rev Cancer, 1870*(2), 239-246. doi:10.1016/j.bbcan.2018.06.004

Iguchi, T., Yamashita, N., Aishima, S., Kuroda, Y., Terashi, T., Sugimachi, K., . . . Tsuneyoshi, M. (2009). A comprehensive analysis of immunohistochemical studies in intrahepatic cholangiocarcinoma using the survival tree model. *Oncology, 76*(4), 293-300. doi:10.1159/000207506

Invrea, F., Rovito, R., Torchiaro, E., Petti, C., Isella, C., & Medico, E. (2020). Patient-derived xenografts (PDXs) as model systems for human cancer. *Curr Opin Biotechnol, 63*, 151-156. doi:10.1016/j.copbio.2020.01.003

Ioka, T., Kanai, M., Kobayashi, S., Sakai, D., Eguchi, H., Baba, H., . . . Kansai Hepatobiliary Oncology, G. (2022). Randomized phase III study of Gemcitabine, Cisplatin plus S-1 (GCS) versus Gemcitabine, Cisplatin (GC) for Advanced Biliary Tract Cancer (KHBO1401-MITSUBA). *J Hepatobiliary Pancreat Sci*. doi:10.1002/jhbp.1219

Ishiguro, T., Ohata, H., Sato, A., Yamawaki, K., Enomoto, T., & Okamoto, K. (2017). Tumor-derived spheroids: Relevance to cancer stem cells and clinical applications. *Cancer Sci, 108*(3), 283-289. doi:10.1111/cas.13155

Ivanov, D. P., & Grabowska, A. M. (2017). Spheroid arrays for high-throughput single-cell analysis of spatial patterns and biomarker expression in 3D. *Scientific Reports*.

Ivascu, A., & Kubbies, M. (2006). Rapid generation of single-tumor spheroids for high-throughput cell function and toxicity analysis. *J Biomol Screen, 11*(8), 922-932. doi:10.1177/1087057106292763

Jabbour, E., & Kantarjian, H. (2012). Chronic myeloid leukemia: 2012 update on diagnosis, monitoring, and management. *Am J Hematol, 87*(11), 1037-1045. doi:10.1002/ajh.23282

Jaros, J., Petrov, M., Tesarova, M., & Hampl, A. (2017). Revealing 3D Ultrastructure and Morphology of Stem Cell Spheroids by Electron Microscopy. *Methods Mol Biol, 1612*, 417-431. doi:10.1007/978-1-4939-7021-6_30

Jiao, Y., Pawlik, T. M., Anders, R. A., Selaru, F. M., Streppel, M. M., Lucas, D. J., . . . Wood, L. D. (2013). Exome sequencing identifies frequent inactivating mutations in BAP1, ARID1A and PBRM1 in intrahepatic cholangiocarcinomas. *Nat Genet, 45*(12), 1470-1473. doi:10.1038/ng.2813

Jin, M. Z., & Jin, W. L. (2020). The updated landscape of tumor microenvironment and drug repurposing. *Signal Transduct Target Ther, 5*(1), 166. doi:10.1038/s41392-020-00280-x

Jogi, A., Vaapil, M., Johansson, M., & Pahlman, S. (2012). Cancer cell differentiation heterogeneity and aggressive behavior in solid tumors. *Ups J Med Sci, 117*(2), 217-224. doi:10.3109/03009734.2012.659294

Johnson, C., Huynh, V., Hargrove, L., Kennedy, L., Graf-Eaton, A., Owens, J., . . . Francis, H. (2016). Inhibition of Mast Cell-Derived Histamine Decreases Human Cholangiocarcinoma Growth and Differentiation via c-Kit/Stem Cell Factor-Dependent Signaling. *Am J Pathol, 186*(1), 123-133. doi:10.1016/j.ajpath.2015.09.016

Johnson, K. A., & Krishnan, A. (2022). Robust normalization and transformation techniques for constructing gene coexpression networks from RNA-seq data. *Genome Biol, 23*(1), 1. doi:10.1186/s13059-021-02568-9

Jones, H., Hargrove, L., Kennedy, L., Meng, F., Graf-Eaton, A., Owens, J., . . . Francis, H. (2016). Inhibition of mast cell-secreted histamine decreases biliary proliferation and fibrosis in primary sclerosing cholangitis Mdr2(-/-) mice. *Hepatology, 64*(4), 1202-1216. doi:10.1002/hep.28704

Jung, I. H., Kim, D. H., Yoo, D. K., Baek, S. Y., Jeong, S. H., Jung, D. E., . . . Chung, Y. Y. (2018). In Vivo Study of Natural Killer (NK) Cell Cytotoxicity Against Cholangiocarcinoma in a Nude Mouse Model. *In Vivo, 32*(4), 771-781. doi:10.21873/invivo.11307

Jung, J., Seol, H. S., & Chang, S. (2018). The Generation and Application of Patient-Derived Xenograft Model for Cancer Research. *Cancer Res Treat, 50*(1), 1-10. doi:10.4143/crt.2017.307

Jung, Y., McCall, S. J., Li, Y. X., & Diehl, A. M. (2007). Bile ductules and stromal cells express hedgehog ligands and/or hedgehog target genes in primary biliary cirrhosis. *Hepatology, 45*(5), 1091-1096. doi:10.1002/hep.21660

Kabashima, A., Hirsova, P., Bronk, S. F., Hernandez, M. C., Truty, M. J., Rizvi, S., . . . Gores, G. J. (2018). Fibroblast growth factor receptor inhibition induces loss of matrix MCL1 and necrosis in cholangiocarcinoma. *J Hepatol, 68*(6), 1228-1238. doi:10.1016/j.jhep.2018.01.026

Kapalczynska, M., Kolenda, T., Przybyla, W., Zajaczkowska, M., Teresiak, A., Filas, V., . . . Lamperska, K. (2018). 2D and 3D cell cultures - a comparison of different types of cancer cell cultures. *Arch Med Sci, 14*(4), 910-919. doi:10.5114/aoms.2016.63743

Kaplan, R. N., Riba, R. D., Zacharoulis, S., Bramley, A. H., Vincent, L., Costa, C., . . . Lyden, D. (2005). VEGFR1-positive haematopoietic bone marrow progenitors initiate the pre-metastatic niche. *Nature, 438*(7069), 820-827. doi:10.1038/nature04186

Karnoub, A. E., Dash, A. B., Vo, A. P., Sullivan, A., Brooks, M. W., Bell, G. W., . . . Weinberg, R. A. (2007). Mesenchymal stem cells within tumour stroma

promote breast cancer metastasis. *Nature, 449*(7162), 557-563. doi:10.1038/nature06188

Kaur, G., & Dufour, J. M. (2012). Cell lines: Valuable tools or useless artifacts. *Spermatogenesis, 2*(1), 1-5. doi:10.4161/spmg.19885

Kawamoto, M., Umebayashi, M., Tanaka, H., Koya, N., Nakagawa, S., Kawabe, K., . . . Morisaki, T. (2018). Combined Gemcitabine and Metronidazole Is a Promising Therapeutic Strategy for Cancer Stem-like Cholangiocarcinoma. *Anticancer Res, 38*(5), 2739-2748. doi:10.21873/anticanres.12516

Kelm, J. M., Timmins, N. E., Brown, C. J., Fussenegger, M., & Nielsen, L. K. (2003). Method for generation of homogeneous multicellular tumor spheroids applicable to a wide variety of cell types. *Biotechnol Bioeng, 83*(2), 173-180. doi:10.1002/bit.10655

Kennedy, L., Hargrove, L., Demieville, J., Karstens, W., Jones, H., DeMorrow, S., . . . Francis, H. (2018). Blocking H1/H2 histamine receptors inhibits damage/fibrosis in Mdr2(-/-) mice and human cholangiocarcinoma tumorigenesis. *Hepatology, 68*(3), 1042-1056. doi:10.1002/hep.29898

Khakoo, A. Y., Pati, S., Anderson, S. A., Reid, W., Elshal, M. F., Rovira, II, . . . Finkel, T. (2006). Human mesenchymal stem cells exert potent antitumorigenic effects in a model of Kaposi's sarcoma. *J Exp Med, 203*(5), 1235-1247. doi:10.1084/jem.20051921

Khalil, C., Moussa, M., Azar, A., Tawk, J., Habbouche, J., Salameh, R., . . . Alaaeddine, N. (2019). Anti-proliferative effects of mesenchymal stem cells (MSCs) derived from multiple sources on ovarian cancer cell lines: an in-vitro experimental study. *J Ovarian Res, 12*(1), 70. doi:10.1186/s13048-019-0546-9

Khan, A. S., & Dageforde, L. A. (2019). Cholangiocarcinoma. *Surg Clin North Am, 99*(2), 315-335. doi:10.1016/j.suc.2018.12.004

Khan, S. A., Genus, T., Morement, H., Murphy, A., Rous, B., & Tataru, D. (2019). Global trends in mortality from intrahepatic and extrahepatic cholangiocarcinoma. *J Hepatol, 71*(6), 1261-1262. doi:10.1016/j.jhep.2019.07.024

Khan, S. A., Tavolari, S., & Brandi, G. (2019). Cholangiocarcinoma: Epidemiology and risk factors. *Liver Int, 39 Suppl 1*, 19-31. doi:10.1111/liv.14095

Kim, J. A., Shim, J. S., Lee, G. Y., Yim, H. W., Kim, T. M., Kim, M., . . . Oh, I. H. (2015). Microenvironmental remodeling as a parameter and prognostic factor of heterogeneous leukemogenesis in acute myelogenous leukemia. *Cancer Res, 75*(11), 2222-2231. doi:10.1158/0008-5472.can-14-3379

Kim, M., Yun, H. W., Park, D. Y., Choi, B. H., & Min, B. H. (2018). Three-Dimensional Spheroid Culture Increases Exosome Secretion from Mesenchymal Stem Cells. *Tissue Eng Regen Med, 15*(4), 427-436. doi:10.1007/s13770-018-0139-5

Kim, S. W., Roh, J., & Park, C. S. (2016). Immunohistochemistry for Pathologists: Protocols, Pitfalls, and Tips. *J Pathol Transl Med, 50*(6), 411-418. doi:10.4132/jptm.2016.08.08

Kittirat, Y., Techasen, A., Thongchot, S., Loilome, W., Thanan, R., Yongvanit, P., . . . Namwat, N. (2018). Suppression of 14-3-3zeta in cholangiocarcinoma cells inhibits proliferation through attenuated Akt activity, enhancing chemosensitivity to gemcitabine. *Oncol Lett, 15*(1), 347-353. doi:10.3892/ol.2017.7326

Knight, E., & Przyborski, S. (2015). Advances in 3D cell culture technologies enabling tissue-like structures to be created in vitro. *J Anat, 227*(6), 746-756. doi:10.1111/joa.12257

Ko, S. F., Yip, H. K., Zhen, Y. Y., Lee, C. C., Lee, C. C., Huang, C. C., . . . Lin, J. W. (2015). Adipose-Derived Mesenchymal Stem Cell Exosomes Suppress Hepatocellular Carcinoma Growth in a Rat Model: Apparent Diffusion Coefficient, Natural Killer T-Cell Responses, and Histopathological Features. *Stem Cells Int, 2015*, 853506. doi:10.1155/2015/853506

Kopper, O., de Witte, C. J., Lohmussaar, K., Valle-Inclan, J. E., Hami, N., Kester, L., . . . Clevers, H. (2019). An organoid platform for ovarian cancer captures intra- and interpatient heterogeneity. *Nat Med, 25*(5), 838-849. doi:10.1038/s41591-019-0422-6

Korita, P. V., Wakai, T., Ajioka, Y., Inoue, M., Takamura, M., Shirai, Y., & Hatakeyama, K. (2010). Aberrant expression of vimentin correlates with dedifferentiation and poor prognosis in patients with intrahepatic cholangiocarcinoma. *Anticancer Res, 30*(6), 2279-2285.

Korner, M., Hayes, G. M., Rehmann, R., Zimmermann, A., Scholz, A., Wiedenmann, B., . . . Reubi, J. C. (2006). Secretin receptors in the human liver: expression in biliary tract and cholangiocarcinoma, but not in hepatocytes or hepatocellular carcinoma. *J Hepatol, 45*(6), 825-835. doi:10.1016/j.jhep.2006.06.016

Ku, J. L., Yoon, K. A., Kim, I. J., Kim, W. H., Jang, J. Y., Suh, K. S., . . . Park, J. G. (2002). Establishment and characterisation of six human biliary tract cancer cell lines. *Br J Cancer, 87*(2), 187-193. doi:10.1038/sj.bjc.6600440

Kukurba, K. R., & Montgomery, S. B. (2015). RNA Sequencing and Analysis. *Cold Spring Harb Protoc, 2015*(11), 951-969. doi:10.1101/pdb.top084970

Lamarca, A., Palmer, D. H., Wasan, H. S., Ross, P. J., Ma, Y. T., Arora, A., . . . Valle, J. W. (2021). Second-line FOLFOX chemotherapy versus active symptom control for advanced biliary tract cancer (ABC-06): a phase 3, open-label, randomised, controlled trial. *Lancet Oncol, 22*(5), 690-701. doi:10.1016/s1470-2045(21)00027-9

Lamberti, D., Cristinziano, G., Porru, M., Leonetti, C., Egan, J. B., Shi, C. X., . . . Segatto, O. (2019). HSP90 Inhibition Drives Degradation of FGFR2 Fusion Proteins: Implications for Treatment of Cholangiocarcinoma. *Hepatology, 69*(1), 131-142. doi:10.1002/hep.30127

Lamouille, S., Xu, J., & Derynck, R. (2014). Molecular mechanisms of epithelial-mesenchymal transition. *Nat Rev Mol Cell Biol, 15*(3), 178-196. doi:10.1038/nrm3758

Lancaster, M. A., & Knoblich, J. A. (2014). Organogenesis in a dish: modeling development and disease using organoid technologies. *Science, 345*(6194), 1247125. doi:10.1126/science.1247125

Lang, C. M. R., Chan, C. K., Veltri, A., & Lien, W. H. (2019). Wnt Signaling Pathways in Keratinocyte Carcinomas. *Cancers (Basel), 11*(9). doi:10.3390/cancers11091216

Langer, R., & Vacanti, J. P. (1993). Tissue engineering. *Science, 260*(5110), 920-926. doi:10.1126/science.8493529

Langley, R. R., & Fidler, I. J. (2011). The seed and soil hypothesis revisited--the role of tumor-stroma interactions in metastasis to different organs. *Int J Cancer, 128*(11), 2527-2535. doi:10.1002/ijc.26031

Laohaviroj, M., Chamgramol, Y., Pairojkul, C., Mulvenna, J., & Sripa, B. (2016). Clinicopathological Significance of Osteopontin in Cholangiocarcinoma

Cases. *Asian Pac J Cancer Prev, 17*(1), 201-205. doi:10.7314/apjcp.2016.17.1.201

Law, A. M. K., Rodriguez de la Fuente, L., Grundy, T. J., Fang, G., Valdes-Mora, F., & Gallego-Ortega, D. (2021). Advancements in 3D Cell Culture Systems for Personalizing Anti-Cancer Therapies. *Front Oncol, 11*, 782766. doi:10.3389/fonc.2021.782766

Law, C. W., Alhamdoosh, M., Su, S., Dong, X., Tian, L., Smyth, G. K., & Ritchie, M. E. (2016). RNA-seq analysis is easy as 1-2-3 with limma, Glimma and edgeR. *F1000Res, 5*. doi:10.12688/f1000research.9005.3

Lawrence, T. S., Beers, W. H., & Gilula, N. B. (1978). Transmission of hormonal stimulation by cell-to-cell communication. *Nature, 272*(5653), 501-506. doi:10.1038/272501a0

Lazzari, G., Nicolas, V., Matsusaki, M., Akashi, M., Couvreur, P., & Mura, S. (2018). Multicellular spheroid based on a triple co-culture: A novel 3D model to mimic pancreatic tumor complexity. *Acta Biomater, 78*, 296-307. doi:10.1016/j.actbio.2018.08.008

Levental, K. R., Yu, H., Kass, L., Lakins, J. N., Egeblad, M., Erler, J. T., . . . Weaver, V. M. (2009). Matrix crosslinking forces tumor progression by enhancing integrin signaling. *Cell, 139*(5), 891-906. doi:10.1016/j.cell.2009.10.027

Li, E., Lin, L., Chen, C. W., & Ou, D. L. (2019). Mouse Models for Immunotherapy in Hepatocellular Carcinoma. *Cancers (Basel), 11*(11). doi:10.3390/cancers11111800

Li, G. C., Ye, Q. H., Dong, Q. Z., Ren, N., Jia, H. L., & Qin, L. X. (2013). Mesenchymal stem cells seldomly fuse with hepatocellular carcinoma cells and are mainly distributed in the tumor stroma in mouse models. *Oncol Rep, 29*(2), 713-719. doi:10.3892/or.2012.2174

Li, L. T., Jiang, G., Chen, Q., & Zheng, J. N. (2015). Ki67 is a promising molecular target in the diagnosis of cancer (review). *Mol Med Rep, 11*(3), 1566-1572. doi:10.3892/mmr.2014.2914

Li, X., & Wang, C. Y. (2021). From bulk, single-cell to spatial RNA sequencing. *Int J Oral Sci, 13*(1), 36. doi:10.1038/s41368-021-00146-0

Li, Y., & Kumacheva, E. (2018). Hydrogel microenvironments for cancer spheroid growth and drug screening. *Sci Adv, 4*(4), eaas8998. doi:10.1126/sciadv.aas8998

Liberzon, A., Birger, C., Thorvaldsdottir, H., Ghandi, M., Mesirov, J. P., & Tamayo, P. (2015). The Molecular Signatures Database (MSigDB) hallmark gene set collection. *Cell Syst, 1*(6), 417-425. doi:10.1016/j.cels.2015.12.004

Lis, R., Touboul, C., Mirshahi, P., Ali, F., Mathew, S., Nolan, D. J., . . . Rafii, A. (2011). Tumor associated mesenchymal stem cells protects ovarian cancer cells from hyperthermia through CXCL12. *Int J Cancer, 128*(3), 715-725. doi:10.1002/ijc.25619

Liu, C., Kelnar, K., Liu, B., Chen, X., Calhoun-Davis, T., Li, H., . . . Tang, D. G. (2011). The microRNA miR-34a inhibits prostate cancer stem cells and metastasis by directly repressing CD44. *Nat Med, 17*(2), 211-215. doi:10.1038/nm.2284

Liu, C. Y., Lin, H. H., Tang, M. J., & Wang, Y. K. (2015). Vimentin contributes to epithelial-mesenchymal transition cancer cell mechanics by mediating cytoskeletal organization and focal adhesion maturation. *Oncotarget, 6*(18), 15966-15983. doi:10.18632/oncotarget.3862

Liu, J., Han, G., Liu, H., & Qin, C. (2013). Suppression of cholangiocarcinoma cell growth by human umbilical cord mesenchymal stem cells: a possible role of Wnt and Akt signaling. *PLoS One, 8*(4), e62844. doi:10.1371/journal.pone.0062844

Liu, L. Z., Yang, L. X., Zheng, B. H., Dong, P. P., Liu, X. Y., Wang, Z. C., . . . Gao, Q. (2018). CK7/CK19 index: A potential prognostic factor for postoperative intrahepatic cholangiocarcinoma patients. *J Surg Oncol, 117*(7), 1531-1539. doi:10.1002/jso.25027

Liu, S., Wang, Z., Zhu, R., Wang, F., Cheng, Y., & Liu, Y. (2021). Three Differential Expression Analysis Methods for RNA Sequencing: limma, EdgeR, DESeq2. *J Vis Exp*(175). doi:10.3791/62528

Ljujic, B., Milovanovic, M., Volarevic, V., Murray, B., Bugarski, D., Przyborski, S., . . . Stojkovic, M. (2013). Human mesenchymal stem cells creating an immunosuppressive environment and promote breast cancer in mice. *Sci Rep, 3*, 2298. doi:10.1038/srep02298

Ljung, B. M., Mayall, B., Lottich, C., Boyer, C., Sylvester, S. S., Leight, G. S., . . . Smith, H. S. (1989). Cell dissociation techniques in human breast cancer--variations in tumor cell viability and DNA ploidy. *Breast Cancer Res Treat, 13*(2), 153-159. doi:10.1007/BF01806527

Loeuillard, E., Fischbach, S. R., Gores, G. J., & Rizvi, S. (2019). Animal models of cholangiocarcinoma. *Biochim Biophys Acta Mol Basis Dis, 1865*(5), 982-992. doi:10.1016/j.bbadis.2018.03.026

Lorsakul, A. A., E.; Harring, V. S.; Sade, H.; Grimm, O.; Bredno J. (2017). Automated wholeslide analysis of multiplex-brightfield IHC images for cancer cells and carcinoma-associated fibroblasts. *Medical Imaging 2017: Digital Pathology, 10140*.

Love, M. I., Huber, W., & Anders, S. (2014). Moderated estimation of fold change and dispersion for RNA-seq data with DESeq2. *Genome Biol, 15*(12), 550. doi:10.1186/s13059-014-0550-8

Lu, H., & Stenzel, M. H. (2018). Multicellular Tumor Spheroids (MCTS) as a 3D In Vitro Evaluation Tool of Nanoparticles. *Small, 14*(13), e1702858. doi:10.1002/smll.201702858

Lu, L., Chen, G., Yang, J., Ma, Z., Yang, Y., Hu, Y., . . . Wang, X. (2019). Bone marrow mesenchymal stem cells suppress growth and promote the apoptosis of glioma U251 cells through downregulation of the PI3K/AKT signaling pathway. *Biomed Pharmacother, 112*, 108625. doi:10.1016/j.biopha.2019.108625

Luchini, C., Robertson, S. A., Hong, S. M., Felsenstein, M., Anders, R. A., Pea, A., . . . Wood, L. D. (2017). PBRM1 loss is a late event during the development of cholangiocarcinoma. *Histopathology, 71*(3), 375-382. doi:10.1111/his.13234

Ma, Y. S., Yang, X. L., Xin, R., Wu, T. M., Shi, Y., Dan Zhang, D., . . . Fu, D. (2021). The power and the promise of organoid models for cancer precision medicine with next-generation functional diagnostics and pharmaceutical exploitation. *Transl Oncol, 14*(8), 101126. doi:10.1016/j.tranon.2021.101126

Machado, M. V., & Diehl, A. M. (2018). Hedgehog signalling in liver pathophysiology. *J Hepatol, 68*(3), 550-562. doi:10.1016/j.jhep.2017.10.017

Maffey, A., Storini, C., Diceglie, C., Martelli, C., Sironi, L., Calzarossa, C., . . . Bianco, F. (2017). Mesenchymal stem cells from tumor microenvironment favour breast cancer stem cell proliferation, cancerogenic and metastatic potential, via

ionotropic purinergic signalling. *Sci Rep, 7*(1), 13162. doi:10.1038/s41598-017-13460-7

Maier, C. F., Zhu, L., Nanduri, L. K., Kuhn, D., Kochall, S., Thepkaysone, M. L., . . . Scholch, S. (2021). Patient-Derived Organoids of Cholangiocarcinoma. *Int J Mol Sci, 22*(16). doi:10.3390/ijms22168675

Mancarella, S., Serino, G., Dituri, F., Cigliano, A., Ribback, S., Wang, J., . . . Giannelli, G. (2020). Crenigacestat, a selective NOTCH1 inhibitor, reduces intrahepatic cholangiocarcinoma progression by blocking VEGFA/DLL4/MMP13 axis. *Cell Death Differ, 27*(8), 2330-2343. doi:10.1038/s41418-020-0505-4

Mancarella, S., Serino, G., Gigante, I., Cigliano, A., Ribback, S., Sanese, P., . . . Giannelli, G. (2022). CD90 is regulated by notch1 and hallmarks a more aggressive intrahepatic cholangiocarcinoma phenotype. *J Exp Clin Cancer Res, 41*(1), 65. doi:10.1186/s13046-022-02283-8

Mao, Z. Y., Guo, X. C., Su, D., Wang, L. J., Zhang, T. T., & Bai, L. (2015). Prognostic Factors of Cholangiocarcinoma After Surgical Resection: A Retrospective Study of 293 Patients. *Med Sci Monit, 21*, 2375-2381. doi:10.12659/MSM.893586

Martinez Lyons, A., & Boulter, L. (2021). The developmental origins of Notch-driven intrahepatic bile duct disorders. *Dis Model Mech, 14*(9). doi:10.1242/dmm.048413

Massa, A., Varamo, C., Vita, F., Tavolari, S., Peraldo-Neia, C., Brandi, G., . . . Aglietta, M. (2020). Evolution of the Experimental Models of Cholangiocarcinoma. *Cancers (Basel), 12*(8). doi:10.3390/cancers12082308

Massani, M., Stecca, T., Fabris, L., Caratozzolo, E., Ruffolo, C., Furlanetto, A., . . . Bassi, N. (2013). Isolation and characterization of biliary epithelial and stromal cells from resected human cholangiocarcinoma: a novel in vitro model to study tumor-stroma interactions. *Oncol Rep, 30*(3), 1143-1148. doi:10.3892/or.2013.2568

McMahon, K. M., Volpato, M., Chi, H. Y., Musiwaro, P., Poterlowicz, K., Peng, Y., . . . Sutton, C. W. (2012). Characterization of changes in the proteome in different regions of 3D multicell tumor spheroids. *J Proteome Res, 11*(5), 2863-2875. doi:10.1021/pr2012472

McNamara, M. G., Bridgewater, J., Palmer, D. H., Faluyi, O., Wasan, H., Patel, A., . . . Valle, J. W. (2021). A Phase Ib Study of NUC-1031 in Combination with Cisplatin for the First-Line Treatment of Patients with Advanced Biliary Tract Cancer (ABC-08). *Oncologist, 26*(4), e669-e678. doi:10.1002/onco.13598

Melzer, C., von der Ohe, J., & Hass, R. (2018). Concise Review: Crosstalk of Mesenchymal Stroma/Stem-Like Cells with Cancer Cells Provides Therapeutic Potential. *Stem Cells, 36*(7), 951-968. doi:10.1002/stem.2829

Melzer, C., von der Ohe, J., & Hass, R. (2019). In Vivo Cell Fusion between Mesenchymal Stroma/Stem-Like Cells and Breast Cancer Cells. *Cancers (Basel), 11*(2). doi:10.3390/cancers11020185

Merino-Azpitarte, M., Lozano, E., Perugorria, M. J., Esparza-Baquer, A., Erice, O., Santos-Laso, A., . . . Banales, J. M. (2017). SOX17 regulates cholangiocyte differentiation and acts as a tumor suppressor in cholangiocarcinoma. *J Hepatol, 67*(1), 72-83. doi:10.1016/j.jhep.2017.02.017

Mertens, J. C., Fingas, C. D., Christensen, J. D., Smoot, R. L., Bronk, S. F., Werneburg, N. W., . . . Gores, G. J. (2013). Therapeutic effects of deleting cancer-associated fibroblasts in cholangiocarcinoma. *Cancer Res, 73*(2), 897-907. doi:10.1158/0008-5472.CAN-12-2130

Mischiati, C., Ura, B., Roncoroni, L., Elli, L., Cervellati, C., Squerzanti, M., . . . Agostinelli, E. (2015). Changes in protein expression in two cholangiocarcinoma cell lines undergoing formation of multicellular tumor spheroids in vitro. *PLoS One, 10*(3), e0118906. doi:10.1371/journal.pone.0118906

Montel, F., Delarue, M., Elgeti, J., Malaquin, L., Basan, M., Risler, T., . . . Joanny, J. F. (2011). Stress clamp experiments on multicellular tumor spheroids. *Phys Rev Lett, 107*(18), 188102. doi:10.1103/PhysRevLett.107.188102

Montel, F. D., M.; Elgeti, J.; Vignjevic, D.; Cappello, G.; Prost, J. (2019). Isotropic stress reduces cell proliferation in tumor spheroids. *New Journal of Physics, 14*.

Morales, J., & Alpaugh, M. L. (2009). Gain in cellular organization of inflammatory breast cancer: A 3D in vitro model that mimics the in vivo metastasis. *BMC Cancer*.

Morisaki, T., Umebayashi, M., Kiyota, A., Koya, N., Tanaka, H., Onishi, H., & Katano, M. (2012). Combining cetuximab with killer lymphocytes synergistically inhibits human cholangiocarcinoma cells in vitro. *Anticancer Res, 32*(6), 2249-2256.

Morton, J. J., Bird, G., Refaeli, Y., & Jimeno, A. (2016). Humanized Mouse Xenograft Models: Narrowing the Tumor-Microenvironment Gap. *Cancer Res, 76*(21), 6153-6158. doi:10.1158/0008-5472.CAN-16-1260

Moscona, A. (1961). Rotation-mediated histogenetic aggregation of dissociated cells. A quantifiable approach to cell interactions in vitro. *Exp Cell Res, 22*, 455-475. doi:10.1016/0014-4827(61)90122-7

Murphy-Ullrich, J. E. (2001). The de-adhesive activity of matricellular proteins: is intermediate cell adhesion an adaptive state? *J Clin Invest, 107*(7), 785-790. doi:10.1172/jci12609

Mwesige, B., Lee, M. R., Lee, Y. S., Han, N. Y., Im, J. E., Kim, J. K., . . . Kim, Y. H. (2022). Establishment of Patient-derived Preclinical Models for Invasive Papillary Cholangiocarcinoma. *Anticancer Res, 42*(1), 599-608. doi:10.21873/anticanres.15517

Nagaraju, G. P., & Sharma, D. (2011). Anti-cancer role of SPARC, an inhibitor of adipogenesis. *Cancer Treat Rev, 37*(7), 559-566. doi:10.1016/j.ctrv.2010.12.001

Nakagawa, H., Suzuki, N., Hirata, Y., Hikiba, Y., Hayakawa, Y., Kinoshita, H., . . . Koike, K. (2017). Biliary epithelial injury-induced regenerative response by IL-33 promotes cholangiocarcinogenesis from peribiliary glands. *Proc Natl Acad Sci U S A, 114*(19), E3806-E3815. doi:10.1073/pnas.1619416114

Nakamura, H., Arai, Y., Totoki, Y., Shirota, T., Elzawahry, A., Kato, M., . . . Shibata, T. (2015). Genomic spectra of biliary tract cancer. *Nat Genet, 47*(9), 1003-1010. doi:10.1038/ng.3375

Nakanuma, Y., Sato, Y., Harada, K., Sasaki, M., Xu, J., & Ikeda, H. (2010). Pathological classification of intrahepatic cholangiocarcinoma based on a new concept. *World J Hepatol, 2*(12), 419-427. doi:10.4254/wjh.v2.i12.419

Nakayama, G. R., Caton, M. C., Nova, M. P., & Parandoosh, Z. (1997). Assessment of the Alamar Blue assay for cellular growth and viability in vitro. *J Immunol Methods, 204*(2), 205-208. doi:10.1016/s0022-1759(97)00043-4

Nallanthighal, S., Heiserman, J. P., & Cheon, D. J. (2019). The Role of the Extracellular Matrix in Cancer Stemness. *Front Cell Dev Biol, 7*, 86. doi:10.3389/fcell.2019.00086

Nath, S., & Devi, G. R. (2016). Three-dimensional culture systems in cancer research: Focus on tumor spheroid model. *Pharmacol Ther, 163*, 94-108. doi:10.1016/j.pharmthera.2016.03.013

Nelson, J. W., Sklenar, J., Barnes, A. P., & Minnier, J. (2017). The START App: a web-based RNAseq analysis and visualization resource. *Bioinformatics, 33*(3), 447-449. doi:10.1093/bioinformatics/btw624

Nepal, C., O'Rourke, C. J., Oliveira, D., Taranta, A., Shema, S., Gautam, P., . . . Andersen, J. B. (2018). Genomic perturbations reveal distinct regulatory networks in intrahepatic cholangiocarcinoma. *Hepatology, 68*(3), 949-963. doi:10.1002/hep.29764

Ng, M. R., & Brugge, J. S. (2009). A stiff blow from the stroma: collagen crosslinking drives tumor progression. *Cancer Cell, 16*(6), 455-457. doi:10.1016/j.ccr.2009.11.013

Nguyen Ho-Bouldoires, T. H., Claperon, A., Mergey, M., Wendum, D., Desbois-Mouthon, C., Tahraoui, S., . . . Fouassier, L. (2015). Mitogen-activated protein kinase-activated protein kinase 2 mediates resistance to hydrogen peroxide-induced oxidative stress in human hepatobiliary cancer cells. *Free Radic Biol Med, 89*, 34-46. doi:10.1016/j.freeradbiomed.2015.07.011

Nissen, N. I., Karsdal, M., & Willumsen, N. (2019). Collagens and Cancer associated fibroblasts in the reactive stroma and its relation to Cancer biology. *J Exp Clin Cancer Res, 38*(1), 115. doi:10.1186/s13046-019-1110-6

Nociari, M. M., Shalev, A., Benias, P., & Russo, C. (1998). A novel one-step, highly sensitive fluorometric assay to evaluate cell-mediated cytotoxicity. *J Immunol Methods, 213*(2), 157-167. doi:10.1016/s0022-1759(98)00028-3

Nowell, P. C. (1976). The clonal evolution of tumor cell populations. *Science, 194*(4260), 23-28. doi:10.1126/science.959840

Nuciforo, S., Fofana, I., Matter, M. S., Blumer, T., Calabrese, D., Boldanova, T., . . . Heim, M. H. (2018). Organoid Models of Human Liver Cancers Derived from Tumor Needle Biopsies. *Cell Rep, 24*(5), 1363-1376. doi:10.1016/j.celrep.2018.07.001

Nunes, A. S., Barros, A. S., Costa, E. C., Moreira, A. F., & Correia, I. J. (2019). 3D tumor spheroids as in vitro models to mimic in vivo human solid tumors resistance to therapeutic drugs. *Biotechnol Bioeng, 116*(1), 206-226. doi:10.1002/bit.26845

O'Brien, J., Wilson, I., Orton, T., & Pognan, F. (2000). Investigation of the Alamar Blue (resazurin) fluorescent dye for the assessment of mammalian cell cytotoxicity. *Eur J Biochem, 267*(17), 5421-5426. doi:10.1046/j.1432-1327.2000.01606.x

Obchoei, S., Weakley, S. M., Wongkham, S., Wongkham, C., Sawanyawisuth, K., Yao, Q., & Chen, C. (2011). Cyclophilin A enhances cell proliferation and tumor growth of liver fluke-associated cholangiocarcinoma. *Mol Cancer, 10*, 102. doi:10.1186/1476-4598-10-102

Oh, D. Y., Lee, K. H., Lee, D. W., Yoon, J., Kim, T. Y., Bang, J. H., . . . Kim, J. W. (2022). Gemcitabine and cisplatin plus durvalumab with or without tremelimumab in chemotherapy-naive patients with advanced biliary tract cancer: an open-label, single-centre, phase 2 study. *Lancet Gastroenterol Hepatol, 7*(6), 522-532. doi:10.1016/S2468-1253(22)00043-7

Oh, I. R., Raymundo, B., Kim, M., & Kim, C. W. (2020). Mesenchymal stem cells co-cultured with colorectal cancer cells showed increased invasive and

proliferative abilities due to its altered p53/TGF-β1 levels. *Biosci Biotechnol Biochem, 84*(2), 256-267. doi:10.1080/09168451.2019.1676692

Ohgushi, M., Matsumura, M., Eiraku, M., Murakami, K., Aramaki, T., Nishiyama, A., . . . Sasai, Y. (2010). Molecular pathway and cell state responsible for dissociation-induced apoptosis in human pluripotent stem cells. *Cell Stem Cell, 7*(2), 225-239. doi:10.1016/j.stem.2010.06.018

Okabe, H., Beppu, T., Hayashi, H., Horino, K., Masuda, T., Komori, H., . . . Baba, H. (2009). Hepatic stellate cells may relate to progression of intrahepatic cholangiocarcinoma. *Ann Surg Oncol, 16*(9), 2555-2564. doi:10.1245/s10434-009-0568-4

Okusaka, T., Nakachi, K., Fukutomi, A., Mizuno, N., Ohkawa, S., Funakoshi, A., . . . Nimura, Y. (2010). Gemcitabine alone or in combination with cisplatin in patients with biliary tract cancer: a comparative multicentre study in Japan. *Br J Cancer, 103*(4), 469-474. doi:10.1038/sj.bjc.6605779

Onion, D., Argent, R. H., Reece-Smith, A. M., Craze, M. L., Pineda, R. G., Clarke, P. A., . . . Grabowska, A. M. (2016). 3-Dimensional Patient-Derived Lung Cancer Assays Reveal Resistance to Standards-of-Care Promoted by Stromal Cells but Sensitivity to Histone Deacetylase Inhibitors. *Mol Cancer Ther, 15*(4), 753-763. doi:10.1158/1535-7163.MCT-15-0598

Ott, P. A., Bang, Y. J., Piha-Paul, S. A., Razak, A. R. A., Bennouna, J., Soria, J. C., . . . Lunceford, J. K. (2019). T-Cell-Inflamed Gene-Expression Profile, Programmed Death Ligand 1 Expression, and Tumor Mutational Burden Predict Efficacy in Patients Treated With Pembrolizumab Across 20 Cancers: KEYNOTE-028. *J Clin Oncol, 37*(4), 318-327. doi:10.1200/JCO.2018.78.2276

Paget, S. (1989). The distribution of secondary growths in cancer of the breast. 1889. *Cancer Metastasis Rev, 8*(2), 98-101.

Pal, A., Ashworth, J. C., Collier, P., Probert, C., Jones, S., Leza, E. P., . . . Grabowska, A. M. (2020). A 3D Heterotypic Breast Cancer Model Demonstrates a Role for Mesenchymal Stem Cells in Driving a Proliferative and Invasive Phenotype. *Cancers (Basel), 12*(8). doi:10.3390/cancers12082290

Pearson, A. T., Finkel, K. A., Warner, K. A., Nör, F., Tice, D., Martins, M. D., . . . Nör, J. E. (2016). Patient-derived xenograft (PDX) tumors increase growth rate with time. *Oncotarget, 7*(7), 7993-8005. doi:10.18632/oncotarget.6919

Pellat, A., Vaquero, J., & Fouassier, L. (2018). Role of ErbB/HER family of receptor tyrosine kinases in cholangiocyte biology. *Hepatology, 67*(2), 762-773. doi:10.1002/hep.29350

Peraldo Neia, C., Cavalloni, G., Chiorino, G., Ostano, P., Aglietta, M., & Leone, F. (2016). Gene and microRNA modulation upon trabectedin treatment in a human intrahepatic cholangiocarcinoma paired patient derived xenograft and cell line. *Oncotarget, 7*(52), 86766-86780. doi:10.18632/oncotarget.13575

Peraldo-Neia, C., Cavalloni, G., Soster, M., Gammaitoni, L., Marchio, S., Sassi, F., . . . Leone, F. (2014). Anti-cancer effect and gene modulation of ET-743 in human biliary tract carcinoma preclinical models. *BMC Cancer, 14*, 918. doi:10.1186/1471-2407-14-918

Petersen, O. W., Ronnov-Jessen, L., Howlett, A. R., & Bissell, M. J. (1992). Interaction with basement membrane serves to rapidly distinguish growth and differentiation pattern of normal and malignant human breast epithelial cells. *Proc Natl Acad Sci U S A, 89*(19), 9064-9068. doi:10.1073/pnas.89.19.9064

Philips, T., Kusmartseva, I., Gerling, I. C., Campbell-Thompson, M., Wasserfall, C., Pugliese, A., . . . Kaddis, J. S. (2017). Factors That Influence the Quality of RNA From the Pancreas of Organ Donors. *Pancreas, 46*(2), 252-259. doi:10.1097/mpa.0000000000000717

Piersma, B., Hayward, M. K., & Weaver, V. M. (2020). Fibrosis and cancer: A strained relationship. *Biochim Biophys Acta Rev Cancer, 1873*(2), 188356. doi:10.1016/j.bbcan.2020.188356

Piha-Paul, S. A., Oh, D. Y., Ueno, M., Malka, D., Chung, H. C., Nagrial, A., . . . Doi, T. (2020). Efficacy and safety of pembrolizumab for the treatment of advanced biliary cancer: Results from the KEYNOTE-158 and KEYNOTE-028 studies. *Int J Cancer, 147*(8), 2190-2198. doi:10.1002/ijc.33013

Pilarski, R., Cebulla, C. M., Massengill, J. B., Rai, K., Rich, T., Strong, L., . . . Abdel-Rahman, M. H. (2014). Expanding the clinical phenotype of hereditary BAP1 cancer predisposition syndrome, reporting three new cases. *Genes Chromosomes Cancer, 53*(2), 177-182. doi:10.1002/gcc.22129

Pinto, B., Henriques, A. C., Silva, P. M. A., & Bousbaa, H. (2020). Three-Dimensional Spheroids as In Vitro Preclinical Models for Cancer Research. *Pharmaceutics, 12*(12). doi:10.3390/pharmaceutics12121186

Pittenger, M. F., Discher, D. E., Peault, B. M., Phinney, D. G., Hare, J. M., & Caplan, A. I. (2019). Mesenchymal stem cell perspective: cell biology to clinical progress. *NPJ Regen Med, 4*, 22. doi:10.1038/s41536-019-0083-6

Pompili, L., Porru, M., Caruso, C., Biroccio, A., & Leonetti, C. (2016). Patient-derived xenografts: a relevant preclinical model for drug development. *J Exp Clin Cancer Res, 35*(1), 189. doi:10.1186/s13046-016-0462-4

Pompura, S. L., & Dominguez-Villar, M. (2018). The PI3K/AKT signaling pathway in regulatory T-cell development, stability, and function. *J Leukoc Biol*. doi:10.1002/JLB.2MIR0817-349R

Primrose, J. N., Fox, R. P., Palmer, D. H., Malik, H. Z., Prasad, R., Mirza, D., . . . group, B. s. (2019). Capecitabine compared with observation in resected biliary tract cancer (BILCAP): a randomised, controlled, multicentre, phase 3 study. *Lancet Oncol, 20*(5), 663-673. doi:10.1016/S1470-2045(18)30915-X

Prior, N., Inacio, P., & Huch, M. (2019). Liver organoids: from basic research to therapeutic applications. *Gut, 68*(12), 2228-2237. doi:10.1136/gutjnl-2019-319256

Pungpak, S., Viravan, C., Radomyos, B., Chalermrut, K., Yemput, C., Plooksawasdi, W., . . . Bunnag, D. (1997). Opisthorchis viverrini infection in Thailand: studies on the morbidity of the infection and resolution following praziquantel treatment. *Am J Trop Med Hyg, 56*(3), 311-314. doi:10.4269/ajtmh.1997.56.311

Qian, M., Yan, F., Wang, W., Du, J., Yuan, T., Wu, R., . . . He, Q. (2021). Deubiquitinase JOSD2 stabilizes YAP/TAZ to promote cholangiocarcinoma progression. *Acta Pharm Sin B, 11*(12), 4008-4019. doi:10.1016/j.apsb.2021.04.003

Qiang, Z., Zhang, W., Jin, S., Dai, K., He, Y., Tao, L., & Yu, H. (2021). Carcinoembryonic antigen, α-fetoprotein, and Ki67 as biomarkers and prognostic factors in intrahepatic cholangiocarcinoma: A retrospective cohort study. *Ann Hepatol, 20*, 100242. doi:10.1016/j.aohep.2020.07.010

Qiao, L., Zhao, T. J., Wang, F. Z., Shan, C. L., Ye, L. H., & Zhang, X. D. (2008). NF-kappaB downregulation may be involved the depression of tumor cell

proliferation mediated by human mesenchymal stem cells. *Acta Pharmacol Sin, 29*(3), 333-340. doi:10.1111/j.1745-7254.2008.00751.x

Quante, M., Tu, S. P., Tomita, H., Gonda, T., Wang, S. S., Takashi, S., . . . Wang, T. C. (2011). Bone marrow-derived myofibroblasts contribute to the mesenchymal stem cell niche and promote tumor growth. *Cancer Cell, 19*(2), 257-272. doi:10.1016/j.ccr.2011.01.020

Quent, V. M., Loessner, D., Friis, T., Reichert, J. C., & Hutmacher, D. W. (2010). Discrepancies between metabolic activity and DNA content as tool to assess cell proliferation in cancer research. *J Cell Mol Med, 14*(4), 1003-1013. doi:10.1111/j.1582-4934.2010.01013.x

Raggi, C., Correnti, M., Sica, A., Andersen, J. B., Cardinale, V., Alvaro, D., . . . Invernizzi, P. (2017). Cholangiocarcinoma stem-like subset shapes tumor-initiating niche by educating associated macrophages. *J Hepatol, 66*(1), 102-115. doi:10.1016/j.jhep.2016.08.012

Raggi, C., Invernizzi, P., & Andersen, J. B. (2015). Impact of microenvironment and stem-like plasticity in cholangiocarcinoma: molecular networks and biological concepts. *J Hepatol, 62*(1), 198-207. doi:10.1016/j.jhep.2014.09.007

Ramasamy, T. S., Yu, J. S., Selden, C., Hodgson, H., & Cui, W. (2013). Application of three-dimensional culture conditions to human embryonic stem cell-derived definitive endoderm cells enhances hepatocyte differentiation and functionality. *Tissue Eng Part A, 19*(3-4), 360-367. doi:10.1089/ten.tea.2012.0190

Rambhatla, L., Chiu, C. P., Glickman, R. D., & Rowe-Rendleman, C. (2002). In vitro differentiation capacity of telomerase immortalized human RPE cells. *Invest Ophthalmol Vis Sci, 43*(5), 1622-1630.

Rampersad, S. N. (2012). Multiple applications of Alamar Blue as an indicator of metabolic function and cellular health in cell viability bioassays. *Sensors (Basel), 12*(9), 12347-12360. doi:10.3390/s120912347

Razumilava, N., Gradilone, S. A., Smoot, R. L., Mertens, J. C., Bronk, S. F., Sirica, A. E., & Gores, G. J. (2014). Non-canonical Hedgehog signaling contributes to chemotaxis in cholangiocarcinoma. *J Hepatol, 60*(3), 599-605. doi:10.1016/j.jhep.2013.11.005

rdrr.io. (2020). removeBatchEffect: Remove Batch Effect. Retrieved from https://rdrr.io/bioc/limma/man/removeBatchEffect.html

Rea, D. J., Munoz-Juarez, M., Farnell, M. B., Donohue, J. H., Que, F. G., Crownhart, B., . . . Nagorney, D. M. (2004). Major hepatic resection for hilar cholangiocarcinoma: analysis of 46 patients. *Arch Surg, 139*(5), 514-523; discussion 523-515. doi:10.1001/archsurg.139.5.514

Reich, M., Deutschmann, K., Sommerfeld, A., Klindt, C., Kluge, S., Kubitz, R., . . . Keitel, V. (2016). TGR5 is essential for bile acid-dependent cholangiocyte proliferation in vivo and in vitro. *Gut, 65*(3), 487-501. doi:10.1136/gutjnl-2015-309458

Reimand, J., Isserlin, R., Voisin, V., Kucera, M., Tannus-Lopes, C., Rostamianfar, A., . . . Bader, G. D. (2019). Pathway enrichment analysis and visualization of omics data using g:Profiler, GSEA, Cytoscape and EnrichmentMap. *Nat Protoc, 14*(2), 482-517. doi:10.1038/s41596-018-0103-9

Reynolds, D. S., Tevis, K. M., Blessing, W. A., Colson, Y. L., Zaman, M. H., & Grinstaff, M. W. (2017). Breast Cancer Spheroids Reveal a Differential Cancer Stem Cell Response to Chemotherapeutic Treatment. *Sci Rep, 7*(1), 10382. doi:10.1038/s41598-017-10863-4

RG., H. (1906). Observations on the living developing nerve fiber. *Proceedings of the Society for Experimental Biology and Medicine, 4*(1). doi:10.3181/00379727-4-98

Richmond, A., & Su, Y. (2008). Mouse xenograft models vs GEM models for human cancer therapeutics. *Dis Model Mech, 1*(2-3), 78-82. doi:10.1242/dmm.000976

Ridge, S. M., Sullivan, F. J., & Glynn, S. A. (2017). Mesenchymal stem cells: key players in cancer progression. *Mol Cancer, 16*(1), 31. doi:10.1186/s12943-017-0597-8

Riffle, S., Pandey, R. N., Albert, M., & Hegde, R. S. (2017). Linking hypoxia, DNA damage and proliferation in multicellular tumor spheroids. *BMC Cancer, 17*(1), 338. doi:10.1186/s12885-017-3319-0

Ritchie, M. E., Phipson, B., Wu, D., Hu, Y., Law, C. W., Shi, W., & Smyth, G. K. (2015). limma powers differential expression analyses for RNA-sequencing and microarray studies. *Nucleic Acids Res, 43*(7), e47. doi:10.1093/nar/gkv007

Rizvi, S., & Borad, M. J. (2016). The rise of the FGFR inhibitor in advanced biliary cancer: the next cover of time magazine? *J Gastrointest Oncol, 7*(5), 789-796. doi:10.21037/jgo.2016.08.12

Rizzo, A., Ricci, A. D., & Brandi, G. (2021). Pemigatinib: Hot topics behind the first approval of a targeted therapy in cholangiocarcinoma. *Cancer Treat Res Commun, 27*, 100337. doi:10.1016/j.ctarc.2021.100337

Russo, F. P., Alison, M. R., Bigger, B. W., Amofah, E., Florou, A., Amin, F., . . . Forbes, S. J. (2006). The bone marrow functionally contributes to liver fibrosis. *Gastroenterology, 130*(6), 1807-1821. doi:10.1053/j.gastro.2006.01.036

Saborowski, A., Saborowski, M., Davare, M. A., Druker, B. J., Klimstra, D. S., & Lowe, S. W. (2013). Mouse model of intrahepatic cholangiocarcinoma validates FIG-ROS as a potent fusion oncogene and therapeutic target. *Proc Natl Acad Sci U S A, 110*(48), 19513-19518. doi:10.1073/pnas.1311707110

Saentaweesuk, W., Araki, N., Vaeteewoottacharn, K., Silsirivanit, A., Seubwai, W., Talabnin, C., . . . Wongkham, C. (2018). Activation of Vimentin Is Critical to Promote a Metastatic Potential of Cholangiocarcinoma Cells. *Oncol Res, 26*(4), 605-616. doi:10.3727/096504017x15009778205068

Saha, S. K., Gordan, J. D., Kleinstiver, B. P., Vu, P., Najem, M. S., Yeo, J. C., . . . Bardeesy, N. (2016). Isocitrate Dehydrogenase Mutations Confer Dasatinib Hypersensitivity and SRC Dependence in Intrahepatic Cholangiocarcinoma. *Cancer Discov, 6*(7), 727-739. doi:10.1158/2159-8290.CD-15-1442

Saijyo, S., Kudo, T., Suzuki, M., Katayose, Y., Shinoda, M., Muto, T., . . . Matsuno, S. (1995). Establishment of a new extrahepatic bile duct carcinoma cell line, TFK-1. *Tohoku J Exp Med, 177*(1), 61-71. doi:10.1620/tjem.177.61

Salati, M., Caputo, F., Baldessari, C., Galassi, B., Grossi, F., Dominici, M., & Ghidini, M. (2020). IDH Signalling Pathway in Cholangiocarcinoma: From Biological Rationale to Therapeutic Targeting. *Cancers (Basel), 12*(11). doi:10.3390/cancers12113310

Santini, M. T., & Rainaldi, G. (1999). Three-dimensional spheroid model in tumor biology. *Pathobiology, 67*(3), 148-157. doi:10.1159/000028065

Sasai, N., Toriyama, M., & Kondo, T. (2019). Hedgehog Signal and Genetic Disorders. *Front Genet, 10*, 1103. doi:10.3389/fgene.2019.01103

Satelli, A., & Li, S. (2011). Vimentin in cancer and its potential as a molecular target for cancer therapy. *Cell Mol Life Sci, 68*(18), 3033-3046. doi:10.1007/s00018-011-0735-1

Sato, K., Zhang, W., Safarikia, S., Isidan, A., Chen, A. M., Li, P., . . . Alpini, G. (2021). Organoids and Spheroids as Models for Studying Cholestatic Liver Injury and Cholangiocarcinoma. *Hepatology, 74*(1), 491-502. doi:10.1002/hep.31653

Saunders, J. H., Onion, D., Collier, P., Dorrington, M. S., Argent, R. H., Clarke, P. A., . . . Grabowska, A. M. (2017). Individual patient oesophageal cancer 3D models for tailored treatment. *Oncotarget, 8*(15), 24224-24236. doi:10.18632/oncotarget.12500

Sawanyawisuth, K., Sashida, G., & Sheng, G. (2021). Epithelial-Mesenchymal Transition in Liver Fluke-Induced Cholangiocarcinoma. *Cancers (Basel), 13*(4). doi:10.3390/cancers13040791

Scherzad, A., Steber, M., Gehrke, T., Rak, K., Froelich, K., Schendzielorz, P., . . . Hackenberg, S. (2015). Human mesenchymal stem cells enhance cancer cell proliferation via IL-6 secretion and activation of ERK1/2. *Int J Oncol, 47*(1), 391-397. doi:10.3892/ijo.2015.3009

Scherzed, A., Hackenberg, S., Froelich, K., Kessler, M., Koehler, C., Hagen, R., . . . Kleinsasser, N. (2011). BMSC enhance the survival of paclitaxel treated squamous cell carcinoma cells in vitro. *Cancer Biol Ther, 11*(3), 349-357. doi:10.4161/cbt.11.3.14179

Schiffman, S. C., Nowacki, M. R., Spencer, L., McMasters, K. M., Scoggins, C. R., & Martin, R. C. (2014). Molecular factors associated with recurrence and survival following hepatectomy in patients with intrahepatic cholangiocarcinoma: a guide to adjuvant clinical trials. *J Surg Oncol, 109*(2), 98-103. doi:10.1002/jso.23459

Schmidt, A., Ladage, D., Schinkothe, T., Klausmann, U., Ulrichs, C., Klinz, F. J., . . . Bloch, W. (2006). Basic fibroblast growth factor controls migration in human mesenchymal stem cells. *Stem Cells, 24*(7), 1750-1758. doi:10.1634/stemcells.2005-0191

Seehawer, M., Heinzmann, F., D'Artista, L., Harbig, J., Roux, P. F., Hoenicke, L., . . . Zender, L. (2018). Necroptosis microenvironment directs lineage commitment in liver cancer. *Nature, 562*(7725), 69-75. doi:10.1038/s41586-018-0519-y

Sergushichev, A. (2016). An algorithm for fast preranked gene set enrichment analysis using cumulative statistic calculation. *bioRxiv*.

Serhal, R., Saliba, N., Hilal, G., Moussa, M., Hassan, G. S., El Atat, O., & Alaaeddine, N. (2019). Effect of adipose-derived mesenchymal stem cells on hepatocellular carcinoma: In vitro inhibition of carcinogenesis. *World J Gastroenterol, 25*(5), 567-583. doi:10.3748/wjg.v25.i5.567

Shah, A. A., Kulkarni, D., Ingale, Y., Koshy, A. V., Bhagalia, S., & Bomble, N. (2017). Kerosene: Contributing agent to xylene as a clearing agent in tissue processing. *J Oral Maxillofac Pathol, 21*(3), 367-374. doi:10.4103/jomfp.JOMFP_14_15

Shah, K., & Kazi, J. U. (2022). Phosphorylation-Dependent Regulation of WNT/Beta-Catenin Signaling. *Front Oncol, 12*, 858782. doi:10.3389/fonc.2022.858782

Shroff, R. T., Javle, M. M., Xiao, L., Kaseb, A. O., Varadhachary, G. R., Wolff, R. A., . . . Borad, M. J. (2019). Gemcitabine, Cisplatin, and nab-Paclitaxel for the Treatment of Advanced Biliary Tract Cancers: A Phase 2 Clinical Trial. *JAMA Oncol, 5*(6), 824-830. doi:10.1001/jamaoncol.2019.0270

Shroff, R. T., Kennedy, E. B., Bachini, M., Bekaii-Saab, T., Crane, C., Edeline, J., . . . Maithel, S. K. (2019). Adjuvant Therapy for Resected Biliary Tract Cancer: ASCO Clinical Practice Guideline. *J Clin Oncol, 37*(12), 1015-1027. doi:10.1200/JCO.18.02178

Shu, Y., Xu, Q., Xu, Y., Tao, Q., Shao, M., Cao, X., . . . Bu, H. (2021). Loss of Numb promotes hepatic progenitor expansion and intrahepatic cholangiocarcinoma by enhancing Notch signaling. *Cell Death Dis, 12*(11), 966. doi:10.1038/s41419-021-04263-w

Singh, D., Febbo, P. G., Ross, K., Jackson, D. G., Manola, J., Ladd, C., . . . Sellers, W. R. (2002). Gene expression correlates of clinical prostate cancer behavior. *Cancer Cell, 1*(2), 203-209. doi:10.1016/s1535-6108(02)00030-2

Singh, D., Singh, P. K., Chaudhary, S., Mehla, K., & Kumar, S. (2012). Exome sequencing and advances in crop improvement. *Adv Genet, 79*, 87-121. doi:10.1016/B978-0-12-394395-8.00003-7

Singrang, N., Kittisenachai, S., Roytrakul, S., Svasti, J., & Kangsamaksin, T. (2019). NOTCH1 regulates the viability of cholangiocarcinoma cells via 14-3-3 theta. *J Cell Commun Signal, 13*(2), 245-254. doi:10.1007/s12079-018-0488-9

Siolas, D., & Hannon, G. J. (2013). Patient-derived tumor xenografts: transforming clinical samples into mouse models. *Cancer Res, 73*(17), 5315-5319. doi:10.1158/0008-5472.CAN-13-1069

Sirica, A. E. (2011). The role of cancer-associated myofibroblasts in intrahepatic cholangiocarcinoma. *Nat Rev Gastroenterol Hepatol, 9*(1), 44-54. doi:10.1038/nrgastro.2011.222

Sirica, A. E., & Gores, G. J. (2014). Desmoplastic stroma and cholangiocarcinoma: clinical implications and therapeutic targeting. *Hepatology, 59*(6), 2397-2402. doi:10.1002/hep.26762

Sirica, A. E., Strazzabosco, M., & Cadamuro, M. (2021). Intrahepatic cholangiocarcinoma: Morpho-molecular pathology, tumor reactive microenvironment, and malignant progression. *Adv Cancer Res, 149*, 321-387. doi:10.1016/bs.acr.2020.10.005

Sirisinha, S., Tengchaisri, T., Boonpucknavig, S., Prempracha, N., Ratanarapee, S., & Pausawasdi, A. (1991). Establishment and characterization of a cholangiocarcinoma cell line from a Thai patient with intrahepatic bile duct cancer. *Asian Pac J Allergy Immunol, 9*(2), 153-157.

Siva Sankar, P., Che Mat, M. F., Muniandy, K., Xiang, B. L. S., Ling, P. S., Hoe, S. L. L., . . . Mohana-Kumaran, N. (2017). Modeling nasopharyngeal carcinoma in three dimensions. *Oncol Lett, 13*(4), 2034-2044. doi:10.3892/ol.2017.5697

Smout, M. J., Sripa, B., Laha, T., Mulvenna, J., Gasser, R. B., Young, N. D., . . . Loukas, A. (2011). Infection with the carcinogenic human liver fluke, Opisthorchis viverrini. *Mol Biosyst, 7*(5), 1367-1375. doi:10.1039/c0mb00295j

Sonnaert, M., Papantoniou, I., Luyten, F. P., & Schrooten, J. I. (2015). Quantitative Validation of the Presto Blue Metabolic Assay for Online Monitoring of Cell Proliferation in a 3D Perfusion Bioreactor System. *Tissue Eng Part C Methods, 21*(6), 519-529. doi:10.1089/ten.TEC.2014.0255

Sorrentino, G., Rezakhani, S., Yildiz, E., Nuciforo, S., Heim, M. H., Lutolf, M. P., & Schoonjans, K. (2020). Mechano-modulatory synthetic niches for liver organoid derivation. *Nat Commun, 11*(1), 3416. doi:10.1038/s41467-020-17161-0

Sripa, B., & Pairojkul, C. (2008). Cholangiocarcinoma: lessons from Thailand. *Curr Opin Gastroenterol, 24*(3), 349-356. doi:10.1097/MOG.0b013e3282fbf9b3

StageBio. (2018). IHC or IF: Which is Best for My Study? Retrieved from https://www.stagebio.com/blog/ihc-or-if-which-is-best-for-my-study

Steinert, P. M., & Roop, D. R. (1988). Molecular and cellular biology of intermediate filaments. *Annu Rev Biochem, 57*, 593-625. doi:10.1146/annurev.bi.57.070188.003113

Strijker, M., Belkouz, A., van der Geest, L. G., van Gulik, T. M., van Hooft, J. E., de Meijer, V. E., . . . Dutch Pancreatic Cancer, G. (2019). Treatment and survival of resected and unresected distal cholangiocarcinoma: a nationwide study. *Acta Oncol, 58*(7), 1048-1055. doi:10.1080/0284186X.2019.1590634

Subramanian, A., Tamayo, P., Mootha, V. K., Mukherjee, S., Ebert, B. L., Gillette, M. A., . . . Mesirov, J. P. (2005). Gene set enrichment analysis: a knowledge-based approach for interpreting genome-wide expression profiles. *Proc Natl Acad Sci U S A, 102*(43), 15545-15550. doi:10.1073/pnas.0506580102

Sueca-Comes, M. R., E. C.; Grabowska, A. M.; Bates D. O. (2022). Looking Under the Lamppost: The Search for New Cancer Targets in the Human Kinome. *Pharmacological Reviews, 74*(4), 1134-1143.

Sulaiman, A., & Wang, L. (2017). Bridging the divide: preclinical research discrepancies between triple-negative breast cancer cell lines and patient tumors. *Oncotarget, 8*(68), 113269-113281. doi:10.18632/oncotarget.22916

Sutherland, R. M., & Durand, R. E. (1984). Growth and cellular characteristics of multicell spheroids. *Recent Results Cancer Res, 95*, 24-49. doi:10.1007/978-3-642-82340-4_2

Sutherland, R. M., McCredie, J. A., & Inch, W. R. (2020). Growth of Multicell Spheroids in Tissue Culture as a Model of Nodular Carcinomas. *JNCI: Journal of the National Cancer Institute, 46*(1), 113-120. doi:10.1093/jnci/46.1.113

Szendroi, M., & Lapis, K. (1985). Distribution of fibronectin and laminin in human liver tumors. *J Cancer Res Clin Oncol, 109*(1), 60-64. doi:10.1007/BF01884256

Tadokoro, A., Kanaji, N., Liu, D., Yokomise, H., Haba, R., Ishii, T., . . . Bandoh, S. (2016). Vimentin Regulates Invasiveness and Is a Poor Prognostic Marker in Non-small Cell Lung Cancer. *Anticancer Res, 36*(4), 1545-1551.

Takagi, S., Miyagawa, S., Ichikawa, E., Soeda, J., Miwa, S., Miyagawa, Y., . . . Kawasaki, S. (2004). Dendritic cells, T-cell infiltration, and Grp94 expression in cholangiocellular carcinoma. *Hum Pathol, 35*(7), 881-886. doi:10.1016/j.humpath.2004.03.016

Takahashi, N., Higa, A., Hiyama, G., Tamura, H., Hoshi, H., Dobashi, Y., . . . Takagi, M. (2021). Construction of in vitro patient-derived tumor models to evaluate anticancer agents and cancer immunotherapy. *Oncol Lett, 21*(5), 406. doi:10.3892/ol.2021.12667

Tanimura, Y., Kokuryo, T., Tsunoda, N., Yamazaki, Y., Oda, K., Nimura, Y., . . . Hamaguchi, M. (2005). Tumor necrosis factor alpha promotes invasiveness of cholangiocarcinoma cells via its receptor, TNFR2. *Cancer Lett, 219*(2), 205-213. doi:10.1016/j.canlet.2004.07.027

Tchoryk, A., Taresco, V., Argent, R. H., Ashford, M., Gellert, P. R., Stolnik, S., . . . Garnett, M. C. (2019). Penetration and Uptake of Nanoparticles in 3D Tumor Spheroids. *Bioconjug Chem, 30*(5), 1371-1384. doi:10.1021/acs.bioconjchem.9b00136

Tentler, J. J., Tan, A. C., Weekes, C. D., Jimeno, A., Leong, S., Pitts, T. M., . . . Eckhardt, S. G. (2012). Patient-derived tumour xenografts as models for oncology drug development. *Nat Rev Clin Oncol, 9*(6), 338-350. doi:10.1038/nrclinonc.2012.61

Tepsiri, N., Chaturat, L., Sripa, B., Namwat, W., Wongkham, S., Bhudhisawasdi, V., & Tassaneeyakul, W. (2005). Drug sensitivity and drug resistance profiles of human intrahepatic cholangiocarcinoma cell lines. *World J Gastroenterol, 11*(18), 2748-2753. doi:10.3748/wjg.v11.i18.2748

Thamavit, W., Bhamarapravati, N., Sahaphong, S., Vajrasthira, S., & Angsubhakorn, S. (1978). Effects of dimethylnitrosamine on induction of cholangiocarcinoma in Opisthorchis viverrini-infected Syrian golden hamsters. *Cancer Res, 38*(12), 4634-4639.

Thippabhotla, S., Zhong, C., & He, M. (2019). 3D cell culture stimulates the secretion of in vivo like extracellular vesicles. *Sci Rep, 9*(1), 13012. doi:10.1038/s41598-019-49671-3

Timaner, M., Letko-Khait, N., Kotsofruk, R., Benguigui, M., Beyar-Katz, O., Rachman-Tzemah, C., . . . Shaked, Y. (2018). Therapy-Educated Mesenchymal Stem Cells Enrich for Tumor-Initiating Cells. *Cancer Res, 78*(5), 1253-1265. doi:10.1158/0008-5472.CAN-17-1547

Tsokos, C. G., Krings, G., Yilmaz, F., Ferrell, L. D., & Gill, R. M. (2016). Proliferative index facilitates distinction between benign biliary lesions and intrahepatic cholangiocarcinoma. *Hum Pathol, 57*, 61-67. doi:10.1016/j.humpath.2016.06.019

Uchibori, R., Tsukahara, T., Mizuguchi, H., Saga, Y., Urabe, M., Mizukami, H., . . . Ozawa, K. (2013). NF-κB activity regulates mesenchymal stem cell accumulation at tumor sites. *Cancer Res, 73*(1), 364-372. doi:10.1158/0008-5472.can-12-0088

UK, C. R. (2018). Worldwide cancer statistics. Retrieved from https://www.cancerresearchuk.org/health-professional/cancer-statistics/worldwide-cancer

UK, C. R. (2021). Survival for bile duct cancer. Retrieved from https://www.cancerresearchuk.org/about-cancer/bile-duct-cancer/survival#collapse-12022-1226093959

Utispan, K., Sonongbua, J., Thuwajit, P., Chau-In, S., Pairojkul, C., Wongkham, S., & Thuwajit, C. (2012). Periostin activates integrin α5β1 through a PI3K/AKT-dependent pathway in invasion of cholangiocarcinoma. *Int J Oncol, 41*(3), 1110-1118. doi:10.3892/ijo.2012.1530

Valle, J., Wasan, H., Palmer, D. H., Cunningham, D., Anthoney, A., Maraveyas, A., . . . Investigators, A. B. C. T. (2010). Cisplatin plus gemcitabine versus gemcitabine for biliary tract cancer. *N Engl J Med, 362*(14), 1273-1281. doi:10.1056/NEJMoa0908721

Valle, J. W., Kelley, R. K., Nervi, B., Oh, D. Y., & Zhu, A. X. (2021). Biliary tract cancer. *Lancet, 397*(10272), 428-444. doi:10.1016/s0140-6736(21)00153-7

Vaquero, J., Aoudjehane, L., & Fouassier, L. (2020). Cancer-associated fibroblasts in cholangiocarcinoma. *Curr Opin Gastroenterol, 36*(2), 63-69. doi:10.1097/MOG.0000000000000609

Vinci, M., Gowan, S., Boxall, F., Patterson, L., Zimmermann, M., Court, W., . . . Eccles, S. A. (2012). Advances in establishment and analysis of three-dimensional tumor spheroid-based functional assays for target validation and drug evaluation. *BMC Biol, 10*, 29. doi:10.1186/1741-7007-10-29

Vis, M. A. M., Ito, K., & Hofmann, S. (2020). Impact of Culture Medium on Cellular Interactions in in vitro Co-culture Systems. *Front Bioeng Biotechnol, 8*, 911. doi:10.3389/fbioe.2020.00911

Vogel, C., & Marcotte, E. M. (2012). Insights into the regulation of protein abundance from proteomic and transcriptomic analyses. *Nat Rev Genet, 13*(4), 227-232. doi:10.1038/nrg3185

Vuoriluoto, K., Haugen, H., Kiviluoto, S., Mpindi, J. P., Nevo, J., Gjerdrum, C., . . . Ivaska, J. (2011). Vimentin regulates EMT induction by Slug and oncogenic H-Ras and migration by governing Axl expression in breast cancer. *Oncogene, 30*(12), 1436-1448. doi:10.1038/onc.2010.509

Walter, S. G., Scheidt, S., Nissler, R., Gaisendrees, C., Zarghooni, K., & Schildberg, F. A. (2021). In-Depth Characterization of Stromal Cells within the Tumor Microenvironment Yields Novel Therapeutic Targets. *Cancers (Basel), 13*(6). doi:10.3390/cancers13061466

Wang, J., Dong, M., Xu, Z., Song, X., Zhang, S., Qiao, Y., . . . Chen, X. (2018). Notch2 controls hepatocyte-derived cholangiocarcinoma formation in mice. *Oncogene, 37*(24), 3229-3242. doi:10.1038/s41388-018-0188-1

Wang, W., Zhong, W., Yuan, J., Yan, C., Hu, S., Tong, Y., . . . Song, G. (2015). Involvement of Wnt/beta-catenin signaling in the mesenchymal stem cells promote metastatic growth and chemoresistance of cholangiocarcinoma. *Oncotarget, 6*(39), 42276-42289. doi:10.18632/oncotarget.5514

Wang, Y., Ding, X., Wang, S., Moser, C. D., Shaleh, H. M., Mohamed, E. A., . . . Roberts, L. R. (2016). Antitumor effect of FGFR inhibitors on a novel cholangiocarcinoma patient derived xenograft mouse model endogenously expressing an FGFR2-CCDC6 fusion protein. *Cancer Lett, 380*(1), 163-173. doi:10.1016/j.canlet.2016.05.017

Wang, Y., Mashock, M., Tong, Z., Mu, X., Chen, H., Zhou, X., . . . Li, X. (2020). Changing Technologies of RNA Sequencing and Their Applications in Clinical Oncology. *Front Oncol, 10*, 447. doi:10.3389/fonc.2020.00447

Wang, Z., Gerstein, M., & Snyder, M. (2009). RNA-Seq: a revolutionary tool for transcriptomics. *Nat Rev Genet, 10*(1), 57-63. doi:10.1038/nrg2484

Warren, A., Chen, Y., Jones, A., Shibue, T., Hahn, W. C., Boehm, J. S., . . . McFarland, J. M. (2021). Global computational alignment of tumor and cell line transcriptional profiles. *Nat Commun, 12*(1), 22. doi:10.1038/s41467-020-20294-x

Weiswald, L. B., Bellet, D., & Dangles-Marie, V. (2015). Spherical cancer models in tumor biology. *Neoplasia, 17*(1), 1-15. doi:10.1016/j.neo.2014.12.004

Whiteley, J. T., Fernandes, S., Sharma, A., Mendes, A. P. D., Racha, V., Benassi, S. K., & Marchetto, M. C. (2022). Reaching into the toolbox: Stem cell models to study neuropsychiatric disorders. *Stem Cell Reports, 17*(2), 187-210. doi:10.1016/j.stemcr.2021.12.015

Williams, C. G., Lee, H. J., Asatsuma, T., Vento-Tormo, R., & Haque, A. (2022). An introduction to spatial transcriptomics for biomedical research. *Genome Med, 14*(1), 68. doi:10.1186/s13073-022-01075-1

Wilson, D. H., Jarman, E. J., Mellin, R. P., Wilson, M. L., Waddell, S. H., Tsokkou, P., . . . Boulter, L. (2020). Non-canonical Wnt signalling regulates scarring in biliary disease via the planar cell polarity receptors. *Nat Commun, 11*(1), 445. doi:10.1038/s41467-020-14283-3

Wong, P. F., Wei, W., Gupta, S., Smithy, J. W., Zelterman, D., Kluger, H. M., & Rimm, D. L. (2019). Multiplex quantitative analysis of cancer-associated fibroblasts and immunotherapy outcome in metastatic melanoma. *J Immunother Cancer, 7*(1), 194. doi:10.1186/s40425-019-0675-0

Wu, L., Amjad, S., Yun, H., Mani, S., & de Perrot, M. (2022). A panel of emerging EMT genes identified in malignant mesothelioma. *Sci Rep, 12*(1), 1007. doi:10.1038/s41598-022-04973-x

Wu, W. R., Shi, X. D., Zhang, R., Zhu, M. S., Xu, L. B., Yu, X. H., . . . Liu, C. (2014). Clinicopathological significance of aberrant Notch receptors in intrahepatic cholangiocarcinoma. *Int J Clin Exp Pathol, 7*(6), 3272-3279.

Xiao, Y., Zhang, B., Cloyd, J. M., Alaimo, L., Xu, G., Du, S., . . . Pawlik, T. M. (2022). Novel Drug Candidate Prediction for Intrahepatic Cholangiocarcinoma via Hub Gene Network Analysis and Connectivity Mapping. *Cancers (Basel), 14*(13). doi:10.3390/cancers14133284

Yamaguchi, N., Morioka, H., Ohkura, H., Hirohashi, S., & Kawai, K. (1985). Establishment and characterization of the human cholangiocarcinoma cell line HChol-Y1 in a serum-free, chemically defined medium. *J Natl Cancer Inst, 75*(1), 29-35.

Yamamoto, K., Ueno, T., Kawaoka, T., Hazama, S., Fukui, M., Suehiro, Y., . . . Hinoda, Y. (2005). MUC1 peptide vaccination in patients with advanced pancreas or biliary tract cancer. *Anticancer Res, 25*(5), 3575-3579.

Yan, S., Chi, X., Chang, X., & Tian, M. (2020). Analysing the meta-interaction between pathways by gene set topological impact analysis. *BMC Genomics*.

Yang, J., Sontag, D. P., Burczynski, F. J., Xi, S., Gong, Y., & Minuk, G. Y. (2022). Comparison of growth features and cancer stem cell prevalence in intrahepatic and extrahepatic cholangiocarcinoma cell lines. *Clin Exp Hepatol, 8*(1), 60-69. doi:10.5114/ceh.2022.114192

Yang, X., Lin, Y., Shi, Y., Li, B., Liu, W., Yin, W., . . . He, R. (2016). FAP Promotes Immunosuppression by Cancer-Associated Fibroblasts in the Tumor Microenvironment via STAT3-CCL2 Signaling. *Cancer Res, 76*(14), 4124-4135. doi:10.1158/0008-5472.CAN-15-2973

Yokoi, K., Kobayashi, A., Motoyama, H., Kitazawa, M., Shimizu, A., Notake, T., . . . Miyagawa, S. I. (2018). Survival pathway of cholangiocarcinoma via AKT/mTOR signaling to escape RAF/MEK/ERK pathway inhibition by sorafenib. *Oncol Rep, 39*(2), 843-850. doi:10.3892/or.2017.6153

Yoon, H. A., Noh, M. H., Kim, B. G., Han, J. S., Jang, J. S., Choi, S. R., . . . Chun, J. H. (2011). Clinicopathological significance of altered Notch signaling in extrahepatic cholangiocarcinoma and gallbladder carcinoma. *World J Gastroenterol, 17*(35), 4023-4030. doi:10.3748/wjg.v17.i35.4023

Yoon, J. H., Gwak, G. Y., Lee, H. S., Bronk, S. F., Werneburg, N. W., & Gores, G. J. (2004). Enhanced epidermal growth factor receptor activation in human cholangiocarcinoma cells. *J Hepatol, 41*(5), 808-814. doi:10.1016/j.jhep.2004.07.016

Yoshida, G. J. (2020). Applications of patient-derived tumor xenograft models and tumor organoids. *J Hematol Oncol, 13*(1), 4. doi:10.1186/s13045-019-0829-z

Yoshida, S., Asanoma, K., Yagi, H., Onoyama, I., Hori, E., Matsumura, Y., . . . Kato, K. (2021). Fibronectin mediates activation of stromal fibroblasts by SPARC in endometrial cancer cells. *BMC Cancer, 21*(1), 156. doi:10.1186/s12885-021-07875-9

Yothaisong, S., Dokduang, H., Techasen, A., Namwat, N., Yongvanit, P., Bhudhisawasdi, V., . . . Loilome, W. (2013). Increased activation of PI3K/AKT signaling pathway is associated with cholangiocarcinoma metastasis and PI3K/mTOR inhibition presents a possible therapeutic strategy. *Tumour Biol, 34*(6), 3637-3648. doi:10.1007/s13277-013-0945-2

Younger, N. T., Wilson, M. L., Martinez Lyons, A., Jarman, E. J., Meynert, A. M., Grimes, G. R., . . . Boulter, L. (2022). In Vivo Modeling of Patient Genetic Heterogeneity Identifies New Ways to Target Cholangiocarcinoma. *Cancer Res, 82*(8), 1548-1559. doi:10.1158/0008-5472.CAN-21-2556

Yu, J., Qin, B., Moyer, A. M., Sinnwell, J. P., Thompson, K. J., Copland, J. A., 3rd, . . . Wang, L. (2017). Establishing and characterizing patient-derived xenografts using pre-chemotherapy percutaneous biopsy and post-chemotherapy surgical samples from a prospective neoadjuvant breast cancer study. *Breast Cancer Res, 19*(1), 130. doi:10.1186/s13058-017-0920-8

Yu, M., Guo, G., Huang, L., Deng, L., Chang, C. S., Achyut, B. R., . . . Cui, Y. (2020). CD73 on cancer-associated fibroblasts enhanced by the A2B-mediated feedforward circuit enforces an immune checkpoint. *Nat Commun, 11*(1), 515. doi:10.1038/s41467-019-14060-x

Zachari, M. A., Chondrou, P. S., Pouliliou, S. E., Mitrakas, A. G., Abatzoglou, I., Zois, C. E., & Koukourakis, M. I. (2014). Evaluation of the alamarblue assay for adherent cell irradiation experiments. *Dose Response, 12*(2), 246-258. doi:10.2203/dose-response.13-024.Koukourakis

Zanoni, M., Cortesi, M., Zamagni, A., Arienti, C., Pignatta, S., & Tesei, A. (2020). Modeling neoplastic disease with spheroids and organoids. *J Hematol Oncol, 13*(1), 97. doi:10.1186/s13045-020-00931-0

Zhang, M., Yang, H., Wan, L., Wang, Z., Wang, H., Ge, C., . . . Yan, X. (2020). Single-cell transcriptomic architecture and intercellular crosstalk of human intrahepatic cholangiocarcinoma. *J Hepatol, 73*(5), 1118-1130. doi:10.1016/j.jhep.2020.05.039

Zhang, S., Song, X., Cao, D., Xu, Z., Fan, B., Che, L., . . . Chen, X. (2017). Pan-mTOR inhibitor MLN0128 is effective against intrahepatic cholangiocarcinoma in mice. *J Hepatol, 67*(6), 1194-1203. doi:10.1016/j.jhep.2017.07.006

Zhang, W., Moore, L., & Ji, P. (2011). Mouse models for cancer research. *Chin J Cancer, 30*(3), 149-152. doi:10.5732/cjc.011.10047

Zhang, Y., Ji, G., Han, S., Shao, Z., Lu, Z., Huo, L., . . . Li, X. (2018). Tip60 Suppresses Cholangiocarcinoma Proliferation and Metastasis via PI3k-AKT. *Cell Physiol Biochem, 50*(2), 612-628. doi:10.1159/000494183

Zhang, Z., Lai, G. H., & Sirica, A. E. (2004). Celecoxib-induced apoptosis in rat cholangiocarcinoma cells mediated by Akt inactivation and Bax translocation. *Hepatology, 39*(4), 1028-1037. doi:10.1002/hep.20143

Zhao, W., Ren, G., Zhang, L., Zhang, Z., Liu, J., Kuang, P., . . . Wang, X. (2012). Efficacy of mesenchymal stem cells derived from human adipose tissue in inhibition of hepatocellular carcinoma cells in vitro. *Cancer Biother Radiopharm, 27*(9), 606-613. doi:10.1089/cbr.2011.1150

Zheng, X., Xu, M., Yao, B., Wang, C., Jia, Y., & Liu, Q. (2016). IL-6/STAT3 axis initiated CAFs via up-regulating TIMP-1 which was attenuated by acetylation of STAT3 induced by PCAF in HCC microenvironment. *Cell Signal, 28*(9), 1314-1324. doi:10.1016/j.cellsig.2016.06.009

Zheng, Y., Zhou, C., Yu, X. X., Wu, C., Jia, H. L., Gao, X. M., . . . Qin, L. X. (2018). Osteopontin promotes metastasis of intrahepatic cholangiocarcinoma through recruiting MAPK1 and mediating Ser675 phosphorylation of beta-Catenin. *Cell Death Dis, 9*(2), 179. doi:10.1038/s41419-017-0226-x

Zhou, B., Xiang, J., Jin, M., Zheng, X., Li, G., & Yan, S. (2021). High vimentin expression with E-cadherin expression loss predicts a poor prognosis after

resection of grade 1 and 2 pancreatic neuroendocrine tumors. *BMC Cancer, 21*(1), 334. doi:10.1186/s12885-021-08062-6

Zhou, J., Tan, X., Tan, Y., Li, Q., Ma, J., & Wang, G. (2018). Mesenchymal Stem Cell Derived Exosomes in Cancer Progression, Metastasis and Drug Delivery: A Comprehensive Review. *J Cancer, 9*(17), 3129-3137. doi:10.7150/jca.25376

Zhou, K. Q., Liu, W. F., Yang, L. X., Sun, Y. F., Hu, J., Chen, F. Y., . . . Wang, Z. (2019). Circulating osteopontin per tumor volume as a prognostic biomarker for resectable intrahepatic cholangiocarcinoma. *Hepatobiliary Surg Nutr, 8*(6), 582-596. doi:10.21037/hbsn.2019.03.14

Zhou, M., Wang, C., Lu, S., Xu, Y., Li, Z., Jiang, H., & Ma, Y. (2021). Tumor-associated macrophages in cholangiocarcinoma: complex interplay and potential therapeutic target. *EBioMedicine, 67*, 103375. doi:10.1016/j.ebiom.2021.103375

Zhou, Q., Wang, Y., Peng, B., Liang, L., & Li, J. (2013). The roles of Notch1 expression in the migration of intrahepatic cholangiocarcinoma. *BMC Cancer, 13*, 244. doi:10.1186/1471-2407-13-244

Zhu, A. X., Finn, R. S., Edeline, J., Cattan, S., Ogasawara, S., Palmer, D., . . . investigators, K.-. (2018). Pembrolizumab in patients with advanced hepatocellular carcinoma previously treated with sorafenib (KEYNOTE-224): a non-randomised, open-label phase 2 trial. *Lancet Oncol, 19*(7), 940-952. doi:10.1016/S1470-2045(18)30351-6

Zhu, A. X., Macarulla, T., Javle, M. M., Kelley, R. K., Lubner, S. J., Adeva, J., . . . Abou-Alfa, G. K. (2021). Final Overall Survival Efficacy Results of Ivosidenib for Patients With Advanced Cholangiocarcinoma With IDH1 Mutation: The Phase 3 Randomized Clinical ClarIDHy Trial. *JAMA Oncol, 7*(11), 1669-1677. doi:10.1001/jamaoncol.2021.3836